The requirements for PCP signalling in early zebrafish endoderm morphogenesis

Lee Barry Miles (B.Sc. Hons)

Doctor of Philosophy

September 2014

School of Biological Sciences
Monash University

Copyright Notices

Notice 1

Notice 2

Abstract

The vertebrate endodermal cell layer gives rise to the intestine and related organs such as the liver and pancreas. The endodermal organs control many critical metabolic processes including the absorption of nutrients, homoeostasis of blood sugar levels, and detoxification of the blood. The cell fate specification and organogenesis of the zebrafish endoderm is well characterised, however the morphogenic processes during migration to the midline at somitogenesis stages and the formation of the primitive endodermal rod were unknown.

This study used the Tg(*sox17:EGFP*) endodermal reporter line to determine the process of endoderm development at somitogenesis stages during two important phases of morphogenesis, the migration to the dorsal midline, and the formation of the endodermal rod (termed "midline aggregation"). Analysis of the polarisation of the microtubule organising centre (MTOC) in respect to the direction of cell migration reveals a contrasting difference between the endoderm and the surrounding mesoderm, indicating the directed migration of these two cell types are not regulated by the same mechanisms.

The Planar cell Polarity (PCP) signalling pathway is known to regulate convergence and extension (C&E) movements of the mesoderm and ectoderm (Topczewski et al., 2001; Jessen et al., 2002). This study analysed endodermal development in the PCP mutants *trilobite* and *knypek,* and reports on the requirements of individual components of the PCP signalling pathway for endoderm development and morphogenesis during somitogenesis stages. The role of PCP signalling components during brain morphogenesis was also investigated, identifying a requirement of specific PCP signalling components for brain vesicle expansion.

This study also describes the generation of a transgenic line that enables the inducible disruption of the PCP signalling to analyse the time-specific roles of this signalling pathway during development. This novel transgenic line enabled the identification of a time-specific role of PCP signalling in the regulation of hindbrain axis morphogenesis.

Declaration

This is to certify that this thesis comprises only my original work towards the PhD degree with the exception of that outlined in the Preface. Due acknowledgements has been made in the text to all other materials used. No material which has been accepted for the award of any other degree or diploma in any university or other institution, and that to the best of my knowledge the thesis contains no material previously published or written by another person, except where due reference is made in the text of the thesis.

Lee B. Miles

Preface

Work presented in this thesis generated with assistance includes the following:

Figure 4.5 B Western gel and blot was preformed by Aminah Giousoh and Evelyn Yip .

Acknowledgements

There are numerous individuals that I would like to thank for their support during my PhD. First and foremost I would like to thank my supervisor Dr. Heather Verkade. I am very grateful to have worked under your supervision. You have always been open to listen to the seemingly never-ending ideas for experiments that I have come up with over the last six years, providing insight, allowing me the freedom to plan experiments, make mistakes (as long as I learnt from them), and provided a sense of faith in my ability to finish this project, even when nothing worked. Not to mention the multiple lessons in grammar – I'm still totally lost with some of them, but that's okay. Thank you!

I would like to thank all my lab members and collaborators over the years: The Verkade lab (Wade Moore, Dr. Xenia Kostoulias, Sarah Sherson, Aminah Giousoh, and Evelyn Yip), the Bryson-Richardson lab (Dr. Rob Bryson-Richardson, Dr. Tamar Sztal, Avnika Ruparelia, Raquel Vaz, Mo Zhao, and Caitlin Williams), and the Currie Lab (Dr. Tom Hall, Dr. Ashley Siegel, Phong Nguyen, and Carmen Sonntag).

I would like to specifically thank Prof. Peter Currie for employing me when my scholarship ran out and providing me with the means and support on numerous occasions to attend meeting and talks. Without his assistance this thesis might not have come to be.

I would like to thank my family. Firstly, I want to thank my parents Varee Lynn and Neville Miles. You have both never faulted in believing in me - even when I was at my worst. My brother Dr. Wayne Miles, you have been a great role model. My sister La Reve Lynn, you have more heart than anyone I know. I must also thank my extended family (Linda Miles, David Hardy, and Glenn Riddell).

Special thanks must also go my fellow PhD students - Tom Dierschke, Victor Yu, Tezz Quon, Wade Moore, and Joe Ryan. I couldn't imagine how I would have turned out without our lunchtime lurkle.

List of abbreviations

EBFP2	enhanced blue fluorescent protein 2
°C	degrees Celsius
cDNA	complimentary deoxyribonucleic acid
C&E	convergence and extension
DNA	deoxyribonucleic acid
dfp	days post fertilisation
ECM	extracellular matrix
EGFP	enhanced green fluorescent protein
h	hours
HMG	high mobility group
hpf	hours post fertilisation
JNK	c-Jun N-terminal Kinase
mCherry	monomeric Cherry
MHB	midbrain hindbrain boundary
mg	milligram
MO	morpholino oligonucleotide
morphant	morpholino oligonucleotide injected embryo
mRNA	messenger RNA
MTOC	microtubule organising centre
ng	nanogram
ON	overnight
ORF	open reading frame
PBS	phosphate buffered saline
PBST	phosphate buffered saline with 0.1% Tween20
PCR	polymerase chain reaction
PCP	Planar cell polarity
RNA	ribonucleic acid
RT-PCR	reverse transcriptase PCR
s	seconds
UTR	untranslated region
YSL	yolk syncytial layer

Table of contents

List of Figures

Chapter 1. Introduction

1.1. Introduction

The overall research area of this study investigates the genetic mechanisms that control development of the endodermal organs. Triploblastic animal embryos are comprised of three cell layers; the endoderm, the mesoderm, and the ectoderm. The endoderm is the innermost layer and gives rise to the gut, intestine, and related organs such as the liver and pancreas (Warga and Nusslein-Volhard, 1999). The endodermal organs control many critical metabolic processes including absorption of nutrients, homeostasis of blood sugar levels, blood oxygenation (in air-breathing vertebrates), and detoxification of the blood.

I used the zebrafish (*Danio rerio*) as a model to investigate vertebrate endoderm development. Zebrafish are an excellent model organism for investigating the genetics of vertebrate development due to their genomic malleability, enabling the generation of transgenic lines. The optical transparency of the developing zebrafish embryo enables cells expressing a fluorescent protein, such as enhanced green fluorescent protein (*EGFP*), to be viewed using fluorescent microscopy; this is vital when investigating deep tissue layers such as the endoderm that would otherwise be blocked by the overlying tissue and not amenable using non-fluorescent microscopy. This provides a powerful tool to investigate cellular migration movements and signalling pathways during development.

The specification of endodermal cell fate (Alexander et al., 1999; Alexander and Stainier, 1999), migration behaviour during very early stages (Pezeron et al., 2008), and organogenesis during late embryonic stages have been extensively studied (Field et al., 2003a; Field et al., 2003b; Ober et al., 2003). However their migration and morphogenesis in the intervening stages have received very little attention. During early development, zebrafish endodermal cells are practically indistinguishable from the overlying mesodermal tissue (Warga and Nusslein-Volhard, 1999) without labelling,

preventing detailed morphological, structural, and developmental analysis. For this reason much work has been focused on understanding the development of the mesoderm, but endoderm specific information is lacking.

In this research project I used the Tg(*sox17:EGFP*) (Mizoguchi et al., 2006) transgenic line as a background genotype. This line has endoderm specific expression of *EGFP*, allowing endodermal cells to be visualised from very early stages (~5 hours post fertilization (hpf)) with the use of a fluorescence microscope. This vital transgenic tool allows endoderm to be easily distinguished from mesoderm.

1.1.1. Development of the zebrafish germ layers

The body plan of zebrafish emerges from a single cell on top of an extra-embryonic yolk ball. Through numerous divisions, cell movements, and rearrangements the embryonic axes are set down to define the body plan (Keller et al., 2008). In zebrafish this occurs within the first 24 hours (Kimmel et al., 1995). Upon fertilization of the oocyte, a single first cell is formed on top of the yolk, and begins to divide. Once the number of cells perched on the yolk ball increases from one cell to many thousands (Kimmel et al., 1995) the process of gastrulation begins. During gastrulation there are three movements, epiboly, involution, and convergence and extension (C&E). Together involution and epiboly work to generate an embryo with three defined germ layers. The ectodermal layer on the outside gives rise to the epidermis and the central nervous system. The endoderm and mesoderm are below the ectoderm. They are sometimes referred to as the mesendoderm, but in fact they do consist of two specified germ layers, with the endodermal cells in the very innermost layer, lying directly over the internal yolk ball (Warga and Nusslein-Volhard, 1999). C&E is the mass migration of cells to the dorsal midline acting to drive the mediolateral narrowing and anterio-posterior lengthening of the embryo. C&E continues into early somitogenesis stages, at which all cell layers are coordinated and the overall body plan is set out (Schier and Talbot, 2005).

1.2. Endodermal development

1.2.1. Endodermal specification

There are three morphological processes that occur during endoderm development up to somitogenesis stages, specification, migration, and midline aggregation. The endodermal cell lineage is specified soon after the onset of gastrulation via the Nodal signalling pathway from a subset of cells in contact with the yolk syncytial layer (YSL)(Alexander and Stainier, 1999)(Figure 1.1). The expression of upstream Nodal activates the induction of a group of high-mobility group (HMG) transcription factors (Alexander et al., 1999; Alexander and Stainier, 1999; Dickmeis et al., 2001; Kikuchi et al., 2001). *Casanova* is a downstream Nodal transcription factor that is responsible (along with *mixer*) for the activation of *sox17* expression. Sox17 is a HMG domain transcription factor that is required for initiation of endodermal differentiation and is the first endoderm specific marker that distinguishes the endoderm from the surrounding mesodermal cells (Alexander and Stainier, 1999; Kikuchi et al., 2001).

1.2.2. Endodermal migration

When the endodermal cells are specified they are in a non-continuous layer of cells overlying the YSL, with an even salt and pepper pattern (Warga and Nusslein-Volhard, 1999)(see Figure 1.1). At this stage endodermal cells are intermingled with the surrounding mesodermal cells, and although these two cell types are morphologically similar, they show contrasting differences in their cell motility during epiboly (Warga and Nusslein-Volhard, 1999). As gastrulation continues the endodermal cells migrate between the surrounding YSL and mesoderm with a random walk characteristic that is unique to the endoderm and independent of the surrounding mesoderm (Pezeron et al., 2008). This migratory behaviour allows the endoderm to spread out over the yolk sac by 75 % epiboly. This random walk migration is in contrast to the migration characteristics of the mesoderm, which exhibit a directed migration to the

dorsal side of the embryo during gastrulation (Sepich et al., 2005; Rohde and Heisenberg, 2007).

At mid-gastrulation (75 % epiboly) the dispersed endodermal cells begin a directed migration towards the dorsal midline (Pezeron et al., 2008). The change in endoderm migratory behaviour at 75 % epiboly from random walk to directed migration also coincides with convergence and extension (C&E) (Figure 1.1). C&E is the process by which all cell layers begin to migrate to the dorsal midline, driving the anteroposterior lengthening and mediolateral narrowing of the embryonic axis. C&E movements are known to be regulated by the Planar cell polarity (PCP) signalling pathway, and disruption of PCP signalling appears to affect the C&E movements of all tissue layers (reviewed in Myers et al., 2002).

A number of factors that specifically control the migration of the endodermal cells to the dorsal midline have been identified. The *sdf1/cxcr4* chemokine pathway is known to regulate aspects of endodermal migration towards the dorsal midline during gastrulation stages. There is evidence that the migrating endodermal cells are attracted towards the surrounding mesoderm via the *sdf1/cxcr4* chemokine pathway after midgastrulation (Mizoguchi et al., 2008). Alternatively, there is also evidence that the endoderm is tethered to the surrounding mesoderm via integrin, and that this is mediated by *sdf1/sxcr4* signalling (Nair and Schilling, 2008). However, the loss of *sdf1/sxcr4* signalling impairs but does not prevent endodermal migration towards the midline at late gastrulation stages (Mizoguchi et al., 2008), indicating additional factors effect endodermal cell migration. Additional evidence for this comes from examination of the extracellular matrix (ECM) component *N-cadherin* mutant *bib*, in which the migration of the mesoderm to the midline is reduced and wider than WT at 100 % epiboly. Interestingly however, the endoderm migration towards the midline is not affected in this mutant and the endoderm is no wider than WT as determined from expression of the endodermal marker *axial* (Warga and Kane, 2007). This is the first demonstrated example of mesodermal migration defects without a disruption of endoderm migration, and does not support the integrin tether, or attractant model of *sdf1/cxcr4* during endoderm migration.

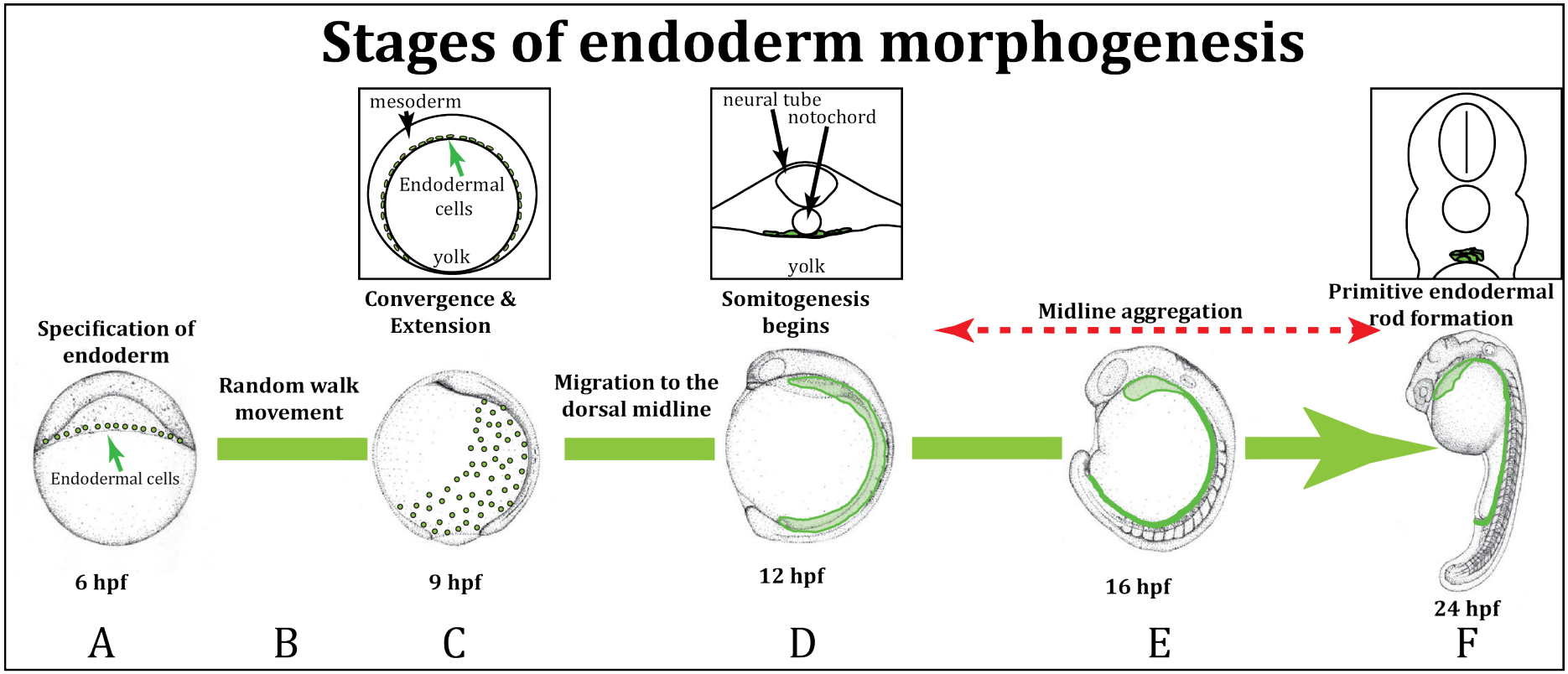
Stages of endoderm morphogenesis
mesoderm
Endodermal cells
yolk
neural tube
notochord
yolk
Specification of endoderm
Endodermal cells
6 hpf
A
Random walk movement
Convergence & Extension
9 hpf
B
C
Migration to the dorsal midline
Somitogenesis begins
12 hpf
D
Midline aggregation
16 hpf
E
Primitive endodermal rod formation
24 hpf
F

Figure 1.1 Stages of endodermal morphogenesis. (A) The endoderm is specified from a subset of cells in contact with the yolk syncytial layer (YSL) at 6 hpf. **(B)** Between 6 and 9 hpf the endoderm undergoes a random walk characteristic to spread out over the yolk. **(C)** At the onset of convergence and extension (C&E) (75 % epiboly) the endoderm starts the migration to the dorsal midline. **(D)** At somitogenesis stages the endoderm forms a broad stripe at the dorsal midline running the anterio-posterior length of the embryo. **(E)** At some point during somitogenesis stages the endoderm undergoes midline aggregation (red line) to form the primitive endodermal rod by 24 hpf **(F).** The green shaded areas represent the location of the endoderm at a particular stage. The green dots represent the pattern of endodermal cells at a particular stage. The box demonstrate the endoderm location in the embryo cross-section at the stages indicated (modified from Kimmel et al., 1995).

Although the *N-cadherin* mutant *bib*, did not display defects in the migration of endodermal cells, the endoderm is known for its specific expression of *E-cadherin* rather than *N-cadherin* (Warga and Kane, 2007). Unfortunately, previous studies into the *E-cadherin* mutant *cdh1*^{rk3} identified an overall convergence and extension defect, but did not investigate the morphology of the endoderm (Shimizu et al., 2005). Therefore a specific role for cadherins in endodermal migration cannot be ruled out.

Recently sphingosine-1-phosphate signalling through S1pr2/Gα13 has been demonstrated to be required specifically and cell autonomously in the endoderm for C&E migration of the anterior endoderm, which will give rise to the pharyngeal endoderm, but is not required for mesodermal C&E movements (Ye and Lin, 2013). However, the *s1pr2* mutant *miles apart* (*mil*) does have defects in the posterior endoderm (Kupperman et al., 2000), suggesting the migration of the posterior endoderm require *s1pr2/gα13* signalling.

The yolk syncytial layer (YSL) has been shown to influence the migration of the anterior endoderm by regulating Fibronectin levels (Sakaguchi et al., 2006). *s1pr2/gα13* signalling has also been shown to regulate the levels of the extra cellular matrix (ECM) protein Fibronectin (Matsui et al., 2007; Osborne et al., 2008). *sdf1/cxcr4* and *s1pr2/gα13* signalling also regulate components of the ECM, indicating a strong role for the ECM in controlling endodermal cell migration. Clearly, more needs to be done to explain the exact role of chemokine attractants and ECM components in controlling endodermal movement.

1.2.3. Midline aggregation

The processes of involution and epiboly are completed at 100 % epiboly, which also is the end of gastrulation. C&E movements in the ectoderm and mesoderm do not stop at 100 % epiboly, but continue into somitogenesis stages while other morphogenic and specification events further refine the body plan.

At mid-somitogenesis stages (11 hpf onwards) the endodermal cells have formed a broad stripe either side of the dorsal midline that runs along the anteroposterior length of the embryo (Figure 1.1). The endoderm has been observed to have formed a primitive endodermal rod at 28 hpf (Field et al.,

2003a), but how the broad stripe seen at earlier stages changes into this structure has not been observed. After the formation of the primitive endodermal rod the cells undergo rearrangements relative to neighbouring cells (Wallingford et al., 2002) to generate the intestine and related organs at 74-76 hpf (Ng et al., 2005).

We have termed the process that changes the single layer of mesenchymal endodermal cells into a midline mesenchymal rod as midline aggregation. The aim of this project was to characterise midline aggregation in detail, and investigate the role that PCP signalling plays in this process.

1.3. The Planar Cell Polarity (PCP) signalling pathway

The Planar cell Polarity (PCP) signalling pathway, also known as the non-canonical Wnt signalling pathway, regulates the polarity of epithelial planes perpendicular to the apical-basal axis (Mlodzik, 1999). PCP signalling was first identified in *Drosophila* (Gubb and Garcia-Bellido, 1982) in which it controls the orientation of the cuticular hairs in relation to neighbouring cells. Since then PCP has been subsequently demonstrated to play a role in the polarisation of a large array of animal structures including intestinal cells, fish scales, hair follicles, and the directionality of inner ear sensory hair bundles in mice (Mlodzik, 1999; Goto and Keller, 2002; Carreira-Barbosa et al., 2003; Fanto and McNeill, 2004; Djiane et al., 2005; Karner et al., 2006; Lopez-Schier and Hudspeth, 2006; Devenport and Fuchs, 2008; Shnitsar and Borchers, 2008; Gomes et al., 2009; Heydeck et al., 2009; Karner et al., 2009; Ravni et al., 2009; Antic et al., 2010; Fenstermaker et al., 2010; Guirao et al., 2010; Kibar et al., 2010; Mapp et al., 2010; Oteiza et al., 2010; Warchol and Montcouquiol, 2010; Wen et al., 2010).

PCP signalling has also been shown to play a major role in the regulation of mesenchymal cell behaviour during gastrulation and C&E in vertebrates (Tada and Smith, 2000; Wallingford et al., 2000; Darken et al., 2002; Goto and Keller, 2002; Jessen et al., 2002; Tada et al., 2002; Carreira-Barbosa et al., 2003; Jenny et al., 2003; Ulrich et al., 2003; Veeman et al., 2003; Miyagi et al., 2004; Torban et al., 2004; Goto et al., 2005; Matsui et al., 2005; Carreira-Barbosa et al., 2008;

Pezeron et al., 2008; Simons and Mlodzik, 2008; Vervenne et al., 2008; Roszko et al., 2009; Sepich et al., 2011; Dohn et al., 2013; Pan et al., 2013). The definitive process by which mesenchymal and epithelial cells generate vertebrate PCP is still not fully understood. Much of the information gained so far about zebrafish PCP comes from studies of mesodermal C&E and neuroepithelial development (Heisenberg et al., 2000; Topczewski et al., 2001; Jessen et al., 2002; Carreira-Barbosa et al., 2003; Kilian et al., 2003; Veeman et al., 2003; Marlow et al., 2004; Goto et al., 2005; Wada et al., 2005; Ciruna et al., 2006; Carreira-Barbosa et al., 2008; Simons and Mlodzik, 2008; Vervenne et al., 2008; Gros et al., 2009; Tada and Kai, 2009; Guirao et al., 2010; Mapp et al., 2010; Dohn et al., 2013), however the role of PCP signalling on endodermal development is lacking.

1.3.1. The downstream effects of PCP signalling

Activation of PCP signalling regulates cellular behaviour through changes in cytoskeletal architecture, and the establishment and modulation of cell polarity (Matsui et al., 2005; Pezeron et al., 2008) (Figure 1.2). PCP signalling also regulates the distribution, organisation, and stability of multiple components of the extracellular matrix (ECM) including Laminin, Fibronectin, and Cadherin to modulate adhesion (Jessen et al., 2002; Coyle et al., 2008; Dohn et al., 2013). PCP signalling is required for the correct localisation of Cadherins within notochord progenitors and the differentiated notochord (Yang and Thorpe, 2011).

PCP signalling also controls cellular behaviours such as the re-establishment of polarity after cell division in the zebrafish neural tube (Ciruna et al., 2006) or the biasing of mesodermal cellular protrusions towards a particular stimulus in migrating prechordal plate mesoderm (Ulrich et al., 2003; Wallingford, 2010). Another known downstream action of PCP signalling is the regulation of cytoskeletal architecture, such as lamellipodia extensions (Wallingford et al., 2000). Although it is evident from these many studies that PCP signalling regulates the dynamics of cytoskeletal structures, it is not exactly clear how PCP signalling deciphers the incoming signals to controls cytoskeletal dynamics.

1.3.2. The PCP signalling pathway

The PCP signalling pathway shares a number of major components with the β-catenin signalling pathway. The common features include the membrane spanning Frizzled (Fzd) receptor and the intercellular mediator Dishevelled (Dvl) (Figure 1.2). Embryos that are homozygote mutant for some components of the PCP signalling pathway display characteristic reduction in convergence and extension movements (Hammerschmidt et al., 1996; Topczewski et al., 2001; Goto and Keller, 2002; Jessen et al., 2002; Kilian et al., 2003; Matsui et al., 2005; Carreira-Barbosa et al., 2008). During PCP signalling Frizzled is activated by Wnt ligands and in turn recruits the intracellular mediator Dishevelled (Dvl) to the plasma membrane (Habas et al., 2001; Ulrich et al., 2003; Habas and Dawid, 2005). This recruitment is reliant on the presence of the transmembrane protein Trilobite (Tri/Vangl2) (Park and Moon, 2002). Frizzled has been shown to localize to regions on the plasma membrane at areas of high PCP signalling activity in ectodermal and mesodermal cells during gastrulation (Witzel et al., 2006). The Frizzled plasma membrane localisations have been shown to co-localize with Dishevelled in epithelial tissues and can act as local adhesion points to hold cells together (Witzel et al., 2006). The roles and functions of the major components of the PCP signalling pathway will now be discussed.

1.3.2.1. Wnt signalling ligands

The Wnt signalling molecules are widely accepted as the ligands that activate PCP signalling. Wnts are secreted extracellular signalling molecules that bind and activate the Frizzled (Fzd) receptor. It is the binding of Wnt ligands to the Frizzled receptor that is thought to initiate the PCP signalling cascade (Gordon and Nusse, 2006; Komiya and Habas, 2008) (Figure 1.2). Wnt molecules are known to form both homodimers and heterodimers (Cha et al., 2008), but it's unknown whether dimer formation influences Frizzled binding. Wnt ligands have also been proposed to activate an independent cascade of PCP signalling via the Ror2 receptor (Gao et al., 2011) (Figure 1.2), although it is unknown if *frizzled* is also required for this interaction.

There are 19 members of the Wnt family known to date (Rothbacher et al., 2000). Wnt ligands are known to interact with multiple Frizzled receptors (Wu and Nusse, 2002). It has also been shown that some Frizzled receptors can have differential affinities for different Wnt ligands (Kilander et al., 2014). Wnt molecules are generally divided into two groups, those that activate the β-catenin signalling pathway, known as canonical Wnt ligands, and those that activate the PCP signalling pathway, or noncanonical Wnt ligands. The four major Wnts known to be responsible for PCP signalling in zebrafish are Wnt11 (Heisenberg et al., 2000; Ulrich et al., 2003; Witzel et al., 2006), Wnt5b (Kilian et al., 2003; Matsui et al., 2005; Witzel et al., 2006), Wnt4 (Matsui et al., 2005) and Wnt11r (Matsui et al., 2005). These proteins have non redundant roles in PCP signalling, as the loss of both *wnt11* and *wnt5b* results a more severe phenotype than either alone (Kilian et al., 2003). Wnt11 predominantly has an effect on both the anterior and posterior regions of the embryo, whereas Wnt5b affects only the posterior region (Ulrich et al., 2003). Zebrafish embryos mutant for the *wnt* PCP genes such as *pipetail/wnt5b (ppt)* (Kilian et al., 2003), or *silberblick/wnt11 (slb)*(Heisenberg et al., 2000), display defective C&E movements and neural tube morphogenesis, demonstrating a role of the noncanonical *wnt* genes and PCP signalling in the regulation of cell migration. During zebrafish gastrulation, Wnt11 has been shown to regulate cellular coherence by modulating the localisation of E-cadherin in the anterior migrating prechordal plate cells, a group of cells that regulated axis extension during gastrulation (Ulrich et al., 2005).

Although the extracellular Wnt signalling molecules are largely accepted to play an important role in the activation of the PCP pathway, the mechanism that determines the directional polarity cue for PCP signalling is not understood. Wnt5b and Wnt11 do not appear to have any pattern of expression to indicate a gradient or the establishment of a gradient (Heisenberg et al., 2000; Kilian et al., 2003), suggesting that Wnts are not the polarizing agents in PCP signalling. It has been proposed that the presence of the Wnt molecules activate cells to a state in which they can detect other signalling molecules that give the gradient signal to determine long range polarity (Barrow, 2006). To date, these other signals have not been identified.

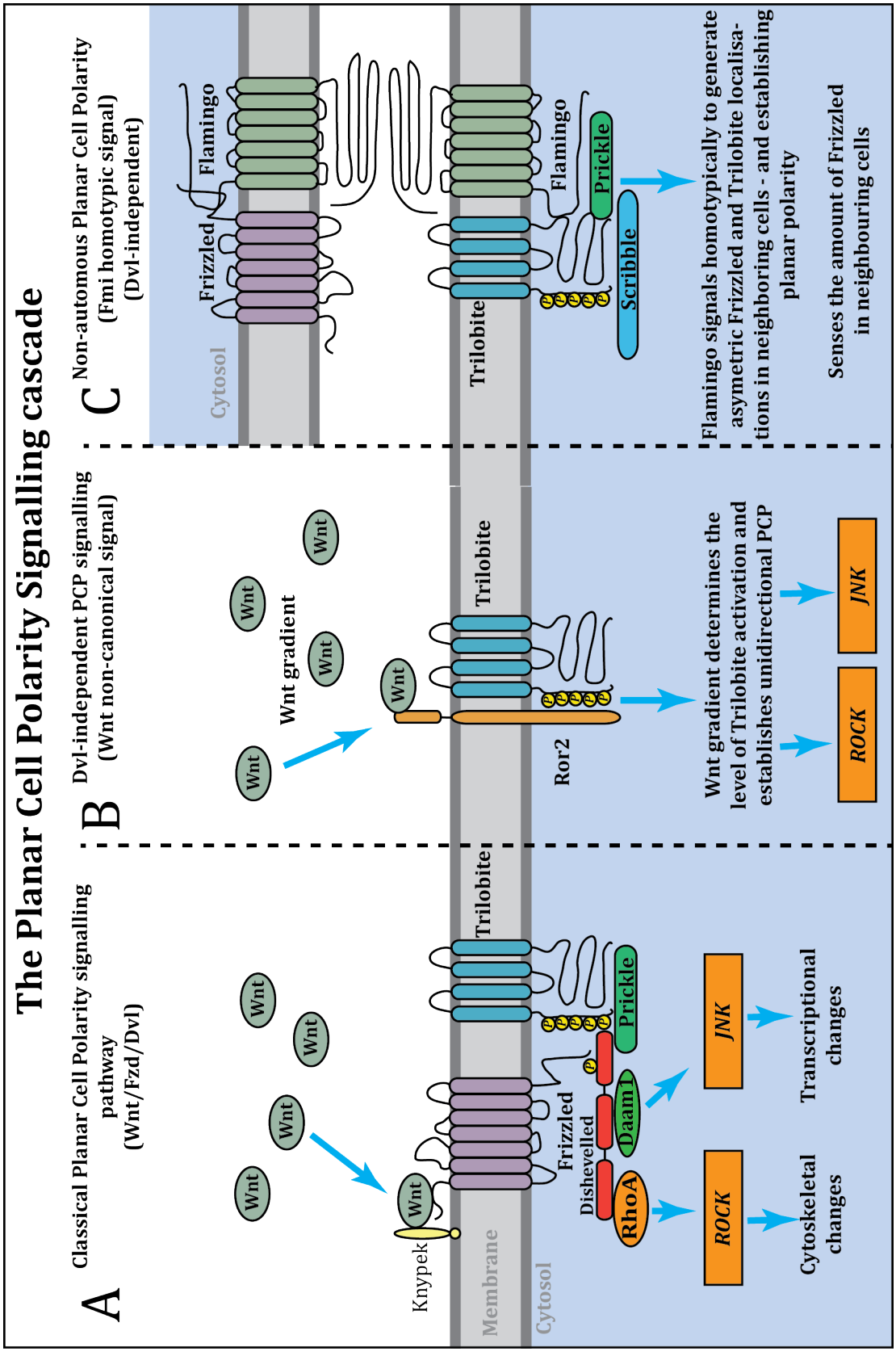
The Planar Cell Polarity Signalling cascade
A
Classical Planar Cell Polarity signalling pathway (Wnt/Fzd/Dvl)
B
Dvl-independent PCP signalling (Wnt non-canonical signal)
C
Non-automous Planar Cell Polarity (Fmi homotypic signal) (Dvl-independent)
Wnt
Wnt gradient
Knypek
Membrane
Cytosol
Trilobite
Frizzled
Dishevelled
Daam1
Prickle
RhoA
ROCK
JNK
Cytoskeletal changes
Transcriptional changes
Ror2
Wnt gradient determines the level of Trilobite activation and establishes unidirectional PCP
Flamingo
Scribble
Flamingo signals homotypically to generate asymetric Frizzled and Trilobite localisations in neighboring cells - and establishing planar polarity
Senses the amount of Frizzled in neighbouring cells

Figure 1.2 The Planar Cell Polarity (PCP) signalling pathway. The PCP signalling pathway currently has three known methods of signal transduction Wnt/Fzd/Dvl, Dvl-independent, and Non-autonomous PCP. **(A)** The classical PCP signalling cascade is generally considered to involve a Wnt/Fzd/Dvl complex. The Wnt ligand is bound by Frizzled with the co-factor Knypek. This in-turn actives and recruits Dishevelled to the plasma membrane to form a complex with Frizzled. The activation and translocation of Dishevelled is dependent on Trilobite. This Fzd-Dvl complex interacts with the small GTPase RhoA and Daam1 to activate the ROCK and JNK pathways respectively. The activation of ROCK and JNK leads to changes in cytoskeletal dynamics and transcriptional changes. **(B)** In Dvl-independent PCP signalling the single pass transmembrane protein Ror2 binds Wnt ligands and forms a complex with Trilobite, inducing the phosphorylation and activation of Trilobite. The activation of Trilobite by Ror2 occurs in a gradient manner, with more Trilobite being activated with more Wnt present. This allows for the establishment of a unidirectional PCP gradient within a cell. **(C)** In Non-autonomous PCP signalling Flamingo forms a complex with Trilobite in one cell, and interacts with a Frizzled-Flamingo complex in a neighbouring cell. This acts a signal between cells, allowing one cell to generate a localisation of Frizzled complexes in the neighbouring cell, as well as sense the level of PCP activation of each cell. (Modified from Gao, 2012).

1.3.2.2. The Frizzled (Fzd) receptor

The Frizzled (Fzd) receptors are responsible for binding extracellular Wnt ligands and transducing this signal to the internal downstream mediators. Frizzled proteins are seven pass transmembrane receptors that are part of the G protein-coupled receptor superfamily (GPCRs) involved in Wnt signalling (Bhanot et al., 1996) (Figure 1.2). The human and mouse genomes each contain 10 *frizzled* genes (KEGG, 2014b; KEGG, 2014d), while the zebrafish genome contains 15 *frizzled* homologs (zfin.org, 2014c).

Traditionally it was thought that PCP signalling and β-catenin signalling used separate Frizzled receptors, but recently Frizzled-4 has been shown to be able to activate either of the two signalling pathways (Robitaille et al., 2002; Ye et al., 2009). Frizzled receptors seem to have the ability to form functional dimers and multimers during Wnt signalling, and it has recently been demonstrated that some individual Frizzled receptors do have preferential selectivity for particular Wnt signalling ligands (Carron et al., 2003; Kaykas et al., 2004; Junge et al., 2009; Kilander et al., 2014). The mechanism of how Frizzled receptor complexes selectively activate either PCP signalling or β-catenin signalling is not fully understood, but Frizzled co-factors that also bind Wnt ligands have been shown to have an influence over this decision.

1.3.2.3. Dishevelled (Dvl)

Dishevelled (Dvl) is the intracellular signalling mediator for both PCP signalling and β-catenin signalling, and is considered to be the central protein in the PCP signalling pathway (Figure 1.2). In vertebrate PCP signal transduction, Frizzled becomes activated upon the reception of Wnt ligands, and this in turn recruits and activates Dishevelled (via phosphorylation) to the plasma membrane (Axelrod et al., 1998; Rothbacher et al., 2000; Habas et al., 2001; Ulrich et al., 2003; Habas and Dawid, 2005). In tissues where PCP signalling is active Dishevelled is localised to the plasma membrane (Axelrod, 2001; Witzel et al., 2006), such as the posterior edge of migrating mesoderm cells (Yin et al., 2008). The activation and membrane recruitment of Dishevelled, meditated by Frizzled,

in the ectoderm and mesoderm in *Xenopus* embryos is dependent on the phosphorylation of the DEP domain (Rothbacher et al., 2000). The membrane recruitment of Dishevelled is also reliant on the transmembrane protein Trilobite (Tri) (Park and Moon, 2002). Once Dishevelled is translocated to the plasma membrane, it causes the endocytosis and internal compartmentalisation of the activated Frizzled receptor within the cell (Yu et al., 2010). The endocytosis of the activated Frizzled receptor is dependent on the Dishevelled DEP domain, and expression of *dishevelled* with either a mutated DEP domain (*Xdd1*) or a deletion of the DEP domain (XDshΔDEP) disrupts this endocytosis in a dominant negative manner and inhibits PCP signalling without affecting β-catenin signalling (Axelrod et al., 1998; Wallingford et al., 2000; Yu et al., 2010). The fact that XDshΔDEP acts a dominant negative is exploited in chapter four to investigate the requirement for PCP signalling at specific time points during endodermal morphogenesis.

Vertebrate Dishevelled uses different conserved domains for β-catenin signalling and PCP signalling (Axelrod, 2001). Dishevelled contains three domains with known function, the DIX domain, which is required for β-catenin signalling (Habas et al., 2001), the PDZ domain, which is required for PCP signalling by binding to Trilobite (Tri/Vangl2) (Park and Moon, 2002), and the DEP domain, which is required specifically for PCP signalling via Prickle (Pk) interaction and endocytosis (Tree et al., 2002; Yu et al., 2010). Dishevelled also has two domains of unknown function, as determined by the Conserved domain database (CDD), the Dishevelled-specific domain and the C-terminal domain (Marchler-Bauer et al., 2013).

dishevelled genes have been identified in all model organisms that have been shown to utilise Wnt signalling, including Hydra*, C. elegans, Xenopus,* zebrafish, mouse, and human (Wharton, 2003). The human and mouse genomes contain three *dvl* genes, (*DVL1*, *DVL2*, and *DVL3*) and (*Dvl1*, *Dvl2*, and *Dvl3*) respectively (KEGG, 2014a; KEGG, 2014c), while zebrafish have five *dvl* family members (*dvl1a*, *dvl1b*, *dvl2*, *dvl3a*, and *dvl3b*)(zfin.org, 2014a). The extra two *dishevelled* genes in zebrafish, compared to mouse and human, are a result of a genome duplication in the teleost lineage (Amores et al., 1998). The role of the

dishevelled gene family in endodermal morphogenesis and the expression patterns of all of the family members is examined in chapter Four.

1.3.2.4. Trilobite (Tri)

There are multiple gene names currently in use for members of this gene family, *trilobite* (*tri*), *van gogh-like-2* (v*angl2*), and *strabismus* (*stbm*). *Van gogh-like-2* (*vangl2*) is the correct nomenclature for vertebrate homologues, and is used in the majority of publications. However, this report refers extensively to the zebrafish *vangl2* mutant *trilobite*, and for simplicity *vangl2* will be referred to as *trilobite* (*tri*) for the remainder of this thesis.

Trilobite (Tri) is a four pass transmembrane tethered protein that is required for PCP signalling in *Drosophila* (Taylor et al., 1998; Wolff and Rubin, 1998), *Xenopus* (Darken et al., 2002; Park and Moon, 2002), mouse (Murdoch et al., 2001), and zebrafish (Jessen et al., 2002) (Figure 1.2). Vertebrate *trilobite* has been shown to be involved in the PCP signalling pathway via epistasis experiments with known PCP mutants (Heisenberg and Nusslein-Volhard, 1997; Marlow et al., 1998). However, overexpression of downstream mediators of PCP, such as XDshΔDEP and Rok2, which are capable of rescuing *wnt11* mutants (Heisenberg et al., 2000; Marlow et al., 2002), are unable to rescue the *trilobite* mutant phenotypes (Jessen et al., 2002). *trilobite* overexpression or knockdown by morpholino antisense oligonucleotide (MO) are unable to rescue the *wnt11* mutant phenotype, but did modify downstream effects of excess Wnt11 (Jessen et al., 2002). Overall these observations indicate that the majority of *tri* function is not in the linear PCP pathway, but rather *tri* acts to modulate PCP signalling.

trilobite is involved in the planar polarisation of primary cilium in mouse and zebrafish (Mahuzier et al., 2012), and is required for correct neural tube closure in mice (Murdoch et al., 2001) and humans (Kibar et al., 2007; Kibar et al., 2010). *tri* mutant zebrafish embryos display a number of distinctive PCP phenotypes, many of which include C&E defects of shortened body axis from a lack of extension, and wider body plans from reduced convergence (Heisenberg et al., 1996; Solnica-Krezel et al., 1996; Jessen et al., 2002). *tri* mutation also disrupts the correct caudal migration of hindbrain motor and facial

branchiomotor neurons (Jessen et al., 2002; Sittaramane et al., 2008). *tri* mRNA is maternally deposited into the zebrafish oocyte, and this mRNA, or deposited protein, contributes to the regulation of C&E movements. Maternal zygotic *tri* (MZ*tri*) mutants, which also lack the maternal component, display a greater reduction in C&E movements than zygotic *tri* mutant embryos (Ciruna et al., 2006).

Although Trilobite is involved in the classical Wnt-Fzd-Dvl PCP signalling cascade, it has also been shown to function in both a *dvl*-independent and a non-autonomous manner to regulate PCP signalling (Seifert and Mlodzik, 2007; Shima et al., 2007; Carreira-Barbosa et al., 2008; Wu and Mlodzik, 2008; Gao et al., 2011) (see Figure 1.2). The *dvl*-independent role of *trilobite* works through an interaction with Ror2, a single-transmembrane protein that is capable of binding the Wnt ligands required for PCP signalling (Hikasa et al., 2002; Oishi et al., 2003). The binding of these Wnt ligands induces the formation of a Ror2-Tri complex, and activation of Trilobite by phosphorylation in a Wnt dose dependent manner, which in turn activates the downstream c-Jun N-terminal kinase (JNK) pathway (Gao et al., 2011) (See Figure 1.2.). Trilobite has been shown to regulate PCP signalling in a non-autonomous manner, by activating Frizzled across the membrane in neighbouring cells, and this interaction is mediated by the PCP protein Flamingo (Gao et al., 2011) (Figure 1.2).

Trilobite contains four transmembrane domains, and a PDZ-domain binding motif (PDZ-DBM) in the C-terminal cytoplasmic region (Jessen et al., 2002). The PDZ-DBM interacts with Dishevelled via its PDZ domain (Park and Moon, 2002), as well as the cytoplasmic PCP protein Prickle (Pk) (Jenny et al., 2003). The interaction between Trilobite and Dishevelled is required for Dishevelled to be translocated to the membrane and interact with Frizzled during PCP signalling (Park and Moon, 2002). Trilobite is capable of forming a homodimer (Belotti et al., 2012), and expression of *trilobite* lacking the PDZ-DBM (*StbmΔPBM*) has been shown to act in a dominant-negative manner (Goto and Keller, 2002). In chapter five I utilise the *StbmΔPBM* dominant negative to generate a transgenic line capable of inducible expression to investigate the *dvl*-independent roles of *tri* during endoderm morphogenesis.

In this research project I utilised the established *tri* mutant to investigate the role of this PCP signalling component and the overall role PCP signalling on endoderm morphogenesis.

1.3.2.5. Knypek (Kny)/ Glypican 4/6

Knypek (kny), also known as glypican 4/6, is an extracellular membrane tethered protein that physically binds noncanonical Wnts, acting as a Frizzled co-factor to promote PCP signalling (Topczewski et al., 2001; Ohkawara et al., 2003; Caneparo et al., 2007; Shao et al., 2009) (Figure 1.2). Kny also binds Dickkopf-1 (Dkk1), a member of the Dickkopf family of secreted proteins that are known to modulate Wnt signals, regulate gastrulation movements, and have inhibitory effects on Frizzled receptors (Caneparo et al., 2007; Cha et al., 2008; Bourhis et al., 2010). The interaction between Kny and Dkk1 acts to promote PCP signalling, while inhibiting β-catenin signalling.

Homozygote mutant *knypek* (*kny*) embryos display a reduction in C&E movements, generating shorter wider embryos at 24 hpf, similar to that observed in *tri, wnt11,* and *wnt5b* mutant embryos (Heisenberg et al., 2000; Topczewski et al., 2001; Jessen et al., 2002; Kilian et al., 2003). In *kny* mutants caudal notochord cells lose the ability to maintain coherence during tail extension and protrusion (Yang and Thorpe, 2011).

In this research project I utilise the *kny* mutant to investigate the role of *kny* and the PCP signalling pathway during endoderm morphogenesis.

1.3.2.6. Flamingo (Fmi)

Flamingo (Fmi), also known as Cadherin EGF LAG seven-pass G-type receptor (Celsr), is a member of the PCP signalling pathway that plays multiple roles in the regulation of PCP signalling (Usui et al., 1999; Gao et al., 2011) (Figure 1.2). Flamingo is a seven-pass transmembrane atypical cadherin that regulates PCP signalling and cell adhesion during epiboly and convergence and extension movements in zebrafish (Carreira-Barbosa et al., 2008). *flamingo* is the only PCP gene shown to play a role during epiboly (Ciruna et al., 2006; Carreira-Barbosa et

al., 2008). *flamingo* can function as an extracellular signalling ligand during non-cell-autonomous PCP signalling, by mediating the interactions between Frizzled and Trilobite (Seifert and Mlodzik, 2007; Shima et al., 2007; Carreira-Barbosa et al., 2008; Chen et al., 2008; Gao et al., 2011) (Figure 1.2).

Flamingo regulates membrane localisation of Prickle, as loss of *flamingo* results in reduced Prickle membrane accumulation (Tree et al., 2002; Ulrich et al., 2003). Flamingo itself localizes at Wnt-induced cell-cell adhesion points in the ectoderm and mesoderm, promoting the accumulation of Frizzled and Dishevelled into distinct puncta on both sides of the contacting plasma membranes (Witzel et al., 2006). The Flamingo localizations are usually the last point of contact between separating cells (Witzel et al., 2006). In *Drosophila,* Flamingo mediates homophilic cell adhesion, which may play a role in cell elongation (Usui et al., 1999). Zebrafish have five *flamingo* genes (*celsr1a, celsr1b, celsr2, celsr2l, celsr3*)(zfin.org, 2014b), whereas there are three genes in the human (*CELSR1, CELSR2,* and *CELSR3*) (NCBI, 2014a) and mouse (*Celsr1, Celsr2,* and *Celsr3*) (NCBI, 2014b) genomes.

1.3.2.7. Prickle (Pk)

Prickle is a cytoplasmic protein that has been show to regulate C&E movements in zebrafish (Carreira-Barbosa et al., 2003) and *Xenopus* (Takeuchi et al., 2003). It is thought to be through physical interactions with Trilobite (Carreira-Barbosa et al., 2003) (Figure 1.2). Epistasis experiments have demonstrated that *prickle* is required for some aspects of Fzd/Dvl-mediated PCP signalling, but is not placed in a linear cascade with *frizzled* and *dishevelled* (Carreira-Barbosa et al., 2003).

Prickle contains four domains that are homologous between *Drosophila,* zebrafish, and *Xenopus* proteins, and can physically bind Trilobite and the DEP/C-terminal domain of Dishevelled (Tree et al., 2002; Carreira-Barbosa et al., 2003; Jenny et al., 2003). In vertebrates Prickle often localises asymmetrically around a cell membrane, often localised with Dishevelled (Veeman et al., 2003). Prickle is recruited to these localized puncta by Trilobite (Jenny et al., 2003; Ciruna et al., 2006). In the neural keel these puncta are asymmetrically localized to the anterior edge of the cell (Ciruna et al., 2006). Contrastingly, in these cells

Dishevelled localises to the opposite side of the cell (Ciruna et al., 2006). Evidence from *Drosophila* suggests that Prickle can destabilise Fzd/Dvl localisations, which acts as a feedback loop to enhance the asymmetric distribution of Fzd/Dvl in a cell, and generate asymmetric polarity of cells (Tree et al., 2002), although this has not been demonstrated in vertebrates.

1.3.2.8. Dishevelled-associated activator of morphogenesis (Daam1)

Dishevelled-associated activator of morphogenesis (Daam1) is required for PCP signalling during *Xenopus* gastrulation, where it functions by binding Dishevelled to mediate the formation of a complex with Dishevelled and the small GTPase RhoA (Habas et al., 2001) (Figure 1.2). The formation of this complex is dependent on the interaction of Frizzled and the noncanonical Wnts. RhoA activation promotes polarised cytoskeleton remodelling via the ROCK kinase pathway (Winter et al., 2001). Daam1 is thought to function in PCP signalling by mediating cytoskeletal dynamics the modulations in cytoskeletal dynamics that are required during gastrulation and C&E (Wharton, 2003).

1.3.2.9. Scribble (Scrib)

scribble (*scrib*) is required for PCP signalling during gastrulation movements in zebrafish. *scribble* maternal-zygotic (MZ*scribble*) mutant embryos display defects in C&E, and morphological defects within the posterior hindbrain/anterior spinal cord region (Wada et al., 2005; Zigman et al., 2011). Scribble physically interacts with Trilobite to regulate PCP signalling and the formation of adherens junctions (Wada et al., 2005; Courbard et al., 2009; Lindqvist et al., 2010) (Figure 1.2). Scribble is also required during neural keel cell division for both the initial spindle positioning, and the rotation into the final correct apicobasal orientation (Zigman et al., 2011).

1.3.2.10. Dickkopf 1 (Dkk1)

Dickkopf 1 (Dkk1) is a member of the Dickkopf family of secreted proteins. The Dickkopf family modulate Wnt signals, gastrulation movements, and have inhibitory effects on Frizzled receptors. Dkk1 binds directly to Knypek to regulate PCP signalling (Caneparo et al., 2007). Dkk1 is first expressed in the zebrafish mesendoderm where it represses β-catenin signalling while increasing PCP signalling (Caneparo et al., 2007). This is achieved by directly binding to LRP5/6, a Frizzled co-factor required for β-catenin signalling, and promoting its endocytosis and subsequent deactivation, while promoting the extracellular localization of Knypek (Caneparo et al., 2007; Bourhis et al., 2010). *dkk1* expression is regulated by β-catenin signalling, where it acts in a negative feedback loop to inhibit β-catenin signalling (Caneparo et al., 2007).

1.4. The aims of this project

Much research has been conducted on early endoderm in regards to specification and migration during gastrulation stages (Alexander and Stainier, 1999; Warga and Nusslein-Volhard, 1999; Dickmeis et al., 2001; Kikuchi et al., 2001; Ober et al., 2004; Mizoguchi et al., 2006; Mizoguchi et al., 2008; Nair and Schilling, 2008; Pezeron et al., 2008). The process of endoderm organogenesis at later stages of development has also received significant attention (Field et al., 2003a; Ober et al., 2003; Jin et al., 2005; Ng et al., 2005; Ober et al., 2006). However, the process of endoderm morphogenesis between these two time points during somitogenesis stages and formation of the primitive endodermal rod (midline aggregation) was unknown at the beginning of this project.

In this project I determined the processes of endoderm morphogenesis at these intervening stages of endoderm development, during somitogenesis stages and during the formation of the primitive endodermal rod. To understand endodermal morphogenesis during these stages I quantified changes in cell behaviour, shape, and polarisation of the endoderm.

The Planar Cell Polarity (PCP) signalling pathway is known to regulate mesodermal convergence and extension (C&E) movements. *tri* and *kny* mutants

have a reduction in the convergence of mesodermal tissues (Topczewski et al., 2001; Jessen et al., 2002). It has also been proposed that the mesoderm has a role in the regulation of endodermal migration (Mizoguchi et al., 2008; Nair and Schilling, 2008). Taken together it was reasoned that the endoderm might also be affected in *tri* and *kny* mutants. If the endoderm is affected in these mutants it raises two possible explanations: one, is that PCP signalling is specifically required in the endoderm; or two, that PCP signalling is required in the mesoderm and that the endoderm require the mesoderm for correct morphogenesis. Therefore in Chapter three I investigate the role of PCP signalling in the regulation of endoderm morphogenesis and midline aggregation. To determine this I characterised endoderm morphogenesis in *tri* and *kny* mutants, and identified a defect in endodermal morphogenesis. In Chapter four I investigate the time specific roles of PCP signalling during midline aggregation. To do this I generated a transgenic line capable of inducing a time specific disruption of PCP signalling, and investigate the role of PCP signalling during brain morphogenesis. In Chapter five I investigate the state of endodermal and mesodermal cell polarisation during endoderm morphogenesis, and identify a difference between the polarisation states of these to cell types during somitogenesis stages. Chapter five also attempts to distinguish between the two possible requirements for PCP signalling in endoderm morphogenesis. To do this I generated multiple tissues specific conditional transgenic lines to disrupt PCP signalling.

Chapter 2. Methods and materials

2.1. List of suppliers and services

Ambion Austin, TX, USA

Applied Biosystems Foster City, CA, USA

Bioline Pty Ltd., Alexandria, NSW, Aust

Bio-Rad Hercules, CA, USA

Crown Scientific Pty Ltd Moorebank, NSW, Aust

Eppendorf Hamburg, Germany

Integrated DNA Technologies, Inc, Aust

Invitrogen Australia Pty Ltd Mt. Waverley, Vic, Aust

Leica Microsystems Gladesville, NSW, Aust

Narishige Scientific Instruments Setagaya-ku, Tokyo, Japan

Nikon Corporation Setagaya-ku, Tokyo, Japan

New England Biolabs Beverly, MA, USA

Olympus Optical Co Ltd Shinjuku-ku, Tokyo, Japan

Promega Madison, WI, USA

Roche Molecular Biochemicals Indianapolis, IN, USA

Scientifix Pty. Ltd., VIC, Aust

Sigma-Aldrich, Castle Hill, NSW, Aust

Sutter Instruments Navato, CA, USA

Thermoline Scientific Smithfield, NSW, Aust

Thermo Fisher Scientific Inc. Waltham, MA, USA

2.2. Standard molecular biology techniques

2.2.1. Preparation of chemically competent cells

A single *E.coli* bacterial colony DH5α strain (Invitrogen) was used to inoculate a 100 ml + Tetracycline culture in Luria broth (LB) medium and grown ON at 37 °C with shaking at 200 rpm. 2 ml of this culture was then inoculated into 100 ml of LB and incubated at 37 °C, with shaking at 200 rpm until an absorbance reading at 590 nm of 0.375 was reached, determined in a DU-65 spectrophotometer (Beckman). 50 ml of this culture was inoculated into each of two 500 ml LB and incubated at 37 °C, with shaking at 200 rpm until an absorbance reading at 590 nm of 0.375 was reached. The cultures were transferred to pre-cooled 250 ml, sterile centrifuge tubes and centrifuged for 10 min (3,000 rpm) at 6 °C in a Sorvall RC6+ centrifuge (Thermo Scientific Inc.). The supernatant was removed and the pellet gently resuspended in 300 ml of ice-cold competence solution (33 % 100 mM $CaCl_2$, 33 % 70 mM $MnCl_2$, 33 % 40 mM sodium acetate (NaAc). This was transferred to 6 x 50 ml flacon tubes and incubated on ice in a 4 °C cold room for 30 min. The falcon tubes were then centrifuged at 3,000 rpm for 10 min in a refrigerated centrifuge. The supernatant was removed and the cells resuspended in 50 ml ice-cold competence solution plus glycerol (42.5 ml competence solution, 7.5 ml glycerol). 100 µl aliquots were dispensed into 1.5 ml eppendorfs on ice and the cells snap frozen in liquid nitrogen. The competent cells were stored at -70 °C.

2.2.2. Transformation of chemically competent cells using heat shock

Competent cells (100 µl) were removed from -70 °C and thawed on ice. ~50 ng plasmid DNA added to the competent cells and incubated on ice for 10 min. The tubes were then placed in a heat block set to 42 °C for 45 sec. The cells were then recovered on ice for 2 min before adding 1 ml sterile LB media and incubating at 37 °C for 1 hour. 100 µl of the culture was then spread on LB plates containing

the appropriate antibiotic (either ampicillin 100 µg/ml, kanamycin 50 µg/ml, or chloramphenicol (30 µg/ml) and grown overnight at 37 °C.

2.2.3. Optimised transformation of Electrocompetent E.coli

Heat inactivation of T4 DNA ligase was performed to improve transformation as per Ymer (1991). To achieve high transformation results the following protocol was modified from Zoller (1992). 1 µl of the heat-inactivated ligation reaction was added to 39 µl sterile H_20 in a PCR tube and placed on ice. 10 µl Electrocompetent cells was added, and the mixture transferred to an ice-cold 2 mm transformation curvette. Transformation was achieved using a BioRad Gene Pulser™ (Cat#165-2078) with settings 2.45 Kv, 200, 25 uF, and pulse time of 4.6 msec. 1 ml LB (+20 uM Glucose) was added to the curvette after transformation and the mixture was transferred to a 1.5 ml microfuge tube and placed in a 37 °C water bath for 1 hour to recover. 150 µl was removed spread on an LB agar plate containing the appropriate antibiotic. The rest of the transformation mixture was centrifuged in a bench top centrifuge at 1000x g for 5 mins. The supernatant was tipped off, leaving ~100 µl. The pellet was re-dissolved, and spread on an LB agar plate containing the appropriate antibiotic and incubated at 37 °C overnight.

2.2.4. Plasmid preparation

Miniprep cultures were prepared by inoculating 15 ml LB (containing the antibiotic selective agent) with a single bacterial colony obtained from the transformation process followed by incubation ON at 37 °C, with shaking (200 rpm). Plasmid DNA was then isolated according to manufacturer's instructions for Wizrad® SV Miniprep kit (Promega). Samples were eluted from columns with 30 µl of H2O.

2.2.5. Glycerol stocks

Glycerol stocks were created by adding 850 µl culture (from miniprep culture) to 150 µl glycerol. The mix was then vortexed and snap frozen in liquid nitrogen. Glycerol stocks were stored at -70 °C.

2.2.6. Restriction digests

Plasmid DNA and PCR products were digested using Promega or Fermentas buffers and enzymes. Promega reactions were generally 0.2-5 µg of DNA, 1 X Reaction Buffer (New England Biolabs) and 1 U/µl restriction enzyme (or a total of 1 U/µl combined for double digests). The reaction mix was incubated for 2 h at 37 °C. Digestes using Fermentas FastDigest® enzymes were generally 0.2-5 µg of DNA, 1x reaction buffer and 1 U/µl. The reaction mix was incubated for 10 min at 37 °C. Digested fragments or plasmids were purified for cloning using Wizard® SV Gel & PCR Clean-up System (Promega) following the manufacturer's instructions, or by ethanol precipitation (see section 2.2.11) in the case of plasmid DNA used for generation of capped mRNAs.

2.2.7. Alkaline phosphatase treatment of digests

To prevent re-ligation of plasmid vectors digested with a single restriction enzyme the purified digested plasmid DNA (see section 2.2.4) was subjected to alkaline phosphatase prior to ligation. Reactions were generally 0.2-1 µg DNA, 1x Shrimp alkaline phosphatase Buffer. The reaction was incubated at 37 °C for 20 min, then the enzyme was inactivate at 65 °C for 10 min. This can now be used straight for ligations.

2.2.8. Ligation of DNA fragments

Ligation of plasmid DNA and PCR products was performed using Promega reagents, using a molar ratio of 1:3 for Vector DNA: Insert DNA, 1 X DNA Ligase buffer, 0.5 U/µl DNA ligase. Reactions were performed either for 1 h at 25 °C or ON at 4 °C.

2.2.9. Cloning techniques

2.2.9.1. Standard cloning

To create the *sox17-EGFP-T2A-KalTA4GI* construct the EGFP-T2A-KalTA4GI fragment was removed from the Kaloop (Distel et al., 2009) vector using SalI and inserted into a SalI opened *sox17-KalTA4GI-IRES-EGFP-pA*. *4xnrUAS:XDshΔDEP-mCherry/cmlc2:EGFP* and *4xnrUAS:StbmΔPBM-mCherry/cmlc2:mCherry* were generated by PCR amplifying SpeI site-*XDshΔDEP-mCherry/cmlc2:EGFP*-SpeI site from the *10xUAS:XDshΔDEP-mCherry/cmlc2:EGFP* vector and SpeI site-*StbmΔPBM-mCherry/cmlc2:mCherry*-SpeI site from the *10xUAS:StbmΔPBM-mCherry/cmlc2:mCherry* respectively. These DNA fragment was then digested with SpeI and inserted into 4xnrUAS:EGFP that had the EGFP fragment removed using SpeI. To create the *4xUAS:EGFP-T2A-KalTA4GI/4xnrUAS:XDshΔDEP-mCherry/cmlc2:EGFP* vector the *4xUAS:EGFP-T2A-KalTA4GI* fragment was removed from the Kaloop vector(Distel et al., 2009) using SacII, and inserted into SacII opened *4xnrUAS:XDshΔDEP-mCherry/cmlc2:EGFP.* To create the *4xUAS:EGFP-T2A-KalTA4GI/4xnrUAS:StbmΔPBM-mCherry/cmlc2:mCherry* vector the *4xUAS:EGFP-T2A-KalTA4GI* fragment was removed from the Kaloop vector(Distel et al., 2009) using SacII, and inserted into SacII opened *4xnrUAS:StbmΔPBM-mCherry/cmlc2:mCherry.* To create the *hsp70i:LoxP-STOP-LoxP-XDshΔDEP-mCherry-pA* vector the STOP cassette was removed from the pBigT-STOP-SLIM vector (see section 2.2.6.3) using SalI and inserted into SalI opened *hsp70i:SalI-XDshΔDEP-mCherry-pA* (see section 2.2.6.3). To create the *hsp70i:LoxP-STOP-LoxP-StbmΔPBM-mCherry/cmlc2:mCherry* vector the STOP cassette was removed from the pBigT-STOP-SLIM vector (see section 2.2.6.3) using KpnI and inserted into KpnI opened *hsp70i:StbmΔPBM-mCherry/cmlc2:mCherry*. pDestTol2CmCherry was generated by inserting cmlc2:mCherry (see section 2.2.6.2) digested with BglII, into the unique BglII site in pDestTol2A and selecting for correct orientation.

2.2.9.2. Fusion PCR cloning

Fusion PCR was used to fuse the mCherry fluorophore to the open reading frame of *XDshΔDEP* to create the transgene *XDshΔDEP-mCherry* and the open reading frame of *StbmΔPBM* to create *StbmΔPBM-mCherry.* mCherry was fused in front of the heart specific promoter cmlc2 (from pDestTol2pAto create cmlc2:mCherry. Fusion PCR relies on overlapping homology of the fragments to be fused. To achieve this the reverse (R) primer of the 5' fragment and the forward (F) primer of the 3' fragment share 50 bp homology – 25 bp of each fragment. The two outermost primers used to amplify the fragments contained attb sites for BP gateway recombination. The two DNA fragments to be fused were first amplified in separate PCR reactions. The 3' fragment was amplified using a F primer that contained homology specific to the start of desired sequence and an upstream attB gateway site for recombination into a plasmid vector. The 3' Reverse primer contained reverse homology to the end of the desired sequence and 25 bp homology to the start of the 5' DNA fragment. The 5' fragment was amplified using a forward primer that contained homology to the start of the desired sequence and homology to the end of the 3' DNA fragment. The 5' Reverse primer contained reverse homology to the end of the desired sequence and a downstream attb gateway site. This results in a 50 bp sequence overlap of the two fragments to be fused. The PCR products of the reactions were purified (see section 2.2.12) and both added to a PCR reaction mix that contained only the F primer of the 5' fragment and the R primer of the 3' fragment. This PCR reaction was run on the following program: 95 °C 10 min, three cycles of 95 °C for 1 min, 62 °C 3 min, 72 °C 2 min, then 30 cycles 95 °C 1 min, 62 °C 1 min, 72 °C 2 min. The resulting product was separated on an agarose gel and the correct size fused fragment was purified (see section 2.2.12) and used in a BP reaction (see section 2.2.6.1). Refer to Appendix 2 for a table of the primers used in this study.

2.2.9.3. Recombination mediated subcloning - Gateway

BP and LR recombination reactions were carried out according to manufacturers' instructions (Gateway® Cloning, Invitrogen). Gateway

recombination was used to clone the complete open reading frame of *XDshΔDEP-mCherry* (from a Fusion PCR reaction; see section 2.2.6.2) and Loxp-*XDshΔDEP-mCherry*-LoxP into the pDONR221 vector (BP recombination reaction, Invitrogen) to create the pME-*XDshΔDEP-mCherry* and pME-LoxP-*XDshΔDEP-mCherry*-LoxP middle entry vectors. *XDshΔDEP-mCherry* and LoxP-*XDshΔDEP-mCherry*-LoxP was then excised and recombined into the pDESTtol2A vector, with p5E-*hsp70l* promoter and p3E-PolyA using the LR recombination reaction, creating the hsp70i:*XDshΔDEP-mCherry*-pA and hsp70i:LoxP-*XDshΔDEP-mCherry*-LoxP-pA plasmids respectively. p5E-*sox17* promoter (created by Xenia Kostoulias in the Verkade lab), pME-*mCherryCAAX*, p3E-polyA, and pDESTtol2A were recombined in an LR reaction to create *sox17:mCherry-pA.* pME-*iCre* recombinase (from Tom Hall, Currie Lab, ARMI, Monash Uni) was recombined in an LR reaction with p5E-*sox17* promoter, p3E-polyA, and pDestTol2CG2 [*cmlc2:EGFP* (cardiac myosin light chain 2 promoter driving EGFP)] to create *sox17:iCre/cmlc2:EGFP.* pME-*KalTA4GI* was recombined in an LR reaction with p5E-*sox17* promoter, p3E-IRES-EGFP-polyA, and pDESTtol2A to create *sox17-KalTA4GI-IRES-EGFP-pA.*

2.2.9.4. In-Fusion Cloning

The In-Fusion® Advantage PCR Cloning System (Clonetec) kit was used according to manufacturer's instructions. The final transgenesis vector used for In-fusion cloning was either the pDestTol2CG2(Kwan et al., 2007) or pDestTol2CmCherry transgenesis vector digested with KpnI and SalI to remove the negative selection cassette. All inserts PCR amplified to be used in In-Fusion cloning contained the required 15 bp homologous overlap at each end of the DNA fragment as specified by the manufacturer. *10xUAS:XDshΔDEP-mCherry/cmlc2:EGFP* was created from p5E-10xUAS and pME-*XDshΔDEP-mCherry. 10xUAS:StbmΔPBM-T2A-EBFP2/cmlc2:mCherry* was created from p5E-10xUAS and pCS2+*StbmΔPBM-T2A-EBFP2* and the final vector pDestTol2CmCherry*. hsp70i:StbmΔPBM-T2A-EBFP2/cmlc2:mCherry* was created from *p5E-hsp70i* promoter, pCS2+StbmΔPBM-T2A-EBFP2 and pDestTol2CmCherry. *hsp70i:LoxP-StbmΔPBM-T2A-EBFP2-LoxP/cmlc2:mCherry*

was created from *p5E-hsp70i* promoter, pCS2+StbmΔPBM-T2A-EBFP2 and pDestTol2CmCherry, with the LoxP sites added in the primer sequence. Refer to Appendix 2 for a table of the primers used in this study.

2.2.9.5. SLIM (Site-directed, Ligase-independent mutatgenesis)

Site-directed, ligase-independent mutagenesis was used as per the published protocol (Chiu et al., 2004) to add restriction sites to the following plasmids: SpeI was added to 4xnrUAS:EGFP to create 4xnrUAS:EGFP-SLIMSpeI, a KpnI site was added to *hsp70i:XDshΔDEP-mCherry*-pA to create *hsp70i-SalI-XDshΔDEP-mCherry*-pA. A KpnI and SalI site was added to pBigT-STOP to create pBigT-STOP-SLIM. Refer to Appendix 2 for a table of the primers used in this study.

2.2.10. Oligonucleotide primer design

Oligonucleotide primers were synthesised by Invitrogen (Invitrogen Australia Pty Ltd Mt. Waverley, Vic, Aust) or IDT (Integrated DNA Technologies, Inc, Aust). The annealing length of the primers were designed to between 18-25 bp with a GC content ranging between 40-60 %, and specific only for the sequence in question. Sequence similarity was determined using a Basic Local Alignment Search Tool (BLAST) search or ApE (A plasmid Editor). Refer to Appendix 2 for a table of the primers used in this study.

2.2.11. Polymerase chain reaction

PCR reactions were performed in either a Bio-Rad S1000TM thermal cycler or a Bio-Rad DNAEngineTM Petlite thermal cycler. The DNA polymerase used was either the Monash *Taq* polymerase (for genotyping) or KOD Hot Start DNA Polymerase (for cloning)(Novagen). Each 20 µl PCR reaction using the Monash *Taq* polymerase contained 0.1-100 ng template DNA, 1x Buffer with $MgSO_4$ (Monash University), 0.2 mM dNTPs, 1 µM F primer, 1 µM R primer, and 1 µl Monash *Taq* polymerase. Reactions were performed with an initial denaturing step of 95 °C for 10 min, followed by 40 cycles of denaturing at 95 °C 20 s;

annealing 20 s (primer specific temperatures); and amplification at 72 °C 1 min/kb depending on desired product size. A final 5 min cycle at 72 °C was performed to allow the complete extension phase to occur. Each 50 µl PCR reaction using the KOD polymerase contained ~10 ng template DNA, 1x KOD buffer, 1.5 mM $MgSO_4$, 0.2 mM dNTPs, 0.3 µM F primer, 0.3 µM R primer, and 0.02 U/µl KOD Hot Start DNA Polymerase. Reactions were performed with an initial denaturing step of 95 °C for 2 min, followed by 20-35 cycles of denaturing at 95 °C 20 s; annealing 10 s (primer specific temperatures); and amplification at 72 °C 10-25 s/kb depending on desired product size. PCR products were separated and visualised on agarose gels and purified for cloning or sequencing or using the Wizard® SV Gel & PCR Clean-up System (Promega). Refer to Appendix 2 for a table of the primers used in this study.

2.2.12. Colony PCR protocol

Overnight Colonies were picked, and mixed with 20 µl Colony PCR master mix in a PCR tube. Master Mix contained the following: 1 µl *Taq* DNA polymerase, 1 µl 10 mM Forward primer, 1 µl 10 mM reverse primer, 2 µl PCR buffer (with $MgCl_2$), 0.6 µl 10 mM dNTPs, and 14.4 Sterile distilled H_20. Colony PCR conditions were as follows: 5 mins at 95 °C, 39 cycles (1 min at 95 °C, 30 sec primer Tm °C, 1 min/kb at 72 °C), 5mins at 72 °C.

2.2.13. Agarose Gel Electrophoresis of DNA fragments

Electrophoresis of DNA was performed as described (Strutt and Strutt, 2009). DNA samples were separated on 0.8-3 % (w/v) multi-purpose agarose (Bioline) prepared in 1 X TBE buffer with the addition of 0.05 µg/ml of ethidium bromide (Promega). The gel loading buffer with dye was added in appropriate volume to the DNA samples and electrophoresis was carried out at 70-120 V. DNA bands were visualised via UV transillumination (λ: 302 nm) and photographed using the GelDoc-ItTM Imaging system (UVP).

2.2.14. DNA purification from agarose gels

DNA fragments were visualised via UV transillumination and the band of interest was quickly excised using a clean scalpel. DNA was purified using Wizard® SV Gel & PCR Clean-up System (Promega) following the manufacturer's instructions. Samples were eluted from columns with 15-30 µl of H2O.

2.2.15. DNA sequencing

300 ng of plasmid DNA were added to a reaction mix containing PRISM Big Dye Terminator® v3.1 Cycle Sequencing Reaction Kit (Applied Biosystems, Foster City, California, USA) as per manufactures' instructions. The reaction was run in a PCR machine on the following settings. Initial denaturing step of 95 °C for 1 min, followed by 30 cycles of denaturing at 96 °C for 10 s; annealing 50 °C for 5 s; and amplification at 60 °C for 4 min. The sample was then held at 5 °C until the clean-up (see section 2.2.14). Sequencing was performed on a 3730 Capillary sequencer (Applied Biosystems) at the Micromon Sequencing facilities.

2.2.16. Clean up of DNA sequencing

The 20 µl DNA sequencing reaction was added to an eppendorf tube containing 3 µl NaAc, 62.5 µl ethanol (96 % technical grade), and 14.5 RO water. This mix was vortexed and incubated at room temperature for 15 min before centrifuging at 1,300 RPM for 20 min in a bench centrifuge. The supernatant was removed and the pellet washed with 200 µl 70 % ethanol. The sample was vortexed before centrifuging 1,300 RPM for 5 min in a bench centrifuge. The supernatant was removed and the pellet dried in a 90 °C heat block for 1 min. After cooling the sample was given to Micromon Sequencing facility at Monash University.

2.2.17. Ethanol precipitation of DNA

Linearised plasmid was precipitated for generation of capped mRNA transcripts for microinjection. DNA was precipitated by adding 1/10 volume 3 M sodium acetate (pH 5.2) and 2.5 volumes absolute ethanol and incubated for 15 min at

room temperature. This mix was then centrifuged at top speed in a bench Centrifuge for 30 min at 4 °C. The supernatant was removed and the pellet washed with 500 µl 70 % ethanol by inverting several times. This was then centrifuged at top speed for 5 min at 4 °C. The supernatant was removed and all residual fluid with a pipette tip. The pellet was air dried (5-10 min) before resuspending in TE or NF-water (generally 20 µl).

2.2.18. In vitro transcription of capped mRNA for microinjection

5 µg of pCS2+(cloned gene) DNA template was digested with *NotI* in a 100 µl reaction and the linearised product purified using ethanol precipitation (see section 2.2.11) . *In vitro* transcription was conducted using a Sp6 mMessage mMachine Kit (Ambion) according to manufacturer's instructions. mRNA was purified using the ProbeQuant G-50 columns (GE) according to manufacturer's instructions. 1 µl of purified mRNA was then subjected to spectrophotometry using the Nanodrop^{1000} to confirm transcription and quality. mRNA was stored at -70 °C.

2.2.19. DNA extraction

2.2.19.1. DNA extraction from an embryo or fin clip

Embryos or fin clips collected for genotyping were either stored in 100 % methanol at -20 °C until DNA extraction or taken directly through the extraction process. For DNA extraction, embryos were placed in 96 well plates, the methanol was removed by pipetting and the embryos dried at 37 °C for 5-10 min on ice until no methanol was present. 50 µl of embryo lysis buffer was added and heated to 98 °C for 10 min. Plates were cooled on ice and then 10 µl of 10 mg/ml Proteinase K (Roche) was added to each well and the plate incubated at 55 °C for 16 h. Proteinase K was inactivated by heating (10 min at 98 °C), the plates cooled on ice. An aliquot of the supernatant was transferred into a new 96 well plates and diluted 1:6 in MilliQ water. 5 µl of this solution was used for PCR genotyping or stored at -20 °C until needed.

2.2.20. Generation of the TA-cloning linker

I aimed to generate multiple vectors to reduce laboratory cloning costs associated with the generation of the vectors needed to analyse endodermal cells in zebrafish. For this, I used a *XcmI* based TA-cloning approach in which two *XcmI* restriction sites are used to generate T-overhangs after digestion. (Schutte et al., 1997; Arashi-Heese et al., 1999; Zhou and Gomez-Sanchez, 2000; Chen et al., 2009; Hong et al., 2009) I generated a *XcmI-EGFP-XcmI* linker containing an EGFP open reading frame flanked by *XcmI* sites (Fig. 1A, B). This linker was then inserted into multiple vectors that are commonly used in zebrafish molecular genetics to enable them to be used in TA-cloning. The *EGFP* gene was included between the *XcmI* sites to serve two functions. Firstly, the size of the *XcmI* digested EGFP fragment is large enough to facilitate easy separation of digested vector, un-digested vector, and EGFP fragment by gel electrophoresis; thus reducing the potential for contamination by un-digested vector or linker in subsequent cloning reactions (a potential problem with small *XcmI* linkers) (Hong et al., 2009). Secondly, in the case of pME-TA, the unmodified vector can be used to generate reporter lines (see pME-TA is a multifunctional vector). An inherent feature of TA-cloning is the lack of defined insert orientation into the T-vector however this can be overcome by performing colony PCR with a vector specific and an insert specific primer, to rapidly identify colonies containing the vectors insert in the correct orientation

2.3. Zebrafish techniques

2.3.1. Animal Husbandry and zebrafish strains

Zebrafish strains used in this study were housed it the lab research aquarium of Dr. Heather Verkade at Monash University using standard husbandry practices. Upon collection, embryos were placed at 28.5 °C in a temperature control incubator (Thermoline Scientific). All experiments were approved by the Monash University Animal Ethics Committee. To raise embryos to adulthood for the next

generation, embryos were first maintained in egg water in a Petri dish in an incubator, at 28.5 °C, with regular cleaning to prevent fungal growth and mould formation. From 5 dpf onwards, larvae were transferred to plastic vessels in the aquarium and fed live paramecium cultures twice daily. From approximately 14 dpf onwards, fry were fed live brine shrimp twice daily, and between 21 dpf to 28 dpf, fry were moved to tanks in the main Aquarium where they were given a combination of live brine shrimp and a pellet feeding regime until they reach sexual maturity between 3-4 months of age, then propagated by pellet food.

2.3.2. Chemical dechorionation

Embryos were chemically dechorionated in 0.2 mg/ml pronase [protease] (Sigma) in egg water for 5 min, then washed three times in egg water.

2.3.3. Needle Preparation protocol

Microinjection needles were created from TW100F-4 borosilicate filamented capillaries (World Precision instruments) using a P-97 Flaming/Brown Micropipette Puller (Sutter Instruments). The machine settings for needle pulling were: Pressure, 300; Heat, 240; Pull, 100; Velocity, 80; Time, 200.

2.3.4. Microinjection of embryos

Embryos were collected from paired matings in breeder boxes approximately 20 min after the dividers were removed and placed in egg water preheated to 28.5 °C. Embryos were placed in grooves on a specialized 4 % agarose block designed to immobilise the embryos via water tension, eliminating the traditional need for a holding pipette during injection. Full specifications of the standard injection mould can be found in The Zebrafish Book (http://zfin.org/zf_info/zfbook/chapt5/5.1.html). Embryos were injected using injection needles (see section 2.3.2), a Femtojet microinjection system (Eppendorf), and a M-152 micromanipulator (Narishige). Injections were performed under the Leica M80 dissecting microscope or Motic SMZ-140

dissecting microscope. Fertilised 1-2 cell embryos were microinjected with ~2 nL of injection mix (see sections 2.3.2.1 and 2.3.2.2). The volume of the injected bolus, assuming that the bolus was a sphere, was calculated using the equation for the volume of a sphere [volume = $1/6\pi d^3$ (d = bolus diameter)]. Hence, 1 nl would approximately be delivered with a bolus diameter of 124 µm. The bolus size was calibrated by injecting into an oil filled (with consistency of the zebrafish yolk) chamber that contained a micrometer.

2.3.4.1. Microinjection of mRNA

Fertilised 1-2 cell embryos were microinjected with ~2 nl of synthetic mRNA traced where appropriate by mixing with 50 mg/ml of rhodamine-dextran (in 0.2M KCl). The injection of mRNA was localized to the embryonic streaming in the yolk.

2.3.4.2. Microinjection of DNA and mRNA for transgenesis

Fertilised 1 cell stage embryos were microinjected with ~2 nl of an injection mix containing synthetic mRNA encoding optimized transposase (50 ng/µl), plasmid DNA of the desired construct (50 ng/µl), Phenol-red (0.05 % w/v) tracer dye, and 0.1M KCl. Injection of DNA was localized directly to the cell body of the embryo.

2.3.5. Fixation of embryos

Embryos were fixed either ON in 4 % PFA (in PBS) at 4 °C, room temperature for 4 hours, or ON in 2 % PFA (in PBS). After fixation the embryos were washed several times in PBT (PBS with 0.01 % Tween) to remove residual PFA. Fixed embryos were either stored at 4 °C for immediate use or dehydrated in a methanol series and stored at -20 °C for longer term storage.

2.3.6. Flat-mounting of zebrafish embryos

Fixed embryos were dechorionated and placed in a Petri dish half filled with solidified 4 % agarose in PBS. For embryos older than 18 somites the tip of the tail was removed using an insect pin and forceps. The PBS was removed, leaving the embryo pinned between the meniscus and the agarose. The embryos were orientated with the yolk against the agarose. Using the insect pin the yolk sac was popped on each side of the embryo and with gentle movements the embryo was pulled flat against the agarose block. All remaining PBS was removed. A drop of liquid 4 % agarose in PBS was applied to a 25 mm circular coverslip (Menzel-Glaser) and this was quickly applied over the flat-mounted embryo. The coverslip was pulled from the agarose block with the embryo attached to the drop of agarose applied. The flat-mounted embryos were placed in PBS and either imaged on the confocal microscope or used for imuno-histochemistry prior to imaging.

2.3.7. Vibratome sectioning of zebrafish embryos

Fixed embryos (as described in section 2.3.3) were embedded in the required orientation in 4 % low melting point agarose. The agarose block containing the embedded embryos was glued to the sectioning platform of the vibratome (Leica VT1200S) with a drop of superglue. The Vibratome was used as per the manufactures' instructions to section the embryos at 200 μM intervals. The sections were placed in PBS on a microscope slide with the sample being encircled with the super pap pen (Invitrogen) to keep the liquid on the slide. Sections were either directly imaged on a confocal microscope or stained before imaging (see section 2.2.22 and 2.2.23).

2.3.8. Rhodamine-Phalloidin (F-actin) Staining

5 μl Rhodamine-Phalloidin was removed from the freezer and placed in an eppendorf tube to allow the methanol to evaporate. This was then resuspended in 200 μl PBS. Vibratome sections to be stained were washed three times with

ice-cold PBS. The sections were then permeabilised with 0.5 % Triton-X 100/PBS at room temperature for 10 min. The sections were then washed three times with ice-cold PBS, before incubating in 2 % Roche blocking reagent in PBT at 4 ^{o}C for 1hr. The blocking solution was removed and the sections washed with ice-cold PBS. The sections were then incubated in Rhodamine-Phalloidin solution for 20 min at room temperature in the dark (TOPRO-3 could also be added at this step – see section 2.2.23). The sections were then washed three times with ice-cold PBS before being imaged on the confocal microscope.

2.3.9. TOPRO-3 staining

TOPRO-3 was diluted 1:10,000 in PBS. This solution was added to vibratome sections and incubated for 20 min at room temp in the dark. The sections were then washed three times with ice-cold PBS before being imaged on the confocal microscope.

2.4. Microscopy and imaging

2.4.1. Low power images

Low power images were collected using an Olympus SZX16 equipped with an Olympus CC-12 camera. Images were imported into Photoshop CS3 (Adobe) for orientation and figure preparation.

2.4.2. Confocal images

Confocal images were taken on either a Leica SP5 confocal microscope or a Nikon C1 upright confocal microscope with an immersion lens (either 20x Fluor 0.5 NA working distance 2.0 mm or 40x Fluor 0.8 NA working distance 2.0 mm).

2.5. Determining the cell shape and aspect ratio

Confocal TIF formatted Images of embryos were exported from either LAS AF lite (Leica) or NIS-Elements Viewer Ver3.20.02 (Nikon) and imported into MetaMorph (Molecular Devices, USA) Version 7.7.4. The images were assembled in a stack and used to produce a maximum projection or a 3D reconstruction. The outline of the endodermal cells was traced freehand in MetaMorph (Molecular Devices, USA). The region measurements tool was used to produce values for the height and width of each cell based on the outline of the cell.

2.6. Statistics

Quantitative data derived from at least three independent experiments or individuals; descriptive statistics are mean ± SEM of data for n individuals or n independent experiments. Microsoft Excel 2007 was used χ squared statistics, $p<0.05$ was used to determine a statistically significant difference. The asterisks refer to the following significant values throughout the thesis: $p<0.05$ (*). GraphPad prism6 was used for unpaired 2-tailied Student-T tests normally-distributed continuous variables. P values are as follows * = $P<0.01$. ** = $P<0.001$, ***=$P<0.005$, **** = $P<0.0001$.

Chapter 3. Endodermal cell midline aggregation, and the role of the PCP signalling pathway in this process

3.1. Introduction

Following endodermal cell specification at gastrulation (50 % epiboly, 5.3 hpf) (Alexander and Stainier, 1999), the endodermal cells undergo a random walk behaviour to spread out anteriorly over the yolk until mid-gastrulation (75 % epiboly) (Pezeron et al., 2008), at which they begin to converge towards the dorsal midline, forming a stripe running the anterio-posterior length of the embryo at 11 hpf. The migratory characteristics of the endoderm from mid-gastrulation (75 % epiboly) through somitogenesis stages have not been previously investigated. Similarly, it is not known when the endoderm undergoes a transition from a monolayer of cells into the primitive endodermal rod that can be seen at 24 hpf (referred to as midline aggregation), and the morphogenic movements required during midline aggregation have not been examined. In this chapter, I describe experiments characterising the migration of the endoderm towards the dorsal midline during somitogenesis stages, and the morphogenic movements undertaken during the process of midline aggregation.

In this chapter, I also investigate the role of the PCP pathway in endodermal movements. Zebrafish embryos that are mutant for components of the PCP pathway, such as *trilobite* (*tri*) and *knypek* (*kny*), display characteristic reductions in embryo length and an increase in width (convergence and extension (C&E) defects) that affects mesodermal and ectodermal tissues (Marlow et al., 1998), but the endodermal tissues have not been examined. Trilobite is a transmembrane membrane protein that plays a role in regulating PCP signalling by interactions with Prickle and Dishevelled (Dvl). *tri* has also been proposed to have a *dvl*-independent role in regulating PCP signalling in

migrating neurons (Jessen et al., 2002). Knypek is an extracellular membrane associated protein that functions to facilitate binding of extracellular Wnt molecules to the Frizzled receptor (Topczewski et al., 2001). As PCP shows movement defects in the other germ layers, I aimed to determine if *tri* and *kny* mutants also develop endodermal defects, and if so, to investigate the roles of these two PCP signalling family members in regulating endodermal morphogenesis.

During early somitogenesis stages it is difficult to distinguish between the endodermal cells and the overlying mesodermal cells without the aid of fluorescent labelling. For this reason, there has been a lack in the number of investigations into the morphogenetic movements and behaviours of the endodermal cells during formation of the endodermal rod. In this study I utilised the early endodermal cell reporter line Tg(*sox17:EGFP*)(Mizoguchi et al., 2008); this line expresses *EGFP* specifically in endodermal cells soon after endodermal specification (50 % epiboly, 5.3 hpf) (Alexander and Stainier, 1999). I utilised this line to fluorescently label endodermal cells and characterise the morphogenetic events that occur in the endoderm as it changes from a single monolayer of cells against the Yolk syncytial layer (YSL) to an endodermal rod.

3.2. Results

3.2.1. Disruption of PCP signalling results in morphological defects in the endoderm

To determine if the Planar Cell Polarity (PCP) signalling pathway has a role in zebrafish trunk endoderm morphogenesis, wildtype, *trilobite* (*tri*), *knypek* (*kny*), and *trilobite*/*knypek* (*tri*/*kny*) double mutant lines were raised in the background of Tg(*sox17*:*EGFP*), and analysed under a fluorescent dissecting microscope. Wildtype embryos have a well-organised endodermal rod at 24 hpf (Figure 3.1 A), with the endodermal cells aligned as a thin stripe of non-epithelial cells along the dorsal midline. *tri* and *kny* mutants develop a shorter anterio-posterior endoderm length than wildtype embryos (Figure 3.1 B,C). *tri* and *kny*

mutant embryos also display a wider and disorganised endodermal stripe compared to wildtype. Occasionally *tri* and *kny* single mutants display a coalescing defect in the endodermal cells just posterior to the pharyngeal endoderm resulting in a hole in the anterior endodermal stripe (Figure 3.1 B, bracket). *tri*/*kny* double mutants display a compounding effect with a drastically shorter and wider endodermal stripe relative to each respective single mutant (Figure 3.1 D, arrowheads). Although single mutants occasionally show a split in the endoderm with low penetrance (Figure 3.1 B bracket), this phenotype is always seen in the double *tri*/*kny* mutants (Figure 3.1 D arrowheads). This indicates that the loss of both *tri* and *kny* causes a greater defect than the loss of *tri* and *kny* alone, and demonstrates that these genes do not play redundant roles during endodermal morphogenesis.

3.2.2. Disruption of PCP signalling results in reduced migration of endodermal cells to the dorsal midline

To characterise endodermal cell migration to the dorsal midline during somitogenesis I measured the width of the endodermal stripe at stages of development from 11 to 21 hpf (3 somites to 24 somites) in wildtype embryos. Three width measurements were taken to determine if the anterior, middle, and posterior regions of the trunk endoderm migrate to the dorsal midline at the same rate (Figure 3.2 A, B). All three regions of the trunk endoderm migrate to the midline at a similar rate with respect to each other (Figure 3.2 C), with the greatest rate of reduction in endodermal width occurring between the 11 hpf (3 somites) and 16 hpf (14 somites). As these regions move in a similar manner, further analysis used the mean of these three widths. To determine the effect of disruption of PCP signalling on endoderm migration to the midline during somitogenesis stages, width measurements were taken from *tri*, *kny*, and *tri*/*kny* homozygous mutant embryos. The endodermal width of both the single PCP mutants *tri* and *kny* was wider than wildtype endodermal width at all stages analysed (Figure 3.2 D). Double *tri/kny* mutants displayed a synergistic effect and a greater reduction in migration to the midline. Contrary to expectations, the overall rate of endodermal migration towards the dorsal midline appears to be

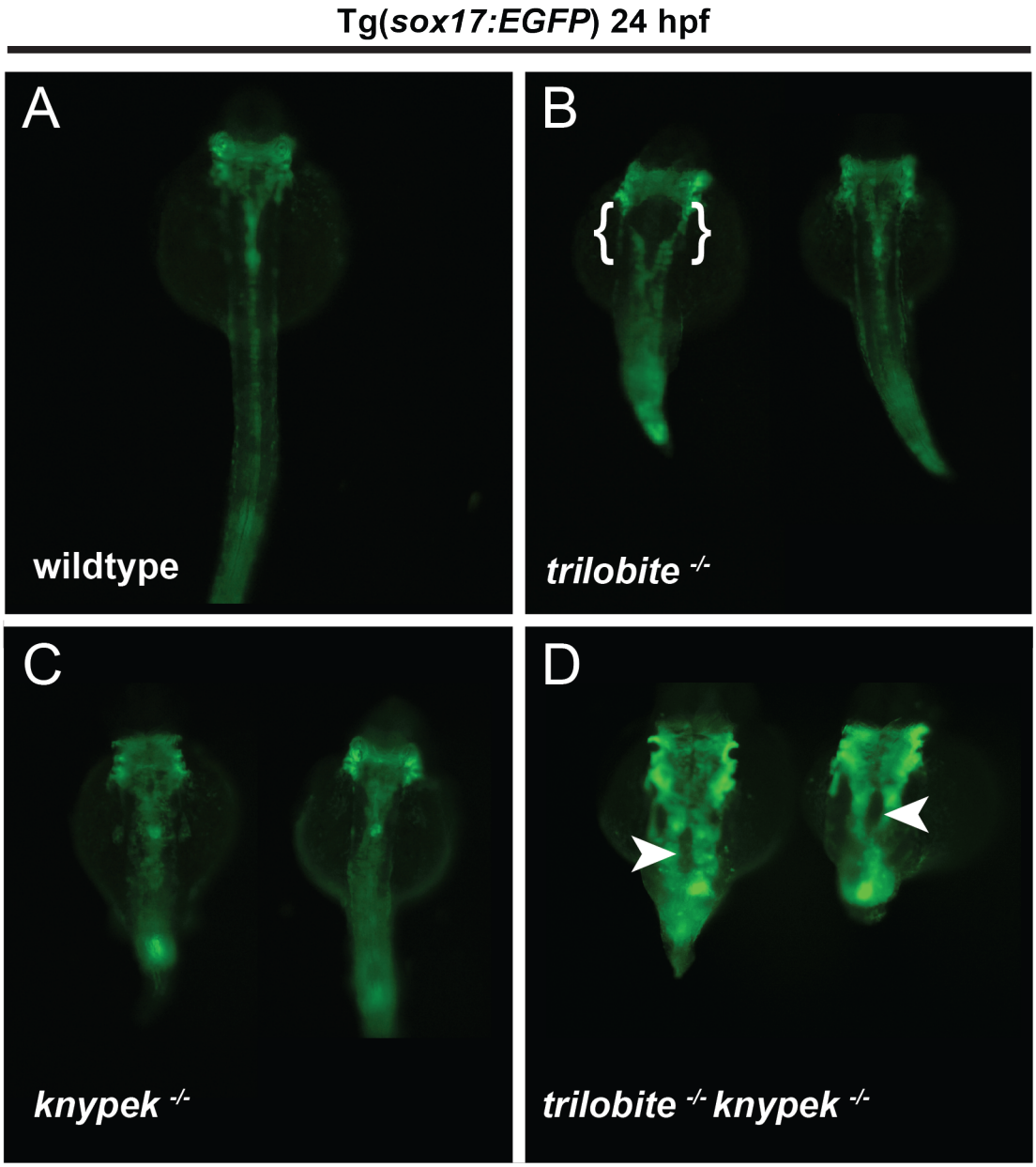

Figure 3.1 Loss of PCP signalling results in disrupted endoderm morphology during development. (A-D) Fluorescent dissecting microscope images of endoderm morphology in (A) 24 hpf wildtype and PCP homozygous mutant embryos (B) *trilobite*, (C) *knypek*, and (D) *trilobite*/*knypek* double mutants in the Tg(*sox17:EGFP*) background. Endoderm morphology in PCP mutants (B, C, and D) has become disorganised and wider than in wildtype (A). Disruption of PCP signalling in the single mutants occasionally results in a splitting of the endoderm posterior to the pharyngeal endoderm as indicated by the brackets in B. *trilobite/knypek* double mutant embryos always have a splitting of the endoderm posterior to the pharyngeal endoderm as indicated by the arrow heads in D.

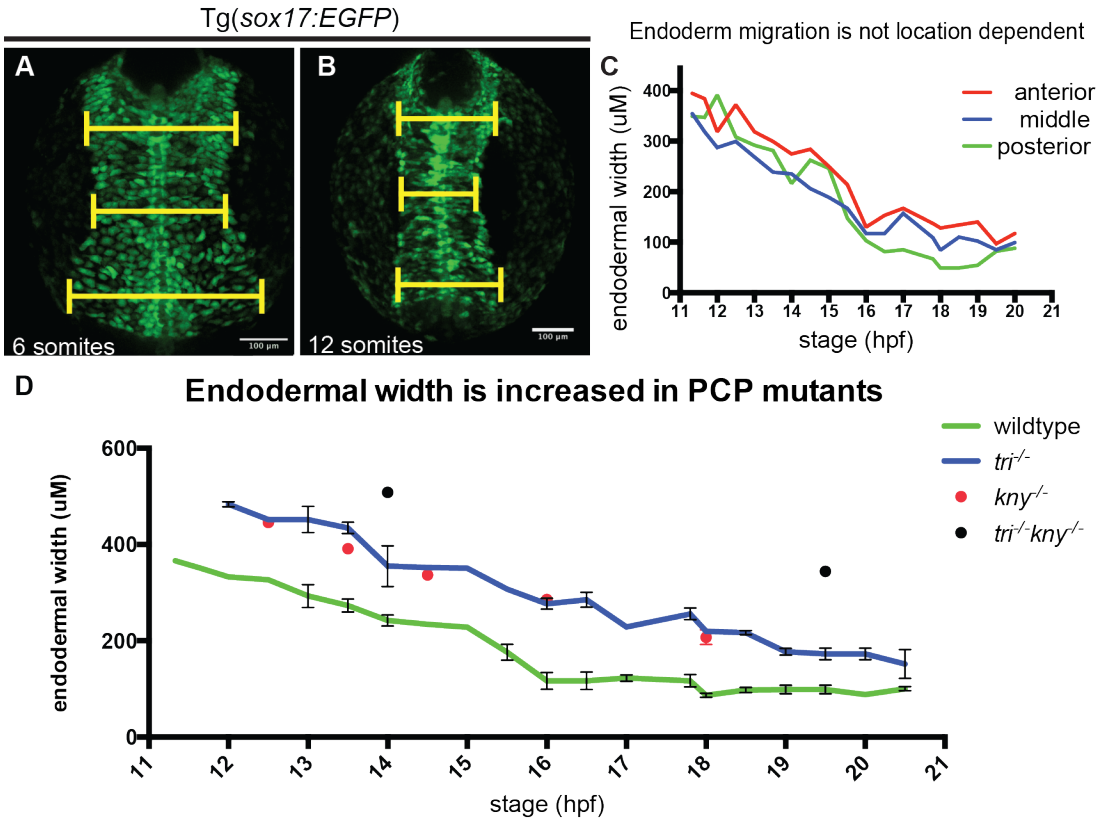

Figure 3.2 PCP signalling is required for correct migration to the dorsal midline during somitogenesis stages. (A-B) Confocal projections of 6 somite (12 hpf) (A) and 12 somite (15 hpf) (B) wildtype Tg(*sox17:*EGFP) embryos. Scale bar indicates 100 µM. Posterior is at the bottom. Yellow bars indicate positions of the three width measurements. **(C)** The anterior, middle, and posterior regions of the endoderm migrate with the same overall rate towards the dorsal midline during somitogenesis stages. **(D)** Endoderm width is increased in homozygote *trilobite* (*tri*) and *knypek* (*kny*) mutants and *tri/kny* double mutant PCP lines. (n= 1-5 embryos per stage). Error bars represent SEM.

equivalent between *tri*, *kny*, and wildtype embryos over the stages analysed (Figure 3.2 D). These results determine that the migration of endodermal cells to the midline during somitogenesis stages is similar along the anterio-posterior embryo axis, and that disruptions in PCP signalling reduce this migration, but do not prevent it.

3.2.3. Morphological characterisation of midline aggregation.

I aimed to characterise the morphogenetic event in which the endodermal cells change from a monolayer of cells against the yolk syncytial layer (YSL) membrane to an endodermal rod, an event we have termed "midline aggregation". The experiments designed to investigate this process are described below.

3.2.3.1. Midline aggregation begins around 14 hpf and is disrupted in the PCP mutants tri and kny

During C&E movements (75 % epiboly to tailbud) the migrating endodermal cells are in a monolayer in contact with the YSL membrane. However, by late somitogenesis stages (24 somites) the endodermal cells have left the monolayer at the midline and formed an endodermal rod, the precursor to the endodermal organs. The time point at which endodermal cells leave the monolayer has not been previously investigated. To determine the timing of this significant change in endoderm morphology, thick vibratome sections of wildtype embryos at stages ranging from 11 to 24 somites were examined using confocal microscopy (Figure 3.3 A-D'). At 11 somites the endoderm is still in a monolayer against the YSL (Figure 3.3 A, A'). By 16 somites a proportion of the endodermal cells have changed their behaviour and started to leave the monolayer, climbing over their neighbouring endodermal cells, and are no longer in contact with the YSL membrane (Figure 3.3 B, B'). Endodermal cells continue to leave the monolayer from 16 somites to 24 somites (Figure 3.3 D, D'), resulting in an endodermal rod at the dorsal midline of the embryo containing a proportion of endodermal cells

wildtype
tri -/-
kny -/-
11 somites
16 somites
18 somites
24 somites
A
A'
E
E'
I
I'
B
B'
F
F'
J
J'
C
C'
G
G'
K
K'
D
D'
H
H'
L
L'

Figure 3.3 Midline aggregation of endodermal cells in wildtype and PCP mutant lines. Confocal images of vibratome sections stained with Rhodamine-Phalloidin to show F-actin (red) at 11 somites, 16 somites, 18 somites, and 24 somites. Endodermal labelled in green by Tg(*sox17:EGFP*). Vibratome sections are in region of the yolk extension to control for A-P position **(A-D)** wildtype embryos (A'-D'). Schematic representations of the endoderm at each stage. **(E-H)** *tri* $^{-/-}$ embryos, showing a wider endodermal region and an increase in endodermal cell number. **(I-L)** *kny* $^{-/-}$ embryos, showing an increase in endodermal cell number and endodermal width. Scale bar indicates 25 μm.

that have left the monolayer, but are still in contact with the other endodermal cells.

I previously demonstrated that the PCP mutants *tri* and *kny* have wider endoderm during somitogenesis stages (Figure 3.2 D). To determine if PCP signalling also plays a role in midline aggregation, vibratome sections of tri and kny mutants from 11 somites to 24 somites were examined (Figure 3.3 E-L). Similar to the wildtype endodermal cells, *tri* mutant endodermal cells had not started to leave the monolayer at 11 somites (Figure 3.3 E-E'). *tri* mutant endodermal cells appeared to be more numerous and disorganised at all stages compared to wildtype. By 24 somites the *tri* mutant had a poorly organised endodermal rod at the midline (Figure 3.3 H-H'). Similar to *tri* mutants, *kny* mutant endodermal cells do not start to leave the monolayer until ~16 somites (Figure 3.3 J-J'), and appear to have a greater number of endodermal cells per section (Figure 3.3 I-L'). *kny* mutant embryos display an unorganised endodermal rod at 24 somites compared to wildtype embryos (Figure 3.3 L-L'). As expected from previous observations, both *tri* and *kny* embryos have a wider endodermal rod at 24 somites than wildtype embryos (Figure 3.3 L-L').

3.2.3.2. Quantification of morphogenetic changes during midline aggregation

To quantify the process of midline aggregation the total number of endodermal cells was determined in cross-section from wildtype embryos at the same stages as in Figure 3.3. The mean cell number of wildtype endodermal cells was constant across all stages analysed, at around 5 cells per section (±0.802 SE) (Figure 3.4 A). The PCP mutants *tri* and *kny* appeared to have higher endodermal cell numbers per section during midline aggregation than wildtype (Figure 3.3 A). Indeed, *tri* mutant embryos had a significantly higher endodermal cell number at 16 somites (6.6 ±0.678 SE) compared to wildtype (5 ±0.366 SE) (Unpaired T-test with equal SD (two-tailed)). The increase in *tri* endodermal cell number continued to increase up to 24 somites (10 ±1.517 SE) when compared to wildtype (5 ±0.816 SE). *kny* mutant embryos also displayed a higher number of endodermal cells per section than wildtype from 18 somites (13 ±2.157 SE) to

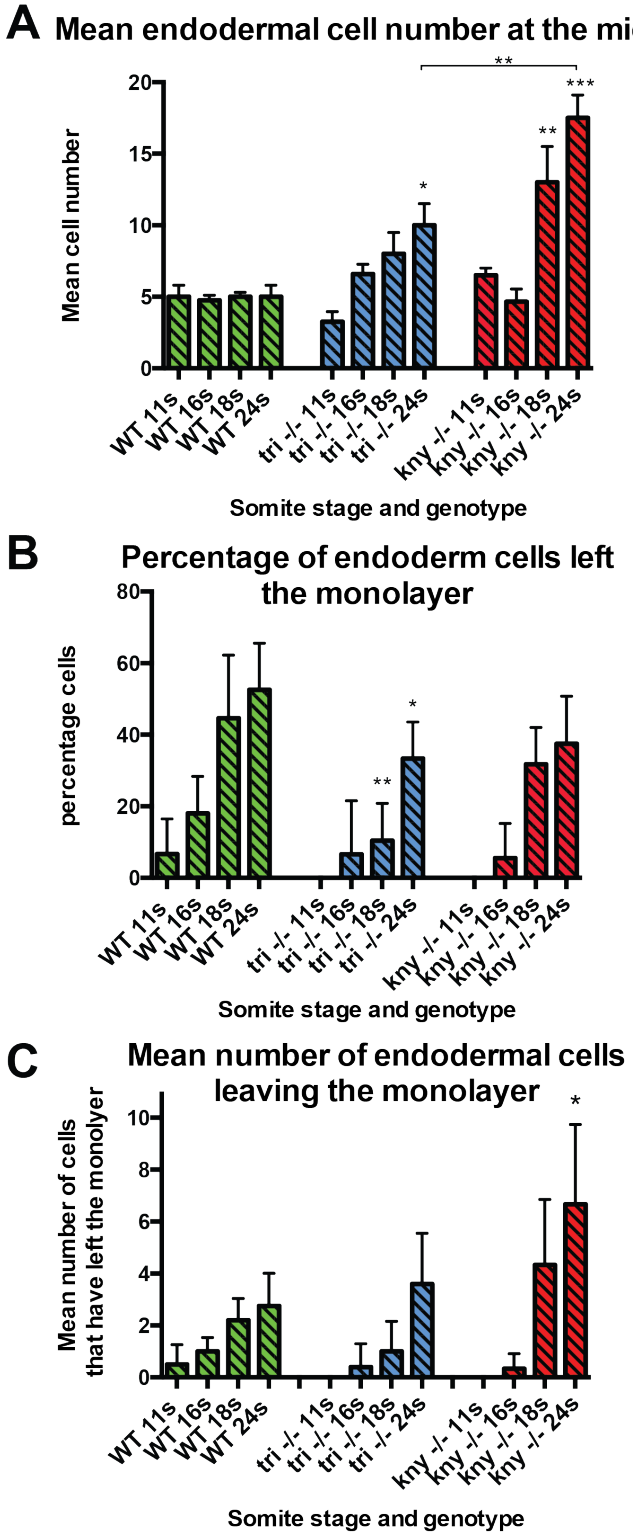

Figure 3.4 Changes in endodermal cell number and position at the midline during midline aggregation. (A) Mean cell number at the dorsal midline from 11 somites to 24 somites of wildtype (wildtype) (green bars), *tri* $^{-/-}$ (blue bars), and *kny* $^{-/-}$ (red bars) embryos. **(B)** Percentage of endodermal cells that have left the monolayer in wildtype (green bars), *tri* $^{-/-}$ (blue bars), and *kny* $^{-/-}$ (red bars) embryos. Thatched bars indicate the percentage of cells still in contact with the YSL. **(C)** Total number of endodermal cells that have left the monolayer in wildtype (green bars), *tri* $^{-/-}$ (blue bars), and *kny* $^{-/-}$ (red bars) embryos. (n=2-8) Error bars represent SEM. Asterisk represents significant as determined by t-test, * = P ≤ 0.05, ** = P ≤ 0.01, *** = P ≤ 0.001, **** = P ≤ 0.0001.

24 somites (17.5 ±1.607 SE)(Figure 3.4 A). Interestingly there were a significantly higher number of endodermal cells at 24 somites in cross-sections of *kny* embryos (17.5 ±1.607 SE) compared to *tri* embryos (10 ±1.517 SE) ($p<0.001$).

As *tri* and *kny* mutants have an increased number of endodermal cells at the midline, there is a chance that overall endodermal cell number might affect the proportion of cells that leave the monolayer. I determined the mean total number of endodermal cells that have left the monolayer in wildtype, *tri* mutant, and *kny* mutant embryos. Wildtype embryos have an increase in the mean number of cells that leave the monolayer from 11 somites until 24 somites, 0.5 (±1.607 SE) and 2.75 (±0.629 SE) respectively (Figure 3.4 C green bars). Surprisingly, *tri* mutant embryos have a similar increase in the total number of cells that leave the monolayer as wildtype, 0.0 and 3.6 (±0.872 SE) respectively (Figure 3.4 C blue bars). Contrastingly, the total number of cells that have left the monolayer in *kny* mutants is significantly larger than wildtype at 24 hpf (6.7 ±1.256 SE) (Figure 3.4 C red bars). These data show that the PCP signalling mutants *tri* and *kny* mutants have multiple defects in endodermal midline aggregation, and that these defects are not identical. To determine if the increase in endodermal cell number identified in Figure 3.4A also resulted in a change in the proportion of cells leaving the monolayer I quantified the percentage of endodermal cells that underwent behavioural changes associated with midline aggregation. This was defined as any cell that no longer remained in contact with the YSL membrane. Wildtype embryos display an increase in the percentage of endodermal cells that have left the monolayer from 11 somites to 24 somites, 6.7 % to 52.6 % respectively (Figure 3.4 B green bars). *tri* and *kny* mutant embryos both display a reduction in the proportion of endodermal cells that leave the monolayer compared to wildtype at all stages analysed until 24 somites (Figure 3.4 B). In summary, although the endodermal cell number is increased in *tri* and *kny* mutants, the overall proportion of cells that have left the monolayer is reduced.

3.2.4. Cell shape changes underlie midline aggregation

Having defined the time point at which the endoderm starts to leave the monolayer and begin midline aggregation (Figure 3.3 A-D, Figure 3.4 B, C) I further investigated the mechanisms involved in this process. Many cellular movements require cell shape changes, for example the elongation of *Xenopus* mesodermal tissues (Keller et al., 2000). To investigate if cell shape changes are required for the onset of midline aggregation the shape of the endodermal cells was measured using dorsal views of live or fixed flat mounted embryos, from 6 somites to 13 somites (Figure 3.5 A, A1, A2). The aspect ratio (width/height) of a cell was used to determine cell elongation along the mediolateral plane. Width (mediolateral) and height (anterio-posterior) measurements were taken from confocal maximum projections and used to calculate the aspect ratio of endodermal cells (Figure 3.5 B). Individual cell outlines were determined using cytoplasmic EGFP. Prior to 7 somites wildtype endodermal cells are essentially circular with an aspect ratio of 1. At around 7 somites the endoderm begins to undergo a cell shape change, reaching a mean maximum aspect ratio of 2 at 10 somites (Figure 3.5). This cell shape change is maintained until 13 somites and is still present at 18 somites (data not shown).

To determine if *tri* and *kny* mutant endodermal cells are able to undergo cell shape changes during midline aggregation, aspect ratios of *tri* and *kny* mutant endodermal cells were determined. At all stages analysed the *tri* and *kny* mutant endodermal cells fail to undergo the change in aspect ratio that is seen in wildtype cells, retaining a constant circularity with an aspect ratio of ~1 from 3 somites to 13 somites (Figure 3.5 D). These data demonstrate that the PCP mutants are unable to carry out this endodermal cell shape change, and indicate that PCP signalling is required for endodermal cell shape changes, and that *tri* and *kny* play a role in the regulation of this process.

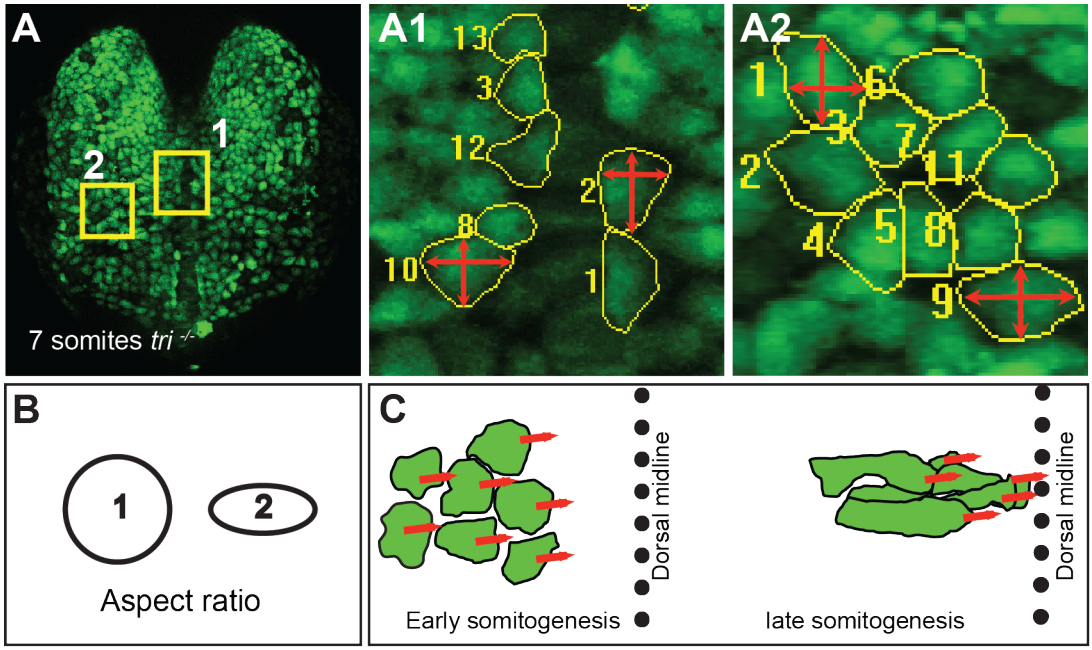

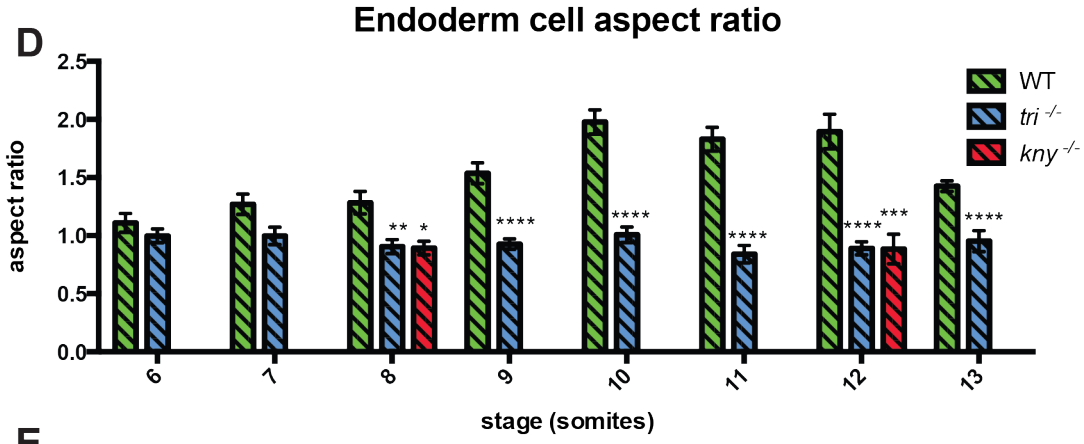

E

stage	6	7	8	9	10	11	12	13
wildtype	1 (16)	1 (4)	2 (23)	3 (33)	2 (22)	2 (13)	1 (10)	3 (41)
tri	1 (17)	1 (11)	2 (21)	2 (32)	3 (16)	1 (6)	2 (7)	1 (8)
kny			1 (11)				2 (6)	

Figure 3.5 PCP signalling is required for correct cell shape changes during midline aggregation. (A, A1, A2) Confocal maximum projections of Tg(*sox17:EGFP*) embryos detailing the width and height measurements taken to calculate the aspect ratio. Measurements were taken at two regions, the midline (A1) and ventral to the midline (A2). **(B)** Schematic representation of two different aspect ratios (width / height). **(C)** Schematic describing the change in cell shape during midline aggregation. **(D)** Graph describing changes in endodermal cell shape of wildtype and PCP mutants, represented by aspect ratio. Error bars represent SEM. Asterisk represents significance as determined by t-test, * = P ≤ 0.05, ** = P ≤ 0.01, *** = P ≤ 0.001, **** = P ≤ 0.0001. **(E)** Number of embryos used per stage and genotype. Number of cells analysed shown in brackets.

3.3. Discussion

3.3.1. Summary of results

My research has been aimed towards characterising and understanding the morphogenic events that underlie endodermal midline aggregation. Although there has been much attention on early endoderm specification (Alexander et al., 1999; Alexander and Stainier, 1999; Warga and Nusslein-Volhard, 1999; Schier and Shen, 2000; Dickmeis et al., 2001; Kikuchi et al., 2001; Schier, 2003; Mazmanian et al., 2010), and later endodermal organ morphogenesis (Field et al., 2003a; Field et al., 2003b; Ng et al., 2005; Niu et al., 2010), the process of midline aggregation remained uncharacterised.

In this study I investigated two major morphogenic movements of the endoderm during early development and the role of PCP signalling in these processes. Firstly, the migration of endodermal cells towards the dorsal midline, and secondly, the morphogenic movement undertaken once they are at the dorsal midline to form the endodermal rod – midline aggregation.

3.3.2. Migration to the midline

Observations of the gross morphology of the endoderm in *tri* and *kny* mutant embryos identified an overall general disorganisation of the endoderm at 24 hpf. Therefore, I investigated if a defect in migration to the dorsal midline was responsible. My results demonstrate that although *tri* and *kny* mutant endodermal cells appear to have a width defect earlier than 3 somites, their rate of migration of endodermal cells during somitogenesis stages is similar to wildtype cells (Figure 3.2 D). This indicates that *kny* and *tri* are both dispensable for endodermal cell migration towards the midline. In line with this, *tri/kny* double mutants also appear to have a similar rate of migration as wildtype endodermal cells (Figure 3.2 D). Despite this, the endodermal stripe is wider than the wildtype at all times. These data demonstrate that PCP signalling is not required for endodermal migration to the dorsal midline during somitogenesis stages, but do have an earlier migration defect during gastrulation, which results

in an overall difference in endoderm migration to the midline. In chapter four I describe the use of a transgenic approach to disrupt PCP signalling at stages after C&E, to avoid the effects of early migration defects, to analyse the role of PCP signalling specifically in the somitogenesis stages, during endodermal midline aggregation.

Interestingly, *kny* and *tri* have both been shown to be dispensable for dorsal-directed cell migration of the lateral mesoderm, during early and midgastrulation (Jessen et al., 2002; Sepich et al., 2005), although PCP signalling is required overall for the process of C&E. Therefore, this is consistent with the observation that PCP is not required for the overall dorsalward migration of the endodermal cells.

3.3.3. Midline aggregation

In this study I have characterised the morphogenesis of the endoderm during midline aggregation in wildtype embryos. Midline aggregation represents a significant change in endodermal behaviour and morphology, from a single monolayer of cells to a rod-like structure. In this study I identified three important areas of interest: cell number, leaving the monolayer, and cell shape change.

3.3.3.1. Cell number at the midline

My results show that there is a constant mean number of 5 endodermal cells in trunk cross-sections of wildtype embryos from 11 hpf to 24 hpf (Section 3.2.3.2). *tri* and kny mutant embryos display an increase in endodermal cell number around 16 somites, and this further increases as the embryos continue to develop. The endodermal cell number increase observed in *tri* and *kny* mutant embryos coincides with the onset of the tail starting to leave the yolk and to extend in wildtype embryos, a process that is highly reduced in *tri* and *kny* mutant embryos (Topczewski et al., 2001; Jessen et al., 2002). This reduction in embryo extension in *tri* and *kny* mutant embryos might explain the increase in endodermal cell number. It is possible that in wildtype embryos the extension

acts to drive the anterio-posterior spreading of the endoderm, in turn thinning the endodermal width and reducing the number of cells in a cross-section. This would explain how the loss of tail extension in PCP mutants results in the increase in endodermal cells at the midline.

An alternative explanation is that PCP is required for endodermal cell proliferation. However PCP does not generally cause changes in cell number. PCP signalling is known to regulate cellular migration, adhesion, and polarity (Fanto and McNeill, 2004; Ciruna et al., 2006; Karner et al., 2006; Dale et al., 2009; Roszko et al., 2009; Segalen and Bellaiche, 2009; Tada and Kai, 2009; Vladar et al., 2009), but not the regulation of cell fate specification or proliferation (Topczewski et al., 2001; Jessen et al., 2002). Therefore it can be concluded that increases in endodermal cell number seen in *tri* and *kny* mutants at 16 somites onwards are unlikely to result from changes in overall endodermal cell number, but rather result from changes in the distribution of existing cells within the embryo due to reduced embryo extension, which would normally change the overall embryo morphology during somitogenesis stages.

These data indicate that the endodermal cell number increase in *tri* and *kny* mutants may result as a secondary defect from the lack of trunk and tail extension. Therefore there is no evidence to support a role of PCP in endodermal cell movement in somitogenesis independent of the roles of PCP in overall embryo morphology.

3.3.3.2. PCP signalling is not required for the endoderm to leave the monolayer

This study identified that endodermal cells begin to leave the monolayer at around 11 somites, and continue to until 50 % of the endodermal cells no longer in contact with the YSL at 24 hpf. *tri* and *kny* mutant embryos both have a delay in the initiation of midline aggregation and endodermal cells leaving the monolayer. *tri* and *kny* mutants also have an increase in the total number of cells that leave the monolayer after 16 somites, but as they do have more endodermal cells in the cross-section this is likely due to defects in overall extension. Surprisingly, the actual proportion of the endodermal cells that leave the

monolayer by 24 hpf is reduced in *tri* and *kny* mutant embryos, suggesting that there is an overall difference. However, it is of interest to note that the cells that do leave the monolayer in the PCP mutants are always centred under the notochord rather than at the ventral edges of the endoderm (Figure 3.3). This suggests that there might be a site-specific cue at the dorsal midline to induce endodermal cells to leave the monolayer, but there is no current candidate molecule for this cue or candidate tissue that secretes it.

Therefore it seems that a requirement for PCP signalling for endodermal cells to leave the monolayer is unlikely, as endodermal cells are still able to leave the monolayer in both PCP mutants studied. Overall, my results demonstrate that PCP signalling does not directly regulate the process by which endodermal cells leave the monolayer during midline aggregation.

3.3.3.3. Endodermal cell shape change is not required for midline aggregation

The mechanisms that underlie endodermal midline aggregation are poorly understood. My results demonstrate that wildtype endodermal cells at the dorsal midline undergo a cell shape change (from an aspect ratio of 1 to 2) around 7 somites. Interestingly, this cell shape change preludes the onset of leaving the monolayer at around 11 somites, suggesting that this cell shape change may be required to leave the monolayer. However, *tri* and *kny* mutant endodermal cells do not undergo this cell shape change and still have the ability to leave the monolayer. It can be concluded from this data that although wildtype endodermal cells undergo a cell shape change that precedes midline aggregation, it is not required for the cells to leave the monolayer.

These results raise a number of interesting questions in regards to the endodermal cell shape changes identified in this study. Firstly, is the endodermal cell shape change observed in wildtype embryos required for correct midline aggregation? *tri* and *kny* endodermal cells do not undergo the cell shape change, but are capable of leaving the monolayer and undergoing midline aggregation. These results demonstrate that the cell shape changes identified are not required for endodermal midline aggregation.

Secondly, is PCP signalling required autonomously within the endodermal cells to under cell shape changes? *tri* and *kny* mutant endodermal cells do not undergo the cell shape change observed in wildtype endodermal cells, suggesting that PCP is required in this process. However, it is possible that the reduction in embryo length results in the loss of cell shape change in *tri* and *kny* mutants, or obscures the function of this cell shape change. Therefore, any role of PCP signalling in endodermal cell shape change during somitogenesis stages is not clear.

It can be concluded that endodermal cell migration to the midline does not specifically require PCP signalling. PCP signalling regulates mesodermal C&E movements and overall embryo elongation, and evidence indicates that the mesoderm has an influence on the migration of the endoderm during gastrulation (Mizoguchi et al., 2008; Nair and Schilling, 2008). My results indicate that PCP signalling is not specifically required for endodermal migration to the dorsal midline during somitogenesis. Together these results supports previous studies indicating that the migration of the endoderm to the dorsal midline is not independent of the mesoderm.

My results demonstrate that endodermal cells begin the process of midline aggregation by starting to leave the monolayer just prior to 11 somites, continuing up to the formation of the primitive endodermal rod at 24 hpf. The PCP signalling pathway, as defined by *tri* and *kny*, is not required for endodermal cells to leave the monolayer; however, the role of the *trilobite* and *knypek* in the regulation of endodermal cell numbers at the dorsal midline in mediolateral cross-sections is not clear.

Chapter 4. The Dishevelled gene family and its role in endoderm development

4.1. Introduction

Members of the *dishevelled* gene family are key intracellular mediators of the PCP signalling pathway, facilitating the signal transduction from the Frizzled receptors, and regulating multiple cellular responses (Axelrod et al., 1998; Rothbacher et al., 2000; Habas et al., 2001; Ulrich et al., 2003; Habas and Dawid, 2005). To date, the zebrafish *dishevelled* gene family has not been very well characterised. Expression data is only available for two members of this family, *dvl2* and *dvl3a*, both displaying ubiquitous expression patterns from the 1 cell stage to 72 hpf (Thisse and Thisse, 2004). Morpholino oligonucleotides targeted against zebrafish *dishevelled* genes have been published for *dvl1b* (Segalen et al., 2010; Yang and Thorpe, 2011), *dvl2*, and *dvl3a* (Angers et al., 2006). In these studies embryos injected with a single *dvl* targeted morpholino reported no gross morphological changes, with the exception of *dvl2* single morphants, that have been reported to have a duplicated neural tube axis (Tawk et al., 2007). In general only co-injection of morpholinos against multiple *dvl* genes generate embryos with gross morphological defects such as reduction in body size (Angers et al., 2006). A number of mutant alleles are reported for this family: *dvl1a*, *dvl1b* (two alleles), *dvl2* (four alleles), *dvl3a* (two alleles)(zfin.org, 2013b; zfin.org, 2013e; zfin.org, 2013a; zfin.org, 2013d; zfin.org, 2013c). However to date no reports have been published utilising these mutants. The mutation sequence data is currently only available for the *dvl1b* sa17495 mutant allele, two *dvl2* alleles (sa6076, and sa20904), and two *dvl3a* alleles (sa14810 and sa19682, Table 1). All of these alleles, with the exception of *dvl3a* sa14810, have mutations within or after the DEP domain, resulting in truncation of the C-terminus. The *dvl3a* sa14810 allele results in a truncation in the 5'- region of the protein.

	Mutation	Effect on protein
dvl1a	---	---
dvl1b	sa17495 T>C:	Truncation of the C-terminal domain
dvl2	sa6076 C > T	causes a truncation in the C-terminal domain
	sa20904 T > A	loss of C-terminal domains.
dvl3a	sa14810 T > C	abolishes a splice site in exon 4 - Probably intron included and early stop
	sa19682 C > T	results in a truncation, including the end of the DEP domain
dvl3b	---	---

Table 1 Effects of known *dishevelled* gene family mutations with available sequence data (from zfin).

Due to *dishevelled* participating in both the PCP signalling and β-catenin signalling pathways, experiments utilising *dvl*-morphants or null mutant *dishevelled* gene members are not useful to specifically investigate the roles of PCP signalling, as both pathways would be affected. In this chapter I describe the use of dominant negative version of *Xenopus dishevelled*-2 that has the DEP domain deleted and replaced by *EGFP* to generate *XDshΔDEP-EGFP* (Sokol, 1996; Heisenberg et al., 2000; Rothbacher et al., 2000; Tada and Smith, 2000; Wallingford et al., 2000; Habas et al., 2001; Yu et al., 2010). The DEP domain is specifically required to function in PCP signalling via phosphorylation and activation of Dishevelled, endocytosis (Yu et al., 2010) and the physical interaction with Prickle (Tree et al., 2002). Over-expression of *XDshΔDEP-EGFP* has been shown to specifically inhibit PCP signalling without disrupting β-catenin signalling (Sokol, 1996). I wished to disrupt the function of Dishevelled proteins in PCP signalling and thus investigate the role of *dishevelled* in endoderm morphogenesis. In order to better understand the genetic landscape that I would be disrupting I characterised the zebrafish *dishevelled* gene family. In this chapter I describe the five members of the zebrafish *dishevelled* gene family, with regards to protein homology and expression patterns during development. I also describe the use of the *dishevelled* dominant negative *XDshΔDEP-EGFP* to develop a transgenic line enable a time specific disruption of PCP signalling, overcoming any potential earlier defects caused in PCP mutant embryos. In addition, this chapter describes the use of this transgenic tool in experiments designed to investigate whether the PCP signalling pathway has a time specific role during endodermal midline aggregation.

4.2. Results

4.2.1. Analysis of the zebrafish dishevelled gene family

4.2.1.1. Zebrafish dishevelled phylogenetic analysis

The zebrafish genome contains five *dishevelled* gene homologs; *dvl1a*, *dvl1b*, *dvl2*, *dvl3a*, and *dvl3b* (ensmbl accession numbers: *dvl1a* ENSDART00000035755, *dvl1b* ENSDART00000103752, *dvl2* ENSDART00000135316, *dvl3a* ENSDART00000097732, and *dvl3b* ENSDART00000007181). To determine the phylogeny of the *dvl* gene family in zebrafish the protein sequences were subjected to phylogenetic analysis by maximum likelihood using MEGA5 (Tamura et al., 2011), using the single *Drosophila* homologue, *Dsh,* as the outlier. The five dvl genes form a phylogenetic tree containing three distinct clades, consisting of the two dvl1 genes (dvl1a and dvl1b), a single dvl2 gene, and a two dvl3 genes (dvl3a and dvl3b) (Figure 4.1). The phylogenetic separation into three groups based on protein sequence is consistent with the naming nomenclature assigned to these genes and with the whole genome duplication known to have occurred in teleosts (Amores et al., 1998).

4.2.1.2. Dishevelled protein structure is conserved

To investigate if all zebrafish *dvl* gene members have a conserved protein domain structure, the amino acid sequences were first aligned using Clustal Omega (Sievers et al., 2011). To identify conserved domains within each protein, the amino acid sequences were analysed using the Conserved Domain Database (CDD) (Marchler-Bauer and Bryant, 2004) (Figure 4.2 A). The overall protein structure and amino acid conservation is highly conserved in all members of the zebrafish Dishevelled family, as indicated by the dark grey highlighted residues (Figure 4.2 A). All zebrafish Dvl proteins contain five conserved Dishevelled protein domains: the DIX domain, the *dishevelled* specific domain, the PDZ domain, the DEP domain, and the *dishevelled* C-terminal domain (Figure 4.2 B).

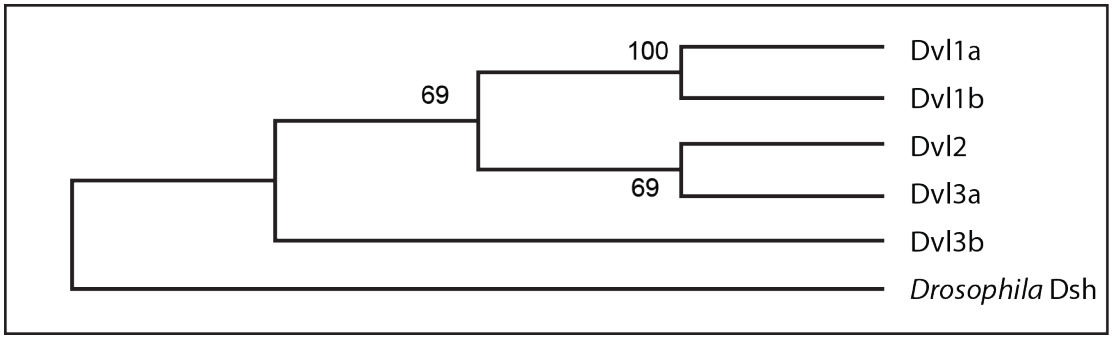

Figure 4.1 Zebrafish Dishevelled protein phylogenetic analysis. The evolutionary history was inferred by using the Maximum Likelihood method based on the JTT matrix-based model (Jones et al., 1992). The bootstrap consensus tree inferred from 500 replicates is taken to represent the evolutionary history of the taxa analysed (Felsenstein, 1985). Branches corresponding to partitions reproduced in less than 50 % bootstrap replicates are collapsed. The percentage of replicate trees in which the associated taxa clustered together in the bootstrap test (500 replicates) are shown next to the branches (Felsenstein, 1985). Initial tree(s) for the heuristic search were obtained automatically as follows. When the number of common sites was < 100 or less than one fourth of the total number of sites, the maximum parsimony method was used; otherwise BIONJ method with MCL distance matrix was used. The analysis involved 6 amino acid sequences. All positions containing gaps and missing data were eliminated. There were a total of 508 positions in the final dataset. Evolutionary analyses were conducted in MEGA5 (Tamura et al., 2011).

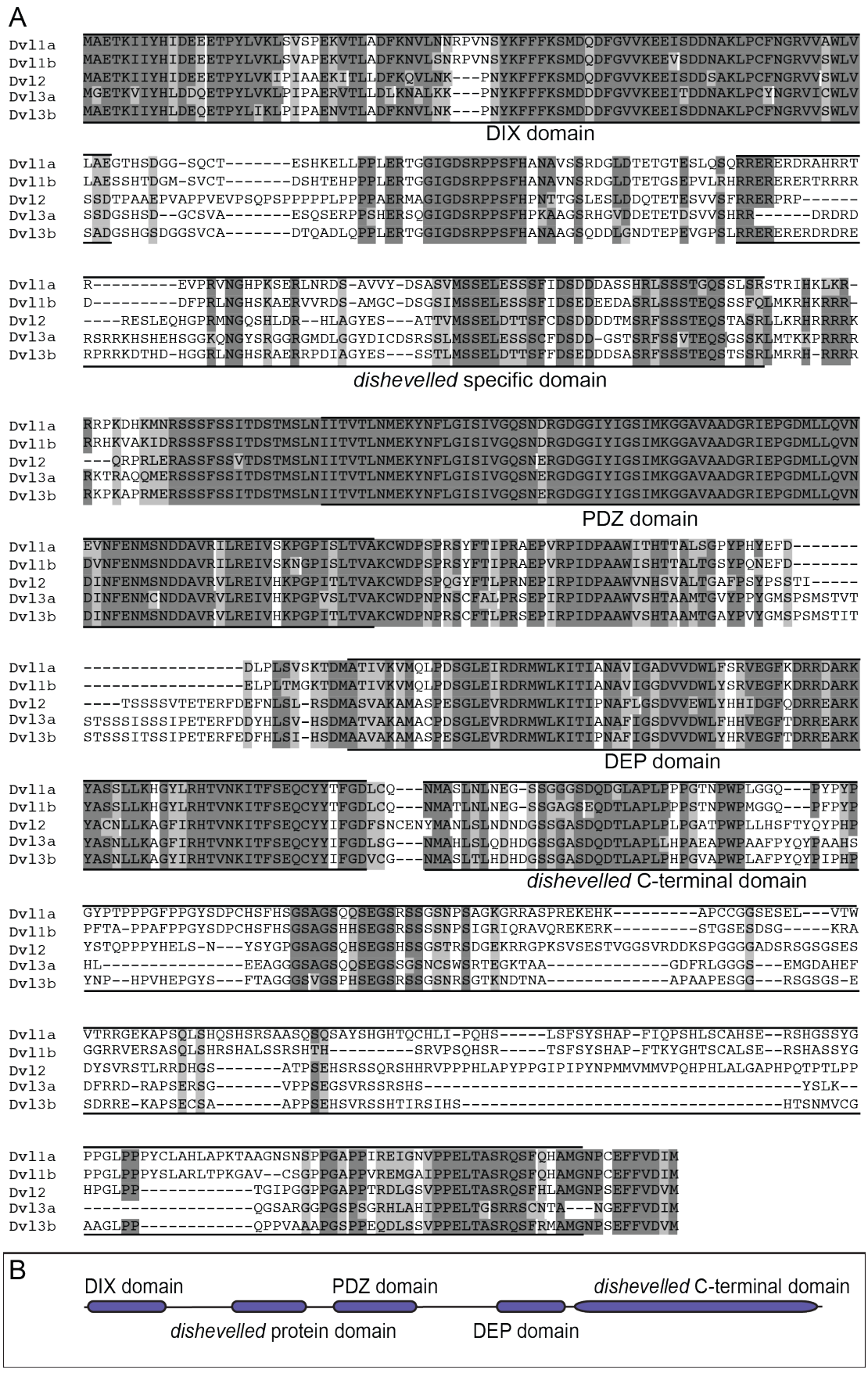
A
Dvl1a
Dvl1b
Dvl2
Dvl3a
Dvl3b
DIX domain
PDZ domain
dishevelled specific domain
DEP domain
dishevelled C-terminal domain
B
DIX domain
PDZ domain
dishevelled C-terminal domain
dishevelled protein domain
DEP domain

Figure 4.2. Zebrafish Dishevelled protein alignment. (A) Dishevelled family protein alignment. Protein sequences were aligned using Clustal Omega from sequences from ensmbl accession numbers as follows: *dvl1a* ENSDART00000035755, *dvl1b* ENSDART00000103752, *dvl2* ENSDART00000135316, *dvl3a* ENSDART00000097732, and *dvl3b* ENSDART00000007181. Highly conserved residues are in dark highlighting. Similar residues are highlighted in light grey. Protein domains are underlined and labelled. **(B)** Zebrafish *dishevelled* protein domain structure. All five zebrafish *dishevelled* genes contain the five *dishevelled* domains: DIX domain, *dishevelled* protein domain, PDZ domain, DEP domain, and the *dishevelled* C-terminal domain.

4.2.1.3. Dishevelled protein similarity

The overall amino acid similarity between the five zebrafish Dvl proteins is shown in Table 1A. The overall residue conservation of all Dvl proteins ranges from between ~60 % and ~80 %. The conservation within the *dvl1* and *dvl3* family groups is fairly high, 79 % and 73 % respectively. As the overall protein structure of all the Dvl proteins is highly conserved (Figure 4.2), I investigated the residue homology specifically within each of the conserved domains. The PDZ, DIX, and DEP domains have the highest level of conservation. The PDZ domain has the highest conservation of all domains, 92 % between *dvl1a*, *dvl1b*, and *dvl3b*, and 100 % conservation between *dvl2* and *dvl3a* (Table 2 D). The DIX domain has a level of residue conservation ranging from 69 % to 95 % (Table 2 B). The DEP domain residues are also highly conserved in all members, ranging from 70 % across the three clade groups, to 100 % and 91 % in the *dvl1* and *dvl3* groups respectively (Table 2 E). The C-terminal domain and the *dishevelled* specific domain have low residue conservation ranging from 42 % to 66 % (Table 2 D) and 45 % to 65 % respectively (Table 2 C).

4.2.1.4. dishevelled gene expression during development

To determine the temporal expression pattern of each member of the *dishevelled* gene family semi-quantitative reverse-transcription polymerase chain reaction (RT-PCR) was performed (25 cycles) to detect the expression during various stages from one cell stage to 72 hpf (Figure 4.3). All *dvl* genes were detected at all stages analysed.

Dishevelled family protein homology

	Dvl1b	Dvl2	Dvl3a	Dvl3b
Dvl1a	79.44	59.16	60.89	66.21
Dvl1b		59.41	61.36	65.74
Dvl2			64.92	69.31
Dvl3a				73.13

DIX domain homology

	Dvl1b	Dvl2	Dvl3a	Dvl3b
Dvl1a	95.29	69.51	80.49	81.71
Dvl1b		68.29	80.49	80.49
Dvl2			76.83	82.93
Dvl3a				85.37

***dishevelled* specific domain homology**

	Dvl1b	Dvl2	Dvl3a	Dvl3b
Dvl1a	63.51	47.89	45.45	47.89
Dvl1b		47.89	45.45	57.75
Dvl2			46.38	56.76
Dvl3a				65.22

PDZ domain homology

	Dvl1b	Dvl2	Dvl3a	Dvl3b
Dvl1a	97.73	93.18	93.18	92.05
Dvl1b		93.18	93.18	92.05
Dvl2			100	96.59
Dvl3a				96.59

DEP domain homology

	Dvl1b	Dvl2	Dvl3a	Dvl3b
Dvl1a	100	70.24	78.57	78.57
Dvl1b		70.24	78.57	78.57
Dvl2			86.9	89.29
Dvl3a				91.67

***dishevelled* C-terminal domain homology**

	Dvl1b	Dvl2	Dvl3a	Dvl3b
Dvl1a	66.07	45.73	36.91	46.43
Dvl1b		43.85	37.96	42.68
Dvl2			44.79	49.46
Dvl3a				52.47

Table 2. Dishevelled amino acid similarity. Percentage protein similarity as determined by Clustal Omega. Dishevelled proteins have a high level of residue conservation, especially within domains.

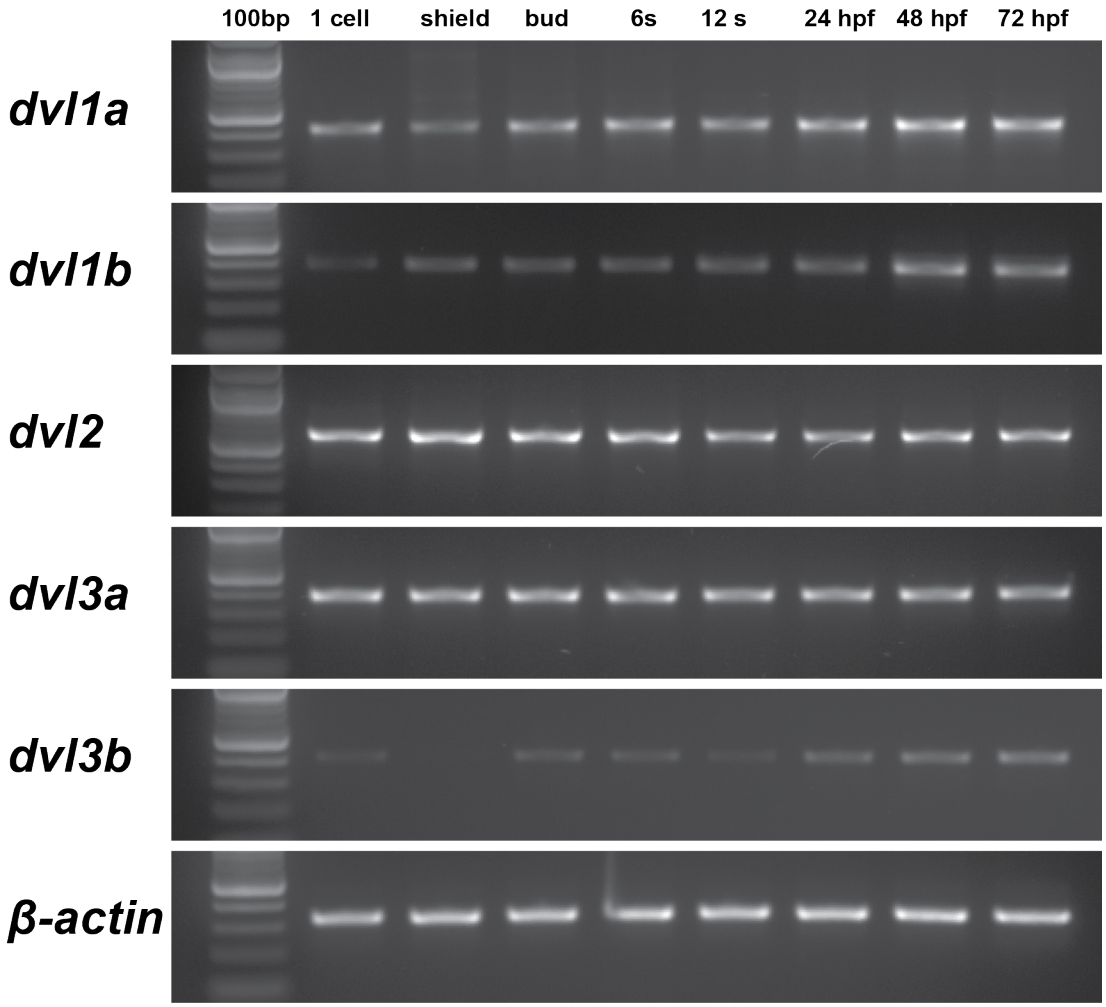

Figure 4.3. Temporal *dishevelled* expression during development. Temporal expression pattern of zebrafish *dishevelled* gene family members as determined from semi-quantitative reverse transcription polymerase chain reaction (RT-PCR) (25 cycles) from 1 cell stage to 96 hpf. 6 s = 6 somites. 12 s = 12 somites. *β-actin* was used as a cDNA control (for Primers see Appendix One).

4.2.1.5. dishevelled gene expression pattern during development

To determine the spatial expression pattern of each *dvl* gene, gene fragments were cloned from a wildtype 24 hpf cDNA library (ensmbl accession numbers: *dvl1a* ENSDART00000035755, *dvl1b* ENSDART00000103752, *dvl2* ENSDART00000135316, *dvl3a* ENSDART00000097732, and *dvl3b* ENSDART00000007181) and used to generate sense and anti-sense riboprobes. As I was interested in endoderm morphogenesis during somitogenesis stages *in situ* hybridisation was performed at the 3 somite stage and 24 hpf (Figure 4.4). All five *dishevelled* genes are ubiquitously expressed throughout the embryo at the 3 somite stage (Figure 4.4 B, F, J, N, R), with expression becoming restricted to the anterior portion of the embryo by 24 hpf (Figure 4.4 D, H, L, P, T).

4.2.2. Generation of a transgenic line to facilitate time specific inducible disruption of PCP signalling

An inherent caveat of using mutant lines to investigate genes that regulate developmental processes is the potential for defects early in development to mask time-specific roles at later developmental stages. The PCP mutants *tri* and *kny* both display significant convergence and extension defects towards the end of epiboly, resulting in the reduction in embryo length and an increase in embryo width (Marlow et al., 1998), as well as endodermal width (Section 3.2.2). These early morphological defects prevent accurate determination of a potential role for PCP signalling specifically during midline aggregation. To investigate if the PCP signalling pathway has a time specific role in endoderm morphogenesis, I generated a transgenic line capable of producing an inducible disruption of PCP signalling. The design and verification of this transgenic line as well as the experiments conducted and outcomes are described in the following sections.

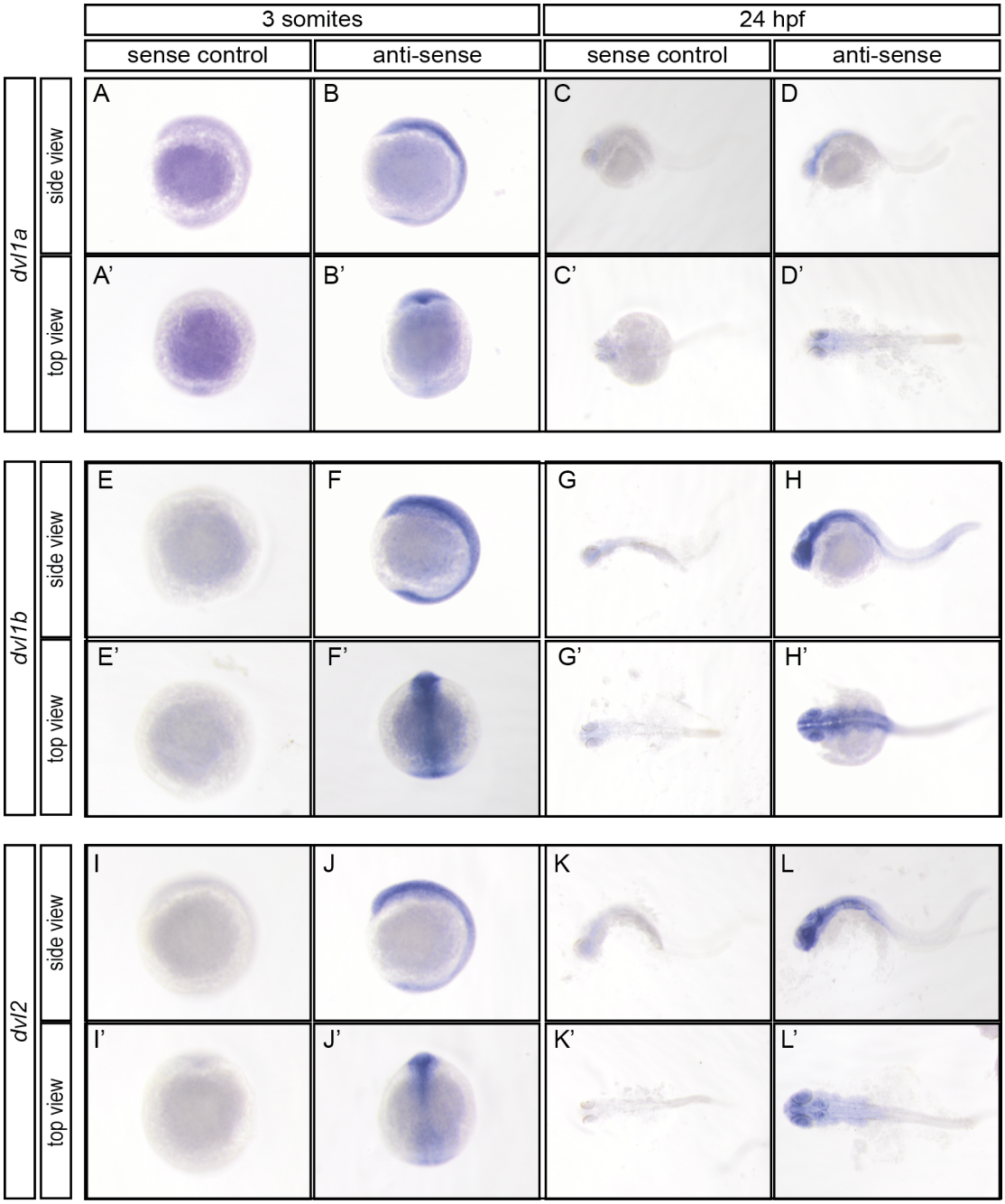
3 somites
24 hpf
sense control
anti-sense
sense control
anti-sense
dvl1a
side view
top view
dvl1b
side view
top view
dvl2
side view
top view
A
B
C
D
A'
B'
C'
D'
E
F
G
H
E'
F'
G'
H'
I
J
K
L
I'
J'
K'
L'

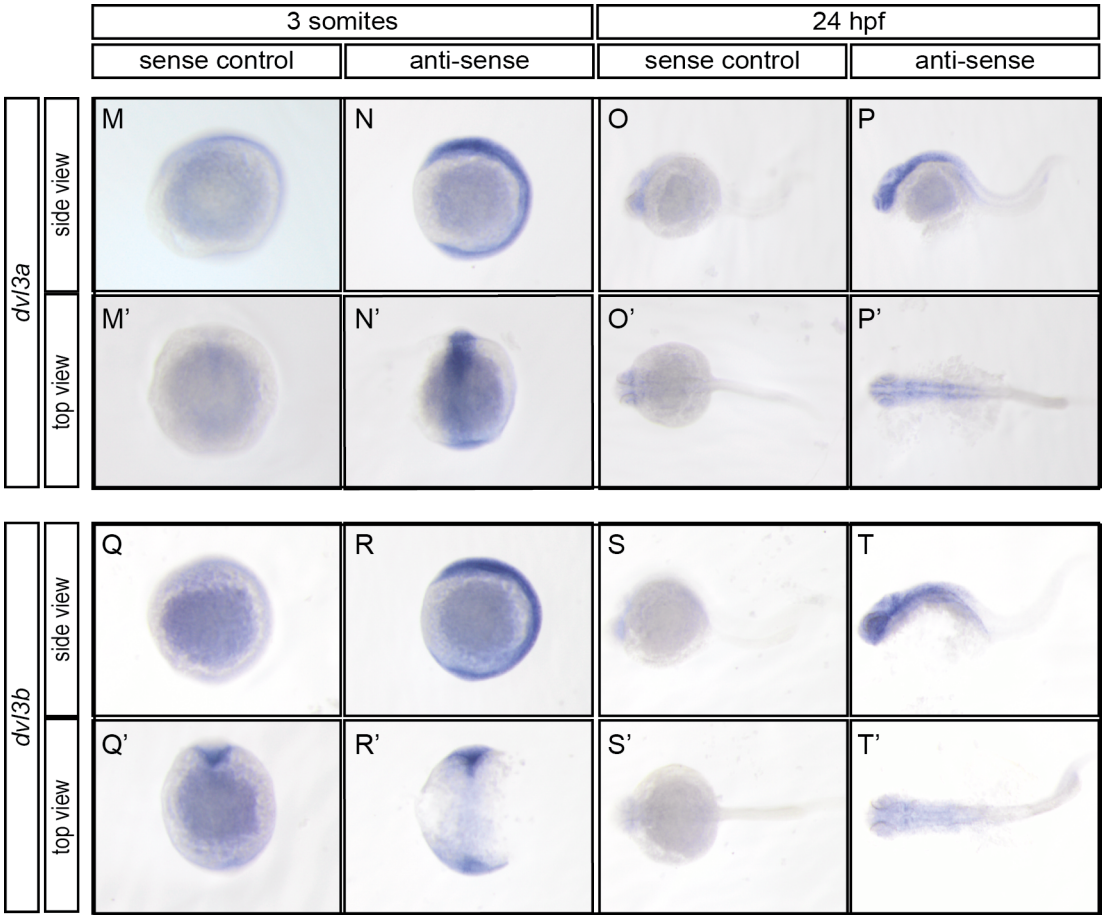

Figure 4.4 Spatial expression of zebrafish *dishevelled* gene family during development. *In situ* hybridisation of *dishevelled* gene expression at 3 somite and 24 somite stages during zebrafish development for *dvl1a* (B-B', D-D'), *dvl1b* (F-F', H-H'), *dvl2* (J-J', L-L'), *dvl3a* (N-N', P-P'), and *dvl3b* (R-R', T-T'). Sense control is also shown *dvl1a* (A-A', C-C'), *dvl1b* (E-E', G-G'), *dvl2* (I-I', K-K'), *dvl3a* (M-M', O-O'), and *dvl3b* (Q-Q', S-S'). See Appendix One for primers and probe sequences.

4.2.2.1. Construct design and HS western and insert mapping

In order to inhibit PCP signalling in a temporal manner I utilised a well documented dominant negative version of *Xenopus dishevelled-2* that has the DEP Domain and C-terminal domain deleted and replaced by *EGFP* to generate *XDshΔDEP-EGFP* (Sokol, 1996; Heisenberg et al., 2000; Rothbacher et al., 2000; Tada and Smith, 2000; Wallingford et al., 2000; Habas et al., 2001; Yu et al., 2010). I wished to generate a transgenic line in the background of the endodermal reporter line Tg(*sox17:EGFP*). To enable endodermal identification in the presence of *XDshΔDEP* over-expression I replaced the *EGFP* ORF with *mCherry* to generate *XDshΔDEP-mCherry*. Using the Tol2kit (Kwan et al., 2007) and Multisite gateway mediated recombination I constructed a Tol2-transgenesis vector that contained *XDshΔDEP-mCherry* under the control of a heat-shock promoter (*hsp70l*) (Figure 4.5 A). This construct was used to generate the stable transgenic line Tg(*hsp70l:XDshΔDEP-mCherry*).

Activation of transgene expression and inhibition of PCP signalling was achieved by subjecting Tg(*hsp70l:XDshΔDEP-mCherry*) embryos to a 1 hour heat shock at 37 **°C**. F_1 embryos subjected to a heat shock at shield stage resulted in *mCherry* positive embryos that displayed convergence and extension defects, phenocopying those seen in *tri* and *kny* mutant embryos at 24 hpf (Figure 4.6).
To determine an accurate time point for inhibition of PCP signalling after heat shock induction, a western blot was performed at various time points of heat shock activation. A poly dsRed antibody was used to detect the presence of protein. Protein is detectable at one hour after the initiation of a heat shock treatment and reaches its peak two hours after heat shock initiation (Figure 4.6 B). It was reasoned that at the time point of highest protein production would coincide with inhibition of PCP signalling, indicating that inhibition of PCP signalling could be inferred at two hours after initiation of the heat shock treatment.

The Tg(*hsp70l:XDshΔDEP-mCherry*) line was outcrossed to the endodermal reporter line Tg(*sox17:EGFP*) and raised for another generation. At this point it became evident that there were large variations in transgene

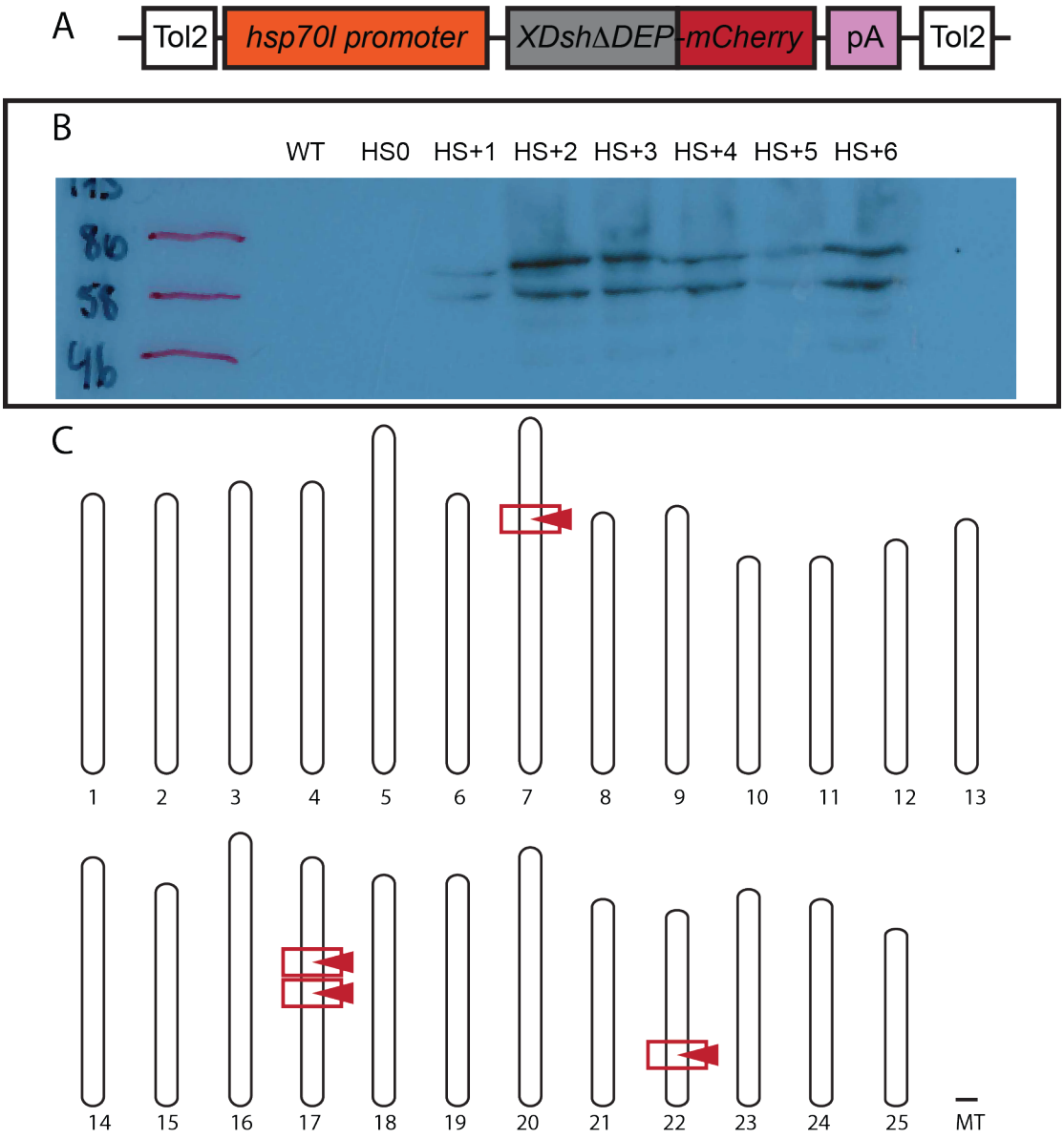

Figure 4.5. Generation of Tg(*hsp70l:XDshΔDEP-mCherry*) a stable transgenic line for heat-inducible disruption of PCP signalling. (A) Construct used to generate Tg(*hsp70l:XDshΔDEP-mCherry*) transgenic line. The dominant negative *dishevelled* gene *XDshΔDEP-mCherry* is under the control of the *hsp70l* heat shock promoter. **(B)** Western blot using polyclonal anti-dsRed against mCherry to detect XDshΔDEP-mCherry protein expression after heat shock induction. Times indicate hours since the start of heat shock induction. Red lines indicate position of ladder bands. The presence of two molecular weight bands is predicted to represent the un-glycosylated and glycosylated state of the XDshΔDEP-mCherry protein **(C)** Schematic of the mapped insertion sites in the genome of the stable transgenic line Tg(*hsp70l:XDshΔDEP-mCherry*).

expression levels in the F_3 embryos (as determined by *mCherry* levels using fluorescent dissecting microscopy after heat shock). At 24 hpf (after heat shock treatment at shield) embryos with high *mCherry* fluorescence displayed the convergence and extension phenotype, whereas embryos with low levels of *mCherry* expression were phenotypically wildtype (Figure 4.6 A-D). It has been demonstrated that transgenic lines generated with the Tol2 transposon mediated system tend to have numerous insertions into the genome (Parinov et al., 2004). It was reasoned that the differences in PCP disruption and *mCherry* expression seen in Figure 11A-D may be due to variations in transgene copy number. In the case of this transgenic it is a particular problem as there are five *dishevelled* genes in the zebrafish genome and their ubiquitous expression profiles makes it likely that high levels of dominant negative expression would be required to disrupt the PCP signalling pathway (Figure 4.4).

To determine the number of transgene insertions this line carried, the insertions were mapped in the F_2 parents as well as in the high and low expressing F_3 embryos using Thermal Asymmetric Interlaced PCR (TAIL-PCR)(Liu and Whittier, 1995) with primers optimised to Tol2 sequences (Parinov et al., 2004).

A total of five insertion events were detected, with four being successfully being mapped to genomic locations: chromosome 7, two on chromosome 17, and chromosome 22 (Figure 4.5 C). All four insertions were in intra-genic regions of the genome (Appendix One). The fifth insertion was unable to be mapped to a specific location as it had inserted into the genome in a Tol2-transposase independent manner, resulting in the retention of a proportion of the vector backbone and preventing accurate mapping using this method. Genotyping primers were generated for all five insertions and used to determine the number of insertions that PCP phenocopying and non- phenocopying 24 hpf embryos carried (after heat shock treatment at shield). Phenocopying embryos were found to carry a minimum of four copies of the transgene, whereas non-phenocopying embryos carried either three copies or less. This confirmed the suspicion that there is a threshold level of *XDshΔDEP-mCherry* expression required to successfully inhibit PCP signalling after heat shock treatment. The F_2

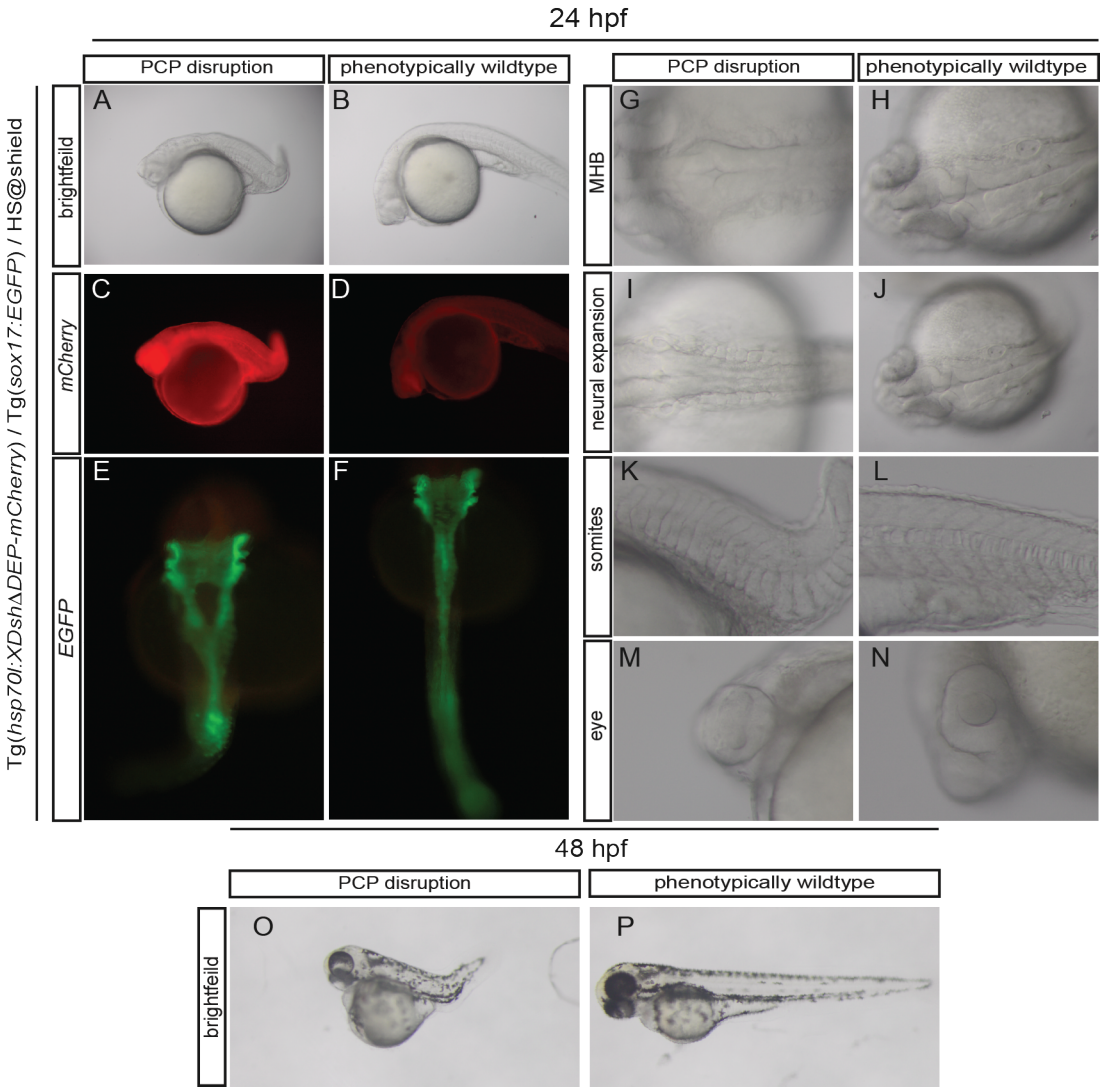

Figure 4.6. Inhibition of PCP signalling at gastrulation using the Tg(*hsp70l:XDshΔDEP-mCherry*) transgenic line. Tg(*hsp70l:XDshΔDEP-mCherry*)/Tg(*sox17:EGFP*) embryos were heat-shocked at shield stage to inhibit PCP signalling during gastrulation. Dissecting microscope images of PCP phenotypic and phenotypically wildtype embryos at 24 hpf (A-N) and 48 hpf (O-P).

parents were genotyped, and only carriers of four or more transgenes were incrossed to generate experimental embryos, and only embryos expressing high levels of *mCherry* after heat shock treatment were selected for further experimental analysis.

4.2.2.2. The Tg(hsp70l:XDshΔDEP-mCherry) line is capable of reproducing PCP mutant C&E phenotypes

To characterise the phenotype of a disruption of PCP signalling from *XDshΔDEP-mCherry* over-expression during gastrulation stages onwards, Tg(*hsp70l:XDshΔDEP-mCherry*)/Tg(*sox17:EGFP*) embryos were heat shocked at shield (here onwards referred to as *Hsp@shield*) and analysed at 24 hpf. Inhibition of PCP signalling caused defects in convergence and extension resulting in shorter, wider embryos (Figure 4.6 A), similar to that seen in the PCP mutant *tri* and *kny* mutant embryos (Section 3.2.1). Wildtype, *tri*, or *kny* heat shock control embryos did not demonstrate phenotypic defects from the heat shock treatment. The reduction in embryo length does not recover by 48 hpf (Figure 4.6 O). *Hsp@shield* embryos have short and wide somites that are less organised than controls (Figure 4.6 K); another characteristic of the PCP mutants *tri* and *kny* (Marlow et al., 1998). In 24 hpf *Hsp@shield* embryos the endoderm appeared to be disorganised, often containing a hole directly posterior to the pharyngeal endoderm (Figure 4.6 E). Inhibition of PCP signalling at gastrulation appeared to disrupt the formation of the midbrain-hindbrain boundary (MHB) (Figure 4.6 G) as well as cause an expansion of the neural tissues posterior to the MHB (Figure 4.6 I). A disruption in the formation of the retina was also observed (Figure 4.6 M). Overall *Hsp@shield* embryos appeared to have a similar phenotype as *tri* and *kny* single mutants. Low expressing embryos (as determined by *mCherry* fluorescence) were phenotypically wildtype in all morphologies analysed (Figure 4.6 B, D, F, H, J, L, N, P).

4.2.2.3. Determination of experimental stages to disrupt PCP signalling

To investigate if PCP signalling has a time specific role during endoderm morphogenesis three developmental time points were selected to disrupt PCP signalling using the Tg(*hsp70l:XDshΔDEP-mCherry*)/Tg(*sox17:EGFP*) line: gastrulation stages (shield stage); the 3 somite stage when the majority of endodermal cells have migrated towards the midline and are undergoing cell shape changes; and finally at the 7 somite stage, just prior to tail elongation and midline aggregation (Figure 4.7).

Firstly, shield stage was chosen (*Hsp@shield*) as it is the earliest time point that embryos can be subjected to a heat shock treatment without killing them. Heat shock treatment at shield stage disrupts PCP signalling during mid-gastrulation stages onwards (75 % epiboly) (Figure 4.7) and enables experimental conditions that can be compared directly to *tri* and *kny* mutant embryos.

Secondly, heat shock treatment at the 3 somite stage (here onwards referred to as *Hsp@3s*) disrupts PCP signalling just prior to the 7 somite stage. This time point was selected as the majority of convergence and extension is complete and the endoderm has migrated from the ventral regions forming an endodermal stripe along the midline, but has not yet begun to leave the monolayer. Disruption of PCP at this stage will allow any defects in endoderm morphology caused by early C&E defects to be bypassed revealing any time specific roles of PCP signalling in endodermal morphogenesis.

Finally, heat shock treatment at the 7 somite stage (here onwards referred to as *Hsp@7s*) disrupts PCP signalling at ~12 somites, prior to two important morphogenic events: 1) when the endodermal cells start leaving the monolayer, and 2) the when the tail begins to leave the yolk sac and start extending. Disruption of PCP at this stage will allow me to investigate potential time specific roles of PCP signalling during midline aggregation, as well as the effect of embryo tail extension on endodermal morphology.

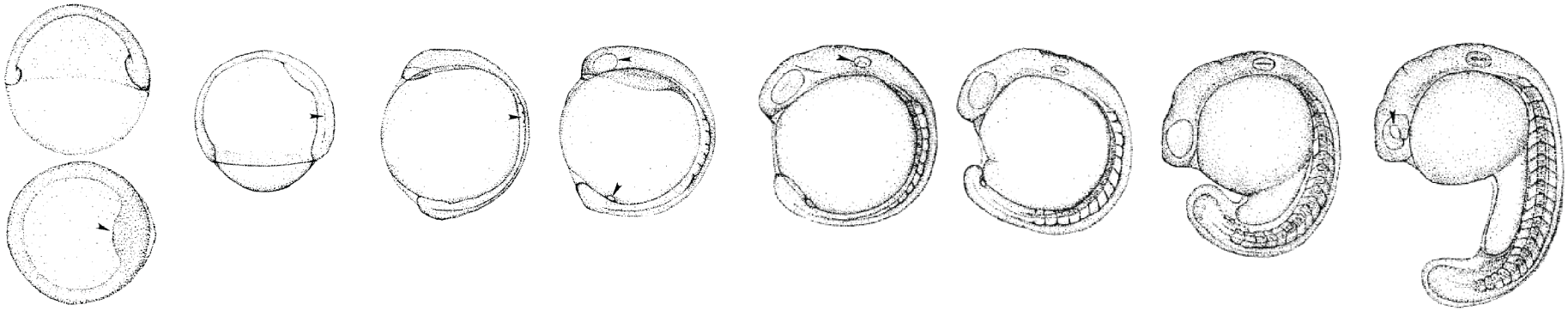

Shield
6 hpf

75% epiboly
8 hpf

3 - somite
11 hpf

6 - somite
12 hpf

10 - somite
14 hpf

14 - somite
16 hpf

18 - somite
18 hpf

21 - somite
19.5 hpf

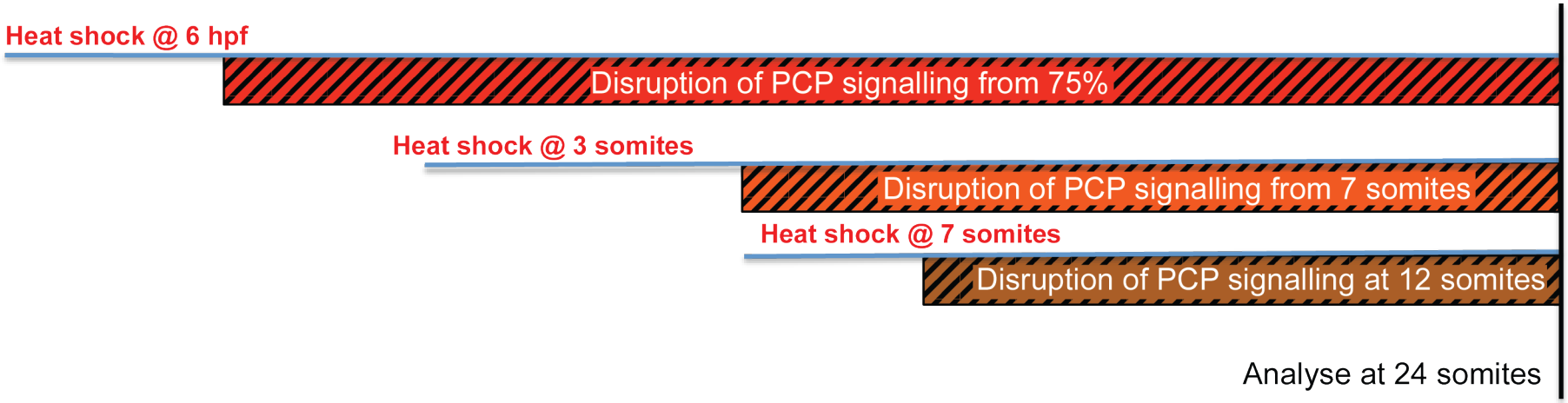

Figure 4.7. Schematic of heat-shock treatment timing. Three time points were chosen for heat shock treatment, shield stage to inhibit PCP signalling from gastrulation onwards, the 3-somite stage to inhibit PCP signalling from 7 somites onwards, and the 7-somite stage to inhibit PCP signalling from 12 somites onwards. Due to the delay in expression, maximum expression is expected 2 hours after heat shock treatment, and therefore the three time points were chosen to take this delay into account. Modified from Kimmel et al; (1995).

4.2.3. Time specific inhibition of PCP signalling pathway highlights the role of tail extension to drive endoderm thinning

To determine if disruption of PCP signalling during endodermal cell migration towards the dorsal midline results in a similar endoderm morphology phenotype as the PCP mutants *tri* and *kny*, endoderm width measurements were taken from confocal images of 24 somite vibratome sections of *Hsp@shield*, *Hsp@3s*, *Hsp@7s*, *tri* mutant, *kny* mutant, and wildtype embryos (Figure 4.8 A). *tri* and *kny* mutant embryos both have a significant increase in endodermal width, however *tri* mutants are not as severe as *kny* mutant embryos (Figure 4.8 A, blue and yellow bars). However the overall embryo width was not significantly different between these two mutants (Figure 4.8 E), suggesting differences in the role of these two genes in regulating embryo and endodermal width. Disruption of PCP signalling from gastrulation onwards (*Hsp@shield*) resulted in a significant increase in endodermal width (Figure 4.8 A, red bar), comparable to *kny* mutants (Figure 4.8 A, yellow bars).

Inhibition of PCP signalling during mid- and late-somitogenesis stages (*Hsp@3s* and *Hsp@7s* respectively) also resulted in a significantly wider endoderm (Figure 4.8 A, orange and brown bars). Surprisingly there was no difference in the severity of endodermal width increase when PCP signalling was inhibited at gastrulation stages or either somitogenesis stages.

To investigate if temporal inhibition of PCP signalling also results in an increase in endodermal cell number along the mediolateral axis as shown in *tri* and *kny* mutants (Figure 1.4), endodermal cell number was quantified from confocal images of vibratome trunk sections of heat shock treated embryos at 24 somites (Figure 4.8). Endodermal cell number is significantly higher in *Hsp@shield* embryos compared to wildtype controls (Figure 4.8 B Red bar). Similar to endodermal width, *Hsp@shield* embryos appeared to have larger cell numbers than *tri* mutants, similar to *kny* mutants, but because of the wider error bars (more variation) in the *Hsp@shield* it is not possible to distinguish amongst them statistically.

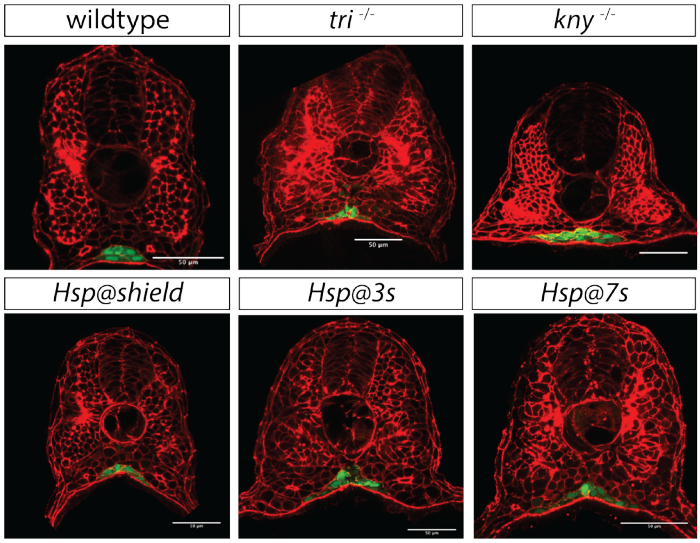

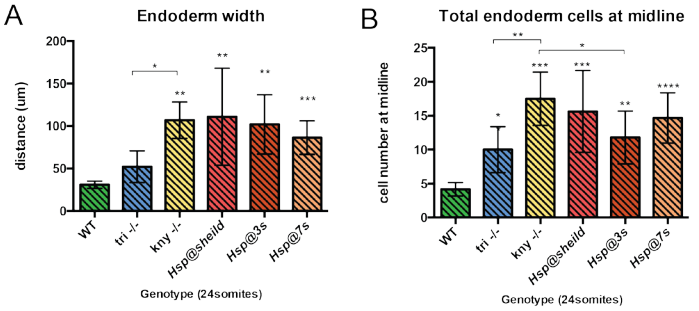

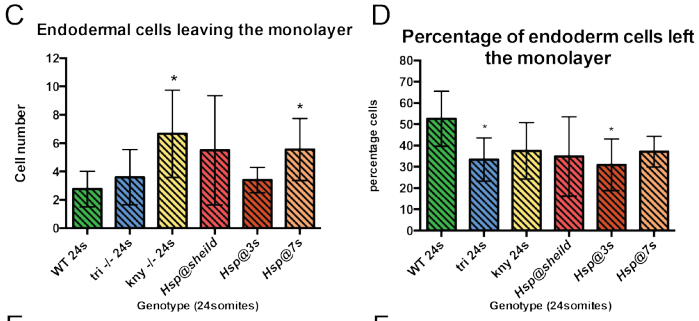

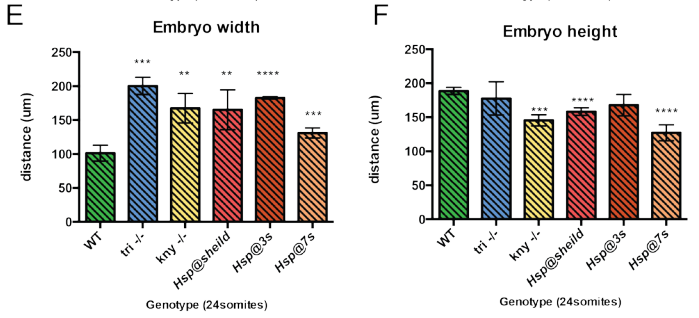

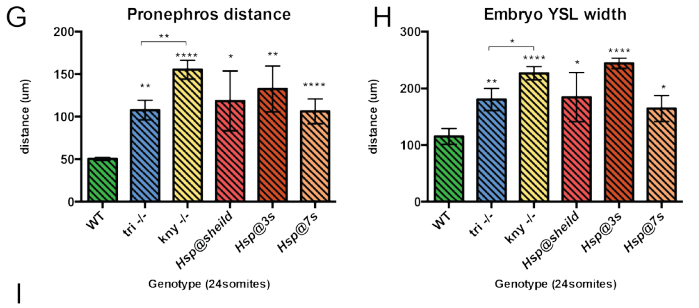

I

Genotype	wildtype	*tri*	*kny*	*Hsp@shield*	*Hsp@3s*	*Hsp@7s*
number of embryos analysed	9	3	4	8	5	9

Figure 4.8. Inhibition of PCP signalling during early development disrupts endoderm morphogenesis. Representative images of wildtype, *tr*i $^{-/-}$, *kny* $^{-/-}$, and Tg(*hsp70l:XDshΔDEP-mCherry*) embryos heat-shocked at either shield (*Hsp@shield*), 3 somites (*Hsp@3s*), or 7 somites (*Hsp@7s*) embryos analysed at 24 hpf. **(A-H)** Graphs of quantitative measurements of wildtype (green bars), *tr*i $^{-/-}$ (blue bars), *kny* $^{-/-}$ (yellow bars), and Tg(*hsp70l:XDshΔDEP-mCherry*) embryos heat-shocked at either shield (*Hsp@shield*)(red bars), 3 somites (*Hsp@3s*) (orange bars), or 7 somites (*Hsp@7s*) (brown bars). **(A)** Mean cell number of trunk endoderm sections at 24 somites. **(B)** Endodermal stripe width. Error bars represent SD. **(C)** Mean number of endodermal cells that have left the monolayer at 24 somites. **(D)** Percentage of endodermal cells that have left the monolayer at 24 somites. **(E)** Mean embryo width, measured at the centre level of the notochord. **(F)** Mean embryo height. Measured through the centre of the notochord. Error bars represent SD. **(G)** Mean distance between the pronephros ducts. Measured distance between the centres of the two pronephros ducts. Error bars represent SD. **(H)** Mean width of the YSL. Measured distance along the YSL to the edge of the mesoderm. **(I)** Number of embryos analysed per genotype. Error bars represent SD. Asterisk on single bars indicate a significant difference to wildtype values, tested using a unbiased two tailed T-test. Asterisk on lines indicate a significant difference between the two values. *p* values are as follows * = $p<0.01$. ** = $p<0.001$, ***=$p<0.005$, **** = $p<0.0001$

Inhibition of PCP signalling at either mid- or late-somitogenesis stages resulted in an increase in endodermal cell number (Figure 4.8 B, Orange and yellow bars). Interestingly there was no significant difference in mediolateral endodermal cell number between mid-, late-somitogenesis, or gastrulation stage inhibition of PCP signalling. These data together with the endodermal width data indicate that in the case of the endoderm PCP signalling is essentially dispensable during C&E movements, but is specifically required during mid-somitogenesis stages (12 somites onwards) for correct endodermal morphogenesis.

4.2.4. Effects of PCP signalling disruption during midline aggregation

In Chapter three I described that *tri* and *kny* mutant embryos have a reduction in the number of cells that leave the monolayer during midline aggregation (Section 3.2.3.2). In order to determine if *dvl*-dependent PCP signalling is required for endodermal cells to leave the monolayer, the number of cells that are no longer in contact with the YSL was determined in 24 hpf *Hsp@shield, Hsp@3s,* and *Hsp@7s* embryos. This results in an increase in the mean number of cells leaving the monolayer in *Hsp@shield* embryos, similar to the increase seen in *kny* mutants (Figure 4.8 C, green, yellow, and red bars). Although disruption of PCP signalling at 7 somites (*Hsp@3s*) appeared to cause a slight increase the mean number of cells, comparable to *tri,* this was not statistically significant (Figure 4.8 C, green, blue, and orange bars). Disruption of PCP signalling at 12 somites (*Hsp@7s*) also resulted in an increase in the mean number of cells leaving the monolayer similar to *kny* mutants (Figure 4.8 C, yellow and brown bars).

Although disruption of PCP signalling in *tri* and *kny* mutants and Tg(*hsp70l:XDshΔDEP-mCherry*) embryos resulted in an increased number of cells leaving the monolayer (Figure 4.8 C), these embryos also had wider endodermal stripes (Figure 4.8 A) and a higher number of cells along the mediolateral axis (Figure 4.8 B). Therefore I was interested in determining if the proportion of the total endodermal cells that leave the monolayer was affected by temporal inhibition of PCP signalling. *tri* mutant embryos showed a significant reduction in the proportion of the total endodermal cells that leave the monolayer (Figure

4.8 D, blue bar). *kny* mutants also appeared to show a reduction in the proportion of cells that leave the monolayer (although this not significant) (Figure 4.8 D, yellow bar). As expected the temporal disruption of PCP signalling at all three experimental heat shock time points results in a reduction in the overall proportion of endodermal cells leaving the monolayer similar to *tri* and *kny* mutants (Figure 4.8 D, red, orange, and brown bars).

4.2.5. The role of PCP signalling in early brain morphogenesis

4.2.5.1. A time specific role for PCP signalling during brain morphogenesis

To investigate the possible further uses of the Tg(*hsp70l:XDshΔDEP-mCherry*) transgenic in dissecting the time-specific requirements to PCP signalling, I investigated the role of the PCP signalling pathway in Midbrain-Hindbrain boundary (MHB) formation, as shown in Figure 4.6 G MHB morphology was analysed using bright field and confocal microscopy at 24 hpf as the MHB is developed and easily observed at this stage (Gutzman et al., 2008). Wildtype embryos display a clearly defined MHB at 24 hpf when viewed under bright field (Figure 4.9 A, B). Confocal imaging of flat mounted wildtype embryos clearly demonstrates the morphology of the forebrain, midbrain, and hindbrain vesicles (Figure 4.9 C); the shape and structure are emphasised in the schematic diagram (Figure 4.9 D). Maximum projection images of wildtype embryos demonstrate the highly organised morphological structure of the MHB at 24 hpf (Figure 4.9 E).

To investigate if PCP signalling is involved in correct MHB morphogenesis I analysed the MHB of *tri* and *kny* mutant embryos at 24 hpf. *tri* mutant embryos have a well-formed and defined MHB as seen under a dissecting microscope (Figure 4.9 F, G) and appear to be similar to wildtype controls. Confocal images of *tri* mutant heads appeared to have a slightly enlarged forebrain vesicle (Figure 4.9 H) and also displayed an opening between the midbrain and the forebrain that is not present in wildtype embryos (Figure 4.9 I). *tri* mutants appeared to have correct MHB folding: however, there is a disruption in the forebrain vesicle folding, resulting in a much larger overall forebrain morphology compared to

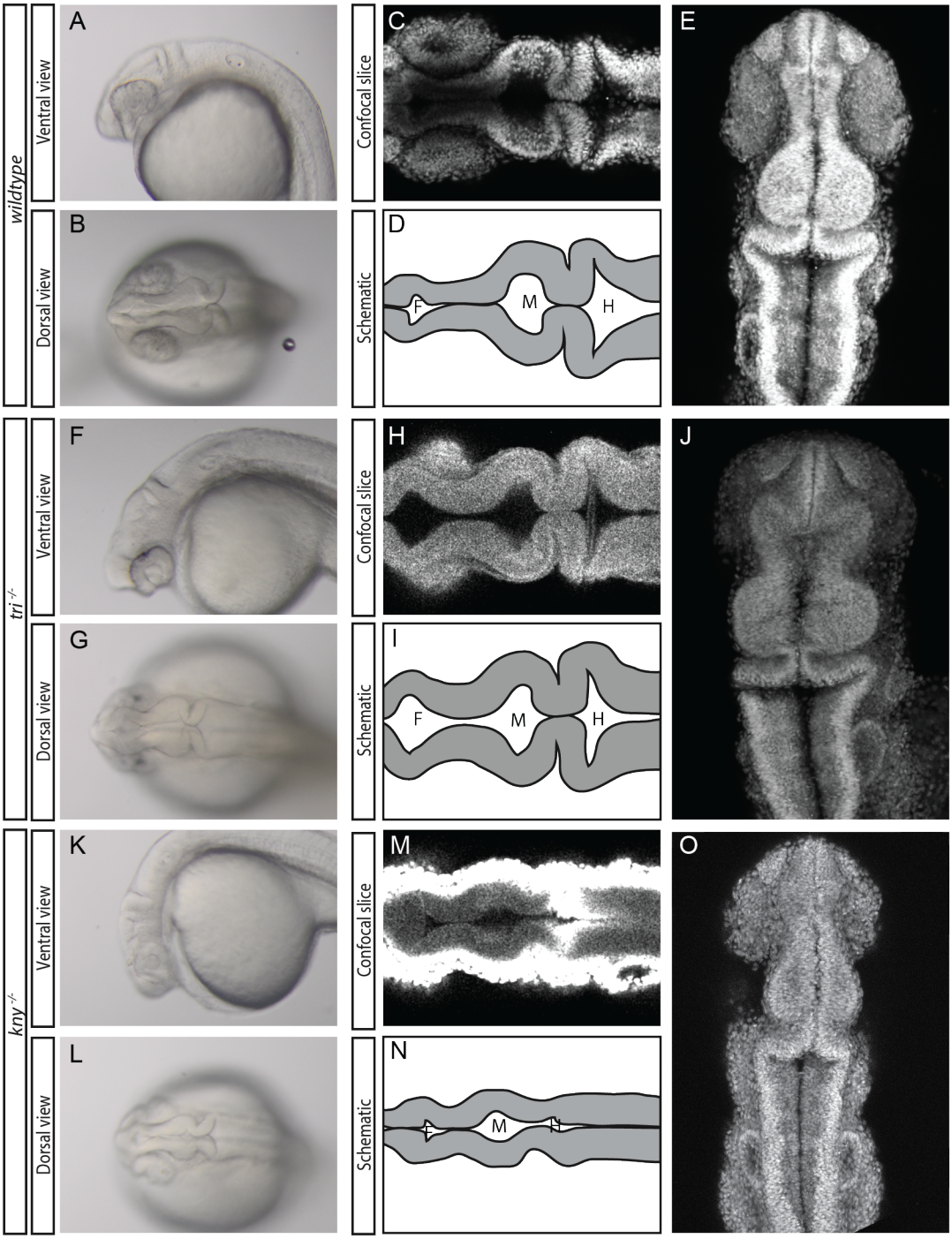
wildtype
tri-/-
kny-/-
Ventral view
Dorsal view
Confocal slice
Schematic
A
B
C
D
E
F
G
H
I
J
K
L
M
N
O
F
M
H

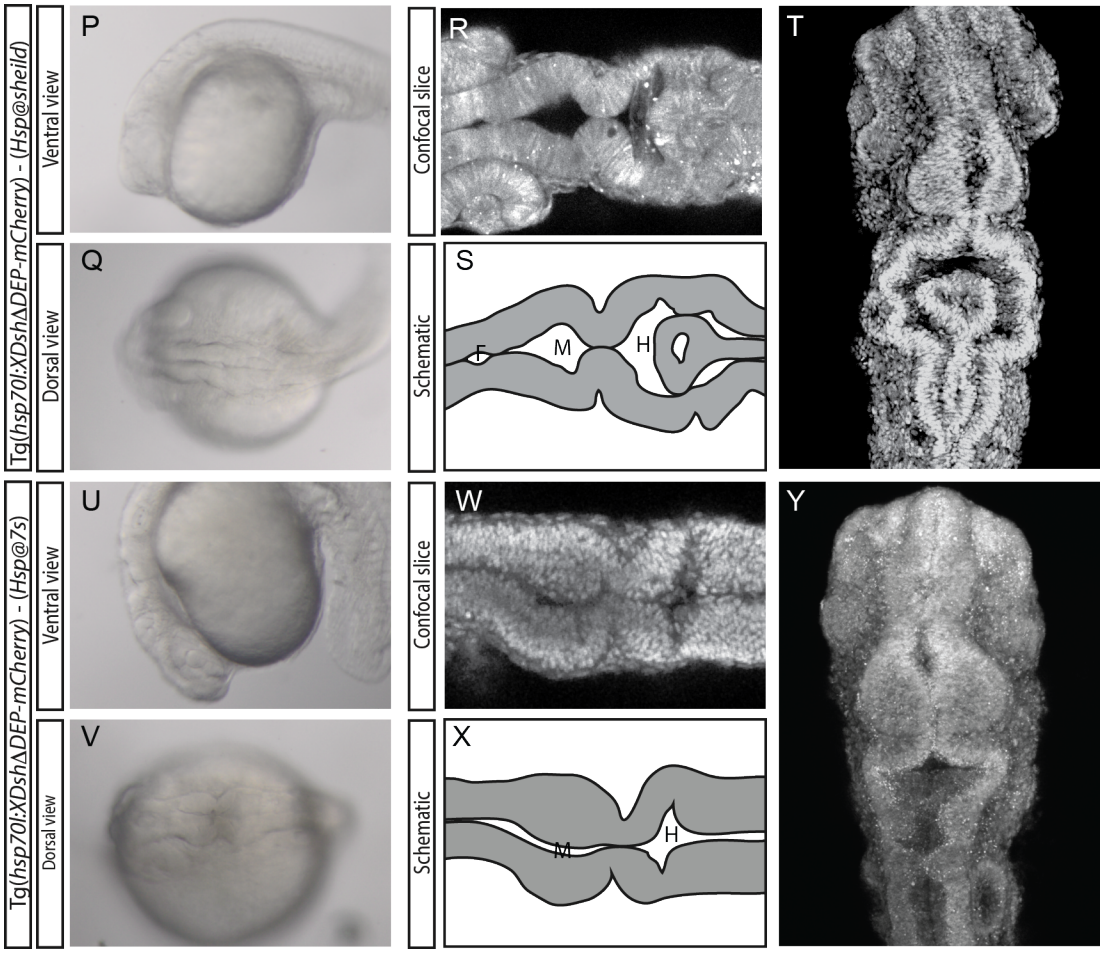

Figure 4.9. PCP signalling plays a role in Midbrain-Hindbrain Boundary formation. MHB formation of wildtype control embryos (A-E), *tri* mutant (F-J), *kny* mutant (K-O), Tg(*hsp70l:XDshΔDEP-mCherry*) (*Hsp@shield*) (P-T), and Tg(*hsp70l:XDshΔDEP-mCherry*) (*Hsp@7s*) (U-Y). Brightfield Images of control embryo MHB (A-B, F-G, K-L, P-Q, U-V). (C, H, M, R, W) Confocal slice showing the brain vesicles. (D, I, N, S, X) Schematic of brain vesicle shape. F, Forebrain vesicle. M, Midbrain vesicle. H, Hindbrain vesicle. (E, J, O, T, Y) Maximum projection image of the MHB and forebrain.

wildtype embryos (Figure 4.9 J). The MHB in *kny* mutants is clearly visible under a dissecting microscope (Figure 4.9 K, L), although it is not as defined as wildtype or *tri* mutant embryos (Figure 4.9 A, B, F, G). Confocal imaging identified that *kny* mutant embryos have reduced MHB folding and comparatively smaller midbrain, hindbrain, and forebrain vesicles (Figure 4.9 M, N), and the overall morphology of the *kny* mutant MHB is also smaller than wildtype (Figure 4.9 O). Inhibiting PCP signalling at gastrulation stages results in a poorly defined MHB with reduced folding under bright field microscopy (Figure 4.9 P, Q). Confocal imaging of *Hsp@shield* heads showed correct folding of the MHB, but identified an ectopic outgrowth within the vesicle of the hindbrain, and an expansion of the neural tube (Figure 4.9 R, S, T). Midbrain and forebrain vesicle size also appeared to be reduced compared to wildtype controls (Figure 4.9 S). Maximum projection imaging of *Hsp@shield* demonstrates a disruption of hindbrain morphology, likely due to the ectopic outgrowth of neural tissue within the hindbrain vesicle (Figure 4.9 T).

To determine if the hindbrain outgrowth phenotype identified in *Hsp@shield* embryos is a timing specific role of PCP signalling during brain formation, or results from an overall disruption of PCP signalling during early development, *Hsp@7s* embryos were analysed at 24 hpf. This time point for PCP signalling inhibition was chosen as it is prior to the initiation of MHB formation/folding at 17 hpf (16 somites) (Gutzman et al., 2008). Inhibition of PCP signalling prior to MHB folding resulted in the formation of a MHB that was observable under bright field microscopy, although it did not appear to be as clearly defined as in wildtype controls (Figure 4.8 U, V). Confocal imaging identified that the midbrain-hindbrain constriction is correctly formed (Figure 4.9 W, N), although all brain vesicle sizes are severely reduced (Figure 4.9 X). Maximum projection imaging identified that although the hindbrain tissue appears to be is slightly enlarged along the ventricle ridges (Figure 4.9 Y), there is no ectopic outgrowth inside the hindbrain ventricle space as seen in *Hsp@shield* embryos.

4.2.5.2. trilobite-independent PCP signalling is required for brain vesicle expansion

To quantify the changes in brain vesicle size from PCP signalling interruption observed in Figure 4.9 (D, I, N, S,), internal vesicle size measurements were taken from confocal slices, at the widest point of each of the forebrain, midbrain, and hindbrain vesicles (Figure 4.10). *tri* mutant embryos have an enlargement of both the forebrain and midbrain vesicles, but the hindbrain vesicle size is unaffected. Contrastingly, *kny* mutants*, Hsp@shield*, and *Hsp@7s* embryos have a reduction in the size of both the forebrain and midbrain vesicles compared to the wildtype controls (Figure 4.10). *kny* and *Hsp@7s* also have a reduction in the size of the hindbrain vesicle. *Hsp@shield* embryos do not have a reduced hindbrain vesicle size, possibly due to the ectopic tissue growth in the internal vesicle of the *Hsp@shield* hindbrain (Figure 4.9 T).

4.2.5.3. Early PCP signalling controls hindbrain tissue morphogenesis

To further investigate the ectopic hindbrain outgrowth identified in *Hsp@shield* embryos (Figure 4.9 P-T), vibratome sections were taken of wildtype controls and *Hsp@shield* embryos at the level of the hindbrain vesicle (Figure 4.11 A, B dotted line). Wildtype control embryos have a clearly formed hindbrain, with two ventral plains of tissue either side of the midline (Figure 4.11 C). Hindbrain sections of *Hsp@shield* embryos clearly show an ectopic duplication of hindbrain tissue (Figure 4.11 D). This ectopic tissue is separated from the surrounding tissue with respect to the basal membrane as determined by *Phalloidin* (F-actin) staining.

I previously observed a neural tube expansion in *Hsp@shield* embryos at 24 hpf under bright field (Figure 4.6 I) and confocal microscopy (Figure 4.9 T). To determine if the ectopic tissue overgrowth in the hindbrain extends down the length of the neural tube, vibratome sections were taken at the level of the first somite. Although the neural tube appears to be expanded compared to wildtype samples, the midline of the neural tube is clearly visible and there is no ectopic tissue growth or axis duplication (Figure 4.11 E, F). 11 out of 13 *Hsp@shield*

embryos display the ectopic hindbrain growth phenotype in Figure 4.11 G, indicating a high level of penetrance. The variation of hindbrain axis duplication is demonstrated in Figure 4.12.

4.2.5.4. A dvl-independent role of neural tube expansion in the somite region

tri (Tawk et al., 2007), maternal-zygotic *tri* (MZ*tri*) (Ciruna et al., 2006) and maternal-zygotic *scribble* (MZ*scribble*) mutants (Zigman et al., 2011) all have an expansion of the neural tube. To compare the neural tube expansion posterior to the brain regions of *tri* and *kny* mutants to *Hsp@shield* and analyse the roles of different components of the PCP signalling pathway during neural tube morphogenesis, vibratome sections were taken at the level of the first somite (Figure 4.13), as was used in these reports. These sections demonstrated that the neural tube axis duplication identified in *Hsp@shield* or *kny* mutants did not extend at the level of the first somite. Interestingly, this expansion of the neural tube in *tri* mutants did extend posteriorly into the somite region (Figure 4.13 F). These results indicate a *dvl*-independent role of *trilobite* in the somite region to regulate neural tube axis formation.

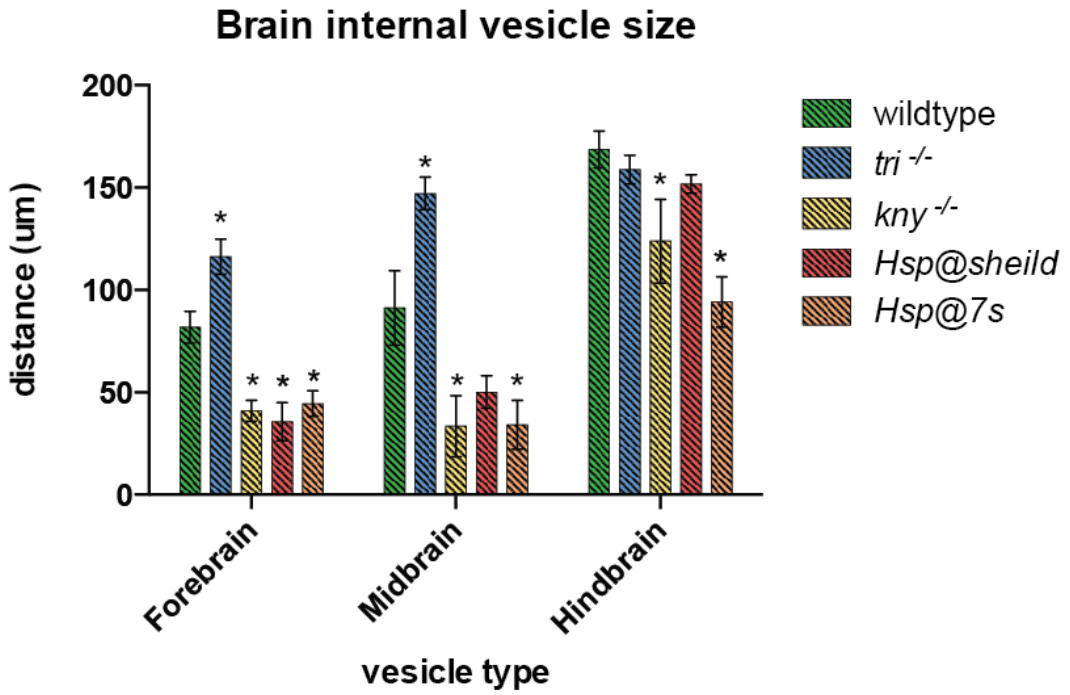

Figure 4.10. PCP signalling controls brain vesicle size. Internal Forebrain, Midbrain, and Hindbrain vesicle size was measured from confocal images of wildtype control, *tri* mutant, *kny* mutant, and Tg(*hsp70l:XDshΔDEP-mCherry*) heat shocked at shield (*Hsp@shield*) or 7 somites (*Hsp@7s*) embryos at 24 hpf. (n=3-4). Asterisk indicate a significant difference to wildtype, to $p<0.05$.

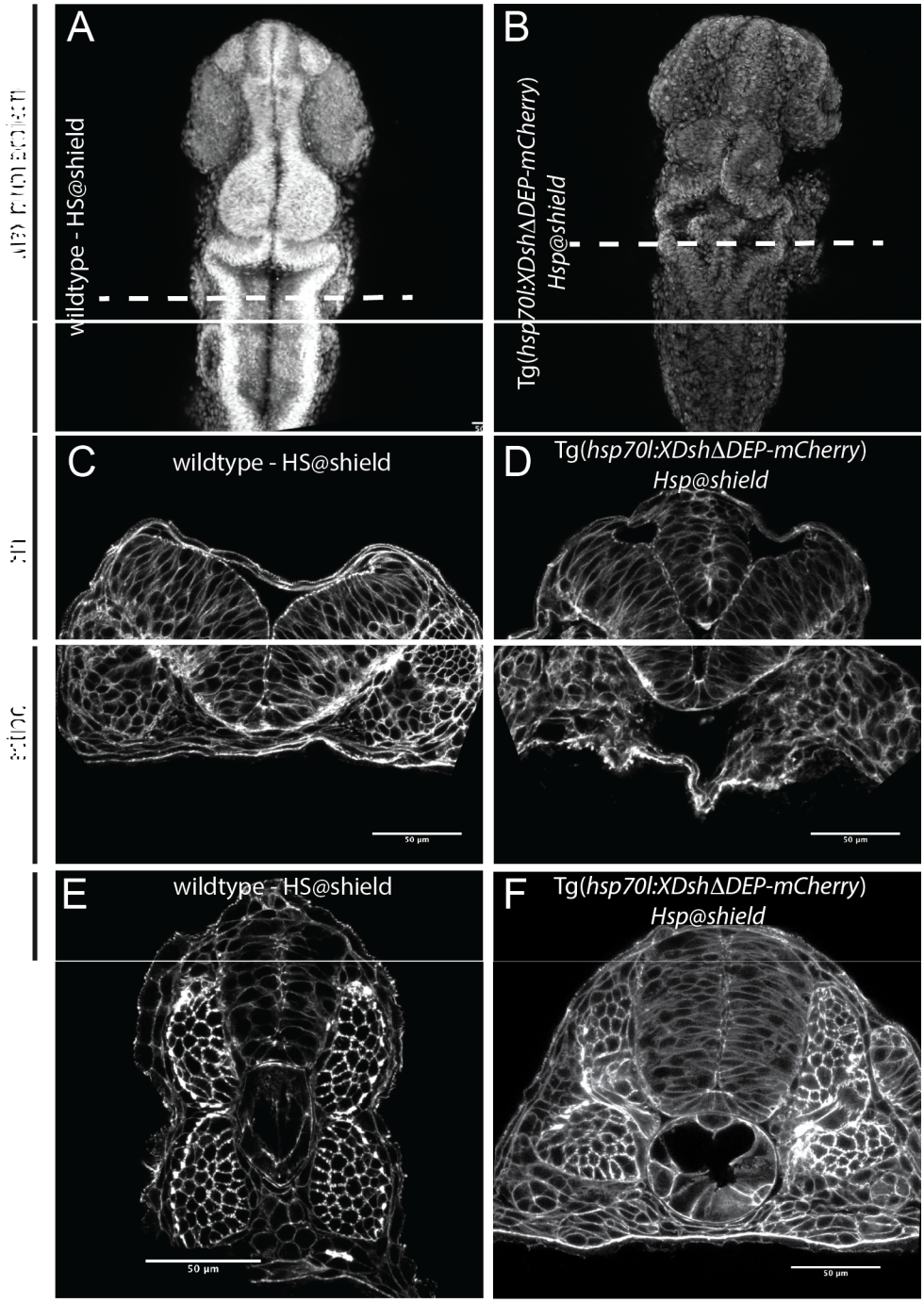

Figure 4.11. Dishevelled mediated control of Hindbrain tissue growth. Confocal images of wildtype heatshock controls and Tg(*hsp70l:XDshΔDEP-mCherry*)(Heat-shocked@shield) embryos at 24 hpf **(A-B)** Maximum projection image of MHB and forebrain in wildtype control embryos (A), and Tg(*hsp70l:XDshΔDEP-mCherry*)/Heat-shocked@shield embryos with ectopic hindbrain growth (B) at 24 somites. Stained with Hoechst 33342. Dotted line indicates the level of Hindbrain vibratome section. 11/13 embryos display this phenotype. Hindbrain section of wildtype control embryo **(C)** and Tg(*hsp70l:XDshΔDEP-mCherry*)/Heat-shocked@shield embryos with ectopic hindbrain tissue **(D)**. Vibratome sections at the level of the first somite in wildtype control embryos **(E)** and Tg(*hsp70l:XDshΔDEP-mCherry*)/Heat-shocked@shield embryos **(F)**. Vibratome sections stained with Rhodamine-Phalloidin. **(G)** Graph of the proportion of Tg(*hsp70l:XDshΔDEP-mCherry*)/Heat-shocked@shield that demonstrate Hindbrain tissue ectopic growth.

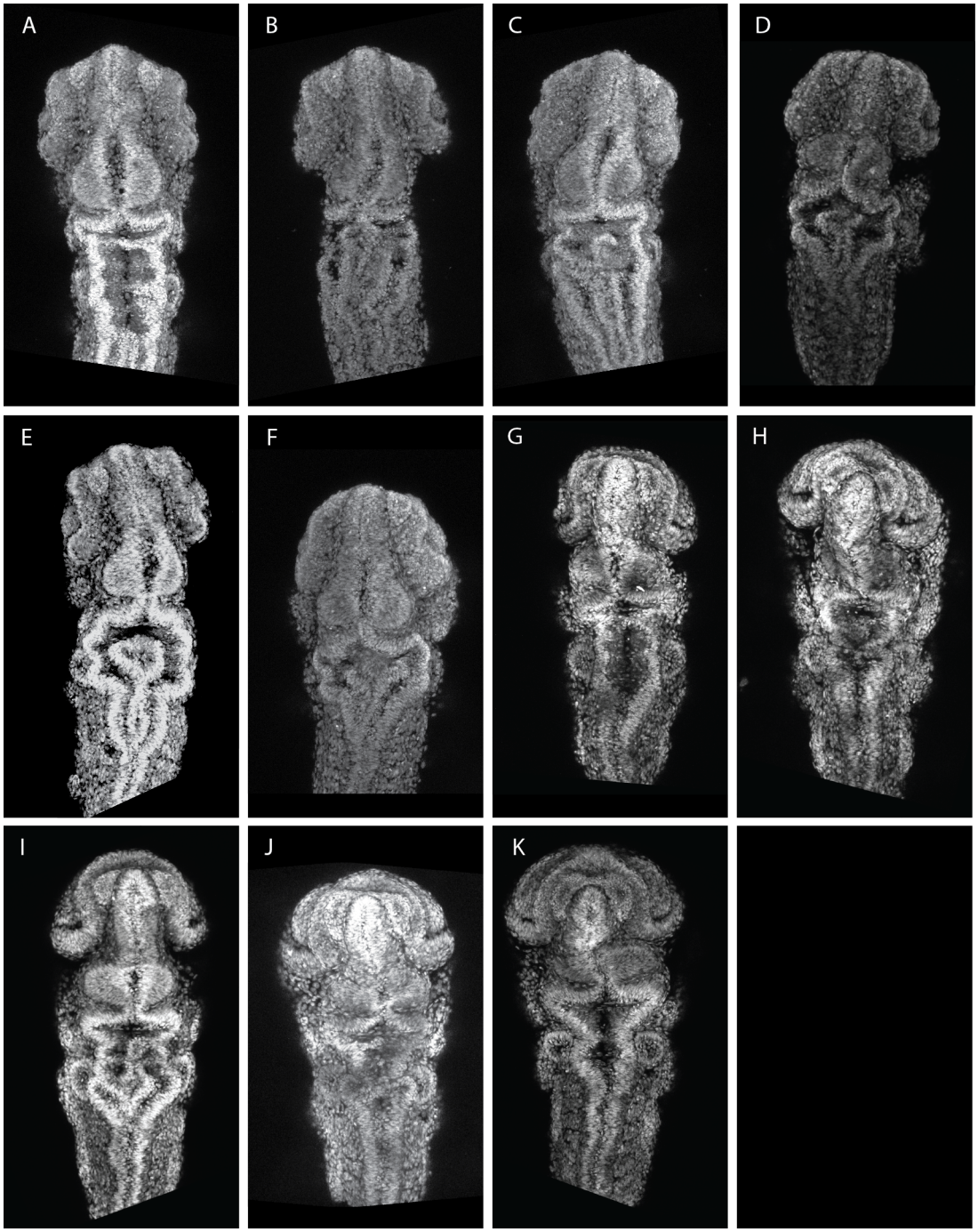

Figure 4.12. Brain morphogenesis phenotypes in Tg(*hsp70l:XDshΔDEP-mCherry*) *Hsp@shield* embryos at 24 hpf. (A-K) Confocal Maximum projection image of MHB and forebrain in Tg(*hsp70l:XDshΔDEP-mCherry*) *Hsp@shield* embryos with ectopic hindbrain growth at 24 somites. Stained with Hoechst 33342.

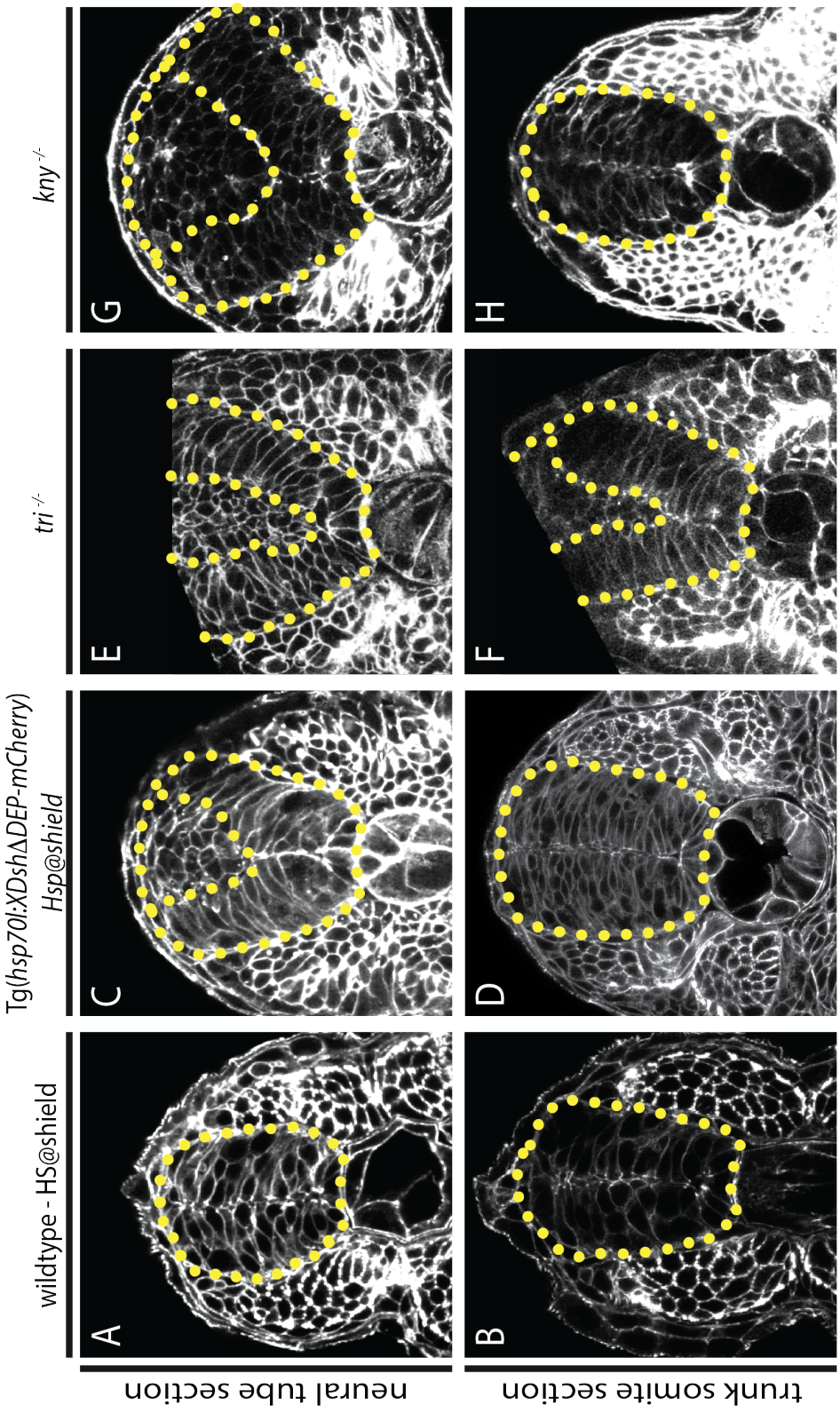

Figure 4.13. tri mutant embryos have a neural tube axis duplication that extends into the somite region. Confocal images of the neural tube and somite level vibratome sections of **(A-B)** wildtype control, **(C-D)** Tg(*hsp70l:XDshΔDEP-mCherry*)/*Hsp@shield*, **(E-F)** *tri* mutant, **(G-H)** and *kny* mutant embryos. *F-actin* labelled with Rhodamine-Phalloidin. Yellow dotted lines indicate the neural tube axis.

4.3. Discussion

4.3.1. Summary of results

In this study I aimed to investigate if the PCP signalling pathway is required in a time specific manner during endoderm development. This chapter describes the use of the dominant negative version of *dishevelled*, *XDshΔDEP-mCherry*, to generate a stable transgenic line capable of a heat-shock inducible disruption of PCP signalling. My results identified a role of PCP signalling during tail extension to drive correct endodermal morphogenesis. I was also able to identify a previously unknown time specific role of PCP signalling during hindbrain morphogenesis.

As I was expressing a *dishevelled* dominant negative during development, a secondary aim of this study was to expand on the current knowledge of the zebrafish *dishevelled* gene family in respect to protein homology, and expression patterns during development. Two members of this family, *dvl1a* and *dvl3b*, have not had any previous investigative data published to date. Phylogenetic analysis and *in situ* hybridisation was used to characterise zebrafish *dishevelled* genes during the first 24 hpf of development. My results show that all *dishevelled* family members are highly conserved at the amino acid level, and have early ubiquitous expression patterns.

4.3.2. The dishevelled gene family

4.3.2.1. Dishevelled protein structure and expression

The teleost genome duplication (Amores et al., 1998) resulted in zebrafish having five *dvl* gene family members (*dvl1a*, *dvl1b*, *dvl2*, *dvl3a*, and *dvl3b*), compared to three in both mouse (*Dvl1*, *Dvl2*, and *Dvl3*) and humans (*DVL1*, *DVL2*, and *DVL3*) (KEGG, 2014a; KEGG, 2014c; zfin.org, 2014a). Although zebrafish have an increased number of *dvl* genes, members of this family have been highly conserved throughout evolution and display a high level of conservation in both the protein structure (Figure 4.2), and residues within

domains (Table 2). This indicates a strong selective pressure against functional specialisation of individual dvl genes.

Although numerous *dishevelled* mutation/truncation studies have been undertaken in multiple model organisms, including *Drosophila*, *Xenopus*, zebrafish, and mice (Yanagawa et al., 1995; Sokol, 1996; Semenov and Snyder, 1997; Axelrod et al., 1998; Heisenberg et al., 2000; Rothbacher et al., 2000; Tada and Smith, 2000; Wallingford et al., 2000; Habas et al., 2001; Wharton, 2003; Angers et al., 2006; Yu et al., 2010), the full functional significance of each Dvl domain has not been determined. As well as mediating PCP signalling, *dishevelled* also participates as the mediator of β-catenin signalling (Yanagawa et al., 1995; Sokol, 1996). My results identified a high level of conservation of both the Dishevelled domains required for PCP signalling or β-catenin signalling (Figure 4.2). This indicates a strong selective pressure for each individual *dvl* gene to function in both Wnt signalling pathways rather than specialising in a specific pathway.

My results demonstrate that all members of the *dvl* gene family have an overlapping expression pattern during the first 24 hpf of development in zebrafish (Figure 4.4). This suggests that individual genes are required and have overlapping functions during development. Previous studies have demonstrated that often morpholino knockdown of single *dvl* genes (*dvl1b* or *dvl3a*) do not result in phenotypic abnormalities during early development, while simultaneous knockdown of genes (*dvl2* and *dvl3a*) result in embryo elongation defects (Angers et al., 2006; Segalen et al., 2010; Lum et al., 2011). This demonstrates that *dvl* genes have a redundancy between different family members. My results showing the overlapping and ubiquitous expression patterns of *dvl* genes support these conclusions. Overall it can be concluded that *dvl* gene family members are functionally redundant during development.

4.3.2.2. Domain conservation of dishevelled members

The Dishevelled DEP domain is specifically required for PCP signalling. It is the site of phosphorylation that is essential for translocation to the membrane and internalisation of the Frizzled-Dishevelled (Fzd-Dvl) complex (Axelrod et al.,

1998; Rothbacher et al., 2000; Wallingford et al., 2000). My results show that the DEP domain has high residue conservation between different orthologue groups, and within homologues (Table 2). This suggests that all five *dvl* genes are capable of participating in PCP signalling. Although it is possible that variations in this domain may translate to differences in downstream PCP signalling actions between different *dvl* genes.

The conserved C-terminal domain of Dishevelled has been overlooked in early investigations into Dvl function, with most studies focusing on the PDZ, DIX, or DEP domains. Deletion screens assessing the function of the DEP domain often utilise a truncated form of *Dvl* missing both the DEP and C-terminal domains (Sokol, 1996; Axelrod et al., 1998; Heisenberg et al., 2000; Rothbacher et al., 2000; Tada and Smith, 2000; Wallingford et al., 2000; Habas et al., 2001; Yu et al., 2010). The significance of this domain in either β-catenin signalling or PCP signalling has not been fully determined, however it has been shown to bind *Klhl12*, an inhibitor the Wnt signalling pathway that regulates Dvl degradation (Angers et al., 2006). Interestingly my results show that the C-terminal domain of zebrafish Dvl has a lower amino acid conservation compared to that of the PDZ, DIX, and DEP domains (Table 2).

The *dishevelled* specific domain has also been overlooked in the early functional truncation studies. This domain has the lowest level of residue conservation of all five dishevelled domains (Table 2). The function of this domain is unknown at present, but the fact that this domain is the only domain that has been subjected to divergence (even within groups) is intriguing. It would be interesting to investigate the role of this domain in the regulation of PCP signalling. Although there has been no investigations yet, It is possible that residue variations within the C-terminal domain, and the *dishevelled* specific domain (as well as the other domains) may allow different *dishevelled* genes to have altered affinities to binding partners, or preferential activation of one of the numerous downstream pathways.

Dishevelled has been shown to both form homodimers (Rothbacher et al., 2000) and heterodimers (Angers et al., 2006). There is no evidence yet but if each *dishevelled* homologue has differential affinities for binding partners, it is easy to speculate that each different Dishevelled heterodimer combination may

have different downstream reactions to the same induction signal. It its also possible that different Dishevelled complexes have different preferences for particular intracellular localisations. As *dvl* genes are partially redundant, a type of differential homo- or hetero-dimer Dishevelled regulation would not be unexpected due to the following three lines of evidence. Firstly, my results show that all *dishevelled* genes have overlapping and ubiquitous expression patterns. Secondly, morpholino knockdown studies against single *dvl* genes often have little effect until multiple *dvl* genes are knockdown (Angers et al., 2006). Thirdly, multiple members of the PCP signalling pathway have been shown to form both homo- and heterodimers; including Trilobite (Belotti et al., 2012), Flamingo (Chen et al., 2008) and Fizzled (Carron et al., 2003; Kaykas et al., 2004; Junge et al., 2009). Taken together these results suggest that dishevelled may have the ability to regulate PCP signalling through different dimer formation. However, I expect that future investigations elucidating the roles of different homo- and hetero-dimeric PCP components will be complex.

Overall it can be concluded that individual *dishevelled* genes are fully functionally redundant and under a high selection pressure to function in both the PCP signalling pathway, and the β-catenin signalling pathway.

4.3.3. PCP signalling during endodermal midline aggregation

In chapter three I described the morphogenic movements during endoderm midline aggregation and how the PCP mutants *tri* and *kny* have a reduction and delay in the number of cells leaving the monolayer (Section 3.2.3.2). In this Chapter I expanded investigations into the role of PCP signalling in a time specific manner during midline aggregation. To investigate the time specific effects of PCP signalling, I used the Tg(*hsp70l:XDshΔDEP-mCherry*) transgenic line I generated to disrupt PCP signalling at various points during endoderm morphogenesis.

Temporal disruption of PCP signalling at the three stages I investigated using Tg(*hsp70l:XDshΔDEP-mCherry*) resulted in endodermal width and cell number defects that closely resemble those seen in *kny* mutants (Figure 4.8 A, B). Interestingly my data also shows a difference in the severity of endodermal

width and mediolateral cell number between *tri* and *kny* mutants (Figure 4.8 A, B). One possible explanation for the difference in endodermal defect severity between the two PCP mutants and the Tg(*hsp70l:XDshΔDEP-mCherry*) experimental embryos is the effect of maternally deposited wildtype mRNA within *tri* mutant embryos partially compensating for the loss of function during early development. MZ*tri* obtained through germ-line replacement lack maternally deposited wildtype mRNA within the oocyte and display a more severe C&E, and neural defects than zygotic *tri* mutants (Ciruna et al., 2006). Contrastingly, MZ*kny* obtained from fertile RNA-rescued adults, do not display an increase in convergent extension defects (Topczewski et al., 2001), indicating that maternal *knypek* mRNA does not play a role in the regulation of C&E movements. PCP signalling disruption from *XDshΔDEP-mCherry* expression overrides any possible maternal *dvl* component. Overall, this suggests that PCP disruption via the Tg(*hsp70l:XDshΔDEP-mCherry*) line represents a complete inhibition of the *dvl*-dependent branch of PCP signalling, and is therefore a valuable tool for examining the role of PCP in developmental processes.

4.3.3.1. A possible localised signal to leave the monolayer

A major aim of this project was to determine if PCP signalling had a role in the regulation of endodermal cells to leave the monolayer during midline aggregation. Disruption of PCP signalling via *XDshΔDEP-mCherry* overexpression from gastrulation stages onwards did not prevent endodermal cells from leaving the monolayer. This data, taken together with the data obtained from *tri* and *kny* mutant embryos (Section 3.3.3), did not identify a conclusive requirement of PCP signalling for endodermal cells to leave the monolayer.

However, I have shown that the *tri* and *kny* mutants, as well as a disruption of PCP signalling at various stages during somitogenesis, result in embryos that are morphologically wider than wildtype embryos at 24 hpf, and that these embryos have more cells leaving the monolayer despite the overall percentage of cells being slightly lower. It is interesting to note that the cells that leave the monolayer are always at the midline in the region of the notochord rather than on the edges of the endodermal stripe (Figure 4.8 and Section 3.2.3).

If the cue to leave the monolayer was autonomous to the endoderm it would be expected that the cells would leave the monolayer along the entire width of the endodermal stripe. However my data does not support this idea. If the surrounding tissues provide the cue to the endoderm it would be expected that wider embryos would result in a wider signalling region, in turn stimulating more endodermal cells to leave the monolayer but still only within a defined region. My data support this idea as *tri* mutant, *kny* mutant, and Tg(*hsp70l:XDshΔDEP-mCherry*) heat-shocked embryos are wider overall than wildtype, and have an increased number of endodermal cells that leave the monolayer, but only within an area restricted to under the notochord. Taken together these two results indicate there is an external signal at the midline, possibly from the surrounding mesoderm to dictate the region of endodermal cells that can leave the monolayer. A similar situation has been shown at later stages during liver organogenesis, where signals from the surrounding mesodermal tissues are required for correct endodermal morphogenesis (Niu et al., 2010).

Unfortunately I was unable to separate the process of the endodermal cells leaving the monolayer, and the increase in endodermal width observed in the PCP mutants via temporal disruption of PCP signalling. This suggests interdependence between these two processes. Therefore from these results it can be concluded that PCP signalling does not have a autonomous role in the regulation of the endodermal cells in leaving the monolayer, but rather suggests that the disruption of PCP signalling at stages earlier than when endodermal cells are leaving the monolayer results in wider embryos, which in turn have a wider signalling region from the surrounding mesoderm, that causes an increase in the number of endodermal cells that leave the monolayer. Overall this suggests that the tissue surrounding the endoderm promotes cells to leave the monolayer, and dictates the region in which this can occur.

4.3.3.2. Embryonic tail extension and its role during endoderm morphogenesis

In chapter three I demonstrated that *tri* and *kny* mutants have an increase in overall endodermal width (Section 3.2.2). In this study I quantified the number of endodermal cells in these mutants. An interesting observation to note is that the increase in mediolateral endodermal cell number in *tri* and *kny* mutants appears to increase in severity at the point where the tail would normally leave the yolk and begin to extend (Figure 4.8 A). This morphogenetic event is severely reduced in *tri* and *kny* mutants, resulting in a shorter embryo.

In order to investigate a potential time specific role of PCP signalling in endoderm morphogenesis during tail-bud extension, I generated and used the Tg(*hsp70l:XDshΔDEP-mCherry*) transgenic line to disrupt PCP signalling at 12 somites, just prior to when the tail bud leaves the yolk and begins to extend at 14 somites. Under these conditions the specific role of tail extension on endoderm morphology could be analysed, bypassing any potential defects caused by PCP signalling disruption during earlier C&E movements. Inhibition of PCP signalling at 12 somites (*Hsp@7s*) resulted in an increase in endodermal width and mediolateral cell number similar to that of *kny* mutants (Figure 4.8 A, B). This result is particularly interesting, as *Hsp@7s* embryos have undergone the majority of C&E movements prior to the disruption of PCP signalling (Figure 4.7). These results suggest that during early convergence and extension movements PCP signalling plays a minor role in regulating overall endodermal width, and raises the possibility that tail extension and elongation may have a significant role in thinning the endoderm.

It is also interesting to note that loss of *kny* and inhibition of PCP signalling at all three heat shock treatment time points result in an endoderm that is wider than *tri* mutants (Figure 4.8 A). My results demonstrating a difference between *tri* mutants and both *kny* mutants and *Hsp@7s* embryos, support previous evidence that shows *tri* also acts in a *dvl*-independent manner (Jessen et al., 2002; Chen et al., 2008; Wu and Mlodzik, 2008; Gao et al., 2011; Torban et al., 2012). Overall these results suggest that *tri* has a *dvl*-independent role in the regulation of endodermal morphogenesis during somitogenesis

stages. However, to determine the full significance of this will require analysis of MZ*tri* mutant embryos. Future experiments using transgenic lines utilising a *trilobite* dominant negative (Pan et al., 2013) might address these questions.

Although both *tri* and *kny* mutants display convergence and extension defects during somitogenesis stages, both proteins have been shown to be dispensable for convergent cell migration during midgastrulation in the lateral mesendoderm (Sepich et al., 2005). Similarly, in chapter 3 my results demonstrated the overall rate of endodermal cell migration towards the dorsal midline in endodermal cells during C&E stages is unaffected in *tri* and *kny* mutant embryos (Section 3.2.2). I have also shown that disruption of PCP signalling after gastrulation and C&E stages at either 7 somites or 12 somites when the majority of convergent cell migration has occurred, results in a similar embryo width (and mediolateral endodermal cell number) to both the *tri* and *kny* mutant embryos at 24 hpf (Figure 4.8 E). These results demonstrate that PCP signalling is dispensable for convergent cell migration in both the mesoderm and endoderm, but is required for overall C&E movements. Overall these results suggest that the C&E defects of *tri* and *kny* mutants may in part result from a reduction in anterior-posterior cell migration causing reduced embryonic extension, which in turn results in wider embryos that appear to be a result of reduced convergence.

4.3.4. A PCP signalling role during brain morphogenesis

4.3.4.1. Disruption of PCP signalling affects brain morphogenesis

My results demonstrate that the *dvl* genes are highly expressed in the brain at 24 hpf (Figure 4.4). *trilobite* is highly expressed in the brain and neural tube from somitogenesis stages onwards (Park and Moon, 2002). *knypek* is expressed in the developing somites at the 16 somite stage, becoming restricted to the midbrain-hindbrain boundary at 48 hpf (Topczewski et al., 2001), but specific expression data for *knypek* at 24 hpf is currently lacking. In order to maximise the Tg(*hsp70l:XDshΔDEP-mCherry*) transgenic line to full effect I investigated the effect of PCP signalling disruption at various time points on brain

morphogenesis. My data indicates that *tri* and *kny* mutants have contrasting roles in the regulation of forebrain and midbrain vesicle expansion, with *tri* mutants having increased vesicle sizes, and *kny* having reduced vesicle sizes (Figure 4.10). Temporal disruption of PCP signalling during gastrulation (*Hsp@shield*) and somitogenesis stages (*Hsp@7s*) closely resembles *kny* mutants in respect to the forebrain and midbrain vesicle size (Figure 4.10). These results suggest that although *tri* is highly expressed in the brain, it is dispensable for the initial stage of brain vesicle expansion, but is required to regulate the correct amount of vesicle expansion. These results also indicate that *kny* and *dvl* and required specifically for the inflation of the brain vesicles. Together this indicates a differential requirement for PCP components during brain vesicle expansion, with a *dvl*-dependent role in vesicle expansion, and a *dvl*-independent role in regulating the level of vesicle expansion. It would be interesting to examine brain vesicle sizes in *tri*/*kny* double mutants, as well as MZ*tri* mutants, to determine if the contrasting effects of the single mutants on brain vesicle expansion are cancelled out, or compounded.

Disruption of PCP signalling from gastrulation onwards (*Hsp@shield*), but not after the 12 somite stage (*Hsp@7s*), results in a duplication of the hindbrain axis (Figure 4.9 T, Y, and Figure 4.11 B, F). This hindbrain axis duplication was not observed in *tri* or *kny* mutants (Figure 4.9 J, O). These results demonstrate a time specific *dvl*-dependent, but *kny*-independent role of PCP signalling prior to 12 somites in the regulation of hindbrain axis morphogenesis. PCP signalling is known to regulate neural tube and neural keel axis morphogenesis by controlling cell re-intercalation across the midline after cell division. *tri* (Tawk et al., 2007), MZ*tri* (Ciruna et al., 2006) and MZ*scribble* mutants (Zigman et al., 2011) display an ectopic neural tube axis duplication that results from a loss of mirror-symmetric cell division, where the two daughter cells of a cell division do not correctly re-intercalate across the dorsal midline. However, in all PCP mutants and morphants investigated to date anterior hindbrain axis defects have not been reported. The ectopic hindbrain axis in *Hsp@shield* embryos is morphologically similar to the duplicated neural tube axis in MZ*tri* (Ciruna et al., 2006), MZ*scribble* (Zigman et al., 2011), and *tri* (Tawk et al., 2007) in respect at the axis duplication occurring at the midline. This suggests by inference that the

ectopic hindbrain axis tissue in *Hsp@shield* embryos likely results from aberrant cell re-intercalation after cell division. In *tri*, MZ*tri,* and MZ*scribble* mutants it has been proposed that a delay in the formation of the neural keel, from a reduction in convergence, is responsible for the mirror-symmetric divisions across the neural plate rather than from downstream PCP signalling defects (Ciruna et al., 2006; Tawk et al., 2007; Zigman et al., 2011). Importantly the hindbrain axis duplication in *Hsp@shield* cannot be solely due to a delay in convergence as suggested by Tawk et al., (2007) as *tri* and *kny* mutant embryos also have a similar increase in embryo width (Figure 4.8), yet do not display hindbrain axis duplication. This indicates that *dvl* has a novel and time specific role in the regulation of hindbrain axis morphogenesis, and this is independent of *tri* and *kny*. It would also be intriguing to examine if the *tri/kny* double mutant embryos also have defects in hindbrain morphogenesis.

tri is known to have a duplication of the neural tube (Ciruna et al., 2006; Tawk et al., 2007). I also observed a duplication of the neural tube axis in *kny* mutants and *Hsp@shield* embryos (Figure 4.13 G). This indicates a requirement for PCP signalling in neural tube axis morphogenesis. Interestingly, the axis duplication in *kny* mutant and *Hsp@shield* embryos was restricted to the region posterior to the hindbrain, but in *tri* mutants this extended into the somite region (Figure 4.13 D, F, H). These results indicate a specific *dvl*-independent role of *tri* during neural tube axis morphogenesis in the somite region. Overall these results demonstrate a general requirement for PCP signalling during axis morphogenesis of the neural tissues, but also a specific requirement of *tri* in the posterior neural tube.

Chapter 5. Biology of Endodermal cell migration to the midline

5.1. Introduction

This chapter aimed to investigate the biology of endodermal cells involved in two major morphogenic movements during the migration towards the dorsal midline and midline aggregation. This chapter describes experiments designed to investigate the state of polarity of endodermal cells as they undergo these processes. It also describes the generation of multiple transgenic lines designed to investigate the autonomy of PCP signalling in the endoderm.

5.1.1. Endodermal cell migration to the midline

During the first half of zebrafish gastrulation endodermal cells undergo an active random walk movement, facilitating the expansion of the endoderm over the yolk syncytial layer (YSL) (Pezeron et al., 2008). This novel migratory behaviour is unique to the endoderm and independent of other cells within the hypoblast. Random-walk migration proceeds up until mid-gastrulation stages (75 % epiboly), at this point the endodermal cells begin to migrate towards the dorsal midline. The dorsal migration of endodermal cells generate a wide stripe of cells running the length of the embryo by 11 hpf that continually reduces in width as development continues (Section 3.2.2). These cells are in a monolayer either side of the dorsal midline until the start of midline aggregation around 11 somites (Section 3.2.3.1). The surrounding mesoderm is suggested to have an influence on the migration of the endoderm, by which the endoderm is physically tethered to the surrounding mesoderm via integrin adhesion molecules, suggesting that endoderm is not actively migrating towards the dorsal midline during late gastrulation stages, but rather is passively migrating with the surrounding mesodermal cells, and this is mediated by *cxcr4* (Nair and Schilling, 2008). An

alternative mechanism has been proposed in which the migration of the endodermal cells towards the dorsal midline is directed towards the Sdf1a chemokine secreted by the surrounding mesoderm (Mizoguchi et al., 2008). *sdf1/cxcr4* signalling plays a role in the migration and proliferation of the endoderm during gastrulation stages, although knockdown of this pathway reduces, but does not fully inhibit endodermal migration to the midline. During somitogenesis stages, however, the mesoderm overlying the endoderm is in the process of generating somites, and therefore undergoing dramatic morphogenetic movements (Hollway et al., 2007). It is unknown if the mesoderm still has an influence on the endodermal layer below as it undergoes midline aggregation.

The mesoderm has been shown to actively migrate to the dorsal midline during gastrulation stages. These cells have a polarised microtubule organising centre (MTOC) orientation that is directed towards the dorsal midline (Sepich et al., 2011). In this chapter I describe experiments to investigate if the endoderm also has a polarised MTOC orientation during migration to the midline. Actively migrating cells often have an MTOC that is preferentially orientated towards the direction of migration (Sepich et al., 2011). The MTOC functions to organise the microtubule cytoskeleton, required for numerous polarised cellular functions such as directed migration, mediolateral intercalation, and orientated cell division (Wallingford et al., 2000; Horne-Badovinac et al., 2001; Jessen et al., 2002; Gong et al., 2004; Ciruna et al., 2006). PCP signalling controls correct MTOC localisation in mesodermal and ectodermal mesenchymal cells during gastrulation, with a loss or disruption of PCP signalling resulting in a randomisation of MTOC localisation in relation to the nucleus (Sepich et al., 2011). Therefore, polarisation of the MTOC orientation represents the standard polarised state observed in directionally migrating cells (Goulimari et al., 2008).

5.1.2. Autonomy of PCP signalling during endodermal cell migration

In Chapter three I demonstrated that the PCP mutants *tri* and *kny* have defects in endodermal morphogenesis (Section 3.2.3). However, it is unknown if PCP

signalling has an autonomous endodermal role during this migration. Examining tissue specific effects and autonomous roles of PCP signalling is not possible in mutant embryos due to all tissue layers being affected. Therefore, in this chapter I describe the generation and characterisation of multiple transgenic lines designed to investigate the autonomous and non-autonomous roles of PCP signalling in endoderm morphogenesis. To aid in the generation of multiple transgenic lines I also developed a number of cloning tools.

5.1.2.1. Development of new tools for rapid and simple generation of transgenics

Advances in tools for zebrafish transgenesis, such as Meganuclease (*I-SceI*)(Grabher et al., 2004), Tol2-transposon mediated transgenesis (Kwan et al., 2007), and ΦC31 integrase (Mosimann et al., 2013) have made the generation of transgenic zebrafish lines feasible for most laboratories. Since the Tol2-mediated transgenesis system was combined with multi-site Gateway cloning system (referred to as the Tol2kit)(Kwan et al., 2007), it has become the standard method for generating constructs to enable stable germ line transgenesis in zebrafish.

Although the Multisite Gateway™ recombination system allows for relatively easy generation of new entry vectors, and enables a large flexibility of promoter/gene of interest combinations, it has four main disadvantages:

1) Generation of new entry vectors requires long *att*B-site containing primers (~60bp) to add the *att*B sites to the desired insert. These primers are costly, often requiring high purification steps to reduce the truncated products that are form during synthesis of primers over 50bp (Sigma-Aldrich, 2014).

2) The recombination reaction between the entry donor vector and the *att*B-site containing PCR product requires expensive BP Clonase™ II Enzyme Mix.

3) Construction of the final transgenesis vector requires expensive LR Clonase™ II Plus Enzyme Mix for each different construct generated.

4) Expensive high transformation efficiency cells are required for both the BP reaction, and multi-site LR reaction transformations. For these reasons, the construction of new Tol2 vectors for zebrafish transgenesis can be costly and time consuming.

I aimed to use the principles of TA-cloning to reduce the cost and efficiency of generating constructs for zebrafish transgenesis, and hence speed up my research outcomes. TA-cloning has been used extensively in molecular cloning (Zhou and Gomez-Sanchez, 2000) and *XcmI* derived TA-linkers have been used for many years to generate a range of cost-efficient TA-cloning plasmids (Schutte et al., 1997; Arashi-Heese et al., 1999; Chen et al., 2009; Hong et al., 2009). In this chapter I describe the generation of four *XcmI* based TA-cloning vectors, p5E-TA, pME-TA, p3E-TA, and pCS2+TA to improves the rate and speed of transgenesis vector generation, and significantly reduce the costs and time of both middle entry generation and final transgenesis vector generation, allowing cheap and rapid generation of expression vectors for use in zebrafish or similar systems.

5.2. Results

5.2.1. Generation of TA-cloning vectors to facilitate rapid and cheap construction of Tol2-transgenesis vectors

5.2.1.1. pCS2+TA – new vectors to replace the expensive T-vectors.

I generated a vector to reduce laboratory cloning costs associated with the generation of vectors for mRNA and *in situ* probe production, the pCS2+TA vector. To generate this vector I replaced the multiple cloning site of pCS2+ with the *XcmI-EGFP-XcmI* TA-cloning linker via *BamHI/SnaBI* digestion (Figure 5.1 A-B, G-J). For cloning applications, the TA-linker is removed by *XcmI* digestion (Figure 5.2 B), and purified A-tailed PCR products can be ligated directly into the purified pCS2+TA T-vector backbone. As TA-cloning does not require restriction digestion of the PCR amplified insert, use of this vector removes the need to

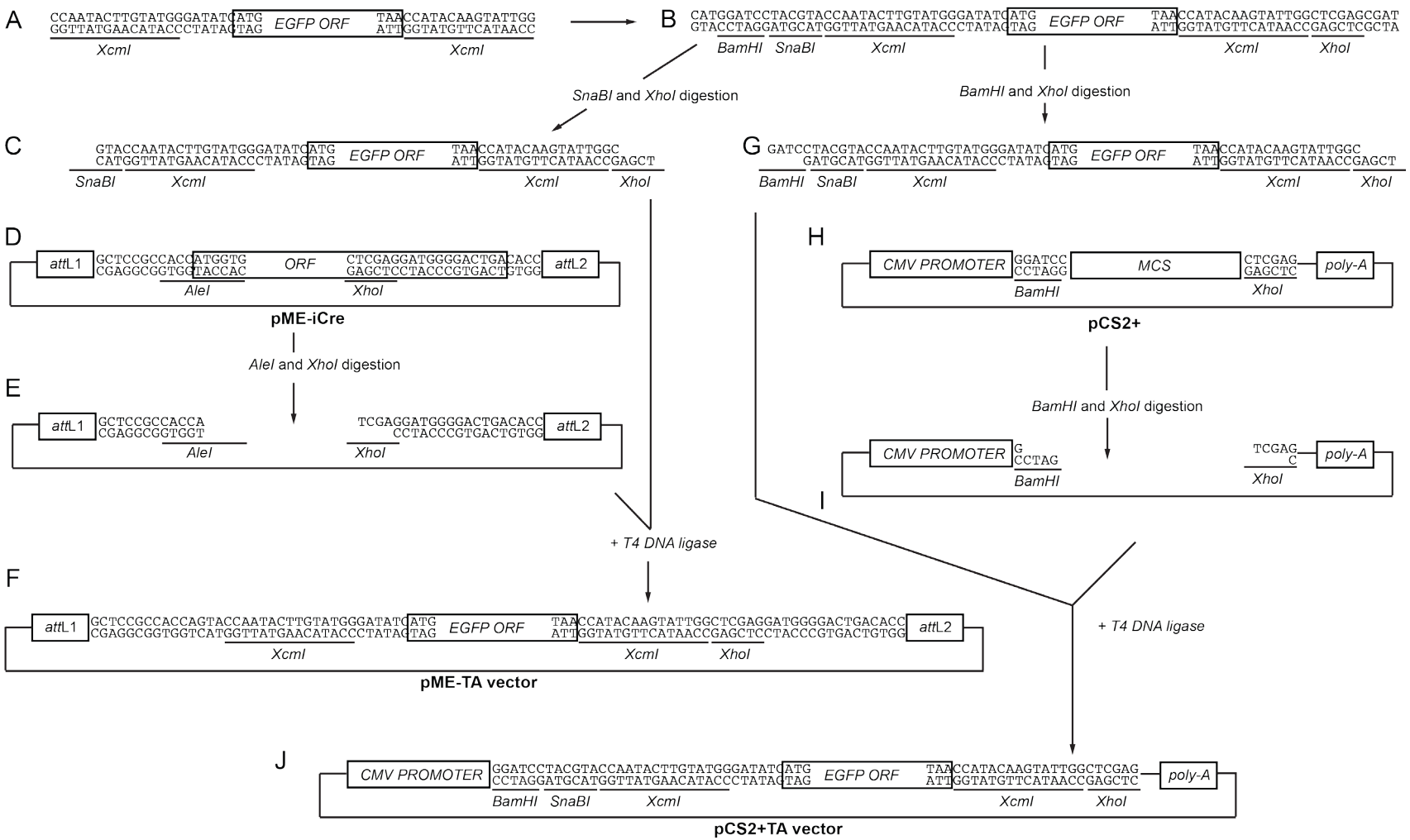
A
CCAATACTTGTATGGGATATCATG EGFP ORF TAACCATACAAGTATTGG
GGTTATGAACATACCCTATAGTAG ATTGGTATGTTCATAACC
XcmI XcmI
B
CATGGATCCTACGTACCAATACTTGTATGGGATATCATG EGFP ORF TAACCATACAAGTATTGGCTCGAGCGAT
GTACCTAGGATGCATGGTTATGAACATACCCTATAGTAG ATTGGTATGTTCATAACCGAGCTCGCTA
BamHI SnaBI XcmI XcmI XhoI
SnaBI and XhoI digestion
BamHI and XhoI digestion
C
GTACCAATACTTGTATGGGATATCATG EGFP ORF TAACCATACAAGTATTGGC
CATGGTTATGAACATACCCTATAGTAG ATTGGTATGTTCATAACCGAGCT
SnaBI XcmI XcmI XhoI
G
GATCCTACGTACCAATACTTGTATGGGATATCATG EGFP ORF TAACCATACAAGTATTGGC
GATGCATGGTTATGAACATACCCTATAGTAG ATTGGTATGTTCATAACCGAGCT
BamHI SnaBI XcmI XcmI XhoI
D
attL1 GCTCCGCCACCATGGTG ORF CTCGAGGATGGGGACTGACACC attL2
CGAGGCGGTGGTACCAC GAGCTCCTACCCGTGACTGTGG
AleI XhoI
pME-iCre
AleI and XhoI digestion
H
CMV PROMOTER GGATCC MCS CTCGAG poly-A
CCTAGG GAGCTC
BamHI XhoI
pCS2+
BamHI and XhoI digestion
E
attL1 GCTCCGCCACCA TCGAGGATGGGGACTGACACC attL2
CGAGGCGGTGGT CCTACCCGTGACTGTGG
AleI XhoI
CMV PROMOTER G CCTAG
BamHI
TCGAG C poly-A
XhoI
I
+ T4 DNA ligase
+ T4 DNA ligase
F
attL1 GCTCCGCCACCAGTACCAATACTTGTATGGGATATCATG EGFP ORF TAACCATACAAGTATTGGCTCGAGGATGGGGACTGACACC attL2
CGAGGCGGTGGTCATGGTTATGAACATACCCTATAGTAG ATTGGTATGTTCATAACCGAGCTCCTACCCGTGACTGTGG
XcmI XcmI XhoI
pME-TA vector
J
CMV PROMOTER GGATCCTACGTACCAATACTTGTATGGGATATCATG EGFP ORF TAACCATACAAGTATTGGCTCGAG poly-A
CCTAGGATGCATGGTTATGAACATACCCTATAGTAG ATTGGTATGTTCATAACCGAGCTC
BamHI SnaBI XcmI XcmI XhoI
pCS2+TA vector

Figure 5.1 How the pME-TA and pCS2+TA vectors were constructed. **(A)** PCR was used to add *XcmI* restriction sites to either side of *EGFP*. **(B)** 5'-*BamHI/SnaBI* sites and a 3'- *XhoI* site was added to *XcmI-EGFP-XcmI* fragment using PCR. **(C-F)** To generate the pME-TA vector: *SnaBI (Blunt)/XhoI* digested TA-linker was inserted into the backbone of an existing Gateway middle entry vector pME-*iCre*, digested with *AleI (Blunt)/XhoI.* **(G-J)** To generate pCS2+TA: *BamHI/XhoI* digested TA-linker was inserted into *BamHI/XhoI* digested pCS2+ backbone. Restriction sites are underlined. p5E-TA and p3E-TA were generated by similar approaches.

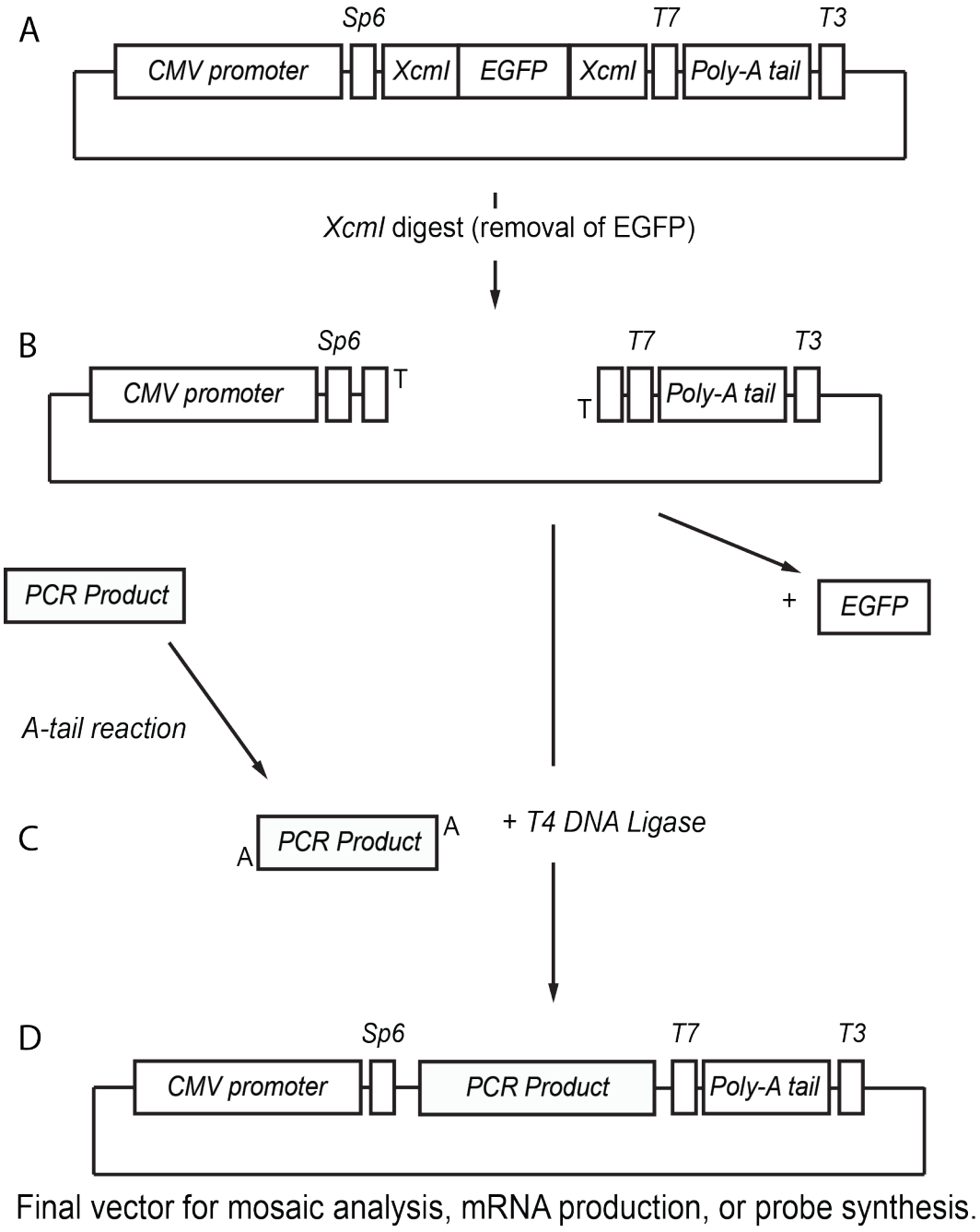

Figure 5.2 pCS2+TA vector design. (A) The multiple cloning site of pCS2+ has been replaced with the TA-linker using *BamHI/XhoI* digestion. **(B)** The TA-linker containing the *EGFP* open reading frame is removed by *XcmI* digestion, leaving T-overhangs. **(C)** The purified *XcmI* digested pCS2+TA vector is ligated to a PCR product that contains A-overhangs. **(D)** The resulting pCS2+ vector containing your PCR product.

identify restriction sites unique to both the vector and insert. The pCS2+TA vector contains all the required sequences for transient gene expression in vertebrates, *in vitro* transcription, and *in situ* hybridisation probe production (Figure 5.2 D). Use of pCS2+TA thus allows the direct cloning of the cDNA into the pCS2+TA vector without subcloning in a commercially prepared T-vector first, replacing the need for expensive pre-prepared T-vectors. I have verified the functionality of pCS2+TA in common zebrafish experiments: injection of DNA for mosaic expression; in vitro transcription followed by injection of mRNA for overexpression; and generation of riboprobes for *in situ* hybridisation, and found that it works in the same manner as the original pCS2+ vector cloned with the same DNA (data not shown).

5.2.1.2. TA-clonable multisite gateway entry vectors

To enable rapid generation of new entry vectors for multisite gateway without the need for BP Clonase™ II Enzyme Mix, I constructed three TA-clonable entry vectors: p5E-TA, pME-TA, and p3E-TA. The generation of the pME-TA vector is outlined in (Figure 5.1). A similar approach was taken to generate p5E-TA and p3E-TA. Flanking the TA-linker are the *att*L and *att*L sites required for the standard multisite LR mediated recombination reaction to generate a final transgenesis vector (Figure 5.3). *XcmI* restriction digestion of these three vectors removes the EGFP cassette, leaving two T-overhangs required for A-tail cloning (Schutte et al., 1997) (Figure 5.3 B). Purified A-tailed PCR products can then be directly ligated into the *XcmI* digested TA-entry vectors (Figure 5.3 B, C). This greatly reduces the cost of generating new middle entry vectors by eliminating the need for both long *att*-site containing primers and BP Clonase™ II Enzyme Mix. Entry vectors generated by this method can then be used in a Multisite Gateway reaction to generate final Tol2-transgenesis vectors (Figure 5.4).

5.2.1.3. multifunctional use of TA-cloning entry vectors

The costs associated with generating final Tol2-transgenesis vectors via the Tol2kit and Gateway mediated recombination can be high, each construct

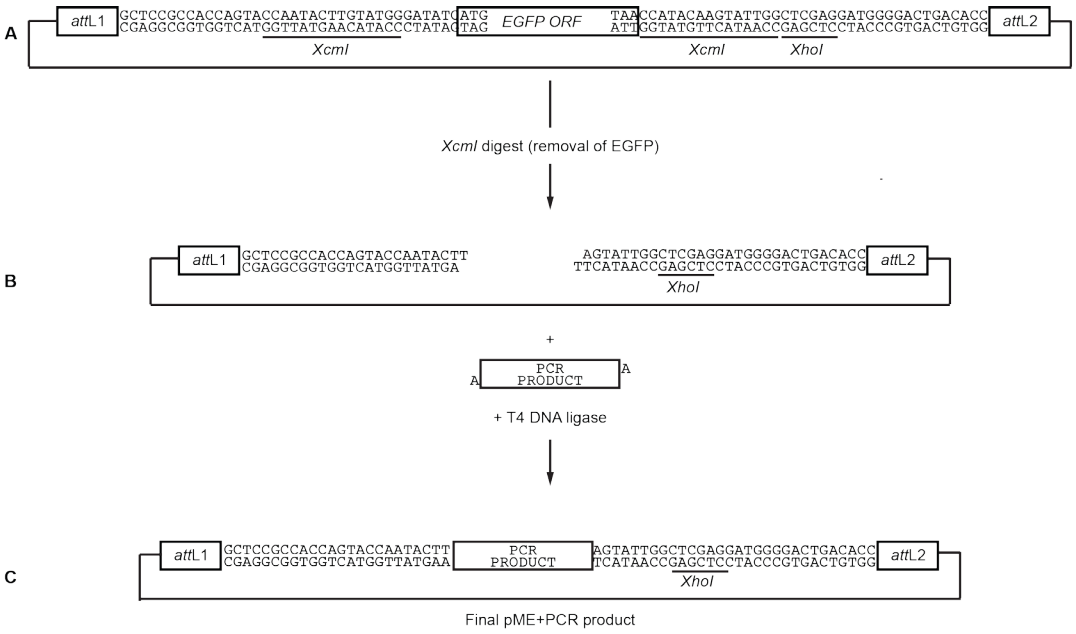

Figure 5.3. pME-TA as an example to rapidly generate new entry vectors without BP-Clonase II enzyme mix. **(A)** The pME-TA vector linker containing the *EGFP* open reading frame. **(B)** The linker is removed using *XcmI* digestion, resulting in a vector with T-overhangs at both ends. The pME-TA vector does not contain any in-frame ATG start codons after digestion with *XcmI.* The purified *XcmI* digested pME-TA T-vector is ligated to a PCR product that contains A-overhangs. **(C)** The resulting middle entry vector containing your PCR product (pME-PCRproduct). Restriction site are underlined. p5E-TA and p3E-TA can be used in the same manner.

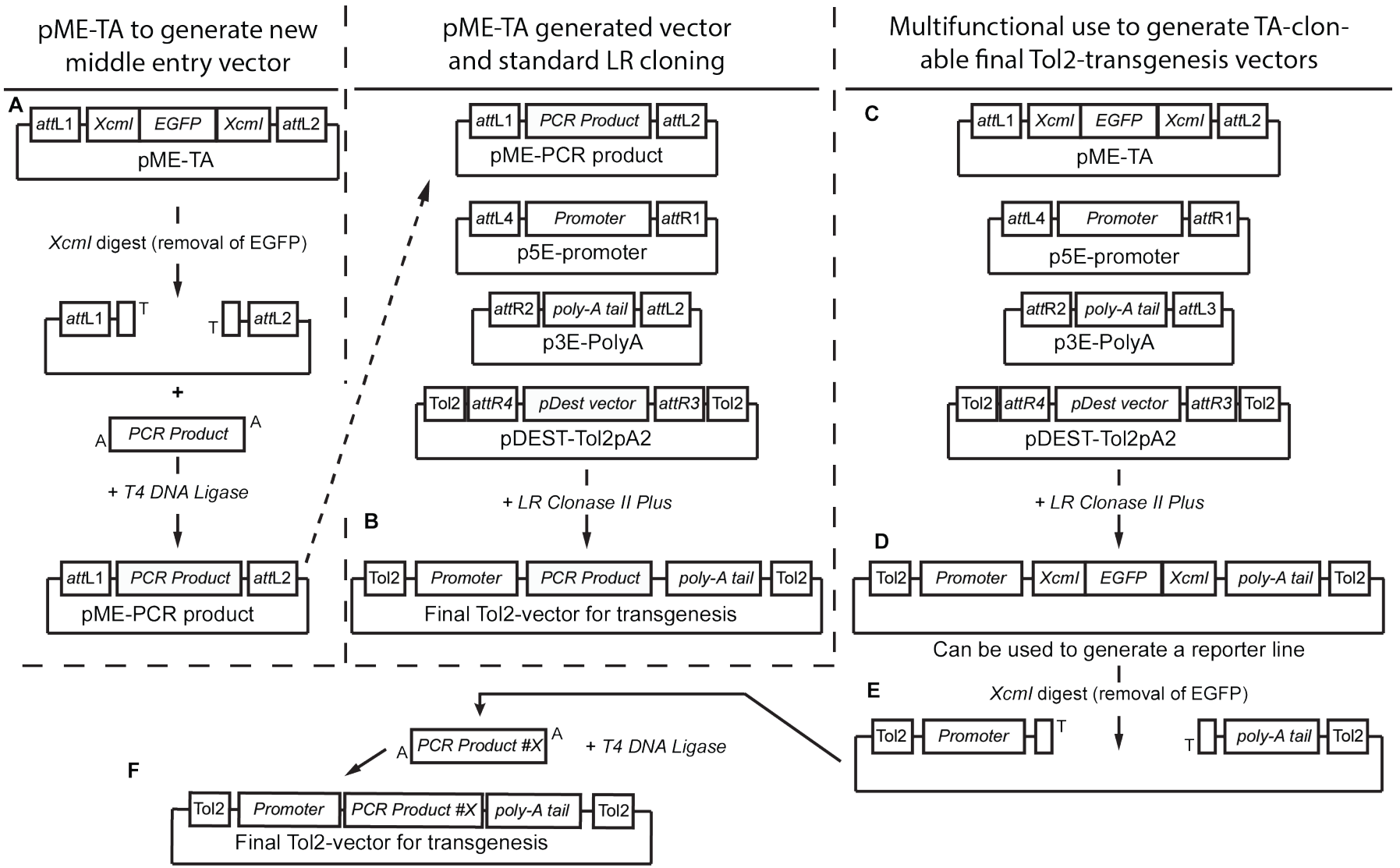
pME-TA to generate new middle entry vector
pME-TA generated vector and standard LR cloning
Multifunctional use to generate TA-clonable final Tol2-transgenesis vectors
A
attL1 XcmI EGFP XcmI attL2
pME-TA
XcmI digest (removal of EGFP)
attL1 T
T attL2
+
A PCR Product A
+ T4 DNA Ligase
attL1 PCR Product attL2
pME-PCR product
attL1 PCR Product attL2
pME-PCR product
attL4 Promoter attR1
p5E-promoter
attR2 poly-A tail attL2
p3E-PolyA
Tol2 attR4 pDest vector attR3 Tol2
pDEST-Tol2pA2
+ LR Clonase II Plus
B
Tol2 Promoter PCR Product poly-A tail Tol2
Final Tol2-vector for transgenesis
C
attL1 XcmI EGFP XcmI attL2
pME-TA
attL4 Promoter attR1
p5E-promoter
attR2 poly-A tail attL3
p3E-PolyA
Tol2 attR4 pDest vector attR3 Tol2
pDEST-Tol2pA2
+ LR Clonase II Plus
D
Tol2 Promoter XcmI EGFP XcmI poly-A tail Tol2
Can be used to generate a reporter line
E
XcmI digest (removal of EGFP)
Tol2 Promoter T
T poly-A tail Tol2
A PCR Product #X A + T4 DNA Ligase
F
Tol2 Promoter PCR Product #X poly-A tail Tol2
Final Tol2-vector for transgenesis

Figure 5.4 The multiple uses of the pME-TA for generating final zebrafish transgenesis vectors. (A-B) pME-TA generated middle entry vectors can subsequently be used in a BP-reaction. (A) A PCR product is cloned into the pME-TA vector using A-tail cloning to generate pME-PCRproduct. (B) pME-PCRproduct is then used in traditional LR gateway cloning using p5E, p3E, and pDest vectors to generate final transgenesis vector. **(C-E)** Generation of a pDestTol2-TA vector, containing the promoter of interest, in order to rapidly generate a related set of final transgenesis vectors. (C) pME-TA vector is used as an entry vector with p5E-yourpromoter, p3E-vector, or pDestTol2 vector in a standard LR-reaction. This can then be stored frozen at -20 °C for use in multiple later reactions (D) The *EGFP*-linker can be removed from the Tol2 vector by *XcmI* digestion to produce pDestTol2-yourpromoter-T, ready for A-tail cloning. (E) Ligation of pDestTol2-T-vector with your A-tailed PCR product to rapidly generate a related set of final transgenesis vectors.

requires the use of BP Clonase™ II Enzyme Mix, LR Clonase™ II Plus Enzyme Mix, and expensive high-competency cells for transformation. The three TA-clonable entry vectors I generated, p5E-TA, pME-TA, and p3E-TA can also be used in a multifunctional way to generate final pDestTol2:TA-clonable transgenesis vectors that enable rapid one step generation of final Tol2-transgenesis vectors. As an example, incorporating an undigested pME-TA entry vector into a multisite LR Gateway reaction generates a final Tol2-transgenesis vector that contains the TA-EGFP-linker in the middle entry position (Figure 5.4 D). As this contains *EGFP* this vector can either be used to generate a reporter line, or more importantly, used as a final pDestTol2:TA-clonable transgenesis vector. *XcmI* digestion results in a final pDestTol2 plasmid with T-overhangs (Figure 5.4 E), allowing purified PCR products to be directly ligated into the middle entry position in one step (Figure 5.4 F). All three TA-clonable entry vectors can be used in this way to generate final pDestTol2:TA-clonable transgenesis vectors, using only one multisite LR reaction (for the initial reaction), no long *attB* primers, and without the need to pass the gene of interest through a middle entry vector; significantly reducing costs and time associated with multisite Gateway mediated cloning. All purified *XcmI* digested vectors can be stored as stocks at -20 °C for later use.

5.2.1.4. Verification of tissue specific expression using a TA-clonable final destination vector

To verify that clones generated using the pME-TA vector are still functional in a multi-site Gateway LR reaction I generated pME-*huTau-mCherry* using *XcmI* digested pME-TA vector. *huTau*-fluorescent protein fusions have been demonstrated to bind and label microtubules in vertebrates (Tomasiewicz et al., 2002). pME-TA-*huTau-mCherry* was taken through a multi-site LR reaction with the p5E-*sox17* promoter (endoderm specific promoter), pDestTol2pA2, and p3E-poly-A tail to generate the final Tol2 transgenesis vector Tol2(*sox17:huTau-mCherry*) (Figure 5.5 A). Injection of this construct into the endodermal reporter line Tg(*sox17:EGFP*) resulted in mosaic blocks of endodermal specific expression of the *huTau-mCherry* transgene and labelling of the microtubules of these cells with mCherry (Figure 5.5 B, C).

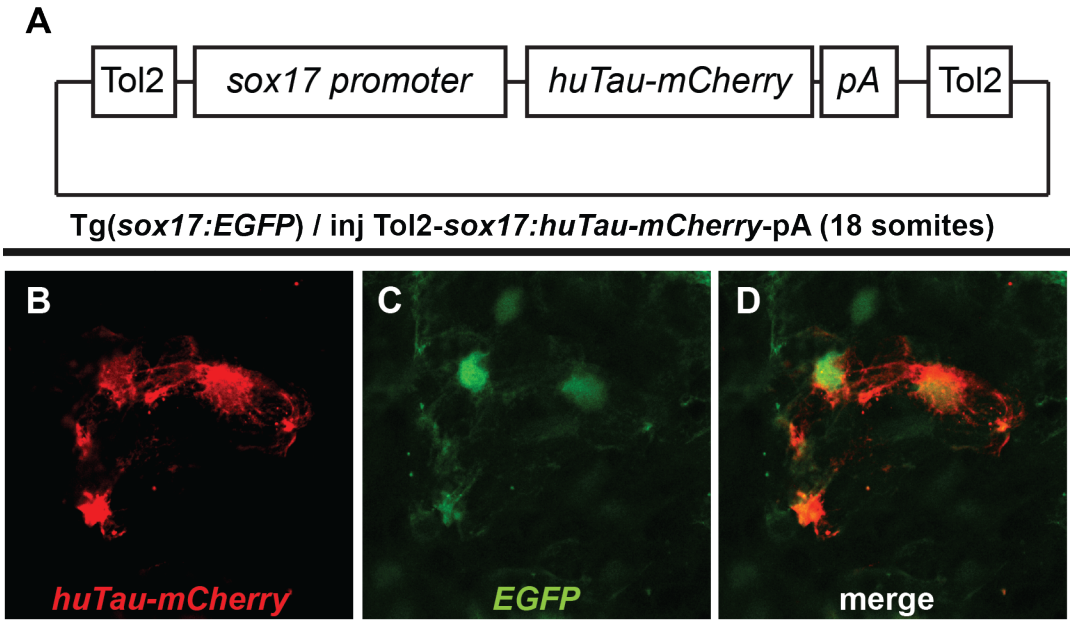

Figure 5.5 Confocal images of endodermal cells mosaically expressing *huTau-mCherry*. (A) *sox17:huTau-mCherry* construct generated using pME-TA and subsequent LR reaction. Tg(*sox17*:*EGFP*) transgenic embryos were injected with *sox17*:*huTau-mCherry* DNA generated using the pME-TA vector. *mCherry* positive embryos were fixed at 18 hpf (hours post fertilisation), flat mounted, and imaged using confocal microscopy. **(B)** *huTAu-mCherry* labels the microtubules of endodermal cells. **(C)** Endodermal cells are labelled by the Tg(*sox17:EGFP*) transgene

.

In order to validate the versatility of the TA-clonable entry vectors to generate TA-clonable final Tol2 transgenesis vectors, an unmodified pME-TA was taken through an LR reaction with p5E-*sox17* promoter, pDestTol2pA2, and p3E-poly-A tail to generate a final 10.7kb Tol2 transgenesis vector *sox17:TA-linker* (similar to Figure 5.4 C-D). The TA-linker was removed with *XcmI* digestion and PCR amplified *huTau-mCherry* was inserted via TA-cloning (as in Figure 5.4 E-F). This 12.3kb Tol2-*sox17*:*huTau-mCherry* vector was injected into Tg(*sox17:EGFP*) embryos, and displayed mosaic endoderm specific microtubule expression, identical to that seen using the Tol2(*sox17*:*huTau-mCherry*) vector generate from pME-TA-*huTau-mCherry* (data not shown), demonstrating the versatility and multifunctional uses of these three TA-cloneable entry vectors in generating constructs for zebrafish transgenesis.

5.2.2. The role of PCP signalling in regulating the polarity of migrating endodermal cells

5.2.2.1. MTOC localisation

The aim of this section of my project was to investigate if the endodermal cells are polarised towards the direction of migration during somitogenesis stages. To visualise the MTOC within cells I utilised *mCherry-Xcentrin,* a fusion protein that binds the centriole (Sepich et al., 2011). I generated a version of *Xcentrin* fused in-frame to the C-terminal to the blue fluorescent protein *TagBFP* (Subach et al., 2008) to give rise to *TagBFP-Xcentrin* (Figure 5.6 A). Co-Injection of *TagBFP-Xcentrin* mRNA and *nuclear-RFP* into Tg(*sox17:EGFP*) embryos resulted in labelling of the MTOC with *TagBFP* and the nucleus with *RFP* (Figure 5.6B-E). The angle of the MTOC relative to the nucleus and the direction of migration (Dorsal midline (Figure 5.6 F dotted line)), was measured from confocal images at a position lateral to the dorsal midline (Figure 5.6 F, G).

Two time points were chosen for investigation, 3 somites (11 hpf) and 16 somites (17 hpf). The 3 somite stage is just prior to when the endodermal cells start to undergo a cell shape change (Section 3.2.4). At 16 somites the endoderm is beginning to leave the monolayer prior to formation of the primitive

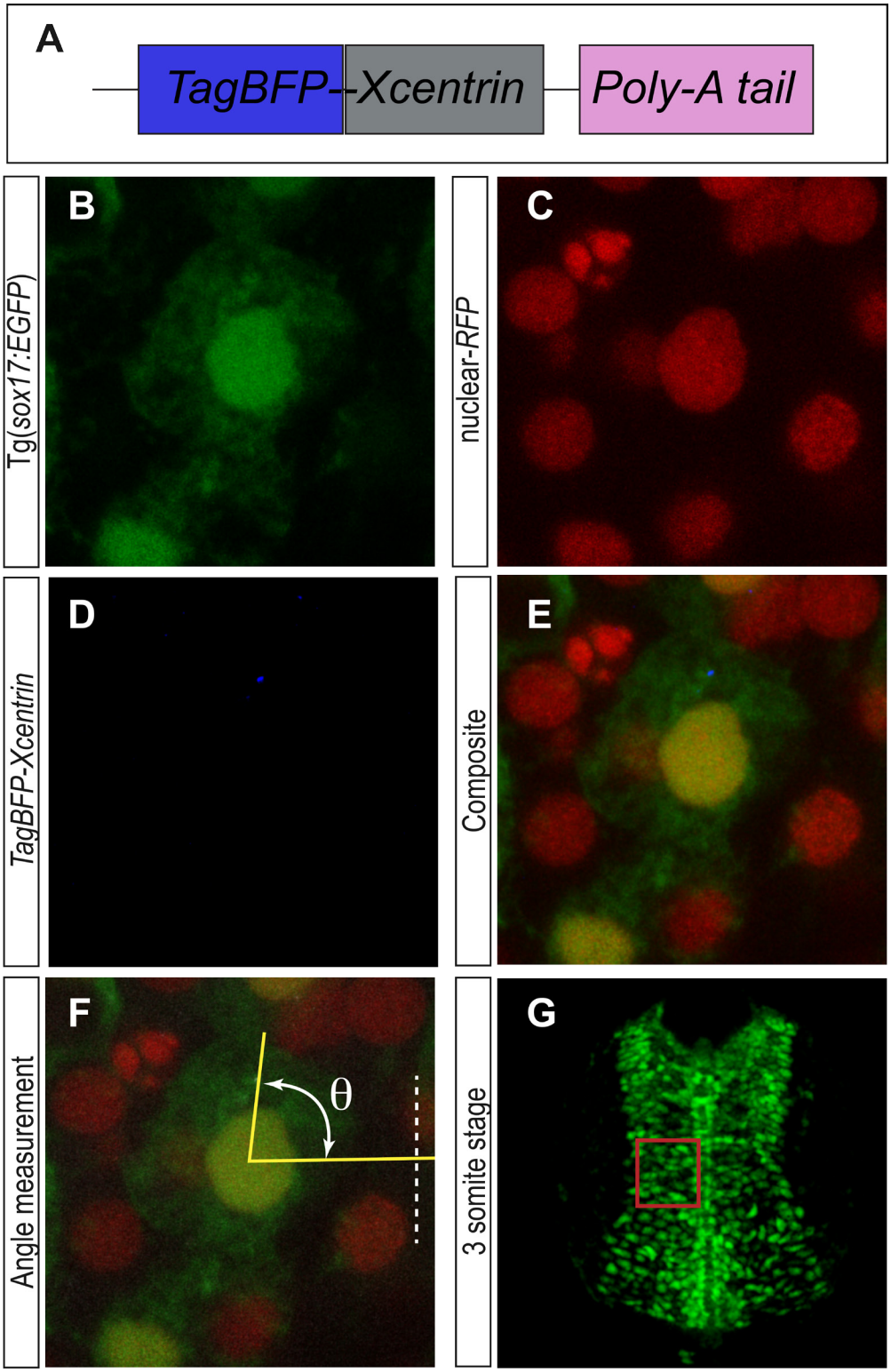

Figure 5.6 Labelling and measurement of the microtubule organising centre (MTOC). (A) mRNA generated from pCS2+*TagBFP-Xcentrin*. **(B-F)** Confocal images of 3-somite Tg(*sox17:EGFP*) embryos injected with *TagBFP-Xcentrin* and nuclear-*RFP* mRNA. Endodermal cells labelled with *EGFP* (green) (B), nucleus labelled with nuclear-*RFP* (red) (C), microtubule organising centre labelled with *TagBFP* (blue) (D), composite image (E). (F) Schematic demonstrating the angle measurement (θ) of the MTOC relative to the centre of the nucleus and the dorsal midline (dotted line). **(G)** Schematic demonstrating the position of the cells analysed (red box) lateral to the midline. Anterior to the top. Posterior to the bottom.

endodermal rod (Section 3.2.3.1). I have demonstrated that endodermal cells undergo a cell shape change at 7 somites prior to, and during midline aggregation (Section 3.2.4). I wished to know if this cell shape change required, or coincided with a polarisation of MTOC orientation.

To test this hypothesis the overall orientation of the MTOC in endodermal cells migrating to the dorsal midline during both early and mid-somitogenesis stages was determined from MTOC angle measurements taken from confocal images of wildtype Tg(*sox17:EGFP*) embryos at 3 and 16 somites respectively (Figure 5.7 C, G blue area). As the mesoderm has a polarised MTOC during gastrulation stages (Sepich et al., 2011) I wished to determine if the mesoderm in a similar niche to the endoderm retained the MTOC polarisation into somitogenesis stages. Therefore, the position of the MTOC in mesoderm cells that occupied the same niche as the endodermal cells was also determined for comparison (Figure 5.7 C, G red area).

PCP signalling has been shown to be required for mesodermal and ectodermal MTOC polarisation (Sepich et al., 2011). To investigate if this was a requirement in the endoderm I also analysed MTOC orientation in *tri* and *kny* mutants, and *Hsp@shield* embryos (Tg(*hsp70l:XDshΔDEP-mCherry*) embryos heat shocked at shield stage). MTOC angle measurements were displayed visually as rose graphs (Figure 5.7 A); 0° is the direction of migration towards the dorsal midline, 90° to the anterior, 180° to the ventral, and 270° to the posterior of the embryo. To generate the rose graphs the data was separated into 12 groups (Figure 5.7 A) each spanning a total of 30°; a 15° window either side of the graph line (Figure 5.7 B). The apparent overall MTOC orientation of each graph is indicated by the arrow. Representative images for each genotype and stage analysed is shown in Figure 5.8.

5.2.2.2. Quantification of MTOC polarised orientations

Previously published evidence for the role of PCP signalling in MTOC orientation was determined without the use of statistical quantification or significance calculations (Sepich et al., 2011). In this investigation I wished to determine if any MTOC localisation changes observed were statistically significant, and

therefore believable. To quantify the changes of MTOC orientation the data was grouped into six quadrants of 60° each, representing anterio-dorsal, dorsal, posterio-dorsal, posterior-ventral, ventral, and anterio-ventral directions relative to the direction of migration towards the dorsal midline (Figure 5.9 A).

Wildtype endodermal cells at 3 somites have a randomised MTOC orientation with respect to their direction of migration (Figure 5.9 C, E). However analysis of the MTOC of mesodermal cells that were closest to the medial axis (within the first two cells away from the YSL) show (or demonstrate) a significant bias towards the overall dorsal direction of cell migration (Figure 5.9 D). At 16 somites endodermal cells have developed a MTOC directed bias specifically towards the dorsal side of the embryo (Figure 5.9 E). Mesodermal cells maintained an overall MTOC polarisation towards the dorsal side of the embryo, but this is no longer specific to any of the three dorsal regions (Figure 5.9 F).

tri mutant endodermal cells have an overall random MTOC distribution at 3 somites (Figure 5.9 C), similar to wildtype cells. Interestingly, *tri* mutant endodermal cells do not generate the polarised MTOC orientation observed in wildtype cells at 16 somites. *tri* mutant mesodermal cells fail to generate a polarised MTOC distribution at both 3 somites and 16 somites (Figure 5.9 D, F). Although *tri* mutant cells appear to have a dorsal polarisation at 16 somites in the endoderm it is not statistically significant (Figure 5.9 E).

kny mutant endodermal cells do not have a polarised MTOC at 3 somites, which is similar to wildtype (Figure 5.9 C). Although it might be predicted that PCP mutant endodermal cells might lack all MTOC polarisation, by 16 somites *kny* mutant endodermal cells do develop a dorsally biased polarisation of the MTOC, similar to that of wildtype endoderm at this stage (Figure 5.9 E). *kny* mutant mesodermal cells fail to generate a polarised MTOC distribution at both stages analysed (Figure 5.9 F).

These results identify that, unlike the mesoderm, the endoderm does not have a polarised MTOC distribution during early somitogenesis stages (3 somites), but does develop a dorsal polarisation of the MTOC by mid-somitogenesis stages (16 somites). Although *tri* and *kny* show the same mesodermal MTOC phenotype, they show a different MTOC phenotype in the

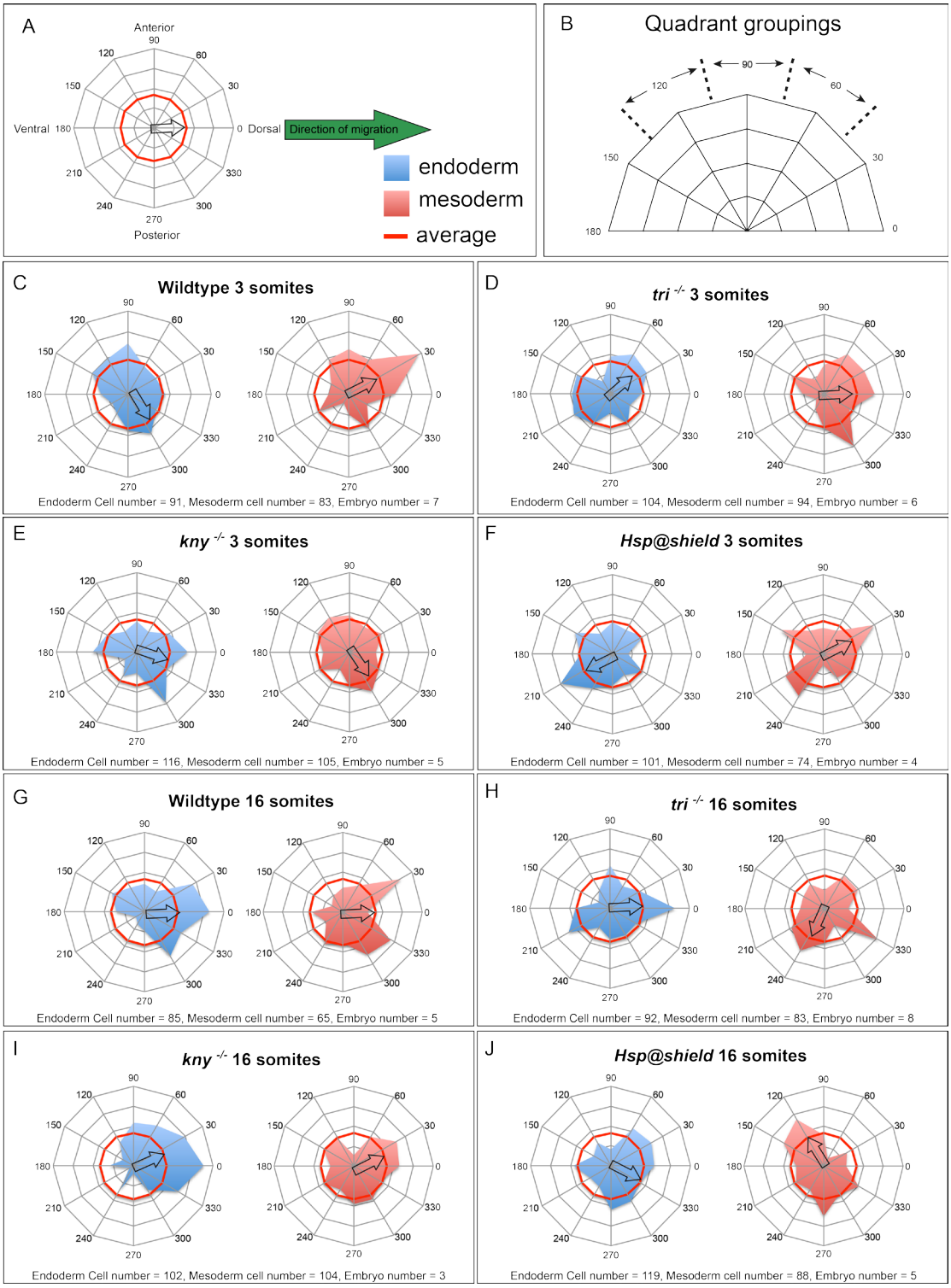

Figure 5.7 The angle of the Microtubule organising centre in wildtype and PCP disrupted embryos. (A) Schematic representing the defined angles relative to the direction of migration to the dorsal midline (green arrow). Endoderm MTOC angels shown in blue shaded area. Mesoderm MTOC angles shown in light red shaded area. The red line shows theoretical average. **(B)** Schematic representation of the 30° window used to group a measurement into one of the twelve regions of the rose graphs. **(C-F)** MTOC angles of 3 somite wildtype (C), *tri* mutant (D), *kny* mutant(E), and Tg(*hsp70l:XDshΔDEP-mCherry*) heat shocked at shield (*Hsp@shield*) (F) embryos. **(G-J)** MTOC angles of 16 somite wildtype (G), *tri* (H), *kny* (I), and Tg(*hsp70l:XDshΔDEP-mCherry*) *Hsp@shield* (J) embryos. Black outline arrows represent apparent overall average direction. Rose graphs represent raw data without statistical analysis (statistically verified in Figure 5.8).

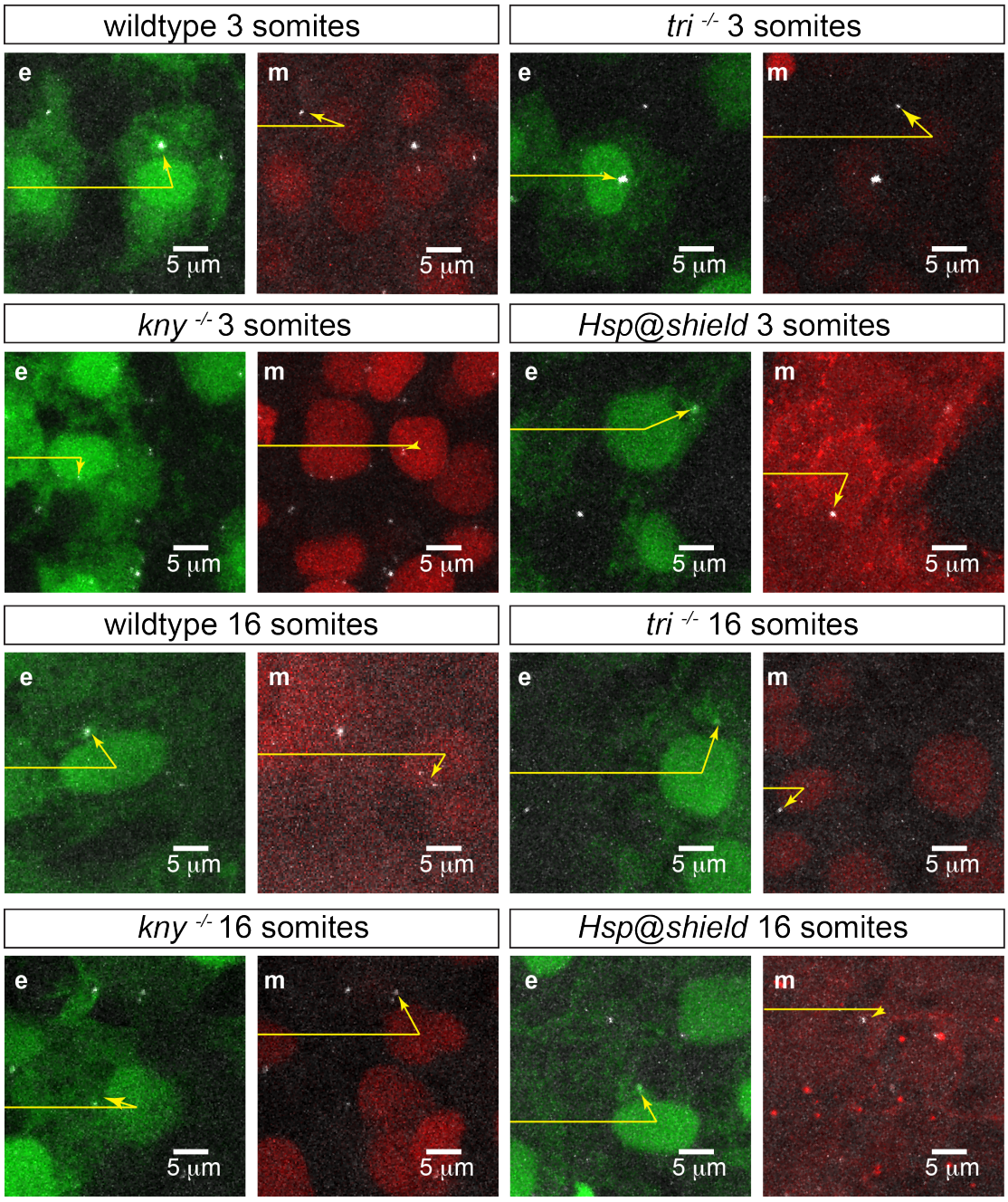

Figure 5.8 Representative images of MTOC polarisation in wildtype and PCP disrupted embryos. Composite confocal images of embryos of wildtype and PCP disrupted embryos injected with *TagBFP-Xcentrin* and nuclear-*RFP* mRNA. Microtubule organising centre (MTOC) labelled with *TagBFP* (white). **(e)** Endodermal cells labelled with *EGFP* (green) and *TagBFP-Xcentrin* (grey). **(m)** Mesodermal cells are labelled nuclear-*RFP* (red) (but *EGFP* negative) and *TagBFP-Xcentrin* (grey). Yellow lines indicate angle measurements of the MTOC relative to the nucleus and dorsal midline. Dorsal midline orientated to the left. Anterior is located at the top. Posterior is located at the bottom. Scale bar indicate 5 µm.

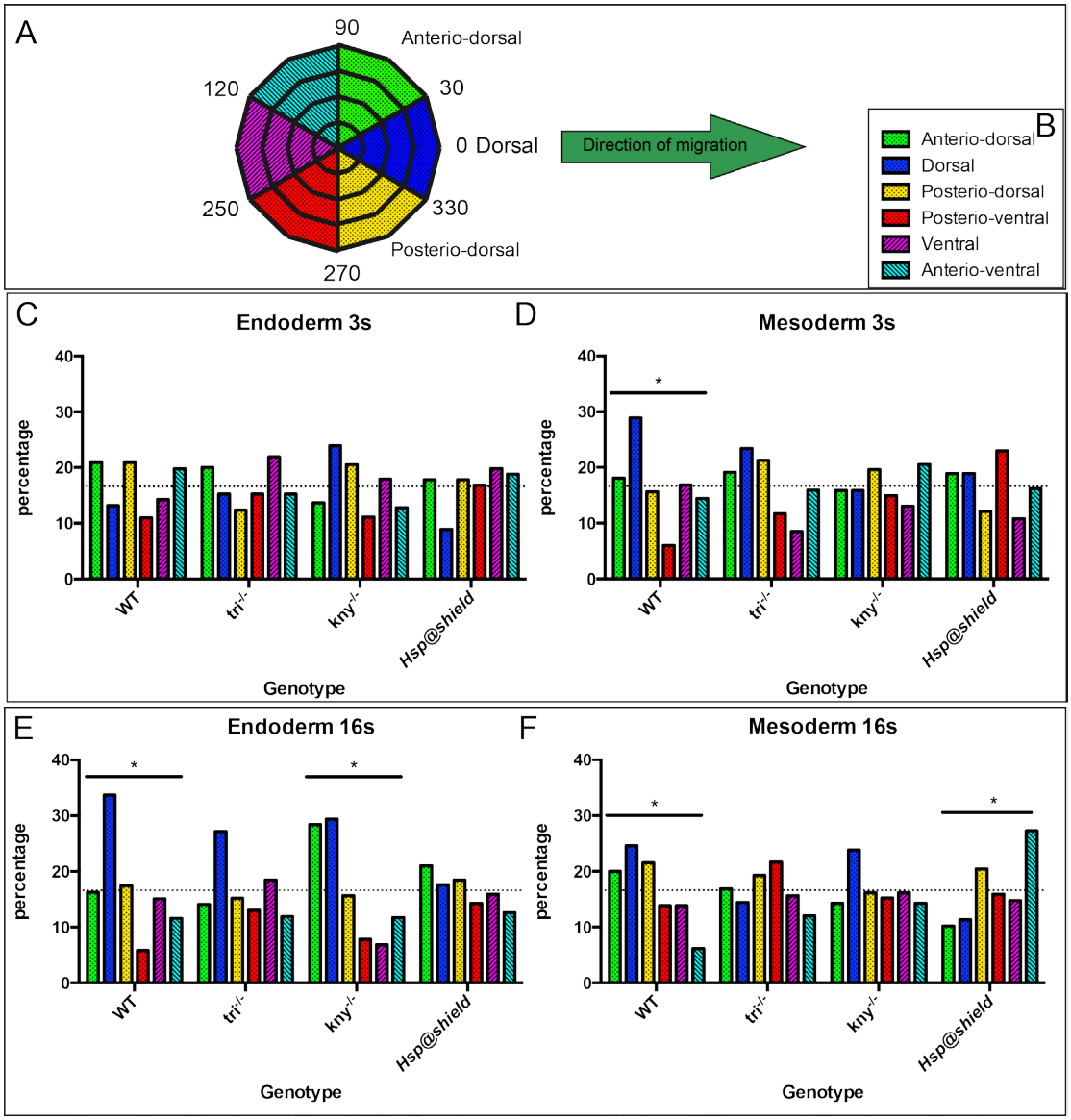

Figure 5.9 Overall distribution MTOC. (A) Schematic highlighting the grouping of MTOC data into six direction groups **(B)** Ledged describing the colour of each of the six spacial groups. **(C-F)** Column graph showing the percentage of MTOC in each of the six quadrants. (C) Endoderm 3 somites. (D) Mesoderm 3 somites. (E) Endoderm 16 somites. (F) Mesoderm 16 somites. Dotted line indicates equal (randomised) mean value. Asterisk represents significant as determined by χ squared test, * = $P \leq 0.05$. See appendix Three for χ squared values testing for equal MTOC distributions over the six quadrants (randomised) and with wildtype observed values as expected values (same of different to wildtype).

endoderm, as *kny* mutant endodermal cells are able to generate a polarised MTOC distribution, but *tri* mutants fail to do this. Taken together these data demonstrate that the mesoderm retains the previously identified MTOC polarisation (Sepich et al., 2011) from gastrulation into somitogenesis stages. These data support previous evidence (Sepich et al., 2011) that the mesoderm of *tri* and *kny* mutants fails to generate a polarised MTOC orientation, and this continues into the somitogenesis stages.

To assess the function of *dvl* in MTOC polarisation Tg(*hsp70l:XDshΔDEP-mCherry*) embryos were heat shock treated at shield (referred to as *Hsp@shield*) and MTOC orientation was determined. Disruption of *dvl* function during gastrulation in *Hsp@shield* embryos resulted in a randomised distribution of the MTOC in the endoderm at both somitogenesis stages (Figure 5.9 C, E). *Hsp@shield* mesodermal cells fail to polarise the MTOC at 3 somites (Figure 5.9 D), but are capable to generating an anterio-ventral directed MTOC polarisation at 16 somites (Figure 5.9 C-F).

Taken together these results demonstrate that loss of *trilobite* prevents the formation of a polarised MTOC in the endoderm. This is consistent with is consistent with previous studies in the mesoderm and ectoderm (Sepich et al., 2011). However these results show that loss of *knypek* does not result in a loss of polarity of the endoderm at 16 somites, despite it losing polarity in the mesoderm.

5.2.3. New transgenic lines to investigate the autonomy of PCP signalling in endoderm morphogenesis

A caveat of using mutant embryos to investigate PCP signalling in endodermal development is the inability to separate the effects of the surrounding mesodermal tissues on endodermal cell behaviour, confusing the endoderm-autonomous, and non-autonomous roles of PCP signalling. The aim of this section of the thesis was to generate a number of transgenic lines utilising the *dvl* dominant negative *XDshΔDEP-mCherry* to disrupt PCP signalling in a tissue specific manner, and enabling investigations into autonomous and non-autonomous roles of PCP signalling during endoderm morphogenesis. A number

of different transgenic approaches were undertaken to generate constitutive or inducible tissue specific knockdowns of PCP signalling.

5.2.3.1. Inhibition of PCP signalling specifically in the endoderm

I aimed to inhibit PCP signalling specifically within the endoderm. To achieve this I utilised the *Gal4/UAS* expression system previously established in zebrafish (Distel et al., 2009) to generate the transgenic line Tg(*sox17:EGFP-T2A-KalTA4GI*) (Figure 5.10). This transgenic line specifically expresses a version of the *Gal4* transcriptional activator *KalTA4* (*EGFP-T2A-KalTA4GI*) linked to *EGFP* with a self-cleaving viral peptide linker (T2A) (Distel et al., 2009). This enables for 1:1 expression of *EGFP* and *KalTA4GI* from a single open reading frame, specifically in the endoderm due to the *sox17* promoter (Figure 5.10 C).

As a partner to the endodermal *Gal4* line I generated Tg(*10xUAS:XDshΔDEP-mCherry/cmlc2:EGFP*) transgenic line, which contains the *XDshΔDEP-mCherry* cassette under the control of a 10xUAS Gal4 response element promoter (Figure 5.10 A). These lines are designed to be crossed together to generate Tg(*sox17:EGFP-T2A-KalTA4GI*)/Tg(*10xUAS:XDshΔDEP-mCherry/cmlc2:EGFP*) double transgenic embryos. These embryos express *EGFP* and *KalTA4* specifically in the endoderm, which in turn results in the activation of the *10xUAS* promoter and expression of *XDshΔDEP-mCherry* specifically in the endoderm, and therefore disrupts PCP signalling (Figure 5.10 A).

Unfortunately, however, in practice the double transgenic embryos expressed both the *EGFP-T2A-KalTA4* activator (Figure 5.10 C) and the *XDshΔDEP-mCherry* dominant negative (Figure 5.10 D) at very low levels. Injection of *KalTA4* mRNA into Tg(*10xUAS:XDshΔDEP-mCherry/cmlc2:EGFP*) embryos also resulted in very low levels of *XDshΔDEP-mCherry* expression (data not shown) indicating either silencing of the highly repetitive *10xUAS* sequences or insertion of the transgene into a region of the genome that represses transcription.

In order to overcome potential silencing I utilised a non-repetitive version of the *UAS* promoter (*4xnrUAS*) that has been shown to be resistant to methylation induced silencing (Akitake et al., 2011). The *4xnrUAS* promoter was

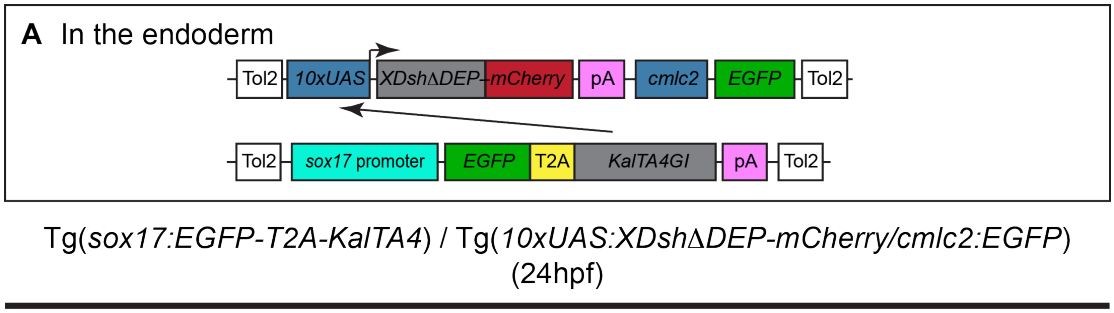

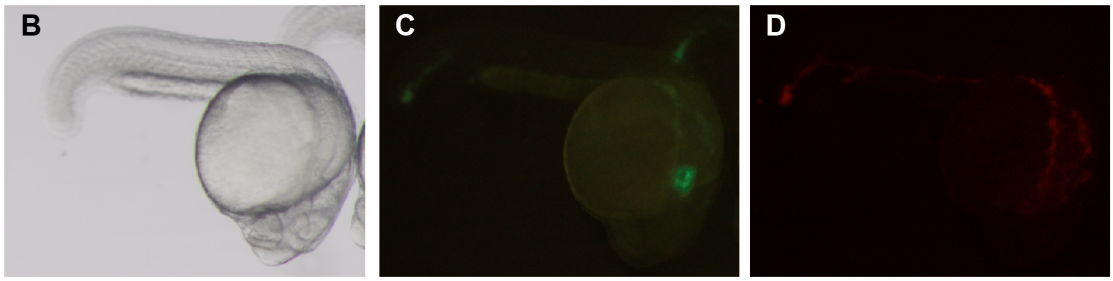

Figure 5.10 Characterising the Tg(*sox17:EGFP-T2A-KalTA4GI*) and Tg(*10xUAS:XDshDEP-mCherry/cmlc2:EGFP*) transgenic lines. (A) Schematic representing the theoretical interaction within an embryo carrying the two transgenes Tg(*sox17:EGFP-T2A-KalTA4GI*) and Tg(*10xUAS:XDshDEP-mCherry/cmlc2:EGFP*) in the endoderm **(B)** Brightfield image. **(C)** Fluorescent image of *EGFP* expression in the heart from the *cmlc2* promoter and the pharyngeal endoderm from the *sox17* promoter. **(D)** Fluorescent image demonstrating low expression of *XDshΔDEP-mCherry* in the endodermal cells.

used to generate the Tg(*4xnrUAS:XDshΔDEP-mCherry/cmlc2:EGFP*) transgenic line. Unfortunately, again only low levels of expression of *XDshΔDEP-mCherry* were seen across multiple founder lines (data not shown). As a third attempt to achieve an endodermal specific expression of *XDshΔDEP-mCherry* I utilized the *Kaloop* amplification cassette (Distel et al., 2009). The *Kaloop* cassette contains the *Gal4* activator *KalTA4* under control of a *UAS* promoter, resulting in a positive feedback loop and enabling the original *KalTA4* signal to be amplified (as in Figure 5.15 A). I generated a Tg(*4xKaloop/4xnrUAS:XDshΔDEP-mCherry/cmlc2:EGFP*) construct. Unfortunately, no founders were recovered from multiple injection rounds suggesting that levels of *Kal4TA* overexpression were toxic even mosaically in the G_0 fish. To overcome the problems associated with expression of *XDshΔDEP-mCherry* specifically in the endodermal cells using the *Gal4/UAS* system I turned to another transgenic approach.

I generated a number of transgenic lines to enable an inducible disruption of PCP signalling specifically in the endoderm. This was done using a codon optimised version of the *Cre/Lox* system to achieve *Cre*-recombinase mediated recombination (Shimshek et al., 2002). The transgenic line Tg(*sox17:iCre/cmlc2:EGFP*) (Figure 5.11) was generated. This line has endodermal specific expression of *iCre* recombinase via the *sox17* promoter (Figure 5.11 A). To verify the function and endoderm-specificity of *iCre* recombinase expression the Tg(*sox17:iCre/cmlc2:EGFP*) line was crossed to a previously established traffic light Tg(*Bactin2:LoxP-mcherry-pA-LoxP-AcGFP-pA*) line (a kind gift from Dr. Thomas Hall) (Figure 5.11). The Tg(*Bactin2:LoxP-mcherry-pA-LoxP-AcGFP-pA*) line ubiquitously expresses *mCherry* in the absence of *iCre* recombinase (Figure 5.11 A). In the presence of *iCre* recombinase the *LoxP-mCherry-LoxP* cassette is excised allowing expression of the green fluorescent protein *AcGFP* (Figure 5.11 B). Embryos carrying both transgenes expressed *mCherry* in all tissues except the endoderm (Figure 5.11 D) and specifically expressed *AcGFP* in the endoderm (Figure 5.11 E). This demonstrated that *iCre* expression in the Tg(*sox17:iCre/cmlc2:EGFP*) transgenic line was specific to the endoderm and retained functional recombinase activity.

To partner the endodermal *iCre* line I generated Tg(*hsp70l:LoxP-EBFP2-pA-LoxP-XDshΔDEP-mCherry*) (Figure 5.12). This line has a *LoxP-EBFP2-pA-LoxP*

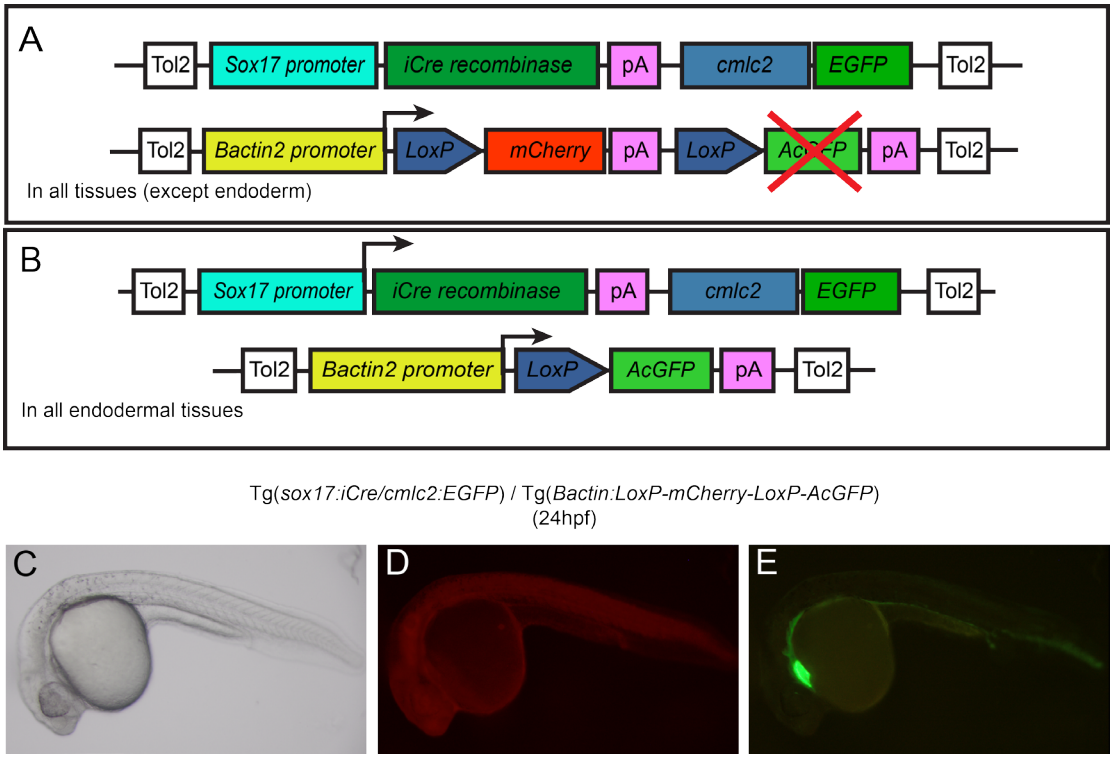

Figure 5.11 Characterising the Tg(*sox17:iCre/cmlc2:EGFP*) transgenic line. (A-B) Schematic representing the theoretical interaction within an embryo carrying the two transgenes Tg(*sox17:iCre/cmlc2:EGFP*) and Tg(*Bactin2:LoxP-mcherry-pA-LoxP-EGFP-pA*) in all tissues except the endoderm (A) and specifically in the endoderm (B). **(C-E)** Bright-field and fluorescent images of an embryo carrying the two Tg(*sox17:iCre/cmlc2:EGFP*) Tg(*Bactin2:LoxP-mcherry-pA-LoxP-EGFP-pA*) transgenes at 24 hpf. (D) Ubiquitous expression of *mCherry* from the *Bactin2* promoter. (E) *EGFP* expression in the heart from the *cmlc2* promoter indicating the embryo carries *iCre* recombinase. *EGFP* expression specifically in the endoderm, indicating specific endodermal *iCre* expression resulting in the excision of the *LoxP-mCherry-pA-LoxP* cassette in the endoderm, and allowing expression of *EGFP* from the *Bactin2* promoter.

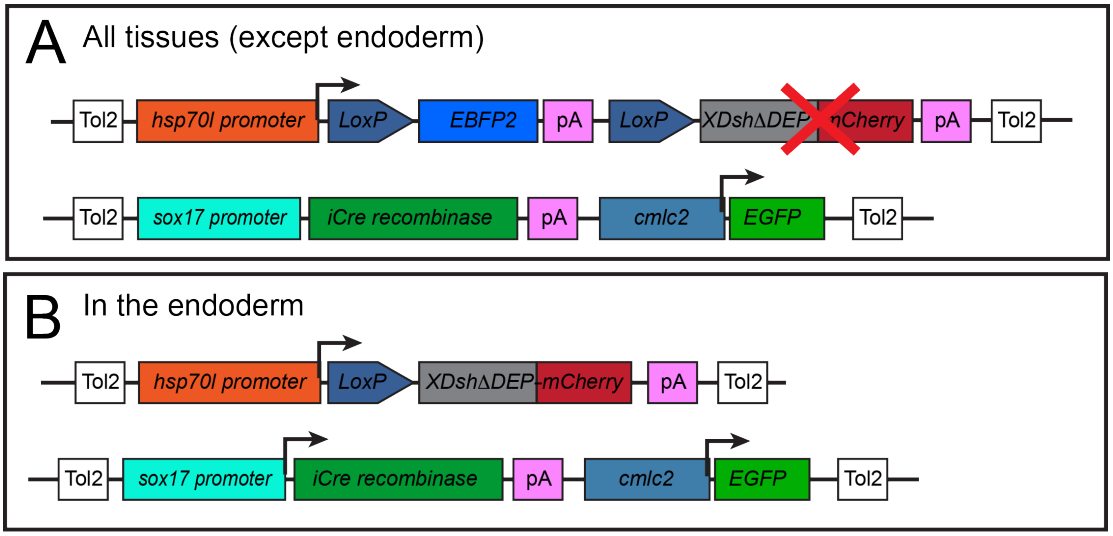

Tg(*hsp70l:LoxP-EBFP2-pA-LoxP-XDshΔDEP-mCherry-pA*)
Heat shock at shield (24 hpf)

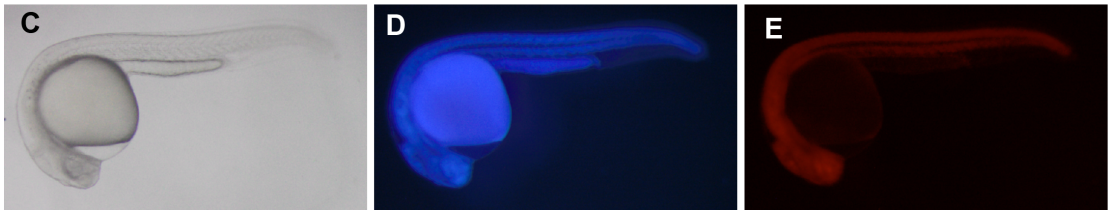

Figure 5.12 Characterising the Tg(*hsp70l:LoxP-EBFP2-pA-LoxP-XDshΔDEP-mCherry*) transgenic line. (A-B) Schematic representing the theoretical interaction within an embryo carrying the two transgenes Tg(*hsp70l:LoxP-EBFP2-pA-LoxPXDshΔDEP-mCherry*) and Tg(*sox17:iCre/cmlc2:EGFP*) in all tissues except the endoderm (A) and specifically in the endoderm (B). (A) *iCre* recombinase is not expressed in non-endodermal cells, and the *LoxP-EBFP2-pA-LoxP* cassette remains intact, preventing expression of *XDshΔDEP-mCherry* (B) In endodermal cells iCre recombinase is expressed from the *sox17* promoter, resulting in the excision of the *LoxP-EBFP2-pA-LoxP* cassette, allowing expression of *XDshΔDEP-mCherry*. **(C-E)** Brightfeild and fluorescent images of a Tg(*hsp70l:LoxP-EBFP2-pA-LoxP-XDshΔDEP-mCherry*) embryo at 24 hpf after a heat shock at shield. (D) Ubiquitous *EBFP2* expression (E) *XDshΔDEP-mCherry* expression without the presence of *iCre* recombinase.

cassette under the control of the *hsp70l* heat shock promoter, followed by a *XDshΔDEP-mCherry* dominant negative transgene (Figure 5.12 A). In the absence of *iCre*, the *EBFP2-pA* cassette is not excised preventing expression of the downstream *XDshΔDEP-mCherry* transgene after heat shock treatment (Figure 5.12 A). Theoretically, in the presence of *iCre* the *EBFP2-pA* cassette is excised and allows expression of *XDshΔDEP-mCherry* after heat shock treatment (Figure 5.12 B). To verify that the presence of the *LoxP-EBFP2-LoxP* cassette prevented expression of *XDshΔDEP-mCherry,* a heat-shock treatment was performed at shield stage on Tg(*hsp70l:LoxP-EBFP2-pA-LoxP-XDshΔDEP-mCherry*) F_2 embryos obtained from an incross of *EBFP2* positive F_1 parents (tested by heat shock treatment of embryos from an outcross). *EBFP2* expression was detected at 24 hpf under a fluorescence dissecting microscope (Figure 5.12 D), but unfortunately *mCherry* expression was also detected (Figure 5.12 E). This indicates the single poly-A sequence was not strong enough to prevent significant read-through expression of the *XDshΔDEP-mCherry* cassette. However, the level of *XDshΔDEP-mCherry* expression was not high enough to disrupt PCP signalling, as heat-shocked embryos were phenotypically wildtype at 24 hpf (Figure 5.12 C).

To confirm the functionality of the *LoxP* sites in excising the *EBFP2* cassette, *iCre* mRNA was injected into Tg(*hsp70l:LoxP-EBFP2-pA-LoxPXDshΔDEP-mCherry*) embryos. Injected embryos were heat-shocked at shield stage and analysed at 24 hpf. Unfortunately, *iCre* mRNA injected and heat-shocked embryos lacked both *EBFP2* and *XDshΔDEP-mCherry* expression (data not shown), indicating an aberrant excision of both transgene cassettes. Sequence analysis could not find any errors in the inserted construct sequence (data not shown). The loss of expression of both transgenes in the presence of *iCre* prevented this line from being useful in further experiments.

In an attempt to prevent read-through expression of *XDshΔDEP-mCherry* in the Tg(*hsp70l:LoxP-EBFP2-pA-LoxP-XDshΔDEP-mCherry*) line, I utilised a previously published STOP cassette. This cassette has a large size of 2.7 kb and contains a transcription stop sequence (triple SV40 polyadenylation sequence) to prevent read-through expression of 3'-cassettes (Srinivas et al., 2001). I generated the Tg(*hsp70l:LoxP-STOP-LoxP-XDshΔDEP-mCherry*) (Figure 5.13)

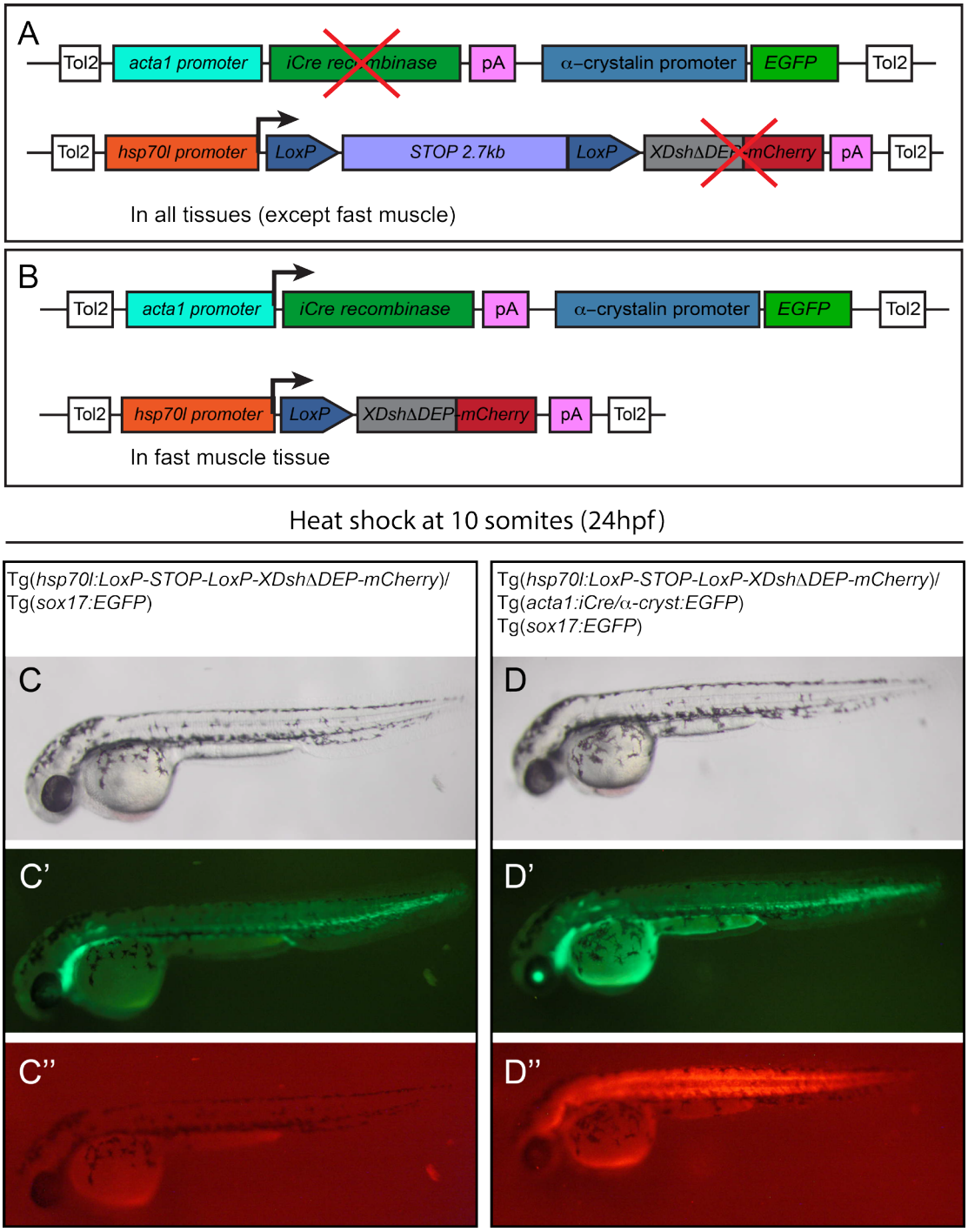

Figure 5.13 Characterising the Tg(*hsp70l:LoxP-STOP-LoxP-XDshΔDEP-mCherry*) transgenic line. (A-B) Schematic representing the theoretical interaction within an embryo carrying the two transgenes Tg(*hsp70l:LoxP-STOP-LoxP-XDshΔDEP-mCherry*) and Tg(*acta1:iCre/ α-cryst:EGFP*) in all tissues except the fast muscle (A) and specifically in fast muscle tissues (B). (A) In all tissues except fast muscle cells no iCre recombinase is expressed and the *LoxP-STOP-LoxP* cassette remains, preventing expression of *XDshΔDEP-mCherry* after a heat shock (B) In fast muscle cells *iCre* recombinase is expressed and excises the *LoxP-EBFP2-LoxP* cassette, allowing expression of *XDshΔDEP-mCherry* after a heat shock. **(C-C")** Brightfeild and fluorescent images of an embryo carrying the two Tg(*hsp70l:LoxP-STOP-LoxP-XDshΔDEP-mCherry*)/Tg(*sox17:EGFP*) transgenes at 24 hpf after a heat shock at shield. (C') no *EGFP* expression in the retina indicates the embryo does not express *iCre* recombinase (C").The *LoxP-STOP-LoxP* cassette is not excised preventing the expression of *XDshΔDEP-mCherry*. **(D-D")** Brightfeild and fluorescent images of an embryo carrying the three Tg(*hsp70l:LoxP-STOP-LoxP-XDshlΔDEP-*

mCherry)/Tg(*sox17:EGFP)*/Tg(*acta1:iCre/α-cryst:EGFP*) transgenes at 24 hpf after a heat shock at shield. (D') *EGFP* expression in the retina from the *α-cryst* promoter indicates the embryo expresses *iCre* recombinase in the fast muscle cells. (D") The *LoxP-STOP-LoxP* cassette has been excised by *iCre* recombinase in fast muscle cells allowing *XDshΔDEP-mCherry* to be expressed.

transgenic line. This line contains a *LoxP* flanked STOP cassette under the control of the *hsp70l* promoter, followed by the *XDshΔDEP-mCherry* cassette. To verify the ability of the STOP cassette to prevent read-through expression Tg(*hsp70l:LoxP-STOP-LoxP-XDshΔDEP-mCherry*)/Tg(*sox17:EGFP*) embryos subjected to a heat-shock treatment at shield were analysed at 24 hpf. *XDshΔDEP-mCherry* expression was not detectable under a fluorescence dissecting microscope (Figure 5.13 C"), indicating the functionality of the STOP cassette to prevent read-through expression.

To verify excision of the STOP cassette in the presence of *iCre*, Tg(*hsp70l:LoxP-STOP-LoxP-XDshΔDEP-mCherry*)/Tg(*sox17:EGFP*) fish were crossed to a previously established Tg(*acta1:iCre/α-cryst:EGFP*) line (a kind gift from Dr. Thomas Hall). Tg(*acta1:iCre/α-cryst:EGFP*) embryos express *EGFP* in the retina and *iCre* specifically in the fast muscle prior to 10 somites. Tg(*hsp70l:LoxP-STOP-LoxP-XDshΔDEP-mCherry*)/Tg(*sox17:EGFP*)/Tg(*acta1:iCre/α-cryst:EGFP*) triple transgenic embryos were subjected to a heat-shock treatment at 10 somites and analysis at 24 hpf. Embryos positive for *iCre* expression (Figure 5.13 D') had detectable *XDshΔDEP-mCherry* expression in the fast muscle cells at 24 hpf (Figure 5.13 D"), demonstrating correct excision of the *LoxP-STOP-LoxP* cassette to enable *XDshΔDEP-mCherry* expression.

To determine if the Tg(*hsp70l:LoxP-STOP-LoxP-XDshΔDEP-mCherry*) line could express *XDshΔDEP-mCherry* at levels high enough to disrupt PCP signalling F_2 embryos generated from an incross of F_1 parents were injected with *iCre* mRNA and subjected to a heat-shocked treatment at shield stage, and analysed at 24 hpf. *XDshΔDEP-mCherry* expression was detected ubiquitously throughout injected embryos, but unfortunately the embryos were phenotypically wildtype (data not shown). This result demonstrated that the transgene is not expressed at a level high enough to disrupt PCP signalling, and therefore this line was not suitable for further experiments.

5.2.3.2. Inhibition of PCP signalling in all tissues except the endoderm

I wished to investigate the non-autonomous influence the surrounding mesoderm had on endodermal morphogenesis, in respect of PCP signalling. To

achieve this I aimed to disrupt PCP signalling in all tissues except the endoderm in an inducible manner. Therefore to investigate the non-autonomous role of PCP signalling I generated the Tg(*hsp70l:LoxP-XDshΔDEP-mCherry-LoxP*) transgenic line (Figure 5.14). This line contains a *LoxP-XDshΔDEP-mCherry-LoxP* cassette under the control of the *hsp70l* promoter. The Tg(*hsp70l:LoxP-XDshΔDEP-mCherry-LoxP*) transgenic line was generated to partner the Tg(*sox17:iCre/cmlc2:EGFP*) line (Figure 5.11) and facilitate inhibition of PCP signalling in all tissues except the endoderm. Theoretically, in the absence of *iCre,* the *XDshΔDEP-mCherry* transgene should be expressed after a heat-shock treatment (Figure 5.14 A). In the presence of *iCre*, the *XDshΔDEP-mCherry* cassette would be excised, eliminating expression (Figure 5.14 B).

To verify the loss of *XDshΔDEP-mCherry* expression in the presence of *iCre* the Tg(*hsp70l:LoxP-XDshΔDEP-mCherry-LoxP*)/Tg(*sox17:EGFP)* line was crossed to the Tg(*acta1:iCre/α-cryst:EGFP*) line (fast muscle *iCre*). Embryos containing only the Tg(*hsp70l:LoxP-XDshΔDEP-mCherry-LoxP*) construct express *XDshΔDEP-mCherry* throughout the embryo at 24 hpf after heat-shock treatment at shield stage, demonstrating that the *hsp70* is capable of directing *XDshΔDEP-mCherry* under heat shock in this line (Figure 5.14 E). Double transgenic Tg(*hsp70l:LoxP-XDshΔDEP-mCherry-LoxP*)/Tg(*acta1:iCre/α-cryst:EGFP*) embryos do not, however, have detectable *XDshΔDEP-mCherry* expression in the fast muscle cells (Figure 5.14 F-H). This demonstrates that the *LoxP* sites retain functionality and can mediate successful excision of the transgene cassette in the presence if *iCre*. Unfortunately these embryos do not display convergence and extension defects at 24 hpf. This indicates that again, the *XDshΔDEP-mCherry* expression is not high enough in this transgenic line to disrupt PCP signalling. F_2 embryos obtained by an incross of positive F_1 parents also failed to give the reduction in convergence and extension that is characteristic of PCP signalling disruption (data not shown). This further demonstrated that with the given strength of the *hsp70l* promoter, transgene copy number was not high enough to facilitate effective disruption of PCP signalling, and this line was unsuitable for use in future experiments.

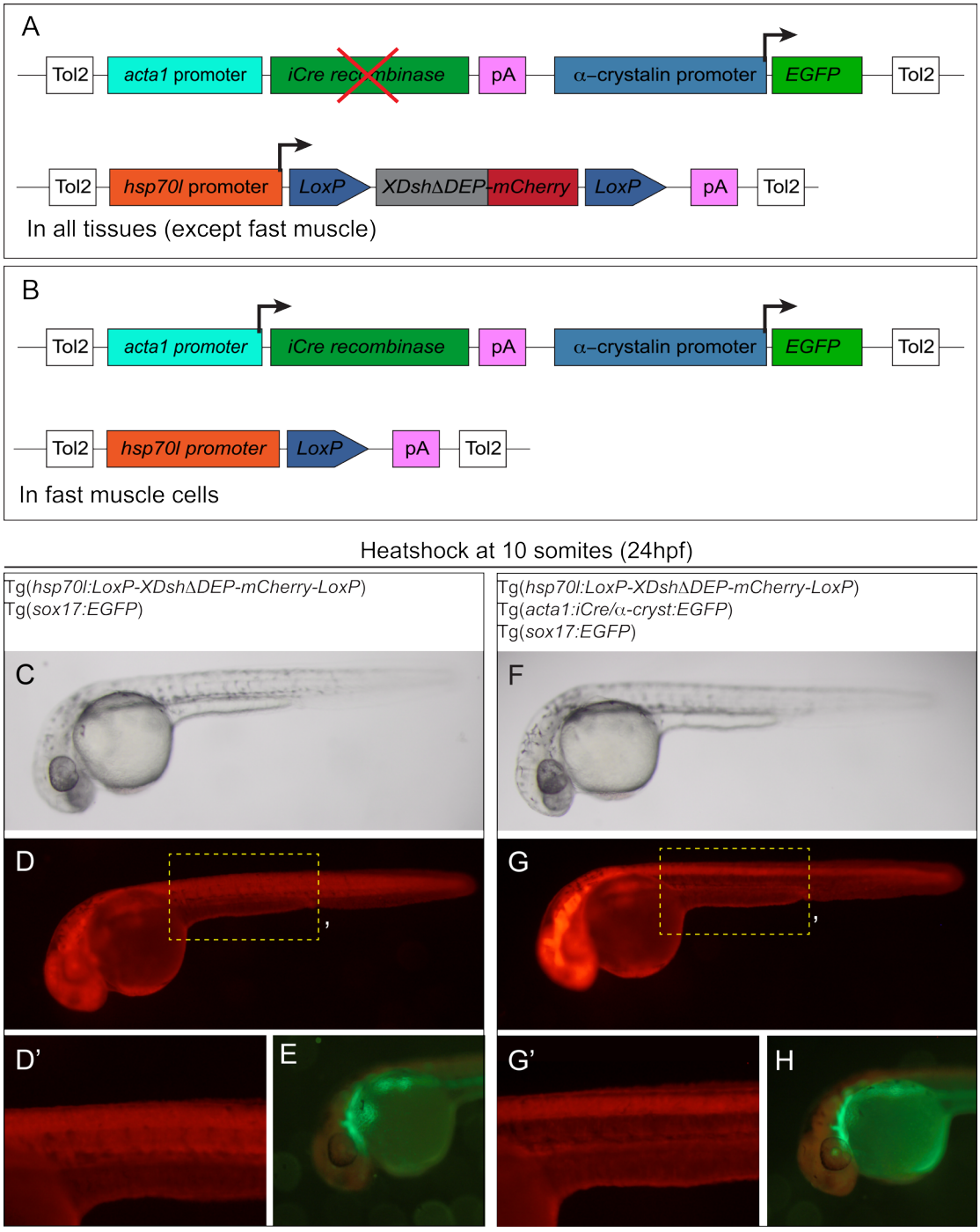

Figure 5.14 Characterising the Tg(*hsp70l:LoxP-XDshΔDEP-mCherry-LoxP*) transgenic line. (A-B) Schematic representing the theoretical interaction within an embryo carrying the two transgenes Tg(*hsp70l:LoxP-XDshΔDEP-mCherry-LoxP*) and Tg(*acta1:iCre/α-cryst:EGFP*) in all tissues except fast muscle (A) and specifically in fast muscle (B). (A) iCre recombinase is not expressed in non-fast muscle cells, and the *LoxP-XDshΔDEP-mCherry-LoxP* cassette remains intact (B) In fast muscle cells *iCre* recombinase is expressed from the *acta1* promoter, and results in the excision of the *LoxP-XDshΔDEP-mCherry-LoxP* cassette. **(C-E)** Brightfeild and fluorescent images of an embryo carrying the two Tg(*hsp70l:LoxP-XDshΔDEP-mCherry-LoxP*)/Tg(*sox17:EGFP)* transgenes at 24 hpf after a heat shock at shield. (D) ubiquitous *XDshΔDEP-mCherry* expression. (D') Zoomed image of the yellow dotted box in D demonstrating the expression of *XDshΔDEP-mCherry* expression in fast muscle cells. (E) no *EGFP* is expressed the retina, indicating the embryos contains not carry iCre recombinase. **(F-H)** Brightfeild and fluorescent images of an embryo carrying the three Tg(*hsp70l:LoxP-XDshΔDEP-mCherry-*

LoxP)/Tg(*sox17:EGFP)*/Tg(*acta1:iCre/α-cryst:EGFP*) transgenes at 24 hpf after a heat shock at shield. (G) *XDshΔDEP-mCherry* expression. (G') Zoomed image of the yellow dotted box in G demonstrating the loss of *XDshΔDEP-mCherry* expression in fast muscle cells, resulting from the *LoxP* cassette being excised by *iCre*. (H) EGFP expression in the retina from the *α-cryst* promoter indicating the embryo contains iCre recombinase.

5.2.3.3. Inhibition of PCP signalling specifically in the endoderm via a Vangl2 dominant negative

In this study, multiple transgenic approaches to achieve a tissue specific disruption of PCP signalling using *XDshΔDEP-mCherry* overexpression have proved unsuccessful. To try a different transgenic approach to disrupting PCP signalling, I utilised a version of the *trilobite* gene lacking the PDZ binding motif (*StbmΔPBM*) that has been demonstrated in *Xenopus* to act as a dominant negative (Goto and Keller, 2002). *trilobite* has two gene family members in the zebrafish genome, however only one is expressed during early developmental stages (Jessen et al., 2002; Jessen and Solnica-Krezel, 2004). It was reasoned that as only one copy of this gene was expressed at the stages examined in this thesis, transgenic lines utilising the *StbmΔPBM* dominant negative might work with lower levels of expression to disrupt PCP signalling than *XDshΔDEP-mCherry.* Therefore I generated a *StbmΔPBM-mCherry* transgene to use in place of *XDshΔDEP-mCherry* to disrupt PCP signalling. Two stable lines were generated: Tg(*4xnrUAS:StbmΔPBM-mCherry/cmlc2:mCherry*) and Tg(*4xKaloop/4xnrUAS:StbmΔPBM-mCherry/cmlc2:mCherry*) (Figure 5.15). Both transgenic lines were crossed to a previously established *Gal4* line, Tg(*acta1:KalTA4GI/a-crystalin:EGFP*) (a kind gift from Dr. Thomas Hall). However, double transgenic embryos for either construct had no detectable *StbmΔPBM-mCherry* expression in fast muscle cells (positive heart *mCherry* and positive retina *EGFP* expression) (Figure 5.15 A). Given this disappointing result, further attempts to generate new stable lines were not made.

5.2.4. Enhancing the heat shock response to generate higher transgene expression

The chemical BGP-15 is a pharmacological inducer of the heat shock response pathway, and has been shown to upregulate heat shock proteins in mice (Chung et al., 2008; Gehrig et al., 2012). I was interested in using this chemical to increase the level of transgene expression after heat shock treatment in the multiple heat inducible transgenic lines that displayed insufficient expression

levels. It was hoped that exposure to BGP-15 would increase transgene expression to a level suitable to disrupt PCP signalling, and allow the lines to be functionally useful.

To test this theory, Tg(*hsp70l:XDshΔDEP-mCherry*) embryos were raised in the presence of either 50mM BGP-15 or eggwater as a control, and subjected to a heat shock treatment at shield stage. Analysis of transgene activation via *mCherry* expression was undertaken 6 hours post heat shock treatment (Figure 5.16). In contrast to what was expected, the presence of BGP-15 significantly reduced the level of transgene expression compared to control embryos (Figure 5.16 B, D). Increasing the concentration to 200mM had the same effect (data not shown). Therefore investigations into increasing transgene expression were not pursued further.

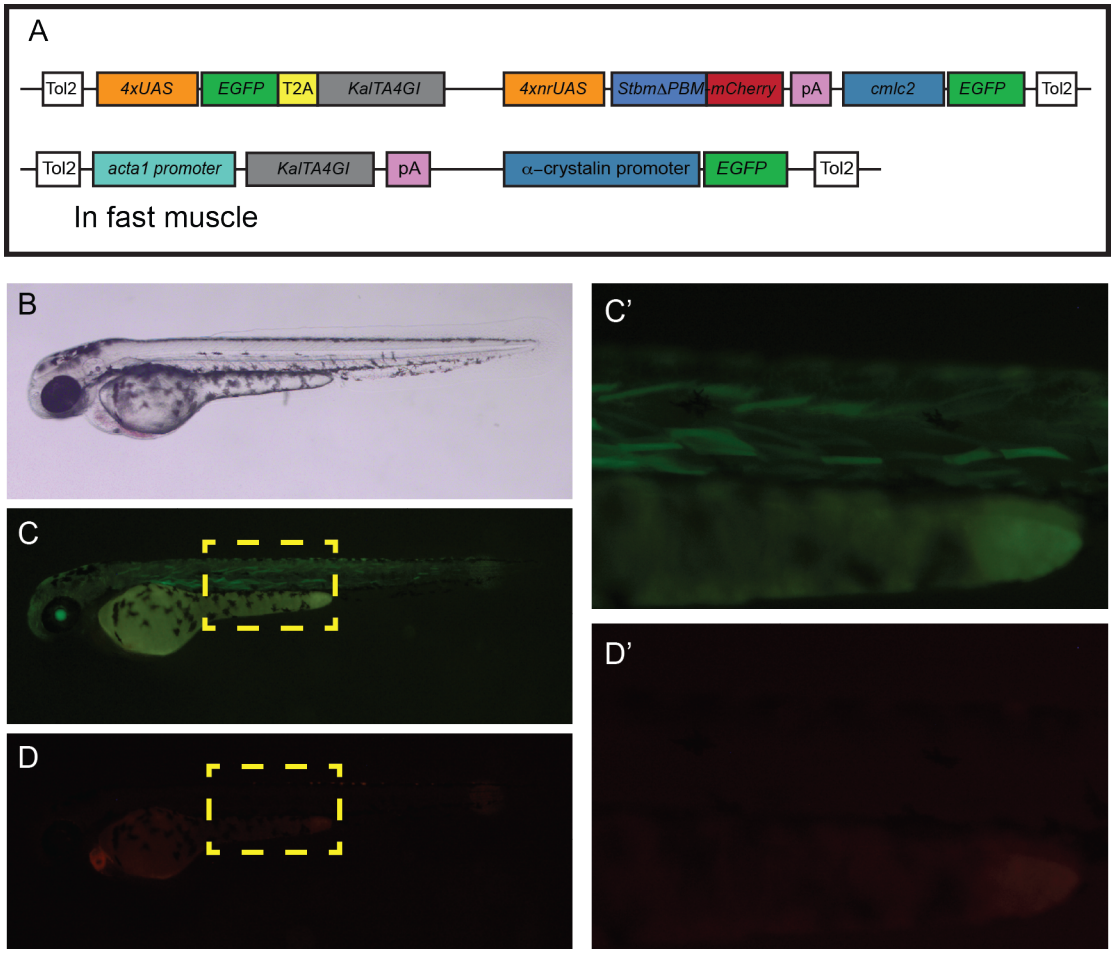

Figure 5.15 Characterising the Tg(*4xKaloop/4xnrUAS-StbmΔPBM-mCherry/cmlc2:mCherry*) transgenic line. (A) Schematic representing the theoretical interaction within an embryo carrying the two transgenes Tg(*4xKaloop/4xnrUAS-StbmΔPBM-mCherry/cmlc2:mCherry*) and Tg(*acta1:KalTA4GI/a-crystalin:EGFP*) in fast muscle cells. **(B-D')** Bright-field and fluorescent images of an embryo carrying the two Tg(*4xKaloop/4xnrUAS-StbmΔPBM-mCherry/cmlc2:mCherry*) and Tg(*acta1:KalTA4GI/a-crystalin:EGFP*) transgenes at 24 hpf. (C) *EGFP* expression in the retina indicating the embryo carries the *acta1:KalTA4GI* cassette. (D) *mCherry* expression in the heart indicates the embryo carries the *4xKaloop/4xnrUAS-StbmΔPBM-mCherry* cassette. (C') Zoomed image of the yellow dotted box in (C) showing *EGFP-T2A-KalTA4GI* expression in the fast muscle of the somites. (D') Zoomed image of the yellow dotted box in D, showing an absence of *StbmΔPBM-mCherry* expression in the fast muscle of the somites.

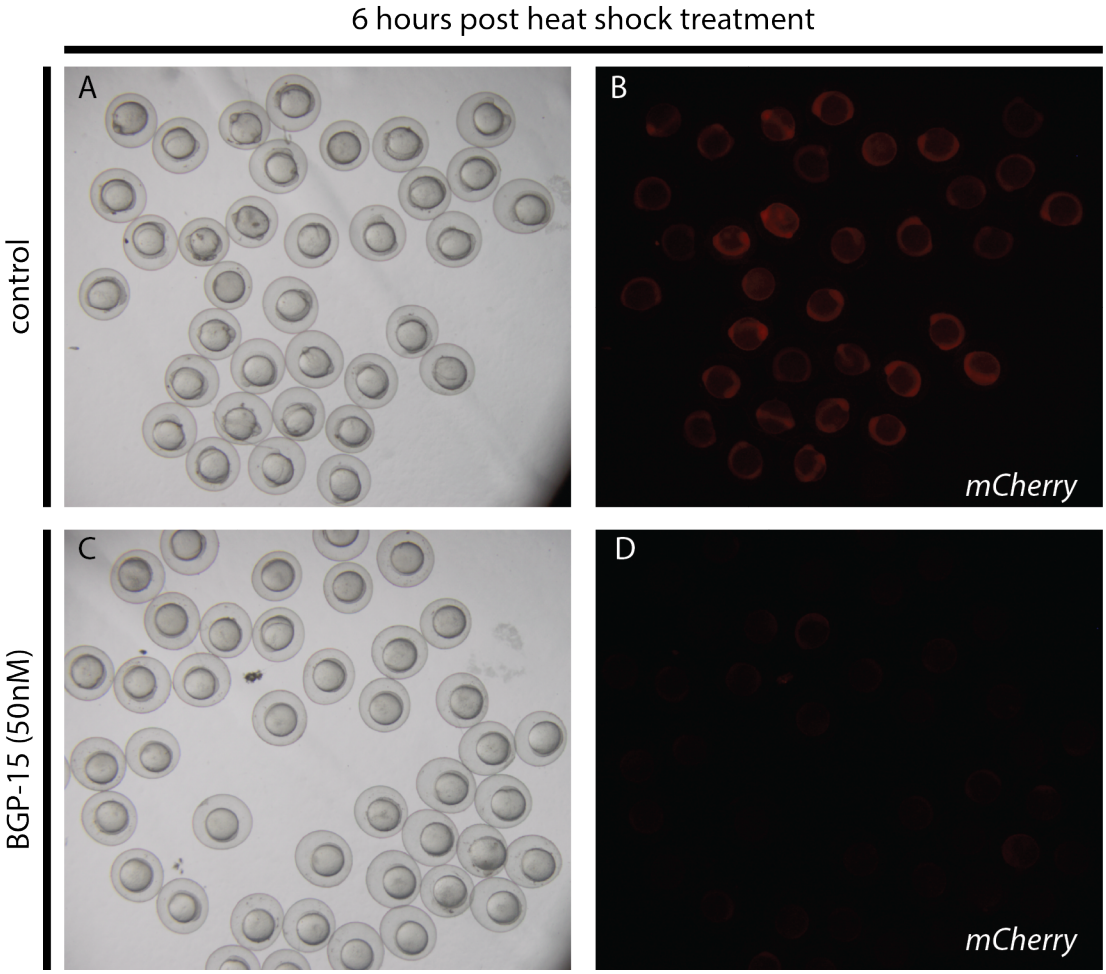

Figure 5.16 The effect of BGP-15 treatment on transgene activation in Tg(*hsp70l:XDshΔDEP-mCherry*) embryos. (A-D) Tg(*hsp70l:XDshΔDEP-mCherry*) embryos were grown in 50mM BGP-15 as previously described, or eggwater as a control. Embryos were subjected to a heat shock treatment at shield stage and *hsp70l* promoter expression levels were determined via *mCherry* fluorescence at 6 hours post heat shock. BGP-15 treatment prior to heat shock treatment resulted in a decrease in transgene activation, as determined by *mCherry* fluorescence. Experiments using 200mM GFP-15 gave similar results.

5.3. Discussion

5.3.1. Summary of results

This chapter I have determined that the polarisation of the MTOC in endodermal cells is not required during migration at early somitogenesis stages.

To investigate the autonomous and non-autonomous roles of PCP signalling during endodermal morphogenesis I generated a number of transgenic lines. To aid in the generation of these transgenic lines I developed a number of molecular cloning tools designed to reduce the time and cost of vector generation. These molecular genetic tools will also be of benefit the zebrafish research community by facilitating rapid generation of Tol2-transgenesis vectors at a significantly reduced expense and time, and have subsequently been published and made publically available (see Appendix Two).

5.3.2. Endodermal MTOC polarisation is present during migration but absent during midline aggregation

Actively migrating mesodermal and ectodermal mesenchymal cells have previously been shown to have a directed MTOC polarity towards the direction of migration at gastrulation stages (Sepich et al., 2011). My results demonstrate that the mesoderm has a dorsally directed MTOC polarisation at somitogenesis stages. Therefore, the somitogenesis stage data generated in this thesis is consistent with these published gastrulation stage MTOC polarisation observations. Together, these results indicate that the previously identified mesodermal MTOC polarisation at gastrulation stages is retained into somitogenesis stages.

I investigated whether the endoderm also has MTOC polarity during somitogenesis stages. The endoderm does not display a polarised MTOC orientation during early somitogenesis stages. It was reasoned that, like the surrounding mesoderm, the endoderm would also have a polarised MTOC during somitogenesis stages. However, my data does not support this, as during early somitogenesis stages the endoderm has a randomised MTOC localisation rather

than directed towards the dorsal side of the embryo (Section 5.2.2.2). This result suggests that although the endoderm is migrating towards the dorsal midline at these stages, unlike the mesoderm, it does not require MTOC polarisation for this process at this stage. My results demonstrate a difference in the MTOC polarisation between the endoderm and the mesoderm during dorsal migration and suggest a difference in migratory behaviour of the endoderm and the mesoderm during somitogenesis stages. Nair and colleagues (2008) suggest that the endoderm is tethered to the overlying mesoderm during early somitogenesis stages, and this represents a passive migrating of the endoderm towards the dorsal midline. My results are consistent with this idea.

At late somitogenesis stages (16 somites, 17 hpf) the endodermal cells gain significant polarisation towards the dorsal midline (Figure 5.9 E). During this stage the endoderm is undergoing midline aggregation and it was reasoned that they would have a polarity directed towards the dorsal midline as they underwent this process. My data support the hypothesis that cell polarisation is involved in this process. However, the absence of MTOC polarisation, as seen in *tri* mutants (Figure 5.9 E), does not prevent endodermal cells leaving the monolayer (Section 3.2.3.2). Overall, these data demonstrate that endodermal cells do not require a polarised MTOC during migration to the midline, but do polarise the MTOC during the stages during midline aggregation.

It would be interesting to investigate the MTOC orientation of endodermal cells actively leaving the monolayer to determine if the process of leaving the monolayer is an active process that requires directed polarity. Unfortunately this would require a third plane to the analysis and was beyond the scope of this thesis.

5.3.3. Mesodermal and endodermal cells require PCP signalling to polarise the orientation of the MTOC during somitogenesis stages

Disruption of PCP signalling has been shown to cause randomisation of MTOC polarity in mesodermal and ectodermal cells during gastrulation stages (Sepich et al., 2011). My results further this by showing that *tri* and *kny* mutant mesodermal cells also have randomised MTOC orientations into somitogenesis

stages. Similarly, *Hsp@shield* mesodermal cells have a randomised MTOC orientation at early somitogenesis stages (3 somites). Interestingly, unlike *tri* and *kny* mutants, *Hsp@shield* mesodermal cells do generate a polarised MTOC by late somitogenesis stages (16 somites), however the direction of this orientation is different from wildtype and predominantly directed towards anterio-ventral regions (Figure 5.9 F). These results are consistent with previous observations that a disruption in PCP signalling results in the disrupted MTOC polarisation in migrating mesodermal cells. Interestingly however, in this study *dvl* appears to be dispensable for cell polarisation in mesodermal cells at late somitogenesis stages, and suggests that *dvl* is required for the correct direction of this polarisation. Taken together, these data suggests that in the mesoderm at late somitogenesis stages *tri* and *kny* are required to establish a polarisation of the MTOC, and *dvl* is required to facilitate the directionality of this polarisation.

During early somitogenesis stages, endodermal cells do not display MTOC polarisation, and therefore would not require PCP signalling in this particular process. However, endodermal cells at later somitogenesis stages during midline aggregation stages display a polarisation of MTOC orientation, directed toward the dorsal midline (Figure 5.9 C). *tri* mutants and *Hsp@shield* embryos do not generate this MTOC polarisation, indicating that both *tri* and *dvl* are required for this process. Interestingly, *kny* mutants are able to generate a polarised MTOC orientation. This indicates that *kny* is dispensable for the polarisation of the endoderm during midline aggregation. Taken together, these data demonstrate a requirement for PCP signalling in endodermal MTOC polarisation during midline aggregation, but independent of *kny*.

Overall, this data demonstrates that migrating endodermal and mesodermal cells have an overall requirement for PCP signalling for MTOC polarisation at somitogenesis stages, but differential requirements for *dvl* and *kny*.

5.3.4. Lessons from failed transgenics

Generating transgenic lines is the gold standard approach for zebrafish genetics experiments. Unfortunately, in this study the numerous transgenic lines

generated to investigate the autonomy of PCP signalling in endodermal morphogenesis did not disrupt PCP signalling, and were unsuitable for use in experimentation. The failure of these transgenic lines to facilitate the required expression levels identified four key considerations that future investigations utilising zebrafish transgenesis may need to address.

5.3.4.1. Level of transgene expression required

When generating stable transgenic lines the desired level of transgene expression needs to be taken into consideration. This is particularly relevant when utilising dominant negative alleles. The level of expression and gene copy number of the dominant negative target protein(s) may influence the level of dominant negative expression required to get an appropriate disruptive interaction with the target protein.

In situations where multiple copies of target genes are expressed, increased levels of the dominant negative may be achieved through expression of multiple copies of the dominant negative allele, linked together via T2A linker sequences, in a single open reading frame. This may overcome any issues with low expression and lack of target knockdown. In this study, the five target *dishevelled* genes for *XDshΔDEP-mCherry* are all expressed during early development (Section 4.2.1.4), and so multiple transgene insertions are required to successfully disrupt PCP signalling. Future transgenic lines utilising multiple *XDshΔDEP-mCherry* transgenes linked via T2A like sequences in a single open reading frame might enable stable transgenic lines with a single (or several) insertions that are capable of inducing a disruption of PCP signalling.

5.3.4.2. Transgene copy number

Insert mapping of Tol2-mediated transgenics has identified that the majority of G_0 parent founders carry as many as 8 or more independent insertions (Parinov et al., 2004). The Tg(*hsp70l: XDshΔDEP-mCherry*) line I generated, characterised, and mapped, was found to contain five transgene insertions after a single outcross (Section 4.1.2.1), with embryos requiring a minimum of four insertions

to achieve successful disruption of the PCP signalling pathway after heat shock treatment (Section 4.2.2.1).

Without identifying the transgene insertion number in a newly generated transgenic line, researchers can be faced with unpredictable variations in expression levels from each subsequent outcross or incross. This effect is often thought to result from transcriptional silencing (methylation), as is the case with repetitive UAS promoter elements (Akitake et al., 2011). However, in lines without repetitive sequences the transgene copy number is often overlooked as a causative reason for variations in expression. This is of particular importance for stable lines that are deposited into centralised services such as ZIRC (zebrafish.org), as subsequent generations may display different expression levels. This is highlighted in the Tg(*hsp70l:XDshΔDEP-mCherry*) line, as it requires multiple transgene insertions to remain functional and therefore sperm freezing and re-establishing the line, or outcrossing and subsequent incrossing, requires a significant amount of genotyping to identify individual fish that carry the correct number of insertions.

Transgene copy number needs to be carefully considered in transgenic lines designed to model human disease, in which mutant alleles of human genes are expressed in wildtype or mutant backgrounds, as the level of transgene expression may influence aetiology. The use of PhiC31 site directed transgenesis appears to have a significant benefit over Tol2-mediated transgenesis in this respect, as it only inserts into engineered genomic locations (Mosimann et al., 2013).

5.3.4.3. Transgene integration site

The transgene integration site can have significant epigenetic effects on the expression of reporter genes. This study utilised the Tg(*sox17:EGFP*) reporter line to label the endoderm during early development via the endoderm specific *sox17* promoter (Mizoguchi et al., 2008). Endogenous *sox17* expression begins at 50 % epiboly and is no longer detectable in the endoderm at the 5 somite stage (Alexander and Stainier, 1999). However, the Tg(*sox17:EGFP*) line has an integration site enhancement and continues to express *EGFP* to at least 60 hpf,

with ectopic expression of *EGFP* in cells other than endoderm after 24 hpf. The two lines I generated utilising the same *sox17* promoter sequence with a fluorescent reporter, Tg(*sox17:EGFP-T2A-KalTA4GI*) and Tg(*sox17:mCherry*) (data not shown), had expression patterns closely resembling expression of endogenous *sox17* with respect to timing and specificity. Expression of *EGFP* in Tg(*sox17:EGFP-T2A-KalTA4GI*) embryos was low and fluorescence levels decreased significantly during somitogenesis stages (Figure 5.10 C) indicating a termination of transcription in the endoderm during these stages and a closer recapitulation of wildtype *sox17* expression patterns than that of Tg(*sox17:EGFP*). The low level and early termination of expression from the *sox17* promoter made it unsuitable to drive expression of the *Gal4* transcriptional activator in this project. Perhaps the use of the highly active *Gal4-VP16* (Distel et al., 2009) under the control of the *sox17* promoter may enhance transcriptional activation. Overall these results demonstrate the importance of carefully selecting founder lines that recapitulate native expression patterns of the promoter used.

5.3.4.4. Positive control for dominant negative expression

In transgenic lines utilising dominant negative alleles, a well-defined phenotype that can be used as a positive readout of correct target knockdown needs to be known to order to direct the screening of possible founders for stable lines. The selection of founder lines solely based on reporter gene fluorescence without a phenotypic readout to verify target knockdown may result in lines that generate inaccurate experimental data. In this study the levels of *XDshΔDEP-mCherry* expression, as determined from *mCherry* fluorescence, in the Tg(*hsp70l:XDshΔDEP-mCherry*) and Tg(*hsp70l:LoxP-XDshΔDEP-LoxP-mCherry*) lines after a heat-shock treatment appeared similar. However only Tg(*hsp70l:XDshΔDEP-mCherry*) had expression levels over the required threshold to produce a disruption of PCP signalling and thus resulted in the characteristic PCP convergence and extension defect phenotype. This demonstrates the need for a phenotype that can be used as a positive selection marker for target gene knockdown when selecting founder lines.

Overall this study identified four key points for consideration when generating transgenic zebrafish lines that should be taken into consideration when selecting founder lines, to avoid potential variations in expression and inaccuracies in experimental data.

5.3.5. TA-cloning vectors as community based tools

In this study I generated and described the use of three TA-clonable Gateway entry vectors p5E-TA, pME-TA, and p3E-TA, as well as a TA-clonable expression vector pCS2+TA. These four vectors contain an *XcmI* based TA-cloning linker approach (*XcmI-EGFP-XcmI*) to facilitate the rapid TA-cloning of PCR products directly into the final vectors. These TA-clonable entry vectors can be used in a multifunctional way to enable rapid one step generation of Tol2-transgenesis vectors. All three TA-clonable entry vectors can be used in this way to generate final pDestTol2:TA-clonable transgenesis vectors, using only one multisite LR reaction (for the initial reaction), no long *attB* primers, and without the need to pass the gene of interest through a middle entry vector.

Recently the ΦC31 integrase system has been demonstrated to work in zebrafish, with stable lines available that containing characterized insertion sites (Mosimann et al., 2013). The *att*B transgenesis backbone vector containing the ΦC31 sites (pDestattB and its derivative pDestattB/CY) also utilizes the Multisite Gateway system to generate final transgenesis vectors, as well as other destination vectors that use the *att*L and *att*L recombination sites. I hope that these tools will enable laboratories generating transgenic zebrafish to reduce the cost and time taken to generate transgenesis vectors.

Chapter 6. Discussion

6.1. Introduction

During gastrulation the endoderm migrates to the dorsal midline as a single layer of cells against the yolk syncytial layer (YSL) (Warga and Nusslein-Volhard, 1999), but the process by which this monolayer coalesces into a primitive endodermal rod was unknown when this project was undertaken. In this thesis, I aimed to identify the process of endoderm morphogenesis from somitogenesis stages up until formation of the primitive endodermal rod at 24 hpf.

The PCP mutants *tri* and *kny* have a reduction in convergence and extension (Topczewski et al., 2001; Jessen et al., 2002), and it was reasoned that endodermal morphogenesis might also be affected in these mutants, which would indicate a role for PCP in endodermal movement. This project aimed to investigate the role of the PCP signalling pathway during various stages of endodermal morphogenesis. I generated transgenic tools to further analyse this problem, and to demonstrate their utility, I analysed the role of the PCP signalling pathway during brain morphogenesis.

6.2. Endodermal morphogenesis

There has been a large amount of research into the movements of the endoderm during gastrulation stages (Warga and Nusslein-Volhard, 1999; Ober et al., 2004; Mizoguchi et al., 2008; Nair and Schilling, 2008; Pezeron et al., 2008). However, the process of endoderm morphogenesis after gastrulation finishes (100 % epiboly) until formation of the primitive endodermal rod (midline aggregation) was previously unknown. I have investigated the process of endodermal migration to the dorsal midline during somitogenesis stages in this thesis.

6.2.1. The polarisation of the Microtubule organising centre (MTOC) is not required for endodermal cell migration

Mesodermal cells have a polarised microtubule organising centre (MTOC) orientation that is directed towards the dorsal midline during gastrulation stages (Sepich et al., 2011). I investigated if the endoderm was similarly polarised in respect to MTOC orientation during migration to the midline at somitogenesis stages. My results demonstrate that endodermal cell shape is relatively circular during early somitogenesis stages (Section 3.2.4), and that the MTOC orientation is not polarised in these cells (Section 5.2.2.2).

The polarised orientation of the MTOC relative to the nucleus is generally considered to reflect the overall cell polarity in migrating cells (Bergmann et al., 1983; Schmoranzer et al., 2003; Prigozhina and Waterman-Storer, 2004). However, the presence of the MTOC at the leading edge of cells is not crucial for migration. In neutrophils the orientation of the MTOC polarisation is not directed towards the leading edge of the cell (Xu et al., 2005). Surprisingly, a fully functional microtubule network is actually dispensable for chemotactic migration in neutrophils, but not in fibroblasts and macrophages (Wittmann and Waterman-Storer, 2001; Xu et al., 2005). It has been shown that the majority of endodermal filopodial processes are orientated toward the direction of migration during gastrulation stages, and the direction of these filopodial processes is regulated by *sdf1/cxcr4* signalling (Mizoguchi et al., 2008). These filopodial extensions are thought to be required for the endoderm to sense the correct direction of migration during gastrulation stages, but it is unknown if they are required during somitogenesis stages. Taking these studies together with the lack of endodermal MTOC polarisation I have observed, it can be concluded that, unlike the mesoderm, a polarised MTOC is not required in endodermal cells for migration to the dorsal midline, but that this does not necessarily preclude an active migration. If filopodial processes are required in the endoderm during somitogenesis stages then a polarised MTOC is not necessary for either filopodial formation or orientation of the filopodial processes.

My results demonstrate that the mesodermal cells that surround the endoderm maintain a polarised MTOC during somitogenesis stages (Section 5.2.2). These results extend upon previous research (Sepich et al., 2011) that identified a MTOC polarisation during gastrulation stages, and demonstrate that the mesoderm remains polarised towards the dorsal midline from gastrulation stages through to mid-somitogenesis stages (16 somites) at least. These results highlight the difference between the polarised states of the mesoderm and the endoderm during migration to the midline from gastrulation stages to somitogenesis stages. Although the mesodermal cells analysed in this study were in a similar location to the endoderm, these two cell types have different physical environments. Endodermal cells occupy a unique embryonic environment during gastrulation until mid-somitogenesis stages. The endoderm is the only cell type to remain in continuous contact with the membrane of the YSL throughout gastrulation. Cell shape and adhesion are known to be important is determining polarisation of the MTOC, and it is likely that the difference between the MTOC polarisation states of the mesoderm and endoderm is due in part to their different physical environments.

6.2.1.1. YSL ECM might regulate endodermal cell polarity

Endodermal cells have a unique flattened cell shape against the YSL during migration stages (Warga and Nusslein-Volhard, 1999), in contrast to mesodermal cells in a similar position, which have a more three-dimensionally round cell shape (Coyle et al., 2008) (Figure 6.1). I identified that endodermal cells are relatively circular during somitogenesis stages (Section 3.2.4). MTOC orientation has been shown to be largely dependent on the state of migration, cell shape, and the influence of surrounding cells (Pouthas et al., 2008; Schmoranzer et al., 2009; Hale et al., 2011), with circular cells tending to have a symmetrical MTOC pattern that reflects the underlying non-polarised state of the cell (Hale et al., 2011). Together this suggests that endodermal cells have more cell surface area in contact with the ECM than the surrounding mesodermal cells. ECM components such as E-cadherin, Fibronectin, and Laminin are enriched at the YSL boundary and tissue boundaries (Montero et al., 2005; Latimer and

Jessen, 2009). The YSL has been suggested to regulate ECM components that serve as a scaffold for the overlying cells to migrate on (Sakaguchi et al., 2006). YSL specific knockdown of the *mix*-family gene *mtx1* has been shown to regulate global embryonic Fibronectin levels, and also results in trunk endodermal defects during organogenesis stages. However, the Fibronectin mutant *natter* did not produce these endodermal defects (Trinh and Stainier, 2004). However, as the maternal contribution of Fibronectin was not investigated, a role for Fibronectin as a YSL regulated candidate molecule can not be eliminated.

S1pr2/Gα13 signalling is required autonomously for anterior endodermal migration (Ye and Lin, 2013). Gα12/13 are both maternally deposited and have been demonstrated to control C&E and epiboly movements by regulating *E-cadherin* function (Lin et al., 2005; Lin et al., 2009). *E-cadherin* is required for correct epiboly movements (Kane et al., 2005; Shimizu et al., 2005; Lin et al., 2009), and is highly enriched at the yolk cell membrane during gastrulation (Montero et al., 2005). Future experiments investigating endodermal cell migration in embryos in which *E-cadherin* or members of the G-protein alpha family are specifically knocked down in the YSL using a morpholino approach may determine the role of the YSL in endodermal cell migration. This can be achieved by injecting morpholino into the yolk after the 1000 cell stage (Trinh and Stainier, 2004).

Overall these results suggest that the mesoderm and endoderm may have different mechanisms regulating the migration to the dorsal midline during early somitogenesis, one in the mesoderm requiring or producing a polarised MTOC orientation, and another in the endoderm where MTOC polarisation is neither required nor produced. The *sdf1/cxcr4* model proposed by Nair et al (2008) and Mizoguchi et al (2008) suggests that the mesoderm and endoderm have very different behaviours during gastrulation. The observations of different MTOC polarisation states in mesodermal and endodermal cells in this study are in keeping with this theory.

6.2.2. A possible role for embryo elongation in driving the thinning and extension of the endoderm

PCP signalling is known to regulate both convergence and extension (C&E) and anterior-posterior (A-P) axis extension of the mesoderm and ectoderm. Disruption of PCP signalling results in a shortened and broadened A-P axis from early somitogenesis stages onwards, as displayed in *tri* and *kny* mutants (Marlow et al., 1998; Topczewski et al., 2001; Jessen et al., 2002; Marlow et al., 2004). My results in Section 3.2.2 demonstrated that that the endoderm in *tri* and *kny* mutants is also wider than in wildtype embryos at all somitogenesis stages analysed. This appears to result either from the endoderm starting dorsal migration later than wildtype endoderm, or from starting at different location than wildtype endodermal cells.

In this study I was able to disrupt PCP signalling in a time specific manner using the Tg(*hsp70l:XDshΔDEP-mCherry*) transgenic line, and investigate the role of PCP signalling after C&E is complete (Figure 6.1). Interestingly, disruption of PCP signalling after C&E stages, during the stages in which tail eversion (when the tail leaves the yolk) and extension occur (Kanki and Ho, 1997), results in an increase in embryo width and endodermal width (Section 4.1.3) similar to when PCP is disrupted during gastrulation stages. This result is highly significant as it demonstrates that PCP plays an important and time-specific role during tail eversion and extension stages, and therefore possibly implicates tail elongation itself in driving the narrowing of the embryo trunk regions including the endoderm.

The ECM protein N-cadherin has been demonstrated to have a specific role in tail extension, with *N-cadherin* (*N-cad*^{m117}) mutants having reduced tail eversion and extension with only minor disruptions to convergence and extension (Harrington et al., 2007). *N-cad*^{m117} mutants develop a normal A-P axis up until 16 somites, coinciding with the onset of tail eversion, and then fail to undergo correct tail extension. A synergistic genetic interaction was also identified between *N-cad* and *tri* in regulating tail extension, implicating PCP in the regulation of tail extension. This suggests that the role of PCP signalling during tail extension may be through the regulation of ECM components.

PCP signalling regulates C&E of mesodermal cells, and *tri* and *kny* mutant embryos have wider, thinner somites a result of this reduced convergence (Hammerschmidt et al., 1996; Topczewski et al., 2001; Jessen et al., 2002). However, PCP signalling does not regulate the formation or specification of the somites (Hammerschmidt et al., 1996; Marlow et al., 1998). My results demonstrate that inhibition of PCP signalling after C&E stages (7 somites), results in embryos that have an increase in embryo width, similar to *tri* and *kny* mutants (Section 4.2.4). This indicates that there is residual migration after the stage at which C&E is generally thought to occur, that has a significant contribution to overall embryo morphology. It also indicates that PCP signalling regulates this post-C&E migration, and that this appears to be independent of somite morphogenesis, as somite formation is not disrupted when PCP signalling is inhibited. Overall, this demonstrates a requirement for PCP signalling during both the C&E stage and mid-somitogenesis stage migration of mesodermal cells to the midline.

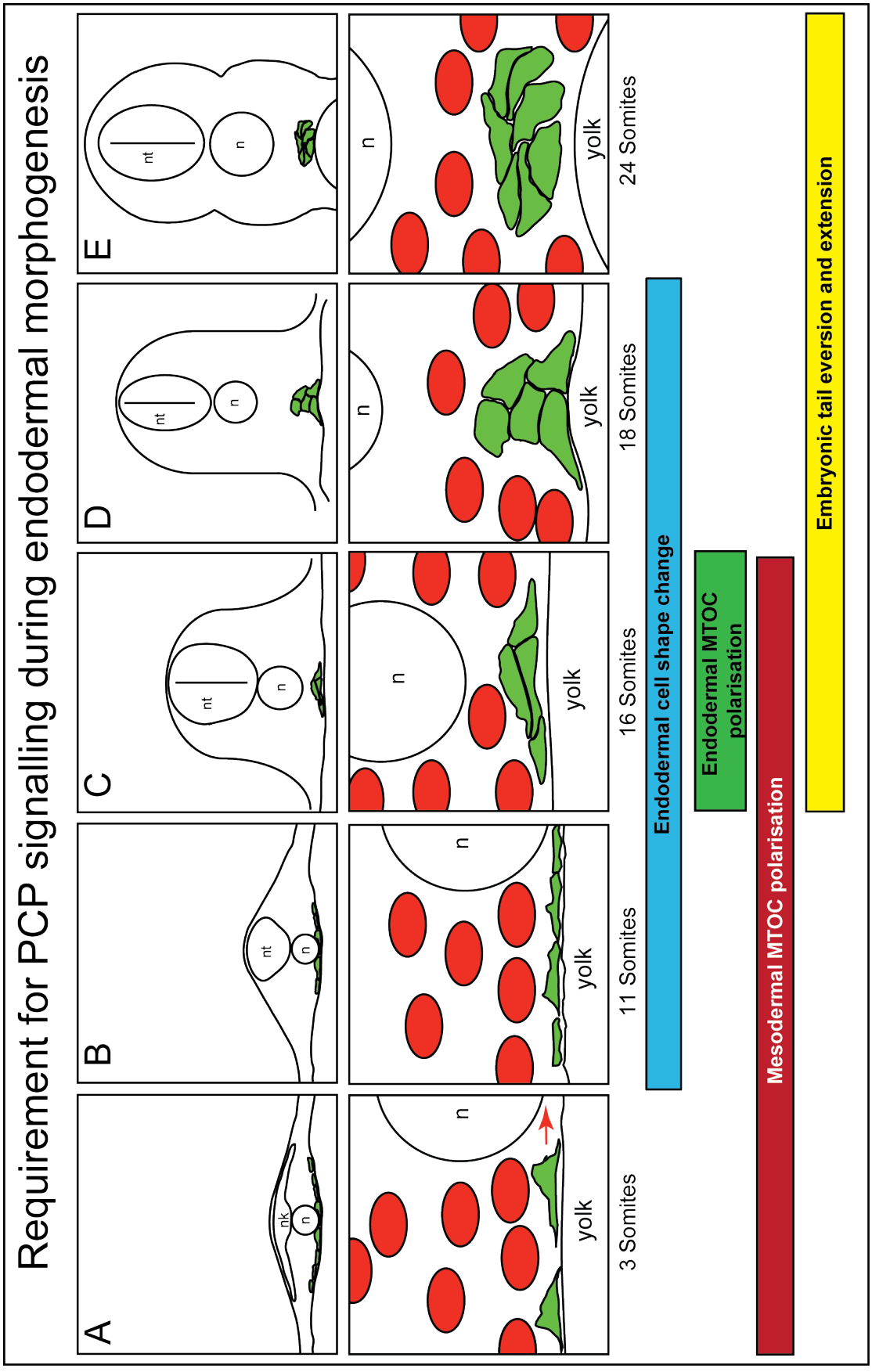
Requirement for PCP signalling during endodermal morphogenesis
A
B
C
D
E
nk
nt
n
yolk
3 Somites
11 Somites
16 Somites
18 Somites
24 Somites
Endodermal cell shape change
Endodermal MTOC polarisation
Mesodermal MTOC polarisation
Embryonic tail eversion and extension

Figure 6.1 Summary of the phases of endodermal morphogenesis and the requirement for PCP signalling. (A) Endoderm morphogenesis begins with the migration of the endodermal cells towards the dorsal midline of the embryo. **(B-E)** At around 11 somites endodermal cells are in a broad stripe along the length of the embryo, and begin to leave the monolayer and contact with the YSL (C), and this continues until 24 somites when the primitive endodermal rod has formed (E). The bars represent the requirement for PCP signalling during the stages of endoderm morphogenesis. PCP is required for the cell shape change at 7 somites, a short period of MTOC polarisation, mesodermal MTOC polarisation, and tail extension. nk – neural keel. n- notochord. nt – neural tube. green cells – endoderm. red cells – mesoderm.

6.2.3. A possible role for the surrounding mesoderm controlling endodermal cells leaving the monolayer during midline aggregation

How the endoderm transitions from a monolayer of cells into the endodermal rod (midline aggregation) was unknown at the start of this study. In chapter three (Section 3.2.3) I defined the process of endoderm midline aggregation, which begins at 11 somites when endodermal cells undergo a behavioural change, leaving contact with the YSL membrane and coalescing to form a primitive endodermal rod at 24 hpf (Figure 6.1).

Disruption of PCP signalling disrupts overall endodermal morphology during midline aggregation, as the *tri* and *kny* mutants have an increase in endodermal width, number of endodermal cells overall per section, and the number of cells leaving the monolayer compared to wildtype (Section 3.2.3.2). However, the overall proportion of endodermal cells leaving the monolayer is reduced in these mutants compared to wildtype. Interestingly, the cells that do leave the monolayer are always at the midline region below the notochord, rather than at the ventral edges (Section 3.2.3.1).

Two conclusions can be drawn from this data. Firstly, it suggests that PCP signalling does not control the signalling mechanism determining the region of endodermal cells that can leave the monolayer, as all three disruptions of PCP signalling tested did not prevent endodermal cells leaving the monolayer (Section 4.1.4). Secondly, it suggests that overall endodermal width might simply be linked to overall embryo width. The increase in endodermal width of *tri* and *kny* mutants is also accompanied by increases in embryo width, although not to the same proportion. In fact, disruption of PCP signalling at 16 somites after the majority of embryonic convergence and extension, in Tg(*hsp70l:XDshΔDEP-mCherry*) embryos, is unable to separate these two morphological defects. This indicates that their morphologies are linked and that the mechanisms that control both occur at the same time, after 16 somites. Since the endoderm is not polarised with respect to MTOC orientation during these stages (Figure 6.1), it further suggests that the endodermal width might be controlled by the overall embryonic width.

In this study, situations that increased the embryonic width all also resulted in higher endodermal cell numbers leaving the monolayer, yet the cells that did leave the monolayer were always located in the region close to the dorsal midline (Section 3.2.3.1). This favours the argument that a localised signalling cue specifically activates endodermal cells to leave the monolayer at the dorsal midline. Considering this, it is likely that the signalling cue to initiate endodermal cells to leave the monolayer is not autonomous to the endoderm, but rather originates from the surrounding mesoderm at the dorsal midline.

These results generate a number of questions regarding midline aggregation. Firstly, what happens to the endodermal cells that have not left the monolayer by 24 hpf at later stages in PCP disrupted embryos, such as during the onset of lumen formation at 43 hpf (Bagnat et al., 2007) or upon completion of lumen formation at 60 hpf? (Horne-Badovinac et al., 2001). Do these cells eventually migrate to the dorsal midline and leave the monolayer at a later time point, or do they remain ventral to the coalescing cells and in contact with the YSL? I have not observed endodermal morphology later than 24 hpf, during organogenesis stages, but as the embryo continues to extend along the A-P axis at stages after 24 hpf, I suspect that the former would be the case.

Secondly, does the signalling cue to leave the monolayer have a specific time-window in which to act on the endoderm? If so then endodermal cells that are not in the correct region to receive the cue when it is presented might miss the time window and never leave the monolayer, regardless if they migrate to the dorsal midline at later stages. There is currently no evidence for this however, and investigation into the signalling mechanisms is a topic for future studies. It would be interesting to continue investigations into the signalling mechanisms regulating endodermal cells leaving the monolayer, and the role of the surrounding tissues in this process. In particular, the identity of the midline signal is not known, nor is the identity of the signalling tissue. As the endodermal cells I observed leaving the monolayer were situated below the notochord, then a midline tissue like the notochord or the hypochord are likely candidates to supply this signalling cue.

6.2.4. Two branches of PCP signalling have different roles during endodermal morphogenesis

Extracellular matrix (ECM) components have well-established roles in the control of C&E movements (Shimizu et al., 2005; Warga and Kane, 2007; Skoglund and Keller, 2010). The PCP signalling pathway is a key regulator of C&E. Multiple members of the PCP signalling pathway have also been demonstrated to regulate components of the ECM (Carreira-Barbosa et al., 2008; Coyle et al., 2008; Cantrell and Jessen, 2009; Latimer and Jessen, 2009; Dohn et al., 2013). *tri* and *kny* have contrasting roles in the regulation of ECM levels. *tri* mutant mesodermal cells have reduced levels of Fibronectin protein, and an overall reduction in the size of the extracellular matrix (ECM) at the end of gastrulation (Dohn et al., 2013). This results from increased proteolysis of Fibronectin, which reduces overall cell-matrix adhesion, and increases the number of cellular membrane protrusions in the mesodermal cells (Jessen et al., 2002; Coyle et al., 2008; Dohn et al., 2013). In contrast, *kny* mutants have an increase in the level of Fibronectin in the ECM, which results in a thicker ECM, and an increased cell adhesion of mesodermal cells at the end of gastrulation. The increased levels of Fibronectin in *kny* mutants result from increased Fibronectin fibril assembly, rather than increased *fibronectin* expression (Dohn et al., 2013). So it seems that although both *tri* and *kny* regulate ECM levels, they have different and independent mechanisms (Dohn et al., 2013), and appear to form two different groups of PCP components based on their roles in regulating ECM levels. This is supported by the fact that *prickle*-morphants have a reduction in ECM components similar to *tri* mutants, while MZ*frizzled7a/7b* mutants have increases in ECM similar to *kny* mutants (Dohn et al., 2013). The different roles of PCP components in the regulation of ECM levels support the general hypothesis that PCP signalling has both linear and non-linear pathways (Lawrence et al., 2007) (reviewed in Figure 1.2).

Although *tri* and *kny* are thought to be in separate arms of the non-linear model of PCP signalling, *tri* and *kny* mutant embryos, and Tg(*hsp70l:XDshΔDEP-mCherry*) heat shocked at gastrulation stages look similar by gross morphology. However, my quantification of embryo morphology using cross-sections (to

measure embryo height, embryo width, YSL width, distance between the pronephric ducts, endodermal width, and endodermal cell number) has identified several differences between these PCP mutant embryos and Tg(*hsp70l:XDshΔDEP-mCherry*) embryos heat shocked as gastrulation stages (Section 4.1.3). The differences in endodermal morphology between *tri* mutant embryos, and *kny* mutant embryos and Tg(*hsp70l:XDshΔDEP-mCherry*) embryos heat shocked at gastrulation stages demonstrates the highly complex role of PCP signalling during endodermal migration to the midline.

These results identified that *kny* mutants have a greater overall increase in multiple width measurements compared to *tri* mutants. This is interesting, especially as the overall embryo width and embryo height is similar in these two mutants (Section 4.1.3). This indicates that *kny* has a specific role in the morphogenesis of the endoderm and tissues in the surrounding region that is not shared by *tri*.

The morphological differences between these two mutants might reflect the putative different roles *tri* and *kny* play in PCP signalling. *kny* is a *frizzled* co-factor, regulating the binding of extracellular Wnt ligands required to activate PCP signalling via *dvl* (Habas et al., 2001; Habas et al., 2003; Ulrich et al., 2003). *tri* is generally thought to be involved in the modulation of the PCP signal via *dvl*, although it is known to have a separate and distinct mechanism from the *dvl*-dependent PCP signalling during convergence and extension movements during gastrulation stages (Dohn et al., 2013). For example, *tri* mutants are not as severely affected as *kny* mutants or Tg(*hsp70l:XDshΔDEP-mCherry*) embryos heat shocked as gastrulation stages with respect to the trunk and endoderm morphology in this study (Section 4.2.3), further supporting the existence of a *dvl*-independent role for *tri* in regulating PCP signalling in controlling embryo morphology. It is of note, however, that the effect of maternally deposited *tri* mRNA and/or protein is currently unknown and was not investigated in this study due to the technical difficulty posed by generating maternal zygotic null embryos, and therefore a partial rescue of the trunk and endoderm morphology phenotypes in *tri* mutants by maternal *tri* cannot be ruled out.

Further support for the idea of two independent arms of the PCP pathway comes from the examination of the *tri/kny* double mutant embryos (Section

3.2.2). These embryos display a more severe convergence and extension phenotype than either single mutant and, interestingly, more severe than Tg(*hsp70l:XDshΔDEP-mCherry*) embryos heat shocked at gastrulation stages. Unfortunately, as generation of *tri*/*kny* double mutants with Mendelian crosses does not generate many embryos, morphological analysis on the *tri*/*kny* double mutants was not attempted in this thesis. However, the synergistic effect of the *tri*/*kny* double mutants on endodermal migration during somitogenesis stages highlights the non-redundant roles *tri* and *kny* play in regulating embryo morphogenesis, and supports the idea of complex interdependent roles of PCP, and therefore perhaps the ECM, during endoderm morphogenesis.

The similar phenotypes observed between *kny* and Tg(*hsp70l:XDshΔDEP-mCherry*) embryos heat shocked at gastrulation stages are to be anticipated. Previous studies indicated that *kny* mutants cause a loss of the interaction between the PCP Wnt ligands and the Frizzled receptor (Topczewski et al., 2001; Kilian et al., 2003; Ohkawara et al., 2003), resulting in no *dishevelled* activation, and hence no downstream *dvl*-mediated roles of PCP signalling. Overall, this indicates that PCP disruption via the Tg(*hsp70l:XDshΔDEP-mCherry*) line represents a disruption of the *dvl*-dependent branch of PCP signalling.

The PCP signalling pathway regulates multiple components of the ECM, including Cadherins (Carreira-Barbosa et al., 2008; Coyle et al., 2008; Cantrell and Jessen, 2009; Latimer and Jessen, 2009; Dohn et al., 2013). The PCP family member Flamingo (Fmi/Celsr) is a seven-pass transmembrane atypical cadherin, that regulates PCP signalling and cell adhesion required for epiboly and convergence and extension movements in zebrafish (Usui et al., 1999; Tree et al., 2002; Ulrich et al., 2003; Carreira-Barbosa et al., 2008). Flamingo has been shown to function as a signalling molecule in a non-cell-autonomous homomeric manner (Chen et al., 2008). It has also been proposed that N-cadherin might function as a signalling molecule, rather than as an adhesion molecule (Harrington et al., 2007). This suggests that, as well as regulating the levels of ECM components, PCP signalling may also play a role in the regulation of cadherin mediated signalling. Overall, these results suggest that the primary role of PCP signalling during endodermal morphogenesis may be through the regulation of cell-adhesion and ECM components.

6.3. PCP signalling controls brain morphogenesis

6.3.1. tri regulates neural tube morphology independently of dishevelled

Numerous members of the PCP pathway have been shown to have a role in neural tube morphogenesis. *tri,* MZ*tri*, *wnt5a, wnt11*, and MZ*scrib* mutants have a duplication of the neural tube posterior to the hindbrain, which results from a reduction in daughter cell re-intercalation after cell division (Ciruna et al., 2006; Tawk et al., 2007; Zigman et al., 2011).

In this study, I identified that both Tg(*hsp70l:XDshΔDEP-mCherry*) embryos heat shocked at gastrulation stages and *kny* mutant embryos also have an expansion of the neural tube that is limited to the region directly posterior to the hindbrain, whereas *tri* mutant embryos have an expansion of the neural tube that extends more posteriorly into the somite region (Section 4.2.5.4). This result is particularly interesting as it is the only morphological feature investigated in this study in which the *tri* mutant has a more severely disrupted morphology than Tg(*hsp70l:XDshΔDEP-mCherry*) embryos heat shocked at gastrulation stages. This is significant, as it indicates that part of the role of *tri* in the expansion of the neural tube at the level of the first somite is independent of *dvl*. This is consistent with a study proposing a non-autonomous role for *tri* during hindbrain motor neuron migration that is independent of both *dvl* and *prickle* (Sittaramane et al., 2013).

Interestingly, PCP disruption via MZ*frizzled7a/7b* double mutants results in a loss of both orientated neurectodermal cell division as well as the correct localisation of these orientated cell divisions, and in turn these mutants do not generate a neural midline (Quesada-Hernandez et al., 2010). This is the first published disruption of PCP signalling that fails to form a neural midline, and it must be independent of *tri* as well as the Wnt signalling ligands, and is thought to represent a direct interaction between apical-basal polarity factors and PCP signalling. In this thesis, Tg(*hsp70l:XDshΔDEP-mCherry*) embryos heat shocked at gastrulation stage are able to generate the neural midline (Section 4.2.4). This result, taken in light of the *MZfrizzled7a/7b* mutant data, would indicate that the

control of neural midline formation is *frizzled* dependent, but independent of multiple of the core PCP proteins including Tri, Kny, Wnt11, Wnt5, and Dvl (Quesada-Hernandez et al., 2010). *frizzled7a* and *frizzled7b* have been shown to function through Wnt11, however, it is unknown if they also participate in β-catenin signalling. Therefore, it is possible that the MZ*frizzled7a/7b* mutants represent a partial disruption of both the β-catenin signalling and PCP signalling pathways, and hence neural midline formation may be regulated by β-catenin signalling rather than PCP signalling. Overall, this suggests a potential role for PCP signalling during neural midline formation that is independent of multiple core PCP components. It would be interesting to analyse the neural midline formation in *tri/kny* double mutants to determine if the neural midline can form in the absence of both these core PCP components.

6.3.2. A role for PCP during vesicle expansion

The mechanisms that regulate overall brain morphogenesis are still poorly understood, although a number of important factors have been identified (Figure 6.2). My results demonstrate that *tri* and *kny* mutants are disrupted in brain morphogenesis, but are able to undergo basal-constriction and correct MHB formation (Section 4.15). Morpholino knockdown of the extracellular matrix component Laminin prevented correct basal constriction during midbrain-hindbrain (MHB) formation, but did not prevent ventricle inflation (Gutzman et al., 2008; Lowery et al., 2009). This is particularly interesting as *kny* and *tri* mutants have both been shown to have altered Laminin levels in mesodermal cells at the end of gastrulation (Dohn et al., 2013). Therefore, if *tri* and *kny* also have altered Laminin levels in the neurectoderm, then this suggests that it does not affect MHB formation in these mutants.

My results (Section 4.1.5.2) identified that *tri* and *kny* appear to have different roles during brain vesicle morphogenesis; *tri* mutants have an increase in the size of the internal forebrain and midbrain vesicles, whereas *kny* mutants have a reduction in the size of these vesicles. These results suggest that *kny* has a specific role during vesicle expansion, but *tri* appears to be dispensable for this process.

It was previously suggested that brain vesicle expansion defects were secondary to circulation defects (Schier et al., 1996), however, more recently it has been shown that the initial stages of ventricle expansion are independent of circulation, but dependent on regulated cell proliferation and ECM components (Lowery and Sive, 2005). My results demonstrate *tri* mutants have an overexpansion of the brain vesicles, whereas *kny* mutants have a reduction in vesicle size. The Fibronectin mutant *natter* (*nat*) displays a disruption in ventricle expansion (Lowery et al., 2009). This is interesting as *tri* mutant mesodermal cells have a reduction in Fibronectin levels, and *kny* mutants have increased levels of multiple components of the ECM, including Fibronectin (Dohn et al., 2013). If *tri* and *kny* also have altered levels of Fibronectin in the neurectoderm, it would suggest that the presence of Fibronectin is critical for ventricle expansion, but reduction in the overall levels does not inhibit the process. These results suggest that PCP signalling has a role during brain vesicle expansion, and that this is possibly through the regulation of ECM component levels. However, further investigations into the levels of ECM components in the brain in *tri* and *kny* mutants will be required to make this conclusion.

The disruption of PCP signalling just prior to the initiation of brain vesicle expansion at 17 somites (Lowery and Sive, 2005) in Tg(*hsp70l:XDshΔDEP-mCherry*) embryos resulted in a decrease in the internal size of the forebrain and midbrain vesicles that was comparable to *kny* mutants (Section 4.1.5). These results are important, as they indicate that PCP signalling via *kny* and *dvl* is required in a time specific manner during brain vesicle expansion from 17 hpf to 24 hpf. *tri* mutants did not have a decrease in brain vesicle size, indicating that *tri* is dispensable for the process of vesicle expansion. The Tg(*hsp70l:XDshΔDEP-mCherry*) transgenic line described here was instrumental in demonstrating this for the first time.

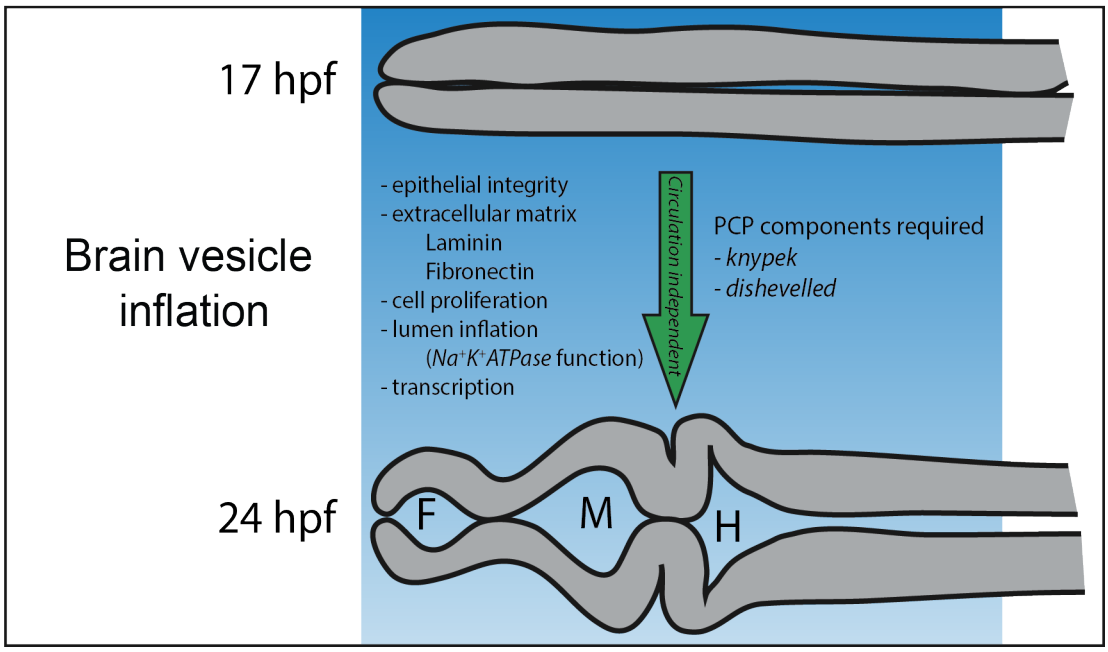

Figure 6.2 Brain vesicle inflation and the role of PCP signalling. Multiple processes are required for brain vesicle expansion from 17 hpf to 24 hpf. The known factors are shown on the left of the blue area (Lowery et al., 2009). The PCP components *knypek* and *dishevelled* required for vesicle inflation, and are shown on the right in the blue area. F= forebrain vesicle. M = midbrain vesicle. H = hindbrain vesicle.

6.3.3. A novel role for PCP during hindbrain axis morphogenesis

PCP signalling is known to have a role in neural tube axis morphogenesis (Ciruna et al., 2006; Zigman et al., 2011), however a role in Hindbrain axis morphogenesis has not been previously reported. I identified a novel role for PCP signalling in the regulation of hindbrain axis morphogenesis via *dishevelled* (Section 4.1.5.3). Interestingly, this appears to be a time specific requirement for *dishevelled,* as Tg(*hsp70l:XDshΔDEP-mCherry*) embryos heat shocked at 16 somites do not have hindbrain axis duplication. Interestingly, hindbrain axis duplication was not present in either the *tri* or *kny* mutants, in this study, or reported in previous studies in MZ*tri* and MZ*scribble* mutants (Ciruna et al., 2006; Zigman et al., 2011). This is significant as it represents the only phenotypic difference between *kny* and Tg(*hsp70l:XDshΔDEP-mCherry*) embryos heat shocked at gastrulation stages that I have identified (Section 4.1.3). These results suggest that *dishevelled* has multiple roles in controlling correct hindbrain axis morphogenesis, and that one of these roles might be independent of both *tri* and *kny*. However, without analysing the effect of the maternal contribution of *tri* (using MZ*tri* embryos) in hindbrain axis formation, or without analysis of hindbrain morphology in *tri*/*kny* double mutants, this conclusion cannot be verified.

tri, MZ*tri,* and MZ*scribble* mutants display a duplication of the neural tube, in the region posterior to the hindbrain, which results from one daughter cell not re-intercalating across the midline after each cell division (Ciruna et al., 2006; Zigman et al., 2011). The hindbrain axis duplication in Tg(*hsp70l:XDshΔDEP-mCherry*) embryos heat shocked at gastrulation stages may represent a similar situation, in which the regulation of daughter cell re-intercalation after division is disrupted in the hindbrain resulting in axis duplication. This implies that PCP signalling is required at some stage prior to 16 somites to establish correct hindbrain morphology, possibly through regulation of the orientated cell division.

6.4. Future thoughts regarding PCP signalling and endodermal morphogenesis

This study focused on the morphogenesis movements of the endoderm during midline aggregation, and the contributions of components of the PCP signalling pathway in this process (for summary see Figure 6.1). To expand this research into future projects, a number of key questions need to be addressed. The first question to address, is whether PCP signalling is required autonomously in the endoderm? To address this, mutant endodermal cells could be replaced with wildtype endodermal cells via transplantation of wildtype endoderm into PCP mutant lines lacking endoderm (due to injection of *cas*-MO (Dickmeis et al., 2001)). Another approach could be the generation of conditional transgenic lines that enable endodermal specific knockdown of PCP signalling, as such a transgenic may allow any endodermal autonomous roles of PCP to be analysed. This may determine if the endoderm specifically requires PCP signalling for midline migration and midline aggregation. The experimental design would need to take into account the knowledge gained from this study about the threshold expression levels required to disrupt PCP signalling via *XDshΔDEP-mCherry* over-expression (Section 4.2.2). This may be achieved by utilising a *trilobite*-dominant negative (Goto and Keller, 2002) under the control of an inducible promoter, such as the *hsp70l* promoter. Indeed, several approaches to carry out the above experiments were attempted in chapter 5, but these were unsuccessful due to low levels of transgene expression, or no transgenic founders being recovered, or silencing of the transgene.

The second question to address is, what is the definitive *dvl*-independent role of *tri* in regulating PCP signalling and embryo morphogenesis? In this study I identified a *dvl*-independent role of *tri* in the regulation of neural tube expansion in the somite region. It would be interesting to generate a *tri*-dominant negative transgenic line under the control of the *hsp70l* promoter, overcoming the maternal contribution of *tri* mRNA, which therefore allows investigation of the roles of *tri* in the PCP signalling pathway in various tissues. Similarly, the generation of a double *tri*-dominant negative and *XDshΔDEP-mCherry* dominant negative transgenic line, would enable one to determine if this has a more severe

effect than either single dominant negative alone. I predict that this would generate a disruption similar to the *tri*/*kny* double mutants.

The primary aims of this thesis focused on investigating endoderm morphogenesis, and the role the PCP signalling pathway plays in this process. However, I also ended up identifying the independent roles of *tri, kny*, and *dvl* in the regulation of multiple stages during endodermal morphogenesis and brain morphogenesis (Figure 6.3).

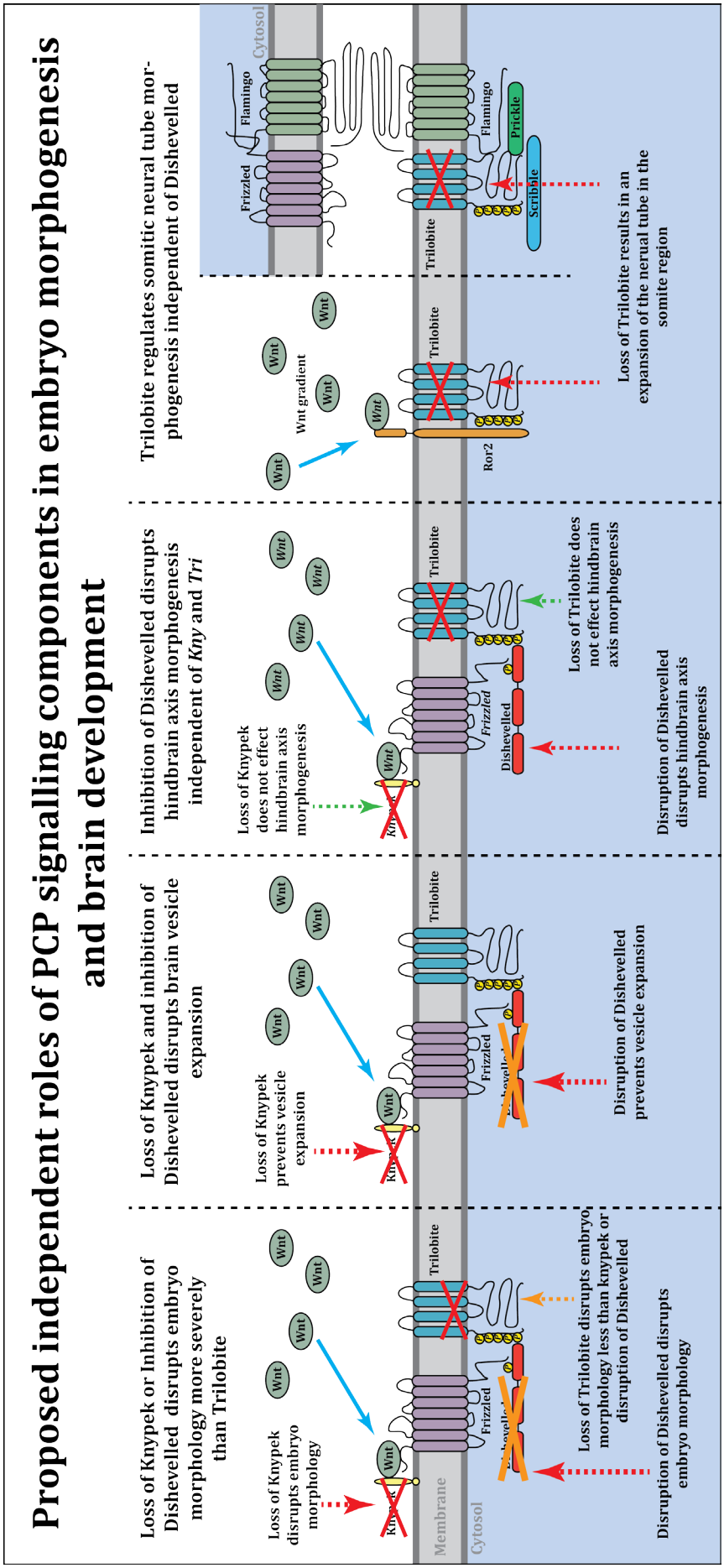
Proposed independent roles of PCP signalling components in embryo morphogenesis and brain development
Loss of Knypek or Inhibition of Dishevelled disrupts embryo morphology more severely than Trilobite
Loss of Knypek and inhibition of Dishevelled disrupts brain vesicle expansion
Inhibition of Dishevelled disrupts hindbrain axis morphogenesis independent of Kny and Tri
Trilobite regulates somitic neural tube morphogenesis independent of Dishevelled
Loss of Knypek disrupts embryo morphology
Loss of Knypek prevents vesicle expansion
Loss of Knypek does not effect hindbrain axis morphogenesis
Membrane
Cytosol
Wnt
Frizzled
Dishevelled
Trilobite
Flamingo
Prickle
Scribble
Ror2
Wnt gradient
Loss of Trilobite disrupts embryo morphology less than knypek or disruption of Dishevelled
Disruption of Dishevelled prevents vesicle expansion
Loss of Trilobite does not effect hindbrain axis morphogenesis
Disruption of Dishevelled disrupts embryo morphology
Disruption of Dishevelled disrupts hindbrain axis morphogenesis
Loss of Trilobite results in an expansion of the nerual tube in the somite region

Figure 6.3. Proposed independent roles of PCP signalling components in embryo morphogenesis and brain development. *kny* mutants and Tg(*hsp70l:XDshΔDEP-mCherry*) embryos heat shocked at gastrulation stages display embryo morphologies that are more severe than *tri* mutants **(First panel)**. *kny* mutants and Tg(*hsp70l:XDshΔDEP-mCherry*) embryos heat shocked at gastrulation or somitogenesis stages fail to expand brain vesicles at 24 hpf. *tri* mutant embryos are capable of brain ventricle expansion, although they are slightly larger than wildtype ventricles **(Second panel).** Inhibition of *dvl* at gastrulation stages results in a duplication of the hindbrain axis. *tri* and *kny* mutants do not have this axis duplication **(Third panel)**. *tri* mutants have an expansion of the neural tube that extends into the somatic region. *kny* mutants and Tg(*hsp70l:XDshΔDEP-mCherry*) embryos heat shocked at gastrulation stages display an expansion of the neural tube, but not posteriorly in the region of the somites **(Fourth panel).**

Chapter 7. Appendix One

Gene	left primer	right primer
dvl1a	dvl1a –F-end	dvl1a-R-UTR
	TGGAAACGTCCCACCAGAAC	ATTTCATGCAACACGATGGCTC
dvl1b	dvl1b middle forward	dvl1b-end-Rev
	GGAGGTGATGTCGTAGACTG	TAGCACTGCGCTGAAATCCA
dvl2	dvl2-F-end	Dvl2-R-UTR
	AGTAGTGGCTCCACACGCAG	CCAGACCCTGTTGCGGTTAATAC
dvl3a	dvl3ch2-Fend	dvl3ch2-R-utr
	GTTTGACTTCCGCCGAGACC	TCGCATGAACAACGACATATCC
dvl3b	dvl3ch18 middle-F	dvl3ch18-end-Rev
	CCGCCACACCGTCAACAAG	CCTAGTGAGTTCTTCGTGGACGTCATGT

Table A1.1 Primers used for sqRT-PCR on the *dishevelled* gene family

7.1. Primers used to clone *dishevelled in situ* probe fragments.

Gene	left primer	right primer
dvl1a	dvl1a –F-end	dvl1a-R-UTR
	TGGAAACGTCCCACCAGAAC	ATTTCATGCAACACGATGGCTC
dvl1b	dvl1b middle forward	dvl1b-end-Rev
	GGAGGTGATGTCGTAGACTG	TAGCACTGCGCTGAAATCCA
dvl2	dvl2-F-end	Dvl2-R-UTR
	AGTAGTGGCTCCACACGCAG	CCAGACCCTGTTGCGGTTAATAC
dvl3a	dvl3ch2-Fend	dvl3ch2-R-utr
	GTTTGACTTCCGCCGAGACC	TCGCATGAACAACGACATATCC
dvl3b	dvl3ch18 middle-F	dvl3ch18-end-Rev
	CCGCCACACCGTCAACAAG	CCTAGTGAGTTCTTCGTGGACGTCATGT

Table A3.2 Primers used to clone *dishevelled* gene fragments for *in situ* hybridisation probes.

7.2. *dishevelled* family probe sequences for in situ hybridisation

7.2.1. dvl1a probe sequence

TGGAAACGTCCCACCAGAACTCACAGCAAGTCGGCAGTCTTTTCAGCACGCTATGGGC
AATCCTTGTGAGTTCTTTGTGGATATTATGTGACAGGAGAGAGTGCCTTCAACATTC
ACTTCATAAGGTTTTGCTACTGACGATCCAATGCCTGCACTGAGAATGTACAAACTG
ATGCACAAATCTAAAGGGAGAGTTCACCTAATGCTGGAAATTCTGTCGTTTGCTCTA
AACTTATTCTGTGAAACAGGAAAATCTGTTTAGTTGACCACAGTTAACTAAAACTGG
GAAATTATTTAATTTATTAAATTTTCTTCGGCTTACTGGCTTAATTCATCAGGAGTC
ACGACAGTGGAATGACCGCCAACTTGTCCAGCATATATTTTGCATAGCAGACGTCCT
TCCAGCCGCAACCCAGTACTGGGAAAAAACCCATACACACTCATACACTAAGGCCAA
TTTAGTTAATTCAATTCACCTATAGTGTATATCTTTGGACTGTGAAGTAAACCGGAG
CACCCGGAGGAAACCCGCACCAACATGGGAAGAACATGCAAACTACACAGAAATGCC
AACTGGTCCAGCCAGGACTAGAAACCAGTGACCTTCTTGCTGTGAGGGGACAGTGCT
AACCACTGAGCCATCGTGTTGCATGAAAT

7.2.2. dvl1b probe sequence

GGAGGTGATGTCGTAGACTGGCTTTACTCAAGGGTGGAAGGATTCAAAGACCGCCGG
GATGCCAGAAAATACGCCAGCAGCTTGCTGAAACACGGCTATCTCAGACACACTGTC
AACAAGATCACATTCTCTGAACAGTGTTACTACACGTTTGGAGATCTCTGCCAAAAC
ATGGCTACGTTAAACTTGAATGAGGGATCGAGTGGTGCTGGTTCAGAGCAGGACACT
TTGGCTCCTCTTCCTCCTCCGTCCACTAACCCGTGGCCCATGGGTGGCCAGCCATTCC
CTTACCCACCCTTCACAGCGCCCCCTGCTTTCCCTCCAGGATATTCAGACCCCTGCCAC
AGTTTCCACAGTGGCAGCGCTGGAAGTCATCACAGTGAGGACTGATGATGGAGGAGG
TTGAGCCCCAGCCCTGGGGTGTCTGAAGTCGCAGCAGTAGTTCCAACCCTAGCATTGG
GAGAATCCAGCGGGCCGTACAGAGGGAAAAGGAGCGCAAATCAACAGGCAGCGAATC
AGATTCAGGCAAGCGAGCAGGAGGGAGGAGGGTTGAGCGTTCAGCCAGCCAACTCAG
CCACCGCAGCCACGCCCTGTCATCCCGTAGCCACACCCACTCACGAGTCCCCTCACAGC
ACAGCCGTACTTCCTTCTCCTACAGCCACGCCCCTTTTACCAAATATGGCCACACGTC
CTGTGCACTCAGCGAACGGAGCCACGCCTCTTCTTATGGGCCCCCAGGTCTGCCTCCT
CCATACAGCCTGGCTAGATTGACTCCTAAAGGGGCCGTCTGCAGTGGGCCCCCGGGGG
CCCCTCCAGTGAGGGAAATGGGGGCCATACCACCTGAACTCACCGCCAGTCGACAGTC
CTTCCAGCATGCAATGGGCAACCCTTGTGAGTTTTTTGTGGATATTATGTAAAATCT
AATGGATTTCAGCGCAGTGCTA

7.2.3. dvl2 probe sequence

AGTAGTGGCTCCACACGCAGCGATGGAGAAAAGAGAAGGGGCCCTAAAAGCGTTTCT
GAGAGTACTGTGGGCGGCAGCGTGCGTGATGATAAATCTCCTGGCGGGGGTGGAGCT
GACTCACGTTCTGGCAGCGGCAGCGAATCAGATTACTCTGTTCGCAGCACCCTGAGAC
GAGATCATGGCTCAGCCACACCCAGCGAACACAGCCGCTCGAGTCAGCGCTCGCATCA
CCGCGTCCCGCCCCCTCACCTCGCCCCGTATCCGCCCGGCATCCCCATCCCATACAACC

CAATGATGGTGATGATGGTGCCCCAACACCCACATCTGGCGCTTGGAGCACCACATCC
GCAAACACCTACTCTGCCGCCCCACCCTGGCTTACCCCCAACCGGCATCCCCGGCGGG
CCTCCAGGAGCTCCCCCGACCCGAGACCTGGGCTCCGTCCCGCCTGAGCTGACTGCTT
CCAGGCAGTCCTTCCACCTGGCCATGGGCAACCCCAGTGAGTTTTTTGTGGATGTGAT
GTAATGAAGGATGTACCCGAGTGAAGGATGGAGGTTTGTAATCACGTGATAACTGTG
AGTTCTGCTCTGCGACGGACAGAGATGTAGTTTACTGTATCAGTGCAGCTCTTTAGA
GTTAGTGTTTGTCCTTGACGGTAGGAACAGGGTTTACGGAAGGGTAGGAAGTCTTGC
ATAGCACAGACTTCAAAATGCATTTGGTTTTTGTGGTATTAACCGCAACAGGGTCTG
G

7.2.4. dvl3a probe sequence

GTTTGACTTCCGCCGAGACCGAGCACCCAGCGAACGCTCGGGCGTGCCCCCCAGCGAG
GGCAGCGTGCGGAGCTCTCGGTCTCACAGCTACAGCCTGAAGCAGGGGTCTGCACGAG
GTGGCCCGGGGTCACCATCCGGCCGACATCTTGCCCACATTCCCCCTGAACTCACTGG
CTCTCGCCGCTCCTGCAACACAGCCAACGGGGAGTTCTTCGTCGACATCATGTGACTT
TACCCAGCAGAAGTGCCCAAACTATTCTTTGCCTTATGGACGAGAAAAAAAAGAAAG
AAACGTGGCCAACTAGAGCAACCGATTAGAATTAGGTTTAGTGCTGATCTAAAAAAT
CAGTAGCTTGTGAGCCCCGACATTACTTAGGCCTTAGAAATTAGTCTACTAAAGCAT
AAGCAAACGTCACTTACAATAACAAAACAACGTTGAACGCGAAATCACCTCGCGGAG
AAATTCAAATAGGAATATTTCCTCTGACGGATGAAAAAAAAGAGGGATTTTTGAGA
GAAATAGCAATAATTGAATGGGATTTAGCTGCAGCGCTACATGGTGTAAGGATTCAT
GGTGAATGTAGTCCAACCGTGGACATAAACGTCAAACTATAAAGAGAAATTTGAGTG
CTTATTAACTTTTTTTTGCCCTCTTTTAACATTTGTACTCTCGGTAAATGTCGGATAT
GTCGTTGTTCATGCGA

7.2.5. dvl3b probe sequence

CCGCCACACCGTCAACAAGATCACCTTCTCTGAGCAGTGCTATTACATCTTTGGAGAC
GTCTGTGGCAATATGGCGAGTCTCACCCTGCATGATCATGACGGTTCTAGTGGAGCG
TCTGACCAGGACACTCTTGCTCCGTTGCCCCATCCTGGAGTGGCTCCCTGGCCACTCG
CTTTCCCTTATCAGTATCCGATTCCTCACCCATACAATCCCCATCCAGTGCACGAGCC
CGGCTACAGCTTCACTGCAGGCGGAGGCAGCGTCGGCAGCCCACACAGCGAAGGCAGT
CGAAGCAGCGGCTCTAATCGCAGCGGTACCAAAAACGACACCAACGCAGCGCCAGCA
GCACCTGAGTCCGGAGGCCGATCGGGGAGCGGCAGCGAGTCCGACAGAAGAGAGAAA
GCTCCCAGCGAGTGCTCAGCAGCACCACCCAGCGAACACAGCGTGCGCAGCTCACACA
CCATCCGCAGCATCCACTCGCACACTTCCAACATGGTGTGTGGAGCCGCAGGACTCCC
TCCACAACCACCCGTGGCTGCAGCTCCCGGATCTCCCCCAGAGCAGGACCTGTCCTCG
GTGCCTCCCGAACTCACGGCCTCGCGACAATCCTTCCGCATGGCCATGGGAAACCCTA
GTGAGTTCTTCGTGGACGTCATGT

7.3. Genomic locations of Tg(*hsp70l:XDshΔDEP-mCherry*) insertions

Chromosome location	Left primer	Right primer	Product size
Chr 17-22 insert	Toil5'-3 CCCCAAAAATAATACTTAAGTACAG	Ch17-22 GCTGTCGTCCTAATTGAAATCC	818 bp
het/homo	Ch17-22 (R-912) GCTTTCTCAGAGTTCCCTCTAC	Ch17-22 GCTGTCGTCCTAATTGAAATCC	912
inside intron	RAS guanyl releasing protein 3 (calcium and DAG-regulated) (*rasgrp3*)		
Chr 17-41 insert	Ch17-41 CAGAGCCACTGCCTTCTAATTC	Toil5'-3 CCCCAAAAATAATACTTAAGTACAG	610
het/homo	Ch17-41 CAGAGCCACTGCCTTCTAATTC	ch17-41 (R-875) AATATGCTCTGCGCCACGAC	875
Chr 22 insert	Toil5'-3 CCCCAAAAATAATACTTAAGTACAG	Ch22 GAGGTGAACTCAATGCAGAAAC	1022
het/homo	Ch22 (R-1197) TTTACCTGTGTGCAGTGGAG	Ch22 GAGGTGAACTCAATGCAGAAAC	1197
Plasmid insert	Toil5'-3 CCCCAAAAATAATACTTAAGTACAG	HSP-plasmid-R TAACCGTATTACCGCCTTTGAG	497

Table A1.3 Mapped genomic locations of transgene insertion in the Tg(*Hsp70l:XDshΔDEP-mCherry*) transgenic line.

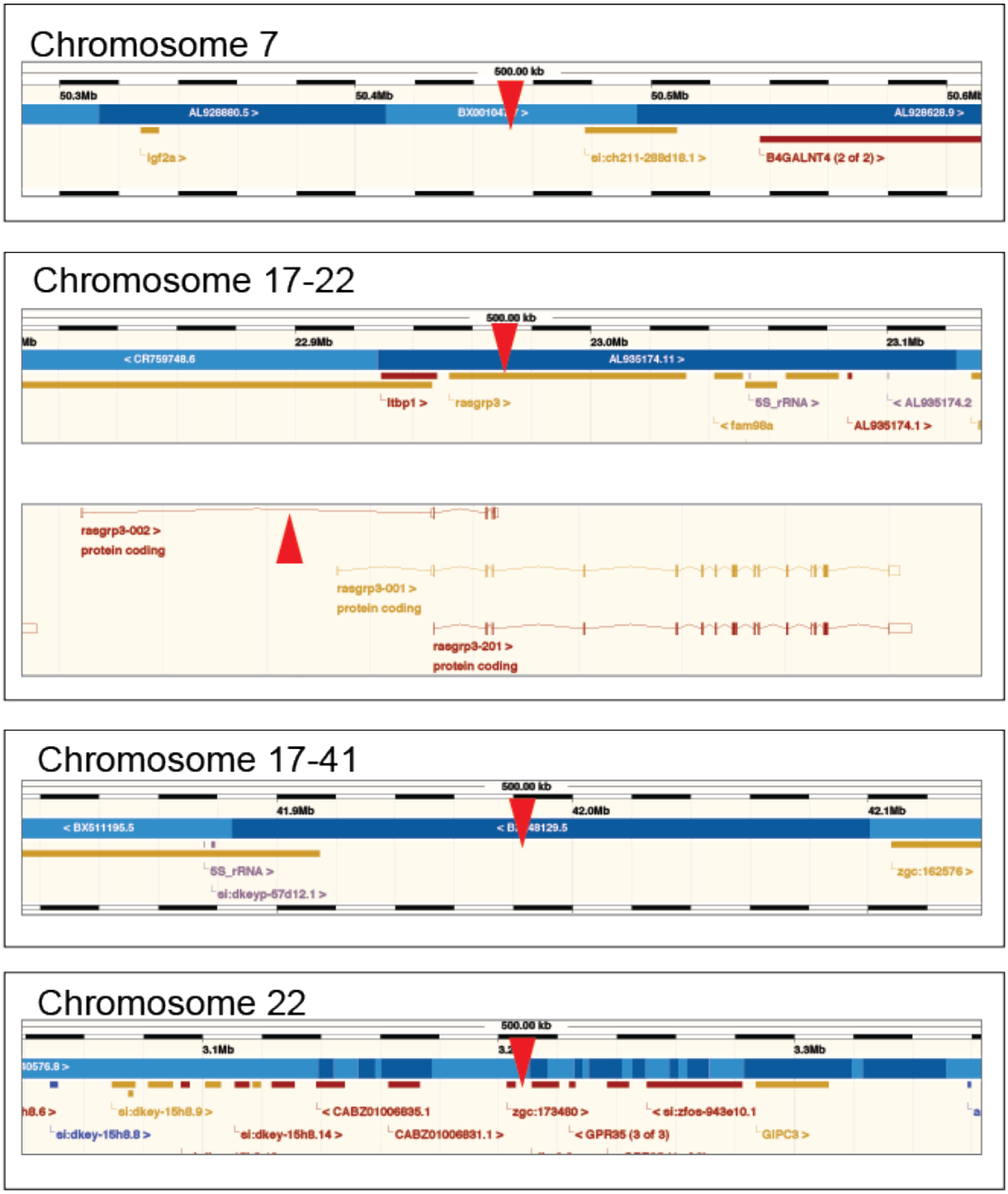

Figure A1.1 Genomic locations of mapped transgene insertion in the Tg(*hsp70l:XDshΔDEP-mCherry*) transgenic line. Red arrowhead indicates insertion site. The insertion in Chromosome 17 at location 22 upstream of the start of the known coding sequence of the *rasgrp3* gene.

Chapter 8. Appendix Two

Published data

ZEBRAFISH
Volume 11, Number 3, 2014

DOI: 10.1089/zeb.2013.0954

TA-Cloning Vectors for Rapid and Cheap Cloning of Zebrafish Transgenesis Constructs

Lee B. Miles and Heather Verkade

HERE WE REPORT the generation and use of three multisite Gateway TA-cloning plasmids, p5E-TA, pME-TA, and p3E-TA, to enable rapid and cheap construction of new entry vectors and final Tol2-transgenesis vectors for zebrafish transgenesis, as well as a TA-cloning expression vector, pCS2+TA, for rapid generation of new expression plasmids. These four vectors contain an *Xcm*I-based

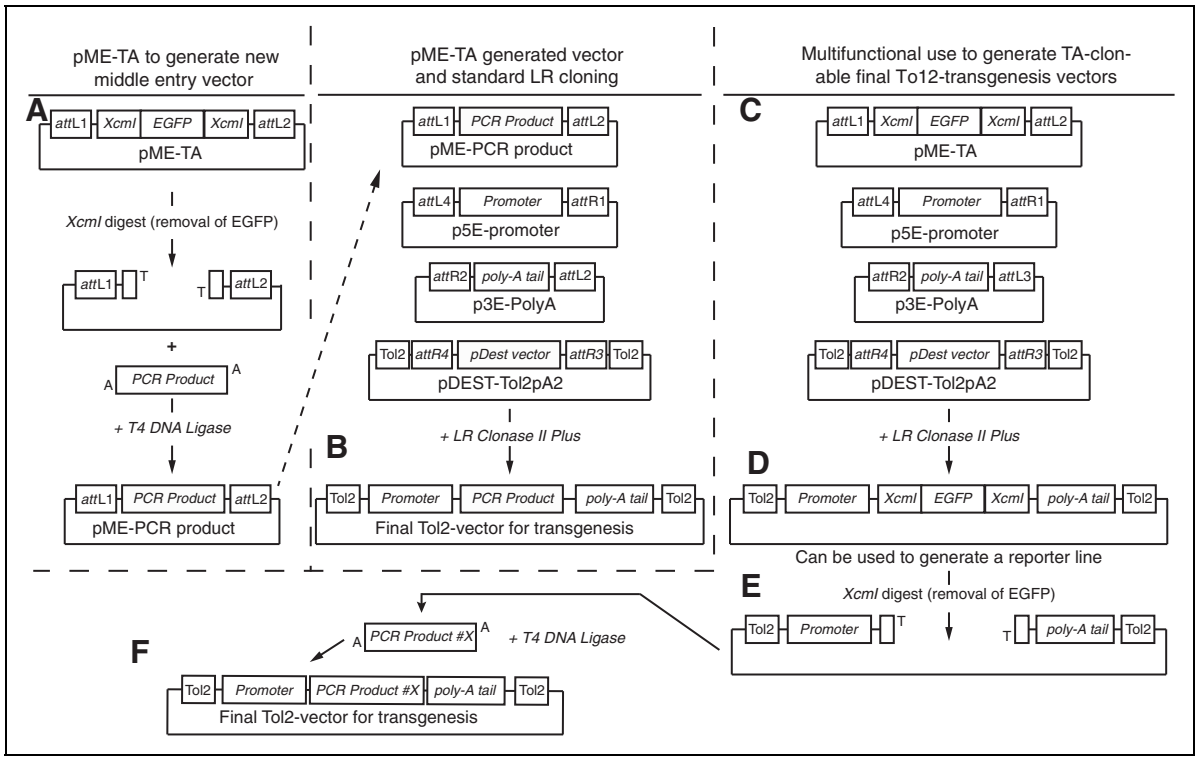

FIG. 1. The multifunctional use of TA clonable multisite gateway entry vectors for generating final zebrafish transgenesis vectors: an example using pME-TA. **(A)** Using pME-TA to generate new middle entry vectors, **(B)** pME-TA generated middle entry vectors can subsequently be used in a multisite LR reaction with p5E, p3E, and pDestTol2 vectors to generate final Tol2-transgenesis vector. **(C–E)** Multifunctional use of TA clonable entry vectors to generate pDestTol2-TA vectors. **(C)** pME-TA vector is used as an entry vector with your desired p5E-promoter, p3E-vector, and pDestTol2 vector in a standard multisite LR reaction. **(D)** If using pME-TA, this vector can be used to generate a reporter line. **(E)** The EGFP linker is removed from the Tol2-TA vector by *Xcm*I digestion to produce the pDest Tol2-your promoter-T-vector, ready for A-tail cloning. **(F)** Ligation of pDestTol2-T-vector with your desired A-tailed PCR products to rapidly generate a related set of final transgenesis vectors, this same procedure can be done with multiple PCR products.

School of Biological Sciences, Monash University, Clayton, Victoria, Australia.

TA-cloning linker approach[1–5] (*Xcm*I-*EGFP*-*Xcm*I) to facilitate rapid TA cloning of PCR products directly into the final vectors. *Xcm*I digestion of these vectors removes the EGFP open reading frame and generates the required T overhangs (Fig. 1A) allowing purified (A-tailed) PCR products to be ligated directly into the purified T-vector backbone. TA cloning does not require restriction digestion of the PCR amplified insert, removing the need to identify restriction sites unique to both the vector and insert. The three multisite gateway TA-cloning vectors p5E-TA, pME-TA, and p3E-TA can be used to rapidly generate new entry vectors without the need for both long *att*-site containing primers and BP Clonase™ II Enzyme Mix. Entry vectors generated with this method can then be used in a LR-Multisite Gateway reaction to generate final transgenesis vectors (Fig. 1B). These TA clonable vectors can be used in a multifunctional way to enable rapid one-step generation of Tol2-transgenesis vectors (Fig. 1C–F). As an example, incorporating undigested pME-TA entry vector into a multisite LR Gateway reaction generates a final Tol2-transgenesis vector that contains the TA-EGFP linker in the middle entry position (Fig. 1D). This can be used to generate a reporter line, but more importantly, subsequent *Xcm*I digestion generates a pDestTol2 plasmid with T overhangs (Fig. 1E) allowing purified PCR products to be directly ligated into the middle entry position in one step (Fig. 1F). All three TA clonable entry vectors can be used in this way to generate final pDestTol2:TA clonable transgenesis vectors, using only one multisite LR reaction (for the initial reaction), no long *attB* primers, and without the need to pass the gene of interest through a middle entry vector. All purified *Xcm*I-digested vectors can be stored as stocks at −20°C for later use. The TA clonable entry vectors reported here are also compatible with any multisite LR destination vector, such as the Tol2kit[6] destination vectors or the ΦC31 integrase destination vectors: pDestattB and its derivative pDestattB/CY.[7] See Supplementary Data (Supplementary Data are available online at www.liebertpub.com/zeb) for a full set of optimized methods of use.

Disclosure Statement

The authors have no competing interests to declare.

Address correspondence to:
Heather Verkade, BSc(hons), PhD
School of Biological Sciences
Monash University
Building 18
Clayton, VIC 3800
Australia

E-mail: [redacted]

Supplementary data

Supplementary Data

Supplementary Materials and Methods

Primers used to generate TA linker and TA vectors

F-*Xcm*I-*Eco*RV-EGFP: CCAATACTTGTATGGGATAT CATGGTGAGCAAGGGCGAG; R-*Sna*BI *Xcm*I Fluro: TTACGTACCAATACTTGTATGGTTACTTGTACAGCT CGTCCA.

F-*Bam*HI-*Xcm*I: AGTGGATCCCCAATACTTGTATGG GATATC; R-*Xho*I-*Xcm*I: ATCGCTCGAGCCAATACTTG TATGGTTACTT.

A-tailing reaction using proofreading polymerase

One to two microliters of purified PCR product, 1 μL Taq DNA polymerase, 1 μL 10 × reaction buffer with $MgCl_2$, 1 μL 10 mM dATP, H_2O to 10 μL were incubated at 70°C for 15 min.

TA linker–vector preparation

TA vectors are prepared through *Xcm*I restriction digestion, and fragments separated using 1% agarose gel electrophoresis. Correct bands were excised and the DNA purified using the Wizard® SV Gel and PCR clean-up system.

Gateway recombination reactions

Gateway recombination reactions were performed as per Kwan *et al.*[6]

Ligation conditions

Fifty or 25 ng of A-tailed PCR product was ligated with *Xcm*I digested TA vector at a ratio ranging from 3:1 to 10:1 as per the optimized T-vector conditions outlined by Schutte *et al.*[3] Ligation reactions were incubated at 16°C for 14 h, and then the ligase was heat inactivated at 65°C for 15 min.

Optimized transformation conditions

Heat inactivation of T4 DNA ligase was performed to improve transformation as per Ymer.[8] To achieve high transformation results, the following protocol was modified from Zoller.[9] One microliter of the heat-inactivated ligation reaction was added to 39 μL sterile H_2O in a PCR tube and placed on ice. Ten microliters of electrocompetent cells was added, and the mixture transferred to an ice-cold 2 mm transformation cuvette. Transformation was achieved using a BioRad Gene Pulser™ (Cat#165-2078) with settings 2.45 Kv, 200, 25 μF, and pulse time of 4.6 ms. One milliliter LB (+20 μM glucose) was added to the cuvette after transformation, and the mixture was transferred to a 1.5-mL microfuge tube and placed in a 37°C water bath for 1 h to recover. One hundred fifty microliters was removed and spread on an LB agar plate containing the appropriate antibiotic. The rest of the transformation mixture was centrifuged in a bench top centrifuge at 1000 *g* for 5 min. The supernatant was tipped off, leaving ~100 μL. The pellet was redissolved, spread on an LB agar plate containing the appropriate antibiotic, and incubated at 37°C overnight.

Colony PCR protocol

Overnight colonies were picked and mixed with 20 μL Colony PCR master mix in a PCR tube. Master Mix contained the following: 1 μL *Taq* DNA polymerase, 1 μL 10 mM forward primer, 1 μL 10 mM reverse primer, 2 μL PCR buffer (with $MgCl_2$), 0.6 μL 10 mM dNTPs, and 14.4 sterile distilled H_2O. Colony PCR conditions were as follows: 5 min at 95°C, 39 cycles (1 min at 95°C, 30 s primer Tm °C, 1 min/kb at 72°C), 5 min at 72°C.

Availability of vectors

The pCS2 + TA vector has been deposited in Addgene.org for easy accessibility (pCS2 + TA ID: 49338). The p5E-TA, pME-TA, and p3E-TA are unable to be deposited in Addgene due to intellectual property issues with Invitrogen and are available upon request from Dr Robert Bryson-Richardson (robert.bryson-richardson@monash.edu).

Acknowledgments

The authors thank Thomas Hall and Peter Currie for the generous gift of the pME-iCre middle entry vector. The work was supported by a project grant from the National Health and Medical Research Council (491087) to H.V.

Disclosure Statement

The authors have no competing interests to declare.

References

1. Zhou MY, Gomez-Sanchez CE. Universal TA cloning. Curr Issues Mol Biol 2000;2:1–7.
2. Arashi-Heese N, Miwa M, Shibata H. XcmI site-containing vector for direct cloning and *in vitro* transcription of PCR product. Mol Biotechnol 1999;12:281–283.
3. Schutte BC, Ranade K, Pruessner J, Dracopoli N. Optimized conditions for cloning PCR products into an XcmI T-vector. Biotechniques 1997;22:40–42.
4. Chen S, Songkumarn P, Liu J, Wang GL. A versatile zero background T-vector system for gene cloning and functional genomics. Plant Physiol 2009;150:1111–1121.
5. Hong SG, Choi JY, Pryor BM, Lee HK. An efficient method to prepare PCR cloning vectors. Mycobiology 2009;37:240–242.
6. Kwan KM, Fujimoto E, Grabher C, Mangum BD, Hardy ME, Campbell DS, *et al.* The Tol2kit: a multisite gateway-based construction kit for Tol2 transposon transgenesis constructs. Dev Dyn 2007;236:3088–3099.
7. Mosimann C, Puller AC, Lawson KL, Tschopp P, Amsterdam A, Zon LI. Site-directed zebrafish transgenesis into

single landing sites with the phiC31 integrase system. Dev Dyn 2013;242:949–963.
8. Ymer S. Heat inactivation of DNA ligase prior to electroporation increases transformation efficiency. Nucleic Acids Res 1991;19:6960.
9. Zoller P. High electro-transformation efficiencies obtained with DNA from ligation mixtures. Bulletin 1359, Bio-Rad Laboratories. Available at: www.bio-radcom/webroot/web/pdf/lsr/literature/Bulletin_1359pdf. (Accessed 11th April 2013), 1992.

Chapter 9. Appendix Three

	3 somites Endoderm	Chi2 value	3 somites Mesoderm	Chi2 value	16 somite Endoderm	Chi2 value	16 somites Mesoderm	Chi2 value
WT (6)	Randomised	0.3353	Directed	0.00611	Directed	0.0001	Directed	0.0194
tri-/- (6)	Randomised	0.5812	Randomised	0.07904	Randomised	0.0923	Randomised	0.6149
tri-/- (WT6)	Different to WT	0.0276	Different to WT	0.02559	Different to WT	0.0409	Different to WT	0.0094
kny-/- (6)	Randomised	0.1906	Randomised	0.78335	Directed	0.0000	Randomised	0.5652
kny-/- (WT6)	Different to WT	0.0005	Different to WT	0.00024	Different to WT	0.0103	Different to WT	0.0140
Hsp@shield (6)	Randomised	0.4618	Randomised	0.27974	Randomised	0.7389	Directed	0.0343
Hsp@shield (WT6)	Same as WT	0.1382	Different to WT	1.77E-10	Different to WT	0.0006	Different to WT	0.0002

Table 4. Statistical values for MTOC polarisation data. χ squared values testing for equal MTOC distributions over the six quadrants (6) (randomised), and with WT observed values as expected values (WT6) (same of different to WT). Green shaded boxes indicate significant difference. $P \leq 0.05$. Red shaded boxes indicate values are not significant.

Chapter 10. References

Akitake, C. M., Macurak, M., Halpern, M. E. and Goll, M. G. (2011) 'Transgenerational analysis of transcriptional silencing in zebrafish', *Dev Biol* 352(2): 191-201.

Alexander, J., Rothenberg, M., Henry, G. L. and Stainier, D. Y. (1999) 'casanova plays an early and essential role in endoderm formation in zebrafish', *Dev Biol* 215(2): 343-57.

Alexander, J. and Stainier, D. Y. (1999) 'A molecular pathway leading to endoderm formation in zebrafish', *Curr Biol* 9(20): 1147-57.

Amores, A., Force, A., Yan, Y. L., Joly, L., Amemiya, C., Fritz, A., Ho, R. K., Langeland, J., Prince, V., Wang, Y. L. et al. (1998) 'Zebrafish hox clusters and vertebrate genome evolution', *Science* 282(5394): 1711-4.

Angers, S., Thorpe, C. J., Biechele, T. L., Goldenberg, S. J., Zheng, N., MacCoss, M. J. and Moon, R. T. (2006) 'The KLHL12-Cullin-3 ubiquitin ligase negatively regulates the Wnt-beta-catenin pathway by targeting Dishevelled for degradation', *Nat Cell Biol* 8(4): 348-57.

Antic, D., Stubbs, J. L., Suyama, K., Kintner, C., Scott, M. P. and Axelrod, J. D. (2010) 'Planar Cell Polarity Enables Posterior Localization of Nodal Cilia and Left-Right Axis Determination during Mouse and Xenopus Embryogenesis', *PLoS ONE* 5(2): e8999.

Arashi-Heese, N., Miwa, M. and Shibata, H. (1999) 'XcmI site-containing vector for direct cloning and in vitro transcription of PCR product', *Mol Biotechnol* 12(3): 281-3.

Axelrod, J. D. (2001) 'Unipolar membrane association of Dishevelled mediates Frizzled planar cell polarity signaling', *Genes Dev* 15(10): 1182-7.

Axelrod, J. D., Miller, J. R., Shulman, J. M., Moon, R. T. and Perrimon, N. (1998) 'Differential recruitment of Dishevelled provides signaling specificity in the planar cell polarity and Wingless signaling pathways', *Genes Dev* 12(16): 2610-22.

Bagnat, M., Cheung, I. D., Mostov, K. E. and Stainier, D. Y. (2007) 'Genetic control of single lumen formation in the zebrafish gut', *Nat Cell Biol* 9(8): 954-60.

Barrow, J. R. (2006) 'Wnt/PCP signaling: a veritable polar star in establishing patterns of polarity in embryonic tissues', *Semin Cell Dev Biol* 17(2): 185-93.

Belotti, E., Puvirajesinghe, T. M., Audebert, S., Baudelet, E., Camoin, L., Pierres, M., Lasvaux, L., Ferracci, G., Montcouquiol, M. and Borg, J. P. (2012) 'Molecular characterisation of endogenous Vangl2/Vangl1 heteromeric protein complexes', *PLoS ONE* 7(9): e46213.

Bergmann, J. E., Kupfer, A. and Singer, S. J. (1983) 'Membrane insertion at the leading edge of motile fibroblasts', *Proc Natl Acad Sci U S A* 80(5): 1367-71.

Bhanot, P., Brink, M., Samos, C. H., Hsieh, J. C., Wang, Y., Macke, J. P., Andrew, D., Nathans, J. and Nusse, R. (1996) 'A new member of the frizzled family from Drosophila functions as a Wingless receptor', *Nature* 382(6588): 225-30.

Bourhis, E., Tam, C., Franke, Y., Bazan, J. F., Ernst, J., Hwang, J., Costa, M., Cochran, A. G. and Hannoush, R. N. (2010) 'Reconstitution of a Frizzled8-Wnt3a-LRP6 signaling complex reveals multiple Wnt and Dkk1 binding sites on LRP6', *J Biol Chem*.

Caneparo, L., Huang, Y. L., Staudt, N., Tada, M., Ahrendt, R., Kazanskaya, O., Niehrs, C. and Houart, C. (2007) 'Dickkopf-1 regulates gastrulation movements by coordinated modulation of Wnt/beta catenin and Wnt/PCP activities, through interaction with the Dally-like homolog Knypek', *Genes Dev* 21(4): 465-80.

Cantrell, V. A. and Jessen, J. R. (2009) 'The planar cell polarity protein Van Gogh-Like 2 regulates tumor cell migration and matrix metalloproteinase-dependent invasion', *Cancer Lett*.

Carreira-Barbosa, F., Concha, M. L., Takeuchi, M., Ueno, N., Wilson, S. W. and Tada, M. (2003) 'Prickle 1 regulates cell movements during gastrulation and neuronal migration in zebrafish', *Development* 130(17): 4037-46.

Carreira-Barbosa, F., Kajita, M., Morel, V., Wada, H., Okamoto, H., Martinez Arias, A., Fujita, Y., Wilson, S. W. and Tada, M. (2008) 'Flamingo regulates epiboly and convergence/extension movements through cell cohesive and signalling functions during zebrafish gastrulation', *Development*.

Carron, C., Pascal, A., Djiane, A., Boucaut, J. C., Shi, D. L. and Umbhauer, M. (2003) 'Frizzled receptor dimerization is sufficient to activate the Wnt/beta-catenin pathway', *J Cell Sci* 116(Pt 12): 2541-50.

Cha, S. W., Tadjuidje, E., Tao, Q., Wylie, C. and Heasman, J. (2008) 'Wnt5a and Wnt11 interact in a maternal Dkk1-regulated fashion to activate both canonical and non-canonical signaling in Xenopus axis formation', *Development* 135(22): 3719-29.

Chen, S., Songkumarn, P., Liu, J. and Wang, G. L. (2009) 'A versatile zero background T-vector system for gene cloning and functional genomics', *Plant Physiol* 150(3): 1111-21.

Chen, W. S., Antic, D., Matis, M., Logan, C. Y., Povelones, M., Anderson, G. A., Nusse, R. and Axelrod, J. D. (2008) 'Asymmetric homotypic interactions of the atypical cadherin flamingo mediate intercellular polarity signaling', *Cell* 133(6): 1093-105.

Chiu, J., March, P. E., Lee, R. and Tillett, D. (2004) 'Site-directed, Ligase-Independent Mutagenesis (SLIM): a single-tube methodology approaching 100% efficiency in 4 h', *Nucleic Acids Res* 32(21): e174.

Chung, J., Nguyen, A. K., Henstridge, D. C., Holmes, A. G., Chan, M. H., Mesa, J. L., Lancaster, G. I., Southgate, R. J., Bruce, C. R., Duffy, S. J. et al. (2008) 'HSP72 protects against obesity-induced insulin resistance', *Proc Natl Acad Sci U S A* 105(5): 1739-44.

Ciruna, B., Jenny, A., Lee, D., Mlodzik, M. and Schier, A. F. (2006) 'Planar cell polarity signalling couples cell division and morphogenesis during neurulation', *Nature* 439(7073): 220-4.

Courbard, J. R., Djiane, A., Wu, J. and Mlodzik, M. (2009) 'The Apical/Basal-polarity determinant Scribble cooperates with the PCP core factor Stbm/Vang and functions as one of its effectors', *Dev Biol*.

Coyle, R. C., Latimer, A. and Jessen, J. R. (2008) 'Membrane-type 1 matrix metalloproteinase regulates cell migration during zebrafish gastrulation: evidence for an interaction with non-canonical Wnt signaling', *Exp Cell Res* 314(10): 2150-62.

Dale, R. M., Sisson, B. E. and Topczewski, J. (2009) 'The emerging role of Wnt/PCP signaling in organ formation', *Zebrafish* 6(1): 9-14.

Darken, R. S., Scola, A. M., Rakeman, A. S., Das, G., Mlodzik, M. and Wilson, P. A. (2002) 'The planar polarity gene strabismus regulates convergent extension movements in Xenopus', *EMBO J* 21(5): 976-85.

Devenport, D. and Fuchs, E. (2008) 'Planar polarization in embryonic epidermis orchestrates global asymmetric morphogenesis of hair follicles', *Nat Cell Biol* 10(11): 1257-68.

Dickmeis, T., Mourrain, P., Saint-Etienne, L., Fischer, N., Aanstad, P., Clark, M., Strahle, U. and Rosa, F. (2001) 'A crucial component of the endoderm formation pathway, CASANOVA, is encoded by a novel sox-related gene', *Genes Dev* 15(12): 1487-92.

Distel, M., Wullimann, M. F. and Koster, R. W. (2009) 'Optimized Gal4 genetics for permanent gene expression mapping in zebrafish', *Proc Natl Acad Sci U S A*.

Djiane, A., Yogev, S. and Mlodzik, M. (2005) 'The apical determinants aPKC and dPatj regulate Frizzled-dependent planar cell polarity in the Drosophila eye', *Cell* 121(4): 621-31.

Dohn, M. R., Mundell, N. A., Sawyer, L. M., Dunlap, J. A. and Jessen, J. R. (2013) 'Planar cell polarity proteins differentially regulate extracellular matrix organization and assembly during zebrafish gastrulation', *Dev Biol* 383(1): 39-51.

Fanto, M. and McNeill, H. (2004) 'Planar polarity from flies to vertebrates', *J Cell Sci* 117(Pt 4): 527-33.

Felsenstein, J. (1985) 'Confidence limits on phylogenies: An approach using the bootstrap', *Evolution* 39: 783-791.

Fenstermaker, A. G., Prasad, A. A., Bechara, A., Adolfs, Y., Tissir, F., Goffinet, A., Zou, Y. and Pasterkamp, R. J. (2010) 'Wnt/planar cell polarity signaling controls the anterior-posterior organization of monoaminergic axons in the brainstem', *J Neurosci* 30(47): 16053-64.

Field, H. A., Dong, P. D., Beis, D. and Stainier, D. Y. (2003a) 'Formation of the digestive system in zebrafish. II. Pancreas morphogenesis', *Dev Biol* 261(1): 197-208.

Field, H. A., Ober, E. A., Roeser, T. and Stainier, D. Y. (2003b) 'Formation of the digestive system in zebrafish. I. Liver morphogenesis', *Dev Biol* 253(2): 279-90.

Gao, B. (2012) 'Wnt regulation of planar cell polarity (PCP)', *Curr Top Dev Biol* 101: 263-95.

Gao, B., Song, H., Bishop, K., Elliot, G., Garrett, L., English, M. A., Andre, P., Robinson, J., Sood, R., Minami, Y. et al. (2011) 'Wnt signaling gradients establish planar cell polarity by inducing Vangl2 phosphorylation through Ror2', *Dev Cell* 20(2): 163-76.

Gehrig, S. M., van der Poel, C., Sayer, T. A., Schertzer, J. D., Henstridge, D. C., Church, J. E., Lamon, S., Russell, A. P., Davies, K. E., Febbraio, M. A. et al. (2012) 'Hsp72 preserves muscle function and slows progression of severe muscular dystrophy', *Nature* 484(7394): 394-8.

Gomes, J. E., Corado, M. and Schweisguth, F. (2009) 'Van gogh and frizzled act redundantly in the Drosophila sensory organ precursor cell to orient its asymmetric division', *PLoS ONE* 4(2): e4485.

Gong, Y., Mo, C. and Fraser, S. E. (2004) 'Planar cell polarity signalling controls cell division orientation during zebrafish gastrulation', *Nature* 430(7000): 689-93.

Gordon, M. D. and Nusse, R. (2006) 'Wnt signaling: multiple pathways, multiple receptors, and multiple transcription factors', *J Biol Chem* 281(32): 22429-33.

Goto, T., Davidson, L., Asashima, M. and Keller, R. (2005) 'Planar cell polarity genes regulate polarized extracellular matrix deposition during frog gastrulation', *Curr Biol* 15(8): 787-93.

Goto, T. and Keller, R. (2002) 'The planar cell polarity gene strabismus regulates convergence and extension and neural fold closure in Xenopus', *Dev Biol* 247(1): 165-81.

Goulimari, P., Knieling, H., Engel, U. and Grosse, R. (2008) 'LARG and mDia1 Link G(alpha)12/13 to Cell Polarity and Microtubule Dynamics', *Mol Biol Cell* 19(1): 30-40.

Grabher, C., Joly, J. S. and Wittbrodt, J. (2004) 'Highly efficient zebrafish transgenesis mediated by the meganuclease I-SceI', *Methods Cell Biol* 77: 381-401.

Gros, J., Serralbo, O. and Marcelle, C. (2009) 'WNT11 acts as a directional cue to organize the elongation of early muscle fibres', *Nature* 457(7229): 589-93.

Gubb, D. and Garcia-Bellido, A. (1982) 'A genetic analysis of the determination of cuticular polarity during development in Drosophila melanogaster', *J Embryol Exp Morphol* 68: 37-57.

Guirao, B., Meunier, A., Mortaud, S., Aguilar, A., Corsi, J. M., Strehl, L., Hirota, Y., Desoeuvre, A., Boutin, C., Han, Y. G. et al. (2010) 'Coupling between hydrodynamic forces and planar cell polarity orients mammalian motile cilia', *Nat Cell Biol* 12(4): 341-50.

Gutzman, J. H., Graeden, E. G., Lowery, L. A., Holley, H. S. and Sive, H. (2008) 'Formation of the zebrafish midbrain-hindbrain boundary constriction requires laminin-dependent basal constriction', *Mech Dev* 125(11-12): 974-83.

Habas, R. and Dawid, I. B. (2005) 'Dishevelled and Wnt signaling: is the nucleus the final frontier?', *J Biol* 4(1): 2.

Habas, R., Dawid, I. B. and He, X. (2003) 'Coactivation of Rac and Rho by Wnt/Frizzled signaling is required for vertebrate gastrulation', *Genes Dev* 17(2): 295-309.

Habas, R., Kato, Y. and He, X. (2001) 'Wnt/Frizzled activation of Rho regulates vertebrate gastrulation and requires a novel Formin homology protein Daam1', *Cell* 107(7): 843-54.

Hale, C. M., Chen, W. C., Khatau, S. B., Daniels, B. R., Lee, J. S. and Wirtz, D. (2011) 'SMRT analysis of MTOC and nuclear positioning reveals the role of EB1 and LIC1 in single-cell polarization', *J Cell Sci* 124(Pt 24): 4267-85.

Hammerschmidt, M., Pelegri, F., Mullins, M. C., Kane, D. A., Brand, M., van Eeden, F. J., Furutani-Seiki, M., Granato, M., Haffter, P., Heisenberg, C. P. et al. (1996) 'Mutations affecting morphogenesis during gastrulation and tail formation in the zebrafish, Danio rerio', *Development* 123: 143-51.

Harrington, M. J., Hong, E., Fasanmi, O. and Brewster, R. (2007) 'Cadherin-mediated adhesion regulates posterior body formation', *BMC Dev Biol* 7: 130.

Heisenberg, C. P., Brand, M., Jiang, Y. J., Warga, R. M., Beuchle, D., van Eeden, F. J., Furutani-Seiki, M., Granato, M., Haffter, P., Hammerschmidt, M. et al. (1996) 'Genes involved in forebrain development in the zebrafish, Danio rerio', *Development* 123: 191-203.

Heisenberg, C. P. and Nusslein-Volhard, C. (1997) 'The function of silberblick in the positioning of the eye anlage in the zebrafish embryo', *Dev Biol* 184(1): 85-94.

Heisenberg, C. P., Tada, M., Rauch, G. J., Saude, L., Concha, M. L., Geisler, R., Stemple, D. L., Smith, J. C. and Wilson, S. W. (2000) 'Silberblick/Wnt11 mediates

convergent extension movements during zebrafish gastrulation', *Nature* 405(6782): 76-81.

Heydeck, W., Zeng, H. and Liu, A. (2009) 'Planar cell polarity effector gene Fuzzy regulates cilia formation and Hedgehog signal transduction in mouse', *Dev Dyn*.

Hikasa, H., Shibata, M., Hiratani, I. and Taira, M. (2002) 'The Xenopus receptor tyrosine kinase Xror2 modulates morphogenetic movements of the axial mesoderm and neuroectoderm via Wnt signaling', *Development* 129(22): 5227-39.

Hollway, G. E., Bryson-Richardson, R. J., Berger, S., Cole, N. J., Hall, T. E. and Currie, P. D. (2007) 'Whole-somite rotation generates muscle progenitor cell compartments in the developing zebrafish embryo', *Dev Cell* 12(2): 207-19.

Hong, S. G., Choi, J. Y., Pryor, B. M. and Lee, H. K. (2009) 'An efficient method to prepare PCR cloning vectors', *Mycobiology* 37(3): 240-2.

Horne-Badovinac, S., Lin, D., Waldron, S., Schwarz, M., Mbamalu, G., Pawson, T., Jan, Y., Stainier, D. Y. and Abdelilah-Seyfried, S. (2001) 'Positional cloning of heart and soul reveals multiple roles for PKC lambda in zebrafish organogenesis', *Curr Biol* 11(19): 1492-502.

Jenny, A., Darken, R. S., Wilson, P. A. and Mlodzik, M. (2003) 'Prickle and Strabismus form a functional complex to generate a correct axis during planar cell polarity signaling', *EMBO J* 22(17): 4409-20.

Jessen, J. R. and Solnica-Krezel, L. (2004) 'Identification and developmental expression pattern of van gogh-like 1, a second zebrafish strabismus homologue', *Gene Expr Patterns* 4(3): 339-44.

Jessen, J. R., Topczewski, J., Bingham, S., Sepich, D. S., Marlow, F., Chandrasekhar, A. and Solnica-Krezel, L. (2002) 'Zebrafish trilobite identifies new roles for Strabismus in gastrulation and neuronal movements', *Nat Cell Biol* 4(8): 610-5.

Jin, S. W., Beis, D., Mitchell, T., Chen, J. N. and Stainier, D. Y. (2005) 'Cellular and molecular analyses of vascular tube and lumen formation in zebrafish', *Development* 132(23): 5199-209.

Jones, D. T., Taylor, W. R. and Thornton, J. M. (1992) 'The rapid generation of mutation data matrices from protein sequences', *Comput Appl Biosci* 8(3): 275-82.

Junge, H. J., Yang, S., Burton, J. B., Paes, K., Shu, X., French, D. M., Costa, M., Rice, D. S. and Ye, W. (2009) 'TSPAN12 regulates retinal vascular development by promoting Norrin- but not Wnt-induced FZD4/beta-catenin signaling', *Cell* 139(2): 299-311.

Kane, D. A., McFarland, K. N. and Warga, R. M. (2005) 'Mutations in half baked/E-cadherin block cell behaviors that are necessary for teleost epiboly', *Development* 132(5): 1105-16.

Kanki, J. P. and Ho, R. K. (1997) 'The development of the posterior body in zebrafish', *Development* 124(4): 881-93.

Karner, C., Wharton, K. A., Jr. and Carroll, T. J. (2006) 'Planar cell polarity and vertebrate organogenesis', *Semin Cell Dev Biol* 17(2): 194-203.

Karner, C. M., Chirumamilla, R., Aoki, S., Igarashi, P., Wallingford, J. B. and Carroll, T. J. (2009) 'Wnt9b signaling regulates planar cell polarity and kidney tubule morphogenesis', *Nat Genet* 41(7): 793-9.

Kaykas, A., Yang-Snyder, J., Heroux, M., Shah, K. V., Bouvier, M. and Moon, R. T. (2004) 'Mutant Frizzled 4 associated with vitreoretinopathy traps wild-type Frizzled in the endoplasmic reticulum by oligomerization', *Nat Cell Biol* 6(1): 52-8.

KEGG, K. E. o. G. a. G. (2014a) Human Dishevelled homologs, http://www.genome.jp/dbget-bin/www_bget?hsa:1855+hsa:1856+hsa:1857, accessed June 2014.

KEGG, K. E. o. G. a. G. (2014b) Human Frizzled receptors, http://www.genome.jp/dbget-bin/www_bget?hsa:11211+hsa:2535+hsa:7855+hsa:7976+hsa:8321+hsa:8322+hsa:8323+hsa:8324+hsa:8325+hsa:8326.

KEGG, K. E. o. G. a. G. (2014c) Mouse Dishevelled homologs, http://www.genome.jp/dbget-bin/www_bget?mmu:13542+mmu:13543+mmu:13544, accessed June 2014.

KEGG, K. E. o. G. a. G. (2014d) Mouse Frizzled receptors, http://www.genome.jp/dbget-bin/www_bget?hsa:11211+hsa:2535+hsa:7855+hsa:7976+hsa:8321+hsa:8322+hsa:8323+hsa:8324+hsa:8325+hsa:8326.

Keller, P. J., Schmidt, A. D., Wittbrodt, J. and Stelzer, E. H. (2008) 'Reconstruction of zebrafish early embryonic development by scanned light sheet microscopy', *Science* 322(5904): 1065-9.

Keller, R., Davidson, L., Edlund, A., Elul, T., Ezin, M., Shook, D. and Skoglund, P. (2000) 'Mechanisms of convergence and extension by cell intercalation', *Philos Trans R Soc Lond B Biol Sci* 355(1399): 897-922.

Kibar, Z., Salem, S., Bosoi, C. M., Pauwels, E., De Marco, P., Merello, E., Bassuk, A. G., Capra, V. and Gros, P. (2010) 'Contribution of VANGL2 mutations to isolated neural tube defects', *Clin Genet*.

Kibar, Z., Torban, E., McDearmid, J. R., Reynolds, A., Berghout, J., Mathieu, M., Kirillova, I., De Marco, P., Merello, E., Hayes, J. M. et al. (2007) 'Mutations in VANGL1 associated with neural-tube defects', *N Engl J Med* 356(14): 1432-7.

Kikuchi, Y., Agathon, A., Alexander, J., Thisse, C., Waldron, S., Yelon, D., Thisse, B. and Stainier, D. Y. (2001) 'casanova encodes a novel Sox-related protein

necessary and sufficient for early endoderm formation in zebrafish', *Genes Dev* 15(12): 1493-505.

Kilander, M. B., Dahlstrom, J. and Schulte, G. (2014) 'Assessment of Frizzled 6 membrane mobility by FRAP supports G protein coupling and reveals WNT-Frizzled selectivity', *Cell Signal*.

Kilian, B., Mansukoski, H., Barbosa, F. C., Ulrich, F., Tada, M. and Heisenberg, C. P. (2003) 'The role of Ppt/Wnt5 in regulating cell shape and movement during zebrafish gastrulation', *Mech Dev* 120(4): 467-76.

Kimmel, C. B., Ballard, W. W., Kimmel, S. R., Ullmann, B. and Schilling, T. F. (1995) 'Stages of embryonic development of the zebrafish', *Dev Dyn* 203(3): 253-310.

Komiya, Y. and Habas, R. (2008) 'Wnt signal transduction pathways', *Organogenesis* 4(2): 68-75.

Kupperman, E., An, S., Osborne, N., Waldron, S. and Stainier, D. Y. (2000) 'A sphingosine-1-phosphate receptor regulates cell migration during vertebrate heart development', *Nature* 406(6792): 192-5.

Kwan, K. M., Fujimoto, E., Grabher, C., Mangum, B. D., Hardy, M. E., Campbell, D. S., Parant, J. M., Yost, H. J., Kanki, J. P. and Chien, C. B. (2007) 'The Tol2kit: a multisite gateway-based construction kit for Tol2 transposon transgenesis constructs', *Dev Dyn* 236(11): 3088-99.

Latimer, A. and Jessen, J. R. (2009) 'Extracellular matrix assembly and organization during zebrafish gastrulation', *Matrix Biol*.

Lawrence, P. A., Struhl, G. and Casal, J. (2007) 'Planar cell polarity: one or two pathways?', *Nat Rev Genet* 8(7): 555-63.

Lin, F., Chen, S., Sepich, D. S., Panizzi, J. R., Clendenon, S. G., Marrs, J. A., Hamm, H. E. and Solnica-Krezel, L. (2009) 'Galpha12/13 regulate epiboly by inhibiting E-cadherin activity and modulating the actin cytoskeleton', *J Cell Biol* 184(6): 909-21.

Lin, F., Sepich, D. S., Chen, S., Topczewski, J., Yin, C., Solnica-Krezel, L. and Hamm, H. (2005) 'Essential roles of G{alpha}12/13 signaling in distinct cell behaviors driving zebrafish convergence and extension gastrulation movements', *J Cell Biol* 169(5): 777-87.

Lindqvist, M., Horn, Z., Bryja, V., Schulte, G., Papachristou, P., Ajima, R., Dyberg, C., Arenas, E., Yamaguchi, T. P., Lagercrantz, H. et al. (2010) 'Vang-like protein 2 and Rac1 interact to regulate adherens junctions', *J Cell Sci* 123(Pt 3): 472-83.

Liu, Y. G. and Whittier, R. F. (1995) 'Thermal asymmetric interlaced PCR: automatable amplification and sequencing of insert end fragments from P1 and YAC clones for chromosome walking', *Genomics* 25(3): 674-81.

Lopez-Schier, H. and Hudspeth, A. J. (2006) 'A two-step mechanism underlies the planar polarization of regenerating sensory hair cells', *Proc Natl Acad Sci U S A* 103(49): 18615-20.

Lowery, L. A., De Rienzo, G., Gutzman, J. H. and Sive, H. (2009) 'Characterization and classification of zebrafish brain morphology mutants', *Anat Rec (Hoboken)* 292(1): 94-106.

Lowery, L. A. and Sive, H. (2005) 'Initial formation of zebrafish brain ventricles occurs independently of circulation and requires the nagie oko and snakehead/atp1a1a.1 gene products', *Development* 132(9): 2057-67.

Lum, W. M., Robertson, J. K. and Van Raay, T. J. (2011) 'Dishevelled2 is a stable protein during early zebrafish development', *Zebrafish* 8(2): 65-71.

Mahuzier, A., Gaude, H. M., Grampa, V., Anselme, I., Silbermann, F., Leroux-Berger, M., Delacour, D., Ezan, J., Montcouquiol, M., Saunier, S. et al. (2012) 'Dishevelled stabilization by the ciliopathy protein Rpgrip1l is essential for planar cell polarity', *J Cell Biol* 198(5): 927-40.

Mapp, O. M., Wanner, S. J., Rohrschneider, M. R. and Prince, V. E. (2010) 'Prickle1b mediates interpretation of migratory cues during zebrafish facial branchiomotor neuron migration', *Dev Dyn* 239(6): 1596-608.

Marchler-Bauer, A. and Bryant, S. H. (2004) 'CD-Search: protein domain annotations on the fly', *Nucleic Acids Res* 32(Web Server issue): W327-31 http://www.ncbi.nlm.nih.gov/Structure/cdd/wrpsb.cgi (accessed 2012).

Marchler-Bauer, A., Zheng, C., Chitsaz, F., Derbyshire, M. K., Geer, L. Y., Geer, R. C., Gonzales, N. R., Gwadz, M., Hurwitz, D. I., Lanczycki, C. J. et al. (2013) 'CDD: conserved domains and protein three-dimensional structure', *Nucleic Acids Res* 41(Database issue): D348-52.

Marlow, F., Gonzalez, E. M., Yin, C., Rojo, C. and Solnica-Krezel, L. (2004) 'No tail co-operates with non-canonical Wnt signaling to regulate posterior body morphogenesis in zebrafish', *Development* 131(1): 203-16.

Marlow, F., Topczewski, J., Sepich, D. and Solnica-Krezel, L. (2002) 'Zebrafish Rho kinase 2 acts downstream of Wnt11 to mediate cell polarity and effective convergence and extension movements', *Curr Biol* 12(11): 876-84.

Marlow, F., Zwartkruis, F., Malicki, J., Neuhauss, S. C., Abbas, L., Weaver, M., Driever, W. and Solnica-Krezel, L. (1998) 'Functional interactions of genes mediating convergent extension, knypek and trilobite, during the partitioning of the eye primordium in zebrafish', *Dev Biol* 203(2): 382-99.

Matsui, T., Raya, A., Callol-Massot, C., Kawakami, Y., Oishi, I., Rodriguez-Esteban, C. and Izpisua Belmonte, J. C. (2007) 'miles-apart-Mediated regulation of cell-fibronectin interaction and myocardial migration in zebrafish', *Nat Clin Pract Cardiovasc Med* 4 Suppl 1: S77-82.

Matsui, T., Raya, A., Kawakami, Y., Callol-Massot, C., Capdevila, J., Rodriguez-Esteban, C. and Izpisua Belmonte, J. C. (2005) 'Noncanonical Wnt signaling regulates midline convergence of organ primordia during zebrafish development', *Genes Dev* 19(1): 164-75.

Mazmanian, G., Kovshilovsky, M., Yen, D., Mohanty, A., Mohanty, S., Nee, A. and Nissen, R. M. (2010) 'The zebrafish dyrk1b gene is important for endoderm formation', *Genesis* 48(1): 20-30.

Miyagi, C., Yamashita, S., Ohba, Y., Yoshizaki, H., Matsuda, M. and Hirano, T. (2004) 'STAT3 noncell-autonomously controls planar cell polarity during zebrafish convergence and extension', *J Cell Biol* 166(7): 975-81.

Mizoguchi, T., Izawa, T., Kuroiwa, A. and Kikuchi, Y. (2006) 'Fgf signaling negatively regulates Nodal-dependent endoderm induction in zebrafish', *Dev Biol*.

Mizoguchi, T., Verkade, H., Heath, J. K., Kuroiwa, A. and Kikuchi, Y. (2008) 'Sdf1/Cxcr4 signaling controls the dorsal migration of endodermal cells during zebrafish gastrulation', *Development*.

Mlodzik, M. (1999) 'Planar polarity in the Drosophila eye: a multifaceted view of signaling specificity and cross-talk', *EMBO J* 18(24): 6873-9.

Montero, J. A., Carvalho, L., Wilsch-Brauninger, M., Kilian, B., Mustafa, C. and Heisenberg, C. P. (2005) 'Shield formation at the onset of zebrafish gastrulation', *Development* 132(6): 1187-98.

Mosimann, C., Puller, A. C., Lawson, K. L., Tschopp, P., Amsterdam, A. and Zon, L. I. (2013) 'Site-directed zebrafish transgenesis into single landing sites with the phiC31 integrase system', *Dev Dyn* 242(8): 949-63.

Murdoch, J. N., Doudney, K., Paternotte, C., Copp, A. J. and Stanier, P. (2001) 'Severe neural tube defects in the loop-tail mouse result from mutation of Lpp1, a novel gene involved in floor plate specification', *Hum Mol Genet* 10(22): 2593-601.

Myers, D. C., Sepich, D. S. and Solnica-Krezel, L. (2002) 'Convergence and extension in vertebrate gastrulae: cell movements according to or in search of identity?', *Trends Genet* 18(9): 447-55.

Nair, S. and Schilling, T. F. (2008) 'Chemokine Signaling Controls Endodermal Migration During Zebrafish Gastrulation', *Science*.

NCBI, T. N. C. f. B. I. (2014a) Human Flamingo homologs, http://www.ncbi.nlm.nih.gov/gene/?term=%28cadherin+EGF+LAG+seven-pass+G-type+receptor%29+AND+%22Homo%22%5Bporgn%3A__txid9605%5D, accessed June 2014.

NCBI, T. N. C. f. B. I. (2014b) Mouse Flamingo homologs, http://www.ncbi.nlm.nih.gov/gene/?term=%28cadherin%2C+EGF+LAG+seven-pass+G-type+receptor%29%28celsr%29+AND+%22Mus+musculus%22%5Bporgn%3A__txid10090%5D, accessed June 2014.

Ng, A. N., de Jong-Curtain, T. A., Mawdsley, D. J., White, S. J., Shin, J., Appel, B., Dong, P. D., Stainier, D. Y. and Heath, J. K. (2005) 'Formation of the digestive system in zebrafish: III. Intestinal epithelium morphogenesis', *Dev Biol* 286(1): 114-35.

Niu, X., Shi, H. and Peng, J. (2010) 'The role of mesodermal signals during liver organogenesis in zebrafish', *Sci China Life Sci* 53(4): 455-61.

Ober, E. A., Field, H. A. and Stainier, D. Y. (2003) 'From endoderm formation to liver and pancreas development in zebrafish', *Mech Dev* 120(1): 5-18.

Ober, E. A., Olofsson, B., Makinen, T., Jin, S. W., Shoji, W., Koh, G. Y., Alitalo, K. and Stainier, D. Y. (2004) 'Vegfc is required for vascular development and endoderm morphogenesis in zebrafish', *EMBO Rep* 5(1): 78-84.

Ober, E. A., Verkade, H., Field, H. A. and Stainier, D. Y. (2006) 'Mesodermal Wnt2b signalling positively regulates liver specification', *Nature* 442(7103): 688-91.

Ohkawara, B., Yamamoto, T. S., Tada, M. and Ueno, N. (2003) 'Role of glypican 4 in the regulation of convergent extension movements during gastrulation in Xenopus laevis', *Development* 130(10): 2129-38.

Oishi, I., Suzuki, H., Onishi, N., Takada, R., Kani, S., Ohkawara, B., Koshida, I., Suzuki, K., Yamada, G., Schwabe, G. C. et al. (2003) 'The receptor tyrosine kinase Ror2 is involved in non-canonical Wnt5a/JNK signalling pathway', *Genes Cells* 8(7): 645-54.

Osborne, N., Brand-Arzamendi, K., Ober, E. A., Jin, S. W., Verkade, H., Holtzman, N. G., Yelon, D. and Stainier, D. Y. (2008) 'The spinster homolog, two of hearts, is required for sphingosine 1-phosphate signaling in zebrafish', *Curr Biol* 18(23): 1882-8.

Oteiza, P., Koppen, M., Krieg, M., Pulgar, E., Farias, C., Melo, C., Preibisch, S., Muller, D., Tada, M., Hartel, S. et al. (2010) 'Planar cell polarity signalling regulates cell adhesion properties in progenitors of the zebrafish laterality organ', *Development* 137(20): 3459-68.

Pan, X., Sittaramane, V., Gurung, S. and Chandrasekhar, A. (2013) 'Structural and temporal requirements of Wnt/PCP protein Vangl2 function for convergence and extension movements and facial branchiomotor neuron migration in zebrafish', *Mech Dev*.

Parinov, S., Kondrichin, I., Korzh, V. and Emelyanov, A. (2004) 'Tol2 transposon-mediated enhancer trap to identify developmentally regulated zebrafish genes in vivo', *Dev Dyn* 231(2): 449-59.

Park, M. and Moon, R. T. (2002) 'The planar cell-polarity gene stbm regulates cell behaviour and cell fate in vertebrate embryos', *Nat Cell Biol* 4(1): 20-5.

Pezeron, G., Mourrain, P., Courty, S., Ghislain, J., Becker, T. S., Rosa, F. M. and David, N. B. (2008) 'Live analysis of endodermal layer formation identifies random walk as a novel gastrulation movement', *Curr Biol* 18(4): 276-81.

Pouthas, F., Girard, P., Lecaudey, V., Ly, T. B., Gilmour, D., Boulin, C., Pepperkok, R. and Reynaud, E. G. (2008) 'In migrating cells, the Golgi complex and the position of the centrosome depend on geometrical constraints of the substratum', *J Cell Sci* 121(Pt 14): 2406-14.

Prigozhina, N. L. and Waterman-Storer, C. M. (2004) 'Protein kinase D-mediated anterograde membrane trafficking is required for fibroblast motility', *Curr Biol* 14(2): 88-98.

Quesada-Hernandez, E., Caneparo, L., Schneider, S., Winkler, S., Liebling, M., Fraser, S. E. and Heisenberg, C. P. (2010) 'Stereotypical cell division orientation controls neural rod midline formation in zebrafish', *Curr Biol* 20(21): 1966-72.

Ravni, A., Qu, Y., Goffinet, A. M. and Tissir, F. (2009) 'Planar Cell Polarity Cadherin Celsr1 Regulates Skin Hair Patterning in the Mouse', *J Invest Dermatol*.

Robitaille, J., MacDonald, M. L., Kaykas, A., Sheldahl, L. C., Zeisler, J., Dube, M. P., Zhang, L. H., Singaraja, R. R., Guernsey, D. L., Zheng, B. et al. (2002) 'Mutant frizzled-4 disrupts retinal angiogenesis in familial exudative vitreoretinopathy', *Nat Genet* 32(2): 326-30.

Rohde, L. A. and Heisenberg, C. P. (2007) 'Zebrafish gastrulation: cell movements, signals, and mechanisms', *Int Rev Cytol* 261: 159-92.

Roszko, I., Sawada, A. and Solnica-Krezel, L. (2009) 'Regulation of convergence and extension movements during vertebrate gastrulation by the Wnt/PCP pathway', *Semin Cell Dev Biol*.

Rothbacher, U., Laurent, M. N., Deardorff, M. A., Klein, P. S., Cho, K. W. and Fraser, S. E. (2000) 'Dishevelled phosphorylation, subcellular localization and multimerization regulate its role in early embryogenesis', *EMBO J* 19(5): 1010-22.

Sakaguchi, T., Kikuchi, Y., Kuroiwa, A., Takeda, H. and Stainier, D. Y. (2006) 'The yolk syncytial layer regulates myocardial migration by influencing extracellular matrix assembly in zebrafish', *Development* 133(20): 4063-72.

Schier, A. F. (2003) 'Nodal signaling in vertebrate development', *Annu Rev Cell Dev Biol* 19: 589-621.

Schier, A. F., Neuhauss, S. C., Harvey, M., Malicki, J., Solnica-Krezel, L., Stainier, D. Y., Zwartkruis, F., Abdelilah, S., Stemple, D. L., Rangini, Z. et al. (1996) 'Mutations affecting the development of the embryonic zebrafish brain', *Development* 123: 165-78.

Schier, A. F. and Shen, M. M. (2000) 'Nodal signalling in vertebrate development', *Nature* 403(6768): 385-9.

Schier, A. F. and Talbot, W. S. (2005) 'Molecular genetics of axis formation in zebrafish', *Annu Rev Genet* 39: 561-613.

Schmoranzer, J., Fawcett, J. P., Segura, M., Tan, S., Vallee, R. B., Pawson, T. and Gundersen, G. G. (2009) 'Par3 and dynein associate to regulate local microtubule dynamics and centrosome orientation during migration', *Curr Biol* 19(13): 1065-74.

Schmoranzer, J., Kreitzer, G. and Simon, S. M. (2003) 'Migrating fibroblasts perform polarized, microtubule-dependent exocytosis towards the leading edge', *J Cell Sci* 116(Pt 22): 4513-9.

Schutte, B. C., Ranade, K., Pruessner, J. and Dracopoli, N. (1997) 'Optimized conditions for cloning PCR products into an XcmI T-vector', *Biotechniques* 22(1): 40-2, 44.

Segalen, M. and Bellaiche, Y. (2009) 'Cell division orientation and planar cell polarity pathways', *Semin Cell Dev Biol*.

Segalen, M., Johnston, C. A., Martin, C. A., Dumortier, J. G., Prehoda, K. E., David, N. B., Doe, C. Q. and Bellaiche, Y. (2010) 'The Fz-Dsh planar cell polarity pathway induces oriented cell division via Mud/NuMA in Drosophila and zebrafish', *Dev Cell* 19(5): 740-52.

Seifert, J. R. and Mlodzik, M. (2007) 'Frizzled/PCP signalling: a conserved mechanism regulating cell polarity and directed motility', *Nat Rev Genet* 8(2): 126-38.

Semenov, M. V. and Snyder, M. (1997) 'Human dishevelled genes constitute a DHR-containing multigene family', *Genomics* 42(2): 302-10.

Sepich, D. S., Calmelet, C., Kiskowski, M. and Solnica-Krezel, L. (2005) 'Initiation of convergence and extension movements of lateral mesoderm during zebrafish gastrulation', *Dev Dyn* 234(2): 279-92.

Sepich, D. S., Usmani, M., Pawlicki, S. and Solnica-Krezel, L. (2011) 'Wnt/PCP signaling controls intracellular position of MTOCs during gastrulation convergence and extension movements', *Development* 138(3): 543-52.

Shao, M., Liu, Z. Z., Wang, C. D., Li, H. Y., Carron, C., Zhang, H. W. and Shi, D. L. (2009) 'Down syndrome critical region protein 5 regulates membrane localization of Wnt receptors, Dishevelled stability and convergent extension in vertebrate embryos', *Development* 136(12): 2121-31.

Shima, Y., Kawaguchi, S. Y., Kosaka, K., Nakayama, M., Hoshino, M., Nabeshima, Y., Hirano, T. and Uemura, T. (2007) 'Opposing roles in neurite growth control by two seven-pass transmembrane cadherins', *Nat Neurosci* 10(8): 963-9.

Shimizu, T., Yabe, T., Muraoka, O., Yonemura, S., Aramaki, S., Hatta, K., Bae, Y. K., Nojima, H. and Hibi, M. (2005) 'E-cadherin is required for gastrulation cell movements in zebrafish', *Mech Dev* 122(6): 747-63.

Shimshek, D. R., Kim, J., Hubner, M. R., Spergel, D. J., Buchholz, F., Casanova, E., Stewart, A. F., Seeburg, P. H. and Sprengel, R. (2002) 'Codon-improved Cre recombinase (iCre) expression in the mouse', *Genesis* 32(1): 19-26.

Shnitsar, I. and Borchers, A. (2008) 'PTK7 recruits dsh to regulate neural crest migration', *Development* 135(24): 4015-24.

Sievers, F., Wilm, A., Dineen, D., Gibson, T. J., Karplus, K., Li, W., Lopez, R., McWilliam, H., Remmert, M., Soding, J. et al. (2011) 'Fast, scalable generation of high-quality protein multiple sequence alignments using Clustal Omega', *Mol Syst Biol* 7: 539.

Sigma-Aldrich (2014) Oligonucleotide Purification Guidelines, http://www.sigmaaldrich.com/life-science/custom-oligos/custom-dna/learning-center/best-purification.html, accessed 30/05/2014.

Simons, M. and Mlodzik, M. (2008) 'Planar Cell Polarity Signaling: From Fly Development to Human Disease', *Annu Rev Genet*.

Sittaramane, V., Pan, X., Glasco, D. M., Huang, P., Gurung, S., Bock, A., Li, S., Wang, H., Kawakami, K., Matise, M. P. et al. (2013) 'The PCP protein Vangl2 regulates migration of hindbrain motor neurons by acting in floor plate cells, and independently of cilia function', *Dev Biol* 382(2): 400-12.

Sittaramane, V., Sawant, A., Wolman, M. A., Maves, L., Halloran, M. C. and Chandrasekhar, A. (2008) 'The cell adhesion molecule Tag1, transmembrane protein Stbm/Vangl2, and Lamininalpha1 exhibit genetic interactions during migration of facial branchiomotor neurons in zebrafish', *Dev Biol*.

Skoglund, P. and Keller, R. (2010) 'Integration of planar cell polarity and ECM signaling in elongation of the vertebrate body plan', *Curr Opin Cell Biol* 22(5): 589-96.

Sokol, S. Y. (1996) 'Analysis of Dishevelled signalling pathways during Xenopus development', *Curr Biol* 6(11): 1456-67.

Solnica-Krezel, L., Stemple, D. L., Mountcastle-Shah, E., Rangini, Z., Neuhauss, S. C., Malicki, J., Schier, A. F., Stainier, D. Y., Zwartkruis, F., Abdelilah, S. et al. (1996) 'Mutations affecting cell fates and cellular rearrangements during gastrulation in zebrafish', *Development* 123: 67-80.

Srinivas, S., Watanabe, T., Lin, C. S., William, C. M., Tanabe, Y., Jessell, T. M. and Costantini, F. (2001) 'Cre reporter strains produced by targeted insertion of EYFP and ECFP into the ROSA26 locus', *BMC Dev Biol* 1: 4.

Strutt, H. and Strutt, D. (2009) 'Asymmetric localisation of planar polarity proteins: Mechanisms and consequences', *Semin Cell Dev Biol*.

Subach, O. M., Gundorov, I. S., Yoshimura, M., Subach, F. V., Zhang, J., Gruenwald, D., Souslova, E. A., Chudakov, D. M. and Verkhusha, V. V. (2008) 'Conversion of red fluorescent protein into a bright blue probe', *Chem Biol* 15(10): 1116-24.

Tada, M., Concha, M. L. and Heisenberg, C. P. (2002) 'Non-canonical Wnt signalling and regulation of gastrulation movements', *Semin Cell Dev Biol* 13(3): 251-60.

Tada, M. and Kai, M. (2009) 'Noncanonical Wnt/PCP Signaling During Vertebrate Gastrulation', *Zebrafish*.

Tada, M. and Smith, J. C. (2000) 'Xwnt11 is a target of Xenopus Brachyury: regulation of gastrulation movements via Dishevelled, but not through the canonical Wnt pathway', *Development* 127(10): 2227-38.

Takeuchi, M., Nakabayashi, J., Sakaguchi, T., Yamamoto, T. S., Takahashi, H., Takeda, H. and Ueno, N. (2003) 'The prickle-related gene in vertebrates is essential for gastrulation cell movements', *Curr Biol* 13(8): 674-9.

Tamura, K., Peterson, D., Peterson, N., Stecher, G., Nei, M. and Kumar, S. (2011) 'MEGA5: molecular evolutionary genetics analysis using maximum likelihood, evolutionary distance, and maximum parsimony methods', *Mol Biol Evol* 28(10): 2731-9.

Tawk, M., Araya, C., Lyons, D. A., Reugels, A. M., Girdler, G. C., Bayley, P. R., Hyde, D. R., Tada, M. and Clarke, J. D. (2007) 'A mirror-symmetric cell division that orchestrates neuroepithelial morphogenesis', *Nature* 446(7137): 797-800.

Taylor, J., Abramova, N., Charlton, J. and Adler, P. N. (1998) 'Van Gogh: a new Drosophila tissue polarity gene', *Genetics* 150(1): 199-210.

Thisse, B. and Thisse, C. (2004) 'Fast Release Clones: A High Throughput Expression Analysis. ', *ZFIN Direct Data Submission (*http://zfin.org*)*.

Tomasiewicz, H. G., Flaherty, D. B., Soria, J. P. and Wood, J. G. (2002) 'Transgenic zebrafish model of neurodegeneration', *J Neurosci Res* 70(6): 734-45.

Topczewski, J., Sepich, D. S., Myers, D. C., Walker, C., Amores, A., Lele, Z., Hammerschmidt, M., Postlethwait, J. and Solnica-Krezel, L. (2001) 'The zebrafish glypican knypek controls cell polarity during gastrulation movements of convergent extension', *Dev Cell* 1(2): 251-64.

Torban, E., Iliescu, A. and Gros, P. (2012) 'An expanding role of Vangl proteins in embryonic development', *Curr Top Dev Biol* 101: 237-61.

Torban, E., Kor, C. and Gros, P. (2004) 'Van Gogh-like2 (Strabismus) and its role in planar cell polarity and convergent extension in vertebrates', *Trends Genet* 20(11): 570-7.

Tree, D. R., Shulman, J. M., Rousset, R., Scott, M. P., Gubb, D. and Axelrod, J. D. (2002) 'Prickle mediates feedback amplification to generate asymmetric planar cell polarity signaling', *Cell* 109(3): 371-81.

Trinh, L. A. and Stainier, D. Y. (2004) 'Fibronectin regulates epithelial organization during myocardial migration in zebrafish', *Dev Cell* 6(3): 371-82.

Ulrich, F., Concha, M. L., Heid, P. J., Voss, E., Witzel, S., Roehl, H., Tada, M., Wilson, S. W., Adams, R. J., Soll, D. R. et al. (2003) 'Slb/Wnt11 controls hypoblast cell migration and morphogenesis at the onset of zebrafish gastrulation', *Development* 130(22): 5375-84.

Ulrich, F., Krieg, M., Schotz, E. M., Link, V., Castanon, I., Schnabel, V., Taubenberger, A., Mueller, D., Puech, P. H. and Heisenberg, C. P. (2005) 'Wnt11 functions in gastrulation by controlling cell cohesion through Rab5c and E-cadherin', *Dev Cell* 9(4): 555-64.

Usui, T., Shima, Y., Shimada, Y., Hirano, S., Burgess, R. W., Schwarz, T. L., Takeichi, M. and Uemura, T. (1999) 'Flamingo, a seven-pass transmembrane cadherin, regulates planar cell polarity under the control of Frizzled', *Cell* 98(5): 585-95.

Veeman, M. T., Slusarski, D. C., Kaykas, A., Louie, S. H. and Moon, R. T. (2003) 'Zebrafish prickle, a modulator of noncanonical Wnt/Fz signaling, regulates gastrulation movements', *Curr Biol* 13(8): 680-5.

Vervenne, H. B., Crombez, K. R., Lambaerts, K., Carvalho, L., Koppen, M., Heisenberg, C. P., Van de Ven, W. J. and Petit, M. M. (2008) 'Lpp is involved in Wnt/PCP signaling and acts together with Scrib to mediate convergence and extension movements during zebrafish gastrulation', *Dev Biol* 320(1): 267-77.

Vladar, E. K., Antic, D. and Axelrod, J. D. (2009) 'Planar Cell Polarity Signaling: The Developing Cell's Compass', *Cold Spring Harbor Perspect Biol* 1(3): a002964.

Wada, H., Iwasaki, M., Sato, T., Masai, I., Nishiwaki, Y., Tanaka, H., Sato, A., Nojima, Y. and Okamoto, H. (2005) 'Dual roles of zygotic and maternal Scribble1 in neural migration and convergent extension movements in zebrafish embryos', *Development* 132(10): 2273-85.

Wallingford, J. B. (2010) 'Planar cell polarity signaling, cilia and polarized ciliary beating', *Curr Opin Cell Biol* 22(5): 597-604.

Wallingford, J. B., Fraser, S. E. and Harland, R. M. (2002) 'Convergent extension: the molecular control of polarized cell movement during embryonic development', *Dev Cell* 2(6): 695-706.

Wallingford, J. B., Rowning, B. A., Vogeli, K. M., Rothbacher, U., Fraser, S. E. and Harland, R. M. (2000) 'Dishevelled controls cell polarity during Xenopus gastrulation', *Nature* 405(6782): 81-5.

Warchol, M. E. and Montcouquiol, M. (2010) 'Maintained Expression of the Planar Cell Polarity Molecule Vangl2 and Reformation of Hair Cell Orientation in the Regenerating Inner Ear', *J Assoc Res Otolaryngol*.

Warga, R. M. and Kane, D. A. (2007) 'A role for N-cadherin in mesodermal morphogenesis during gastrulation', *Dev Biol* 310(2): 211-25.

Warga, R. M. and Nusslein-Volhard, C. (1999) 'Origin and development of the zebrafish endoderm', *Development* 126(4): 827-38.

Wen, S., Zhu, H., Lu, W., Mitchell, L. E., Shaw, G. M., Lammer, E. J. and Finnell, R. H. (2010) 'Planar cell polarity pathway genes and risk for spina bifida', *Am J Med Genet A* 152A(2): 299-304.

Wharton, K. A., Jr. (2003) 'Runnin' with the Dvl: proteins that associate with Dsh/Dvl and their significance to Wnt signal transduction', *Dev Biol* 253(1): 1-17.

Winter, C. G., Wang, B., Ballew, A., Royou, A., Karess, R., Axelrod, J. D. and Luo, L. (2001) 'Drosophila Rho-associated kinase (Drok) links Frizzled-mediated planar cell polarity signaling to the actin cytoskeleton', *Cell* 105(1): 81-91.

Wittmann, T. and Waterman-Storer, C. M. (2001) 'Cell motility: can Rho GTPases and microtubules point the way?', *J Cell Sci* 114(Pt 21): 3795-803.

Witzel, S., Zimyanin, V., Carreira-Barbosa, F., Tada, M. and Heisenberg, C. P. (2006) 'Wnt11 controls cell contact persistence by local accumulation of Frizzled 7 at the plasma membrane', *J Cell Biol* 175(5): 791-802.

Wolff, T. and Rubin, G. M. (1998) 'Strabismus, a novel gene that regulates tissue polarity and cell fate decisions in Drosophila', *Development* 125(6): 1149-59.

Wu, J. and Mlodzik, M. (2008) 'The frizzled extracellular domain is a ligand for Van Gogh/Stbm during nonautonomous planar cell polarity signaling', *Dev Cell* 15(3): 462-9.

Xu, J., Wang, F., Van Keymeulen, A., Rentel, M. and Bourne, H. R. (2005) 'Neutrophil microtubules suppress polarity and enhance directional migration', *Proc Natl Acad Sci U S A* 102(19): 6884-9.

Yanagawa, S., van Leeuwen, F., Wodarz, A., Klingensmith, J. and Nusse, R. (1995) 'The dishevelled protein is modified by wingless signaling in Drosophila', *Genes Dev* 9(9): 1087-97.

Yang, Y. and Thorpe, C. (2011) 'BMP and non-canonical Wnt signaling are required for inhibition of secondary tail formation in zebrafish', *Development* 138(12): 2601-11.

Ye, D. and Lin, F. (2013) 'S1pr2/Galpha13 signaling controls myocardial migration by regulating endoderm convergence', *Development* 140(4): 789-99.

Ye, X., Wang, Y., Cahill, H., Yu, M., Badea, T. C., Smallwood, P. M., Peachey, N. S. and Nathans, J. (2009) 'Norrin, frizzled-4, and Lrp5 signaling in endothelial cells controls a genetic program for retinal vascularization', *Cell* 139(2): 285-98.

Yin, C., Kiskowski, M., Pouille, P. A., Farge, E. and Solnica-Krezel, L. (2008) 'Cooperation of polarized cell intercalations drives convergence and extension of presomitic mesoderm during zebrafish gastrulation', *J Cell Biol* 180(1): 221-32.

Ymer, S. (1991) 'Heat inactivation of DNA ligase prior to electroporation increases transformation efficiency', *Nucleic Acids Res* 19(24): 6960.

Yu, A., Xing, Y., Harrison, S. C. and Kirchhausen, T. (2010) 'Structural analysis of the interaction between Dishevelled2 and clathrin AP-2 adaptor, a critical step in noncanonical Wnt signaling', *Structure* 18(10): 1311-20.

zebrafish.org Zebrafish International Resource Center (ZIRC) http://zebrafish.org.

zfin.org (2013a) dishevelled, dsh homolog 1a, dvl1a, http://zfin.org/ZDB-GENE-090312-40.

zfin.org (2013b) dishevelled, dsh homolog 1b, dvl1b, http://zfin.org/ZDB-GENE-071004-1, accessed December 2013.

zfin.org (2013c) dishevelled, dsh homolog 2, dvl2, http://zfin.org/ZDB-GENE-041118-20.

zfin.org (2013d) dishevelled, dsh homolog 3a, dvl3a, http://zfin.org/ZDB-GENE-010319-1.

zfin.org (2013e) dishevelled, dsh homolog 3b, dvl3b, http://zfin.org/ZDB-GENE-121101-2.

zfin.org (2014a) Zebrafish Dishevelled homologs, http://zfin.org/action/quicksearch/query?pageSize=20&query=dishevelled+homolog&categoryID=GENES, accessed June 2014.

zfin.org (2014b) Zebrafish Flamingo homologs, http://zfin.org/action/quicksearch/query?pageSize=20&query=cadherin+EGF+LAG+seven-pass+G-type+receptor&categoryID=GENES, accessed June 2014.

zfin.org (2014c) Zebrafish Frizzled homologs, http://zfin.org/action/quicksearch/query?pageSize=20&query=frizzled+homolog&categoryID=GENES, accessed 18/06/14.

Zhou, M. Y. and Gomez-Sanchez, C. E. (2000) 'Universal TA cloning', *Curr Issues Mol Biol* 2(1): 1-7.

Zigman, M., Trinh le, A., Fraser, S. E. and Moens, C. B. (2011) 'Zebrafish neural tube morphogenesis requires Scribble-dependent oriented cell divisions', *Curr Biol* 21(1): 79-86.

Zoller, P. (1992) 'High Electro-transformation Efficiencies Obtained With DNA From Ligation Mixtures', *Bulletin 1359, Bio-Rad Laboratories, (*http://www.bio-rad.com/webroot/web/pdf/lsr/literature/Bulletin_1359.pdf*) accessed 11th April 2013*.